Tornado Missile Risk Analysis—Appendixes

EPRI

ywords:
Tornado Missile
Risk Assessment
Design Basis Event

EPRI NP-769
Project 616
Final Report
Appendixes
May 1978

Prepared by
Carolina Power and Light Company
Raleigh, North Carolina

ELECTRIC POWER RESEARCH INSTITUTE

Tornado Missile Risk Analysis
Appendixes — Analytical Models and Data Bases

NP-769
Research Project 616

Final Report, May 1978

Prepared by

CAROLINA POWER AND LIGHT COMPANY
411 Fayetteville Street
Raleigh, North Carolina 27602

Principal Investigator
L. A. Twisdale

Co-Authors
W. L. Dunn
S. T. Lew
T. L. Davis
J. C. Hsu
S. T. Lee

Prepared for

Electric Power Research Institute
3412 Hillview Avenue
Palo Alto, California 94304

EPRI Project Manager
Boyer B. Chu
Nuclear Power Division

ABSTRACT

Mathematical models of the contributing events to the tornado missile hazard at nuclear power plants have been developed in which the major sources of uncertainty have been considered in a probablistic framework. These models have been structured into a sequential event formalism which permits the treatment of both single and multiple missile generation events. A simulation computer code utilizing these models has been developed to obtain estimates of tornado missile event likelihoods. Two case studies have been analyzed: a single unit plant using the current NRC set of missiles and a two unit arrangement using an expanded missile set. Preliminary results suggest that the likelihood of missile strike and that of subsequent plant damage may be acceptably small.

Variable	Units	Symbol
Reference Radius to Maximum Wind Speed (at z_{to})	(ft)	ρ_{tmo}
Reference Rotational Wind Speed at (ρ_{tmo}, z_{to})	(ft/sec)	$(U_{r\theta})_o$
Boundary Layer Thickness	(ft)	$\delta(\rho_t)$
Effective Thickness of Sublayer	(ft)	ζ
Translation Speed	(ft/sec)	U_T
Boundary Wind Speed	(ft/sec)	v_b
Radial Distance To Right, Left Boundaries	(ft)	R_r, R_l
Slope of Vertical Variation of ρ_{tm}		S
Boundary Layer Thickness at ρ_{tmo}	(ft)	δ_m
Maximum Boundary Layer Thickness	(ft)	δ_o
Magnitude of Ratio of Radial to Tangential Wind Speeds at (ρ_{tmo}, z_{to})		γ
Radial Distance to Zero Wind Speed	(ft)	ρ_{to}
Effective Width for Missile Damage	(ft)	W_{te}

Appendix 2. Missile Characterization Methodology

Missile Area	(ft^2)	A
Minimum Impact Area	(in^2)	A_{min}
Maximum Impact Area	(ft^2)	A_{max}
Impact Mode		B
Depth or Diameter	(ft)	d
Width or Thickness	(ft)	b
Availability Mode		I_a
Length	(ft)	L
Mass	(lb_m)	m
Missile Set		S
Volume	(ft^3)	M_v
Origin Zone		O_z
Weight	(lb_f)	W
Weight per Unit Length	(lb_f/ft)	w

CONTENTS

NOTATION

The following is utilized in this report:

Variable	Units	Symbol
Appendix 1. Tornado Event Risk & Windfield Modeling		
Tornado Origin Area	(mi^2)	A_o
Plant Strike Envelope	(mi^2)	A_p
Path Area	(mi^2)	A_t
Updated Tornado F-scale Windspeeds		F'
Probability Density Function		$f(\ )$
Prior Intensity Classification		I
Posterior Intensity Classification		I'
Local Intensity State		I^*
Path Length	(mi)	L_t
Probability of an Event		$P(\ )$
Reference Area	(mi^2)	S
Reference Time Period	(yr)	T
Path Width	(ft)	W_t
Path Direction	(rad)	ϕ_t
Occurrence Rate	(yr^{-1})	ν
Plant Envelope Projection Along Tornado Length	(mi)	Z_1
Plant Envelope Projection Along Tornado Width	(mi)	Z_2
Coordinates in Cylindrical Tornado Frame		(ρ_t, θ_t, z_t)
Radial, Tangential, and Vertical Wind Speeds, Respectively	(ft/sec)	U_r, U_θ, U_z
Rotational Wind Speed	(ft/sec)	$U_{r\theta}$
Dimensionless Wind Speed (Model)		u
Normalized Wind Speed	(ft/sec)	U_o
Radius to Maximum Tangential Wind Speed	(ft)	$\rho_{tm}(z_t)$
Reference Height for Intensity Specification	(ft)	z_{to}

Blank Page

Variable	Units	Symbol
Clearance Height	(in)	Z_c
Storage Height	(in)	Z_s
Solidity Ratio		σ

Appendix 3. Missile Aerodynamics, Injection and Trajectory Analysis

Plant Cartesian Frame		F_p
Plant Cylindrical Frame		F_{pc}
Tornado Cartesian Frame		F_t
Tornado Cylindrical Frame		F_{tc}
Relative Velocity Cartesian Frame		F_r
Wind Frame		F_w
F_p Base Vectors		$\hat{i},\hat{j},\hat{k}$
F_{pc} Base Vectors		$\hat{r},\hat{\theta},\hat{k}$
F_t Base Vectors		$\hat{i},\hat{j},\hat{k}$
F_{tc} Base Vectors		$\hat{r}_t,\hat{\theta}_t,\hat{k}$
F_r Base Vectors		$(\hat{u},\hat{v},\hat{w})$
F_w Base Vectors		$(\hat{v},\hat{P},\hat{L})$
F_p Coordinates		(x,y,z)
F_{pc} Coordinates		(ρ,θ,z)
F_{tc} Coordinates		(ρ_t,θ_t,z)
F_r Coordinates		(u,v,w)
Time	(sec)	t
Missile Position Relative to F_p	(ft)	$\bar{R}$
Missile Position Relative to F_t	(ft)	$\bar{R}_t$
Tornado Position Relative to F_p	(ft)	$\bar{O}_t$
Tornado Touchdown Point, S		(ρ_s,θ_s,z_s)
Missile Orientation Unit Vectors:		
Major Axis		$\hat{MCL}$
Minor Axis		$\hat{MD}$
Missile Center Line Orientation Angles:		
from $\hat{w}$	(rad)	ψ
Azimuthal, from $-\hat{v}$	(rad)	ϕ

Variable	Units	Symbol
from $-\hat{v}$	(rad)	α
Azimuthal, from $\hat{w}$	(rad)	β
Missile Roll Angle	(rad)	δ
Tornado Approach Angle (from $\hat{i}$)	(rad)	τ
Wind Velocity Relative to F_p and in Components Parallel to F_{pc}	(ft/sec)	$\bar{U}=(U_r,U_\theta,U_z)$
Wind Velocity Relative to F_t and in Components Parallel to F_{tc}	(ft/sec)	$\bar{u}_{tc}=(u_{rt},u_{\theta t},u_{zt})$
Wind Velocity Relative to F_t and in Components Parallel to F_{pc}	(ft/sec)	$\bar{u}_{pc}=(u_r,u_\theta,u_z)$
Missile Velocity Relative to F_p and in Components Parallel to F_{pc}	(ft/sec)	$\bar{V}_{pc}=(V_r,V_\theta,V_z)$
Wind-Missile Relative Velocity in Components Parallel to F_{pc}	(ft/sec)	$\bar{v}_{pc}=(v_r,v_\theta,v_z)$
Wind-Missile Relative Velocity in Missile Components (axial, cross flow, depth, width)	(ft/sec)	$\bar{v}=(v_a,v_c,v_b,v_d)$
Magnitude of Relative Velocity	(ft/sec)	v
Coordinate Transformation Matrix from F_a to F_b		$\tilde{L}_{b,a}$
Missile Acceleration in Components Parallel to F_{pc}	(ft/sec^2)	$\bar{a}_{pc}=(a_r,a_\theta,a_z)$
Aerodynamic Force in Components Parallel to F_{pc}	(lb_f)	$\bar{f}=(f_r,f_\theta,f_z)$
Vertical Restraining Force	(lb_f)	$\bar{f}_{OV}$
Horizontal Restraining Force	(lb_f)	$\bar{f}_{OH}$
Aerodynamic Drag Force	(lb_f)	f_D
Aerodynamic Lift Force	(lb_f)	f_L
Aerodynamic Side Force	(lb_f)	f_S
Aerodynamic Lift Force due to Radial Wind Velocity	(lb_f)	$\bar{f}_{LR}$
Aerodynamic Lift Force due to Tangential Wind Velocity	(lb_f)	$\bar{f}_{LT}$
Aerodynamic Drag Force due to Vertical Wind Velocity	(lb_f)	$\bar{f}_{DZ}$

Variable	Units	Symbol
Radial Component of Horizontal Aerodynamic Force	(lb_f)	f_R
Tangential Component of Horizontal Aerodynamic Force	(lb_f)	f_T
Drag Force in Axial, Depth, Cross Flow, and Width Directions, Respectively	(lb_f)	D_a, D_b, D_c, D_d
Reference Aerodynamic Area	(ft^2)	A_{REF}
Effective Aerodynamic Area Normal to $\bar{v}$	(ft^2)	A
Gravitational Acceleration	(ft/sec^2)	g
Air Density	($slugs/ft^3$)	ρ_a
Drag Coefficient		C_D
Lift Coefficient		C_L
Side Force Coefficient		C_S
Maximum Drag Coefficient		C_{Dm}
Tumbling Drag Coefficient		C_{Dt}
Lift Coefficient due to u_r		C_{LR}
Lift Coefficient due to u_θ		C_{LT}
Lift Coefficient due to u_z		C_{LZ}
Drag Coefficient due to u_r		C_{DR}
Drag Coefficient due to u_θ		C_{DT}
Drag Coefficient due to u_z		C_{DZ}
Side Force Coefficient due to u_r		C_{SR}
Side Force Coefficient due to u_θ		C_{ST}
Side Force Coefficient due to u_z		C_{SZ}
Drag Coefficients for Normal Areas With Flow Parallel to Axial, Depth, and Width Directions		$C_{D_a}, C_{D_b}, C_{D_d}$

Appendix 4. Missile Impact Methodology

Equivalent Missile Diameter	(in)	d_e
Perforation Thickness	(in)	e

Variable	Units	Symbol
Coefficient of Restitution		e_r
Concrete Compressive Strength	(lb/in^2)	f'_c
Gravitational Acceleration	(ft/sec^2)	g
Equivalent Velocity Reduction Coefficient		$g(\theta,\beta)$
Empirical Penetration Constant		K
Missile Shape Factor		K_m
Concrete Penetrability Factor		K_b
Missile Deformability Factor		K_d
Barrier Effective Mass	(lb_m)	M_b
Offset Impact Region		O_r
Reduction Factor for Material Statistical Strength Increase		R_s
Scabbing Thickness	(in)	s
Barrier Thickness	(in)	t_b
Impact Velocity	(ft/sec)	$\bar{V}_i$
Equivalent Impact Velocity	(ft/sec)	V'_i
Velocity of Barrier After Impact	(ft/sec)	V_b
Velocity of Missile After Impact	(ft/sec)	V_m
Penetration Depth	(in)	z
Ricochet Angle	(rad)	α
Angle of $\hat{MCL}$	(rad)	β
Angle of Yaw	(rad)	γ
Angle of Obliquity	(rad)	θ
Yield Stress of Steel Barrier	(lb/in^2)	σ_y
Missile Density	(lb_m/ft^3)	ρ_m

APPENDIX 1
TORNADO EVENT RISK AND WINDFIELD MODELING

1.1 Introduction

The initiating event in the tornado missile event sequence is the occurrence of a tornado and its associated wind distribution at the plant site. For the purposes of tornado missile risk analysis, two basic models are required for the description and numerical assessment of this initiating event: an occurrence model which includes a tornado strike definition and a windfield model which defines the tornado characteristics required for the missile trajectory analysis. In this chapter, methodology and model descriptions are presented for both. The general characteristics of tornadoes, including their small horizontal extent, unpredictable behavior, relatively short life, and extreme variability, place major reliance on indirect measuring techniques and analytical modeling to provide the information necessary for this methodology development. As a result, there are significant sources of uncertainty in both the occurrence statistics and the windfield model.

1.2 Tornado Occurrence and Windspeed Risk Analyses

The assessment of risks associated with tornado events requires the analysis and interpretation of available tornado statistics and the development of a model which relates event success to this input data. The tornado data record is characterized by significant subjective input and subsequent variation in quality and accuracy from one area to another, inflationary reporting and population bias, and a major reliance on indirect measurement techniques and data grouping to quantify the variables of interest. Tornado incidence and/or windspeed risk analyses typically utilize several of the following characteristics: intensity, frequency, location, tornado path variables (length, width, direction), and windfield variables (profile size, shape). Statistical correlation analyses, attributed probabilistic independence, and regional grouping have been applied in varying degrees in previous

tornado occurrence and windspeed risk models. Generally, the event of interest includes tornado path union with a defined point in a region or that any portion of a structure will be subjected to windspeeds exceeding prescribed values. In this section, the salient characteristics of tornado data, including attempts at parameter estimation, and a review of previous tornado risk models are presented. Although tornado occurrence analyses have thus far been applied to tornado incidence rather than tornado missile events, the methods and many of the same variables are useful in modeling the initiating tornado event. The proposed initiating event model and the utilization of tornado incidence statistics are discussed in Section 1.3.

1.2.1 Tornado Data Characteristics

The tornado data which is currently available for event probability estimation can be classified into two basic sources:

(1) That obtained within the framework of a comprehensive and nominally unbiased data gathering system.

(2) That obtained from the observation or measurement of geographically limited, intensity limited, or other "nonrandom" tornado events.

For an accurate assessment of tornado missile risks, the recognition of the data source and its utilization in any statistical sense must be qualified accordingly. Data sources of the first type imply the existence of an essentially unbiased random sampling of the parent tornado event population within a particular region. Thus, probability estimates obtained from such data would provide a logical basis for risk analysis. The tornado variables which are generally assumed to have this type of data base include intensity, path length, path width, path direction, and occurrence frequency. These variables are useful in establishing tornado incidence risks. Data sources of the second type can be employed in a statistical analysis in the associated limited event spaces or in a general event space if the a priori probabilities are known or assumed for each data set resulting from the

tornado event. Frequently, the nonrandom aspect is assumed to be insignificant and the data is applied uniformly to the larger population. The tornado variables for which a data source of this type has developed primarily includes the vortex parameters. Typically, data obtained from selected measurements is much more detailed and comprehensive in terms of evaluating the physical characteristics of tornadoes (e.g., 1-1, 1-2, 1-33, 1-40, 1-55, 1-66). Its main usefulness is in tornado vortex modeling (Section 3.4) and in verifying the indirect measuring systems employed for data of the first type. In this section, further characteristics of tornado occurrence data are discussed and a summary of the significant attempts at statistical parameter estimation is presented.

1.2.1.1 Tornado Recording Systems and Usage

Tornado data sources are characterized by the fundamental errors and uncertainties associated with any observation and measurement system that is significantly dependent upon both observer availablilty and human judgment. As noted by Paultz (1-28), all severe local storms are not observed, all those observed are not reported, and some of those reported are incorrectly classified. The dependence of complete tornado reporting upon a dispersed population is well established (1-43, 1-24, 1-34), and several investigators (1-23, 1-51) have attempted to correct for this potential bias in the data record. Fujita (1-24) notes that reporting efficiency is high in the eastern United States but that correlation of high population centers in the midwest to tornado frequency suggests less efficient reporting. By analyzing annual reporting trends, Fujita concludes that reporting efficiency is far from the saturation value. The number of tornadoes reported has increased significantly in the past 25 years from an annual frequency of approximately 274 in the early 1950's to some 919 annually in the mid 1970's (1-70). This increase in reported tornado frequency is the apparent result of greater population density, improved storm reporting networks and techniques, more trained observers, and the establishment of community warning networks (1-24). Although it is normally desirable to utilize as large a data base as feasible, the potential effect of inflationary reporting, particularly in a regionalized data analysis, should be considered in the analysis of the data record.

The reliance on indirect methods to estimate tornado intensity, path length, and path width is another inherent problem in tornado characterization. Since tornadoes are relatively short-lived and localized phenomena, most are not observed throughout their entire life. Consequently, the only information regarding their characteristics is often the resulting damage. In an attempt to provide a procedure for classifying all tornadoes based upon observed damage patterns and tracks, the FPP scale for tornado intensity, path length, and path width variables was developed by Fujita and Pearson (1-9, 1-25). Each tornado since 1971 has been given an FPP rating by the local Meteorologist-In-Charge of the National Weather Service Office. Other classification systems, notably the Dames & Moore categories (1-51), have also been proposed.

Several unavoidable difficulties arise in the use of a general classification system which is based upon indirect measurement estimations. Because of the subjective judgment required in indirect classification systems, the data record is subject to regional bias. Inherent in this indirect measurement system is the dependence on structure density and location in the tornado path to provide the damage medium for which the method is dependent. The absence or scarcity of such structures necessarily bias the data unconservatively. In addition, a major source of uncertainty is the correlation of tornado characteristics to structural damage and the subsequent intensity classification on the basis of structural damage. The prediction error associated with the dynamic tornado characteristics, prior structural condition, and failure mechanisms is significant. Typically, investigators that have conducted detailed engineering analyses of tornado damaged structures have reported lower windspeed estimates than those bounded by the recorded FPP classification interval (1-22, 1-66). Others (1-50) have recognized the potential for classification error in the data record and made adjustments in the data by assuming 10% of the tornado path lengths could have been underestimated. Recognizing the significance of the extreme events, McDonald et al. (1-23) actually reevaluated the original classification and in some cases modified it on the basis of subjective differences.

Although the current tornado record and classification system have a number of shortcomings, they constitute the major source of information for tornado risk assessment. A major question regarding the use of this data concerns the extent to which regional grouping and analysis of the data is employed. Regional variation of tornado characteristics has long been recognized as any tornado incidence map (1-34, 1-43) clearly illustrates. Recognition of regional data variation in the development of tornado risk models or maps has resulted (e.g., 1-10, 1-12, 1-21, 1-23, 1-50, 1-51, 1-72). The question of optimal regional size is an important one because of the effect of potential local classification bias is more significant the smaller the region. Garson et al. (1-19) use a national data base to characterize tornado parameters in order to minimize regional bias effect. Naturally, the utilization of data covering too large a region can result in unconservative results if applied to the most tornado-prone areas. It is also apparent that optimal tornado regionalization should also consider synoptic conditions for tornado genesis (e.g., 1-21). Much work remains to be done regarding regionalization of tornado risks, particularly in the statistical analysis of existing records and in the propagation of classification error in risk prediction.

1.2.1.2 Probabilistic Tornado Variable Characterization

The tornado occurrence variables of interest to tornado missile risk assessment include arrival process (frequency of occurrence), intensity, path length, path width, and tornado direction. Investigators have employed different data sources, the same data source but for different time periods, and either grouped or continuous data to statistically characterize these variables. Some of the more recent attempts and conclusions regarding tornado occurrence characteristics are summarized here.

The tornado arrival process was first analyzed by Thom (1-6) for central Iowa tornadoes in the period 1916-56. He demonstrated that a Polya process was an appropriate model since tornado events tend to cluster. Wen

and Chu (1-17) compare Polya and Poisson processes for tornado arrival and determine that a conservative and accurate approximation of tornado occurrence in the United States can be given by the expression

$$P(D) \cong \nu T E(V_o) \tag{1.1}$$

where ν = mean rate of tornado occurrence, T = time period of interest, and $E(V_o)$ = expectation taken over the tornado parameters resulting in the event D. Garson et al. (1-19) employed the above results directly in their tornado risk model. Singh et al. (1-52), Wen (1-39), and Wen and Ang (1-65) also utilize this result and assume that the occurrence of tornadoes is a simple Poisson process. Other tornado risk models which imply the utilization of the product of a mean annual rate of tornado occurrence and the number of years considered are assuming the validity of Eq. 1.1 and the basic independence of tornado events. Additionally, the simplification represented by Eq. 1.1 implies that the event space is limited to the consideration of one or more successes in the same event. Because the only original work in tornado arrival characterization has apparently been limited to two investigations (1-6, 1-17), additional work is needed in the statistical analysis of the tornado arrival process. Noticeably absent is an investigation regarding arrival characterization of extreme tornado events. Also, sufficient statistics should now be available to investigate the implications of the assumed constant rate of occurrence instead of the more general time dependent rate.

Characterizations of tornado intensity, path length, path width, and direction variables have largely been limited to graphical displays and simple numerical data grouping techniques. The number of references which contain such information about the above variables is large and will not be summarized here. However, the number of investigators which have utilized basic probability concepts or drawn statistical inferences from such data is quite limited. A brief review of these reported studies follows.

The relationship of tornado intensity, damage path length, and damage path width has been modeled by several investigators. Thom's pioneering work (1-6) suggested that tornado path length and width distributions are jointly lognormally distributed. Three sets of data covering Iowa and Kansas tornadoes in the period 1937-1962 were analyzed, and a correlation coefficient of 0.39 was determined from the Iowa data. The mean value of path length was 3.94 miles, the mean value of path width was 464 feet, and the mean path area was 2.82 square miles. In utilizing this data, Thom rejected tornado path lengths greater than 100 miles and path widths greater than 1000 yards as doubtful observations. Wen and Chu (1-17) analyzed 212 tornadoes classified by the Fujita system (1-9) according to intensity and area characteristics. By using midrange Fujita velocity and area transformations, they found that a joint lognormal distribution with a mean velocity equal to 110 mph and a mean path area of 1.65 square miles was an excellent fit to the data. The correlation coefficient is 0.672. Garson et al. (1-19) employed 1971, 1972, and 70% of the 1973 FPP classified tornadoes and postulated that a joint lognormal distribution for intensity, length, and width variables was an acceptable model. Using midrange transformations, the means were determined as 106 mph, 2.5 miles, and 251 feet for wind velocity, path length, and path width variables. Positive correlation coefficients of approximately 0.45 were found for the three pairs of variables. Other investigators have not performed correlation analyses but have presented cross tabulations of intensity and area variables. Tecson (1-59) classified 1965 tornadoes into Fujita intensity and area scales. Although not performed by the author, a chi-square test for independence of intensity and damage area variables indicates high significance (99%). Fujita and Pearson (1-25) present graphical displays which indicate correlation of path length, width, and intensity variables. Again, a chi-square test on the path length and width data indicates that the independence hypothesis is rejected at both the 95% and 99% confidence level. Howe (1-60) analyzed 1953-70 tornado path length and width data and concluded that lognormal models were not appropriate in eight states representing 40% of the reported tornadoes. In addition, he applied statistical significance tests to

determine if different hypothesized tornado populations for regionally grouped states exists. When path lengths were reduced to consider "skipping" tornadoes or "intermittent ground contact," the lognormal distribution was found to be appropriate.

1.2.2 Tornado Risk Models

Tornado risk assessment methods rely on input data from existing tornado statistics and attempt to quantify the probabilities associated with specific tornado events. In terms of event definition, previous approaches can be categorized into two sets:

(1) Those in which event success is related to tornado incidence or occurrence.

(2) Those in which event success is defined in terms of some windspeed exceedance criterion.

Approaches limited to the first type do not differentiate between tornado intensities whereas the second type models allow for a more useful event definition, as specified by actual windspeed exceedance probabilities. Because of the characteristics of the data record noted earlier, the latter event space requires the transformation of the existing data into actual windspeeds, a process which is a source of considerable uncertainty (cf. Section 1.3.5). In the following, a brief review of tornado risk assessment, with particular emphasis on the windspeed risk models, is presented.

Court (1-43) reviews and classifies attempts at tornado incidence mapping and representations prior to 1969. As noted in the reference, diverse techniques have been employed but the earlier approaches generally involved the counting of the number of tornado within the selected reference

area and the quantification of risk in terms of tornado incidence or occurrence frequency. The first significant attempt at tornado risk assessment was made by Thom (1-6) in 1963. Event success was defined as the union of the tornado path area with any point within a specified region. By utilizing a geometrical interpretation of probability, Thom's point probability calculation is

$$P(H) = \frac{\nu T \hat{A}_t}{S} \tag{1.2}$$

where ν = mean rate of occurrence within S, T = time period, $\hat{A}_t$ = mean path area, and S = reference area. Equation 1.2 assumes that each tornado event is equally likely to occur anywhere within S and that the tornado events are statistically independent. Success of event H is interpreted as: "A given point within S is within the tornado damage path area at least once for the expected ν tornado strikes within time period T." The exact expression for n tornadoes within time T is given by

$$P(H) = 1 - (1 - \frac{\hat{A}_t}{S})^n \tag{1.3}$$

A binomial series expansion of Eq. 1.3 with $\nu T \equiv n$ indicates that Eq. 1.2 is a first order approximation which is accurate for small $\frac{\hat{A}_t}{S}$.

Wen and Chu (1-17) evaluated the tornado arrival process, constructed a joint probability density function of tornado intensity and path area, and developed a windspeed risk model for point strike events. The basic strike probability calculation is approximated by Eq. 1.1 and thus further verifies Thom's model. The windspeed exceedance function, given by $E(V_o)$, is obtained by the midrange transformation of Fujita classified data (F5 corresponds to 289 mph, etc.) to continuous velocity and area values. The authors implicitly assumed that an F-scale tornado has F-scale windspeeds over its entire damage area.

McDonald et al. (3-1) proposed the use of a windspeed profile in a point strike event model. The geometrical approach is the same as Thom's, and the probability that a point in S is not within the specified windspeed damage path is given by

$$P(H) = e^{\frac{-\nu T \hat{A}_t}{S}} \qquad (1.4)$$

Thus, the authors have implicitly assumed a Poisson process for tornado occurrence events. The generalization of Eq. 1.4 for additional time period and its approximation by Eq. 1.1 is straightforward.

Garson et al. (1-16) incorporate a windspeed profile into Wen and Chu's model (1-17) and determine that the overconservatism can approach 180% for the constant intensity assumption. In a subsequent publication (1-19), Garson et al. present a windspeed risk model in which the strike event is defined as tornado path union with any portion of the plan area of a given structure. An expression is derived for tornado damage origin area for rectangular structures and rectangular tornado damage path areas. An example indicates that, for a square building plan as small as 90' per side, a point structure model results in only 76.4% of the total expected damage origin area. The consideration of finite area "targets" requires information for the tornado path direction variable, which the authors assumed to be independent of intensity, path length, and path width variables. Midrange Fujita scale values are utilized in the transformation to continuous windspeed variables.

Markee et al. (1-21) utilize Thom's mean damage path area (1-6), Fujita scale tornado intensity classifications (1-9), and Paultz's frequency data (1-28) to compute tornado point strike probability as given by Eq. 1.2 for 5° latitude-longitude squares. The point probability of windspeed exceedance is given as

$$P(H) = P(S)P(I) \qquad (1.5)$$

where P(S) = point strike probability and P(I) = tornado intensity probability. This is equivalent to assuming the independence of tornado windspeed intensity and tornado strike, or equivalently damage area (i.e., $P(I|S) = P(I)$). Because of the positive correlation of damage area and intensity, this approach could lead to a biased estimate of P(H). Furthermore, the utilization of differenct data sources for variables which have been shown to be correlated is questionable.

McDonald et al. (1-23) propose the utilization of a global region to determine the tornado damage path-intensity relationship and a local region to assess the intensity distribution for specific site windspeed risk analyses. A combined Rankine wind profile is utilized to consider windspeed decay from the tornado center. Although the utilization of different data regions may be advantageous because of existing data record shortcomings, this approach is equivalent to stating

$$f(a,v) = f(a|v_o)f(v_1) \tag{1.6}$$

where a and v denote the area and velocity variables respectively. Obviously, if the intensity marginal density function $f(v_1)$ for the local region is appreciably different from $f(v_o)$ for the global region, results which imply the utilization of Eq. 1.6 to obtain joint density functions are theoretically inconsistent, although perhaps justifiable on the basis of the limited statistics.

Wen and Ang (1-65) extend previous results (1-17) to include finite area structures and variable tornado wind profile. They conclude that, if the structure area is nearly circular and less than 10^5 square feet, the point strike model is satisfactory. A system of n collinear point structures are also considered. Tornado path direction is assumed to be independent and normally distributed. However, a chi-square test for goodness of fit on path directional data (1-34) indicates that the normal distribution hypothesis should be rejected at the 95% confidence level.

Abbey and Fujita (1-50) assess tornado risks by the expression

$$P(H) = \frac{P_L D}{Sy} \qquad (1.7)$$

where P_L is an adjusted total path length, D is referred to as the DAPPLE (Damage Area Per Path Length) index, S is the reference area, and y is the number of years of data. This approach utilizes the results of field damage surveys of the April 3-4, 1974 tornadoes to account for gradations of damage along the tornado path. Total path lengths for all intensity tornadoes are tabulated for the years 1950-1972. The assumption is made that the damage area gradation for the April 3-4, 1974 tornado outbreak is representative of tornadoes in general. This method is the only tornado risk analysis approach thus far which attempts to include tornado intensity variation along its path length as well as across the path width. As expected, this considerably reduces tornado risk for the more intense storms when compared to models which neglect path length intensity variation.

1.3 An Initial Event Tornado Risk Model

As suggested in the previous section, the considerations in the development of a tornado risk model include the tornado strike definition, methods of analysis and utilization of the existing data recording system, and the transformation of FPP data into continuous variables. In addition, since it is tornado missile events which are of interest here, the interface of the tornado risk model with subsequent conditional tornado missile events in the simulation methodology must be recognized. An initial event tornado risk model is presented in this section which includes the proposed tornado strike definition for tornado missile events, new statistical analyses of the pertinent tornado variables, the use of a Bayesian approach to process the error inherent in the data base, and windspeed correlation analysis to F-scale damage descriptions.

1.3.1 Tornado Strike Model

A tornado strike at a nuclear power plant which could result in a missile hazard requires that the tornado pass sufficiently close to the plant such that the missile trajectories could potentially intersect safety-related systems and structures. The injection and trajectory analyses of potential tornado missiles reported in the literature suggest:

(1) Potentially damaging missiles located outside of the 73 mph tornado wind boundary (gale intensity tornado damage) are not generally injected and transported by the tornado.

(2) The trajectories of the potentially damaging missiles which are injected within the tornado track generally remain within the path width defined by the 73 mph wind boundary.

Noting that tornado missile trajectory oddities have been reported (e.g., 1-34), these hypotheses have been evaluated using the random orientation trajectory model presented in Appendix 3. On the basis of a study representing 2250 missile trajectory simulations (reported in Section 3.3.5), the 73 mph tornado strike boundary model envelopes the statistically significant missile impact zone for tornadoes with path widths greater than 1000 ft. However, for tornadoes with less than 1000 ft. to the 73 mph boundaries, the second hypothesis above is not verified. An effective tornado width (W_{te}) is defined (Eq. 3.11) which covers the potential missile impact zone. In the following tornado strike model development, the effective tornado width is implied in the probability strike calculation employing W_t.

The successful event of tornado strike is defined in this study as the union of any point of the plant area containing safety-related components with the tornado path boundary defined above. It can be easily demonstrated

by applying the total probability theorem that this definition is conservative when compared to a tornado strike definition which includes a specified area or percentage of the plant safety structures. For the purposes of tornado strike event definition, the plant itself is modeled as an enclosed area as either a nonreentrant polygon or a circle. As illustrated in Figure 1-1, safety structures and equipment which are to be assessed for potential tornado missile hazards are enclosed in this tornado strike envelope. Some limiting cases of the "point-union" concept of successful tornado strike are also indicated. In the actual strike simulations, tornadoes such as $(A_t)_j$ in Figure 1-1 will pass through the entire plant envelope (i.e., origination or termination of a tornado within the envelope are not considered). This implies that the conditional probability $P(q|r)$ of striking collinear points (q,r) in the path direction is conservatively modeled as unity rather than its theoretical value $1 - \frac{a}{L_t}$.

The utilization of a tornado strike envelope which is considered to have a finite area (rather than a point model) requires that the geometry of the tornado be considered in the tornado strike risk assessment. As noted in Section 1.2, previous investigators (1-19, 1-65) which have accounted for the area of the targets have assumed rectangular tornado damage paths. This idealization not only permits an analytical solution but it is compatible with available tornado data. This rectangular damage representation has a length (L_t) equal to the total path length and a width (W_t) representing the mean path width. As noted by Fujita (1-24), this representation does not in practice give the integrated damage area but is an adequate measure of the tornado-affected area. The rectangular model will be utilized here on the basis of these considerations and the sensitivity study noted in the following.

Given the tornado strike definition, plant tornado strike envelope, and the rectangular tornado missile impact zone (assumed equal to effective path damage area), it is possible to determine the position of the tornado which results in a successful tornado strike event. The area within which the tornado center point must be located to result in a strike is termed the

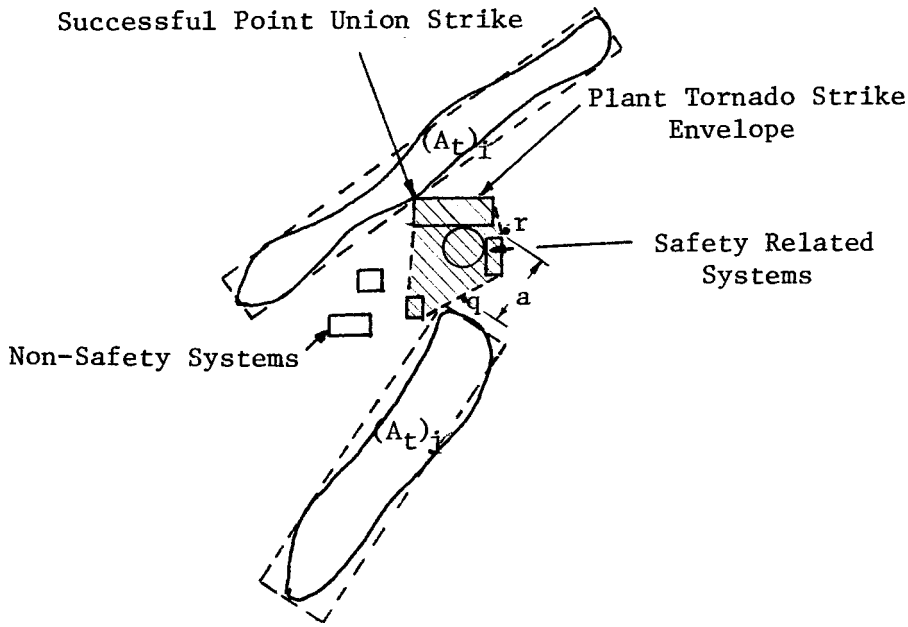

Figure 1-1. Tornado Strike Envelope

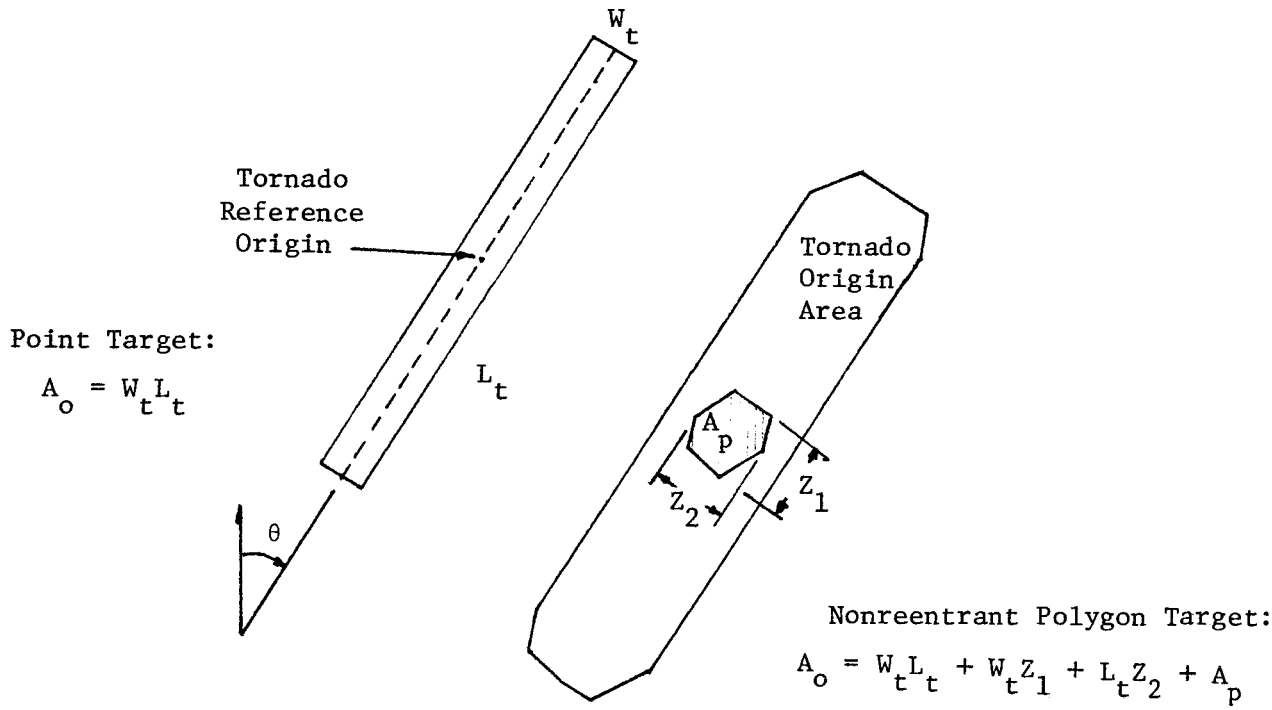

Figure 1-2. Tornado Origin Area For Nonreentrant Polygon

tornado origin area. It can be shown that the tornado origin area (A_o) for any n-sided nonreentrant polygon is given by

$$A_o = W_t L_t + W_t Z_1 + L_t Z_2 + A_p \tag{1.8}$$

where W_t = tornado path width, L_t = tornado path length, Z_1 = projection of polygon in tornado length direction, Z_2 = projection of polygon in tornado width direction, and A_p = area of polygon. It is interesting to note that this general expression is also valid for a line plant model ($A_p = 0$) or a circular strike envelope ($Z_1 = Z_2$ = circle diameter) and agrees with the expressions derived in references 1-19 and 1-65 for rectangular structures. Figure 1-2 illustrates the size of the tornado origin area relative to the tornado area which is used in risk models which model the target as a point. Recognizing the curvature of many tornado tracks (e.g., 1-5, 1-74), a sensitivity study was conducted to examine the adequacy of the rectangular tornado path model. Solutions from Eq. 1.8 were compared to values of A_o obtained from curved tornado path areas. Using a graphical integration procedure and curved tornado tracks represented by sectors from circular arcs, several of the results are presented in Table 1-1. The indication is that for representative nuclear plant strike envelope areas and typical tornado dimensions, the rectangular model yields tornado origin areas only several percent smaller than equal area tornadoes represented by a 30° arc. A comparison of the actual zones is given in Figure 3-3 for a 10 mile tornado track with a 0.25 mile path width (cf. 1-74). Also indicated on the figure is the analytical expression for the extreme curvature case of a tornado track which generates a full circular disc. Since tornadoes have been reported to make U-turns and complete circles (1-5), this expression can be used to compare strike probabilities for such extreme cases. Comparison of this result indicates that the rectangular model is conservative when compared to equal area extreme curvature tracks and thus provides an accurate model for tornado strike analysis utilized in this study.

3.3.2 A Probability Model For Tornado Strike Simulation

The integration of the previously described tornado strike model to the simulation methodology discussed in Volume I is formulated in the

Table 1-1. Comparison of Tornado Origin Areas

Plant Geometry	Tornado Path Length (mi)	Tornado Path Width (mi)	Tornado Origin Area Rectangular (sq mi)	Tornado Origin Area 30° Arc (sq mi)	Comparison % Increase for Arc Shape Tornado
Circular	5	0.25	4.07	4.23	2.29
Envelope	5	0.50	5.42	5.54	3.90
r_p = 0.25 mi	10	0.25	7.82	7.94	1.85
	10	0.50	10.45	10.64	1.57
	20	0.50	20.32	21.22	4.42
	40	0.50	40.45	39.70	-1.85
Rectangle a = 0.1 mi	10	0.25	22.32	21.42	4.05
b = 0.196 mi	20	0.50	49.45	48.02	-3.88

(a) Rectangular Tornado Track

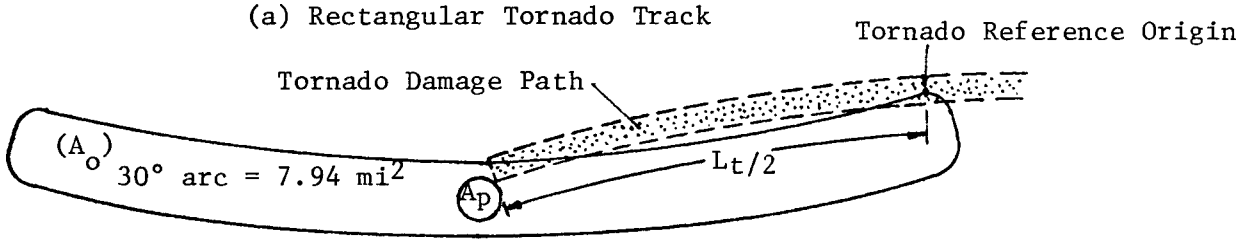

(b) Curved Tornado Track

$$(A_o)_{circle} = 7.50 \text{ mi}^2 = \begin{cases} \pi \left(r_p + \frac{L_t}{2\pi} + \frac{W_t}{2}\right)^2, & \text{if } r_p > \frac{L}{2\pi} - \frac{W}{2} \\ 2L_t\left(r_p + \frac{W_t}{2}\right), & \text{if } r_p < \frac{L}{2\pi} - \frac{W}{2} \end{cases}$$

(c) Circular Tornado Track

Figure 1-4. Comparison of Tornado Origin Areas

following. Tornado intensity is chosen as the primary characteristic, or finest grain structure, of the initiating tornado strike event. This is consistent with the discussion, event trees, and equations presented in Volume I. Because of the conditional event sequence, the tornado strike risk cannot be computed independently and a closed-form type formulation (cf. 1-17, 1-19, 1-65) is not appropriate. The probability estimate for the n^{th} tornado simulation history, $P_n(I_i)$, is required rather than the mean probability estimate $P(I_i)$. Utilizing Wen's conclusions regarding tornado arrival process (Eq. 1.1), $P_n(I_i)$ can be determined by

$$P_n(I_i) = P(H_n \bigcap [(L_t)_n = l_t,\ (W_t)_n = w_t,\ (\Phi_t)_n = \phi_t] \,|\, I = I_i) \qquad (1.9)$$

where H_n denotes a successful tornado strike by the n^{th} tornado history and thus

$$P(H_n) = \begin{cases} \dfrac{\nu_i (A_o)_n T}{S}, & \text{if } (A_o)_n \leq S \\ 1, & \text{if } (A_o)_n > S \end{cases} \qquad (1.10)$$

Substituting for $(A_o)_n$ from Eq. 1.8 and utilizing the n^{th} tornado strike variables from Eq. 1.9 ($(L_t)_n = l_t$, etc.), Eq. 1.10 becomes

$$P_n(I_i) = \begin{cases} \dfrac{\nu_i T}{S} (w_t l_t + w_t Z_1 + l_t Z_2 + A_p), & \text{if } (A_o)_n \leq S \\ 1, & \text{if } (A_o)_n > S \end{cases} \qquad (1.11)$$

In the above, it is assumed that the n^{th} set of tornado variables are obtained by sampling from $f(L_t, W_t, \Phi_t | I_i)$, or its equivalent, by standard Monte Carlo methods. In Eqs. 1.10 and 1.11 ν_i is the mean occurrence rate for tornadoes of intensity i in the reference area S and T is the design life of the plant or other reference time period (e.g., per year). As discussed in Section 1.2.1.2, this approach results in an event space in which success refers to at least one or more successes in the time period T.

1.3.3 Prior Data Analysis of The Recent Tornado Record

The numerical evaluation of the tornado strike model requires the availability of the joint density function $f(L_t, W_t, \Phi_t | I_i)$. In the tornado missile risk assessment of a specific plant site, a sufficiently large regional data base which considers both classification bias potential and synoptic conditions for tornado genesis might be utilized to construct the joint density function. For this methodology oriented investigation, the current NRC regions (1-20) are adopted as the criteria for tornado data grouping and analysis. Specific regional site studies of tornado data are not attempted; however, the methods are valid for any input $f(L_t, W_t, \Phi_t, I)$. Raw FPP classified data for the five years 1971-1975 was obtained for the purpose of constructing the joint density functions necessary in the tornado strike analysis. The year 1971 was selected as a starting point because of the inflationary reporting trend, potential incomplete data sets, and since it corresponds to the commencement of the use of the FPP classification system. Even with this recent data set, out of a total of some 4582 tornado entries, some 2183 do not have direction specified.

To evaluate the homogeneity of the variables within the NRC regions as well as independence among pairs of variables, the hypothesis tests noted in Table 1-2 were performed. The results indicate that with the exception of regional homogeneity of P_L and I variables, the variable groupings are pairwise dependent and are not homogeneous. To further evaluate the conclusion that the homogeneity hypotheses of both P_L and I in the NRC regions 1, 2, and 3 should not be rejected at the 5% level, an analysis of variance was also performed for these two variables. The results indicate that both the reported path length (P_L) and tornado intensity (I) vary significantly in these regions. The difference in these results can be attributed partially to the fact that only 57 and 36 tornadoes (a total of only 2% of the total number) were reported in regions 2 and 3, resulting in low expected values in the chi-square contingency table. Since the chi-square test is not particularly good for small samples and in the interest of consistency, NRC regional data groups will be utilized in the case evaluations in this investigation. Thus, on the basis of these statistical tests, the risk assessment should reflect the dependency among the tornado strike variables and the nonhomogeneity in the NRC regions.

Table 1-2. Summary of Tornado Data Hypothesis Tests

Test No.	Type of Test	Result (at the 5% level)
1.	Homogeneity of P_L in NRC Regions 1, 2, 3	Homogeneous (.3376)
2.	Homogeneity of P_w in NRC Regions 1, 2, 3	Not Homogeneous (.0018)
3.	Homogeneity of I in NRC Regions 1, 2, 3	Homogeneous (.0832)
4.	Homogeneity of ϕ_t in NRC Regions 1, 2, 3	Not Homogeneous (<.0001)
5.	Homogeneity of I Between Data with and without ϕ_t Specified	Not Homogeneous (<.0001)
6.	Homogeneity of P_L Between Data with and without ϕ_t Specified	Not Homogeneous (<.0001)
7.	Homogeneity of P_w Between Data with and without ϕ_t Specified	Not Homogeneous (<.0001)
8.	*Independence of I and ϕ_t	Dependent (<.0001)
9.	*Independence of P_L and ϕ_t	Dependent (<.0001)
10.	*Independence of P_w and ϕ_t	Dependent (<.0001)
11.	*Independence of I and ϕ_t (Exclude data with blank ϕ_T)	Dependent (<.0001)
12.	*Independence of P_L and ϕ_t (Exclude data with blank ϕ_T)	Dependent (<.0001)
13.	*Independence of P_w and ϕ_t (Exclude data with blank ϕ_T)	Dependent (<.0001)
14.	Independence of I and P_L	Dependent (<.0001)
15.	Independence of I and P_w	Dependent (<.0001)
16.	Independence of P_L and P_w	Dependent (<.0001)
17.	Independence of I and P_L (Exclude data with blank direction)	Dependent (<.0001)
18.	Independence of I and P_w (Exclude data with blank direction)	Dependent (<.0001)
19.	Independence of P_L and P_w (Exclude data with blank direction)	Dependent (<.0001)
20.	Independence of P_L and regrouped I ($F_4 + F_5$)	Dependent (<.0001)
21.	Independence of P_w and regrouped I ($F_4 + F_5$)	Dependent (<.0001)

Note: *Indicates approximate test because of circular characteristic of ϕ_t.

The joint frequency of the tornado observations comprising the five year data set is presented in Appendix 5.1 for each of the three NRC regions. These classification tables provide for the most detailed representation of the data and are presented to conveniently allow for independent analysis. The procedures used in the investigation to analyze this data primarily consist of quantitative statistical analysis because of the relatively large number of observations available. Qualitative a priori knowledge of the implied random process has not assumed a major role in the prior analysis.

A major consideration in the data analysis involves the omission of tornado direction in 48% of the observations and the nonhomogeneity of the L_t, W_t, and I populations between the data sets which include and exclude the incomplete entries (cf. tests 5, 6, and 7 in Table 1-2). In addition, direction is a circular variable for which the standard statistical analysis methods are not strictly valid (6-25). A trade-off is thus required since the hypothesis tests (approximate because of the circular characteristic of Φ_t) quantitatively indicate dependence of the direction variable to the other tornado strike variables. On the basis of the above considerations and the difficulty in obtaining joint and marginal distributions (discussed subsequently), independence is attributed to the direction variable, Φ_t. This permits utilization of the 2183 direction observations to model $f(\Phi_t)$ and the use of the total 4582 observations to construct $f(L_t,W_t,I)$. To qualitatively assess the actual dependence of direction to tornado intensity, the frequency polygons in Figure 1-4 were prepared. The correlation of Φ_t and I is not particularly strong as evidenced by the similar shape for all intensities. It is apparent, however, that the weaker tornadoes do not exhibit quite as strong peakedness in the NE direction. Thus, although the chi-square test suggests dependence, the attributed independence to direction in relation to tornado intensity should not significantly affect the results. The empirical histogram for the combined three regions is presented in Figure 1-5. Because of its circular variable characteristic and the ampleness of the data record, these frequencies are proposed to describe $f(\Phi_t)$ in all three regions. Since regions 2 and 3, respectively, had only 27 and 12 directional data points and their frequency polygons are not appreciably different from the combined data, this is

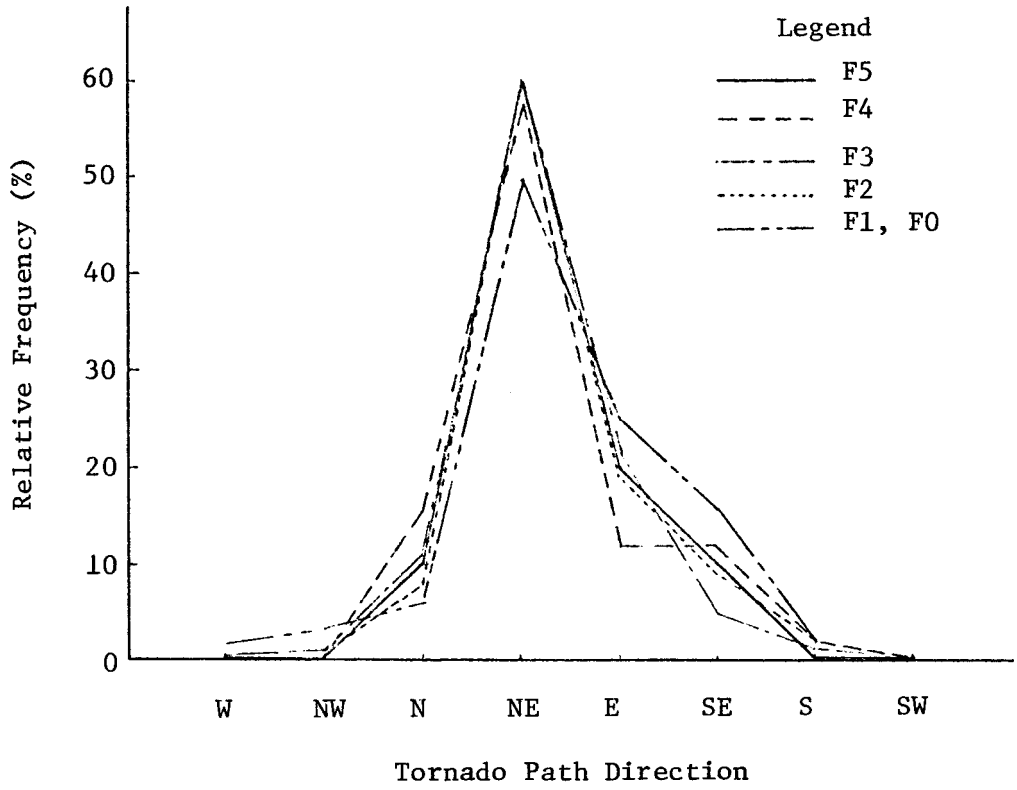

Figure 1-4. Tornado Directional Frequency Polygons

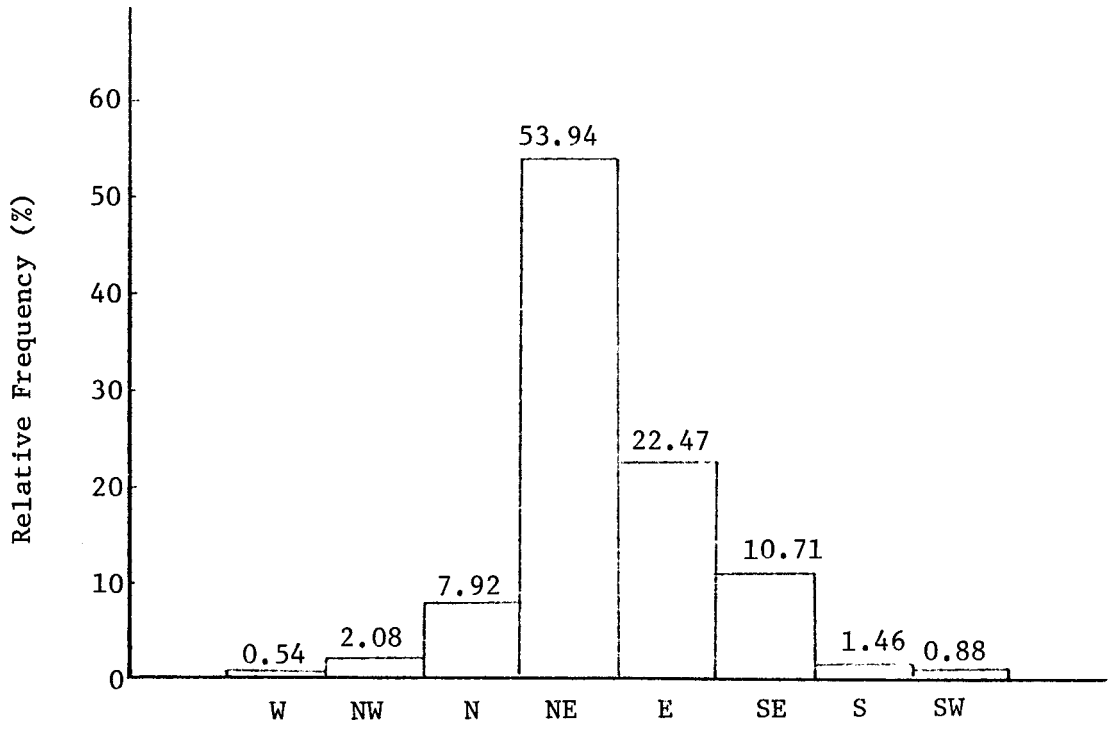

Figure 1-5. Combined Histogram of Tornado Direction

considered an appropriate method to smooth the data considering the statistical uncertainty associated with regions 2 and 3. Naturally, for a particular plant site, $f(\Phi_t)$ can be input to reflect additional regional data or synoptic conditions considered appropriate.

The three remaining tornado strike variables are significantly correlated and thus the determination of an appropriate joint probability model $f(L_t,W_t,I)$ is necessary. Tornado intensity is considered the independent variable and both simple and complex parametric distributions were evaluated to determine an acceptable marginal distribution f(I). By using the conventional midrange intensity windspeed transformation, graphical techniques indicate that of the simple two parameter distributions, the lognormal and gamma models appear to provide an adequate functional fit to the data in all three regions. Quantitative goodness-of-fit tests (chi-square) indicate that at the 5% significance level both models should be rejected in region 1 and neither should be rejected in regions 2 or 3. These results are not unusual considering the large data base in region 1 and the modest data in the other regions. On the basis of the functional fit, the gamma distribution is selected in region 2 and the lognormal in region 3 as noted in Table 1-3. Since neither of these distributions are bounded, they yield finite probabilities for tornado intensities which do not appear in the data base. Unless a physical model which predicts the upper bound is assumed, the assessment of tornado risks in these regions is particularly sensitive to the distribution selected because of the small data base. In region 1, rejection of the appropriate simple distributions suggests that complex distributions (analytical curve fitting) be evaluated. Calculation of the sample skewness (β_1=1.08) and kurtosis (β_2=4.38) implies that both the Johnson and Pearson families are candidates. In the Johnson family, both the S_L (shifted lognormal) and S_B distributions were evaluated; in the Pearson family, type I and type III distributions were checked. Of these, the Johnson S_B provides the best functional fit and is summarized in Table 1-3.

For tornado length and width variables, several simple distributions (lognormal, gamma, exponential) were evaluated as models for the marginals

Table 1-3. Prior Tornado Intensity Distributions

NRC Region	Distribution Model	Model Parameters	F Scale Probabilities F0	F1	F2	F3	F4	F5	≥F6	χ^2 Statistic
1	Observed	-	0.2386	0.4262	0.2377	0.0742	0.0212	0.0022	0	-
	Lognormal	$\hat{\lambda}$=4.566 ζ=0.3842	0.2250	0.4285	0.2455	0.0772	0.0189	0.0039	0.0010	13.39
	*Johnson S_B	ε=0, λ=2500 η=2.465, γ=7.979	0.2440	0.4240	0.2375	0.0735	0.0172	0.0032	0.0005	7.68
2	Observed	-	0.4211	0.2982	0.2105	0.0702	0	0	0	-
	Lognormal	$\hat{\lambda}$=4.440 ζ=0.4055	0.3430	0.4107	0.1820	0.0500	0.0113	0.0022	0.0008	4.23
	*Gamma	λ=0.0608 κ=5.6	0.3559	0.3822	0.2008	0.0520	0.0080	0.0010	0.0001	3.80
3	Observed	-	0.3333	0.5000	0.1111	0.0556	0	0	0	-
	*Lognormal	$\hat{\lambda}$=4.432 ζ=0.3587	0.3336	0.4545	0.1710	0.0347	0.0054	0.0007	0.0001	1.57
	Gamma	λ=0.0813 κ=7.28	0.3620	0.4410	0.1670	0.0275	0.0024	0.0001	0	1.60

Note: *Denotes prior model utilized in this investigation.

$f(L_t)$ and $f(W_t)$ and all are rejected at the 5% significance level. In addition, the conditional density functions $f(L_t|I=F4)$, $f(L_t|I=F4 \cup I=F5)$, $f(W_t|I=F4)$, and $f(W_t|I=F4 \cup I=F5)$ were evaluated and acceptable simple theoretical models were not found. To determine the feasibility of using the data histograms for $f(L_t,W_t|I)$ directly in the risk analysis, the relative frequency charts given in Appendix 5.2 were constructed. The results indicate that in region 1 the data is sufficiently smooth and continuous to permit use of the observed frequencies directly. For regions 2 and 3, because of the small data base, the same joint density function will also be utilized to provide for a continuous representation. If path length and width correlations are necessary for F6 tornadoes, the I_5 frequencies will be utilized.

On the basis of the statistical and qualitative analysis discussed above, the joint density function required for the tornado strike analysis is given by the conditional form

$$f(L_t,W_t,I,\Phi_t) = f(L_t,W_t|I)f(I)f(\Phi_t) \tag{1.12}$$

In the probability sampling, the tornado length and width scale intervals will be modeled as uniform distributions in the transformation from the discrete FPP numbers to actual distances. Similarly, the tornado direction intervals (NE, E, etc.) are assumed to have equally likely direction within any octant. Consideration of the potential classification error in f(I) and its windspeed correlation are discussed in the following sections.

1.3.4 Analysis of Intensity Classification Error

Since the tornado data record is based upon an indirect classification system, a significant question is whether or not the tornado statistics should be utilized without any consideration of the potential classification error. As discussed in Section 1.2.1.1, the sources of uncertainty in the data include variability in observer interpretation, structural damage correlation to tornado characteristics, and structure dispersion within the

tornado path. These error sources are most prevalent in the tornado intensity or F-scale classification (cf. 1-9). Although the existence of uncertainty in the data base is well recognized (e.g., 1-23, 1-28, 1-50, 1-66, 1-71), an analysis of its potential effect in a tornado risk assessment has not yet appeared. In the following, F-scale classification error uncertainty is evaluated parametrically for inclusion in the risk analysis.

For the purposes of modeling and analyzing classification error, the uncertainty is attributed to the following two sources:

(1) Direct Evaluation Error: This results from the subjective variances of the tornado observer, the prediction error associated with the assumed relation of tornado intensity to observed damage, and the variance in structure characteristics (original conditons and response mechanisms).

(2) Random Dispersion Error: The dependence of tornado classification on structure density and dispersion in the tornado path potentially underestimates the tornado characteristics. Statistically, this results from the fact that the method relies on random measurements in terms of structure location and spatial tornado intensity variation.

An estimate of the total error and the resulting uncertainty in the existing tornado data record can thus be obtained through combination of the above sources. A Bayesian treatment of each source of error provides a logical basis for constructing the new or posterior distribution of tornado intensity (6-24). This posterior distribution $f(I')$ can be given in general form as

$$f(I') = \int_I [\alpha f_1(I'|I) + \beta f_2(I'|I)]\, f(I)dI \qquad (1.13)$$

subject to the natural constraints that $\alpha + \beta = 1$, $0 \leq \alpha \leq 1$, and $0 \leq \beta \leq 1$. In this formulation, α is the weight attributed to the direct evaluation error, β is the weight attributed to the random dispersion error, $f_1(I'|I)$ is the

conditional density function associated with the direct evaluation error, and $f_2(I'|I)$ is the conditional density function of the random dispersion error. Basically, f(I) is the prior distribution and the distributions $f_1(I'|I)$ and $f_2(I'|I)$ contain all the information on the error sources such that Eq. 1.13 can be interpreted as an application of the total probability theorem.

Comparison of f(I') to f(I) provides the means of assessing the classification error and the uncertainties associated with tornado intensity statistics. Recognizing the subjective evaluations required for α, β, $f_1(I'|I)$, and $f_2(I'|I)$, a parametric study has been conducted in an attempt to bound f(I') and thus to determine the significance of classification uncertainty. A normal probability distribution is selected to describe the direct evaluation error because its theoretical basis is consistent with the assumed processes contributing to the direct evaluation error. It has been widely used to describe symmetrical error sources in measurements when a number of random effects contribute (6-24, 6-1). A shifted exponential distribution is selected to describe $f_2(I'|I)$ since the upper tails of many distributions are approximated by its analytical form. By restricting the lower bound of the random dispersion classification error to be the next highest F-scale tornado intensity, this distribution provides a realistic model of dispersion error which is theoretically appealing. In the numerical evaluation of Eq. 1.13 it is convenient to construct conditional probability error matrices to represent $f_1(I'|I)$ and $f_2(I'|I)$ in discrete form corresponding to the F-scale classification system. One such matrix is presented for $f_1(I'|I)$ in Table 1-4 using a normal distribution with the mean ($\bar{U}_{max}$) equal to the midpoint of the particular F-scale windspeed interval and the $\bar{U}_{max}$ + 3σ limit as the midpoint of the next interval. This results in the expected bounded error matrix which is very nearly symmetrical (slight unsymmetry is due to the unequal windspeed ranges for the various F scales). From reference to this Table, the model predicts that the probability that a tornado is actually F2 intensity given that it has been classified F2 is $P(I_2'|I_2) = 0.85014$. Correspondingly, due to the error sources noted previously, there are nearly equal probabilities (~0.0749) that classified F2 tornado is actually either F1 or F3 and extremely remote chances that its true intensity is either F0 or F4. This error band is comparable to estimates of F-scale assignment accuracy, including $\pm$50 mph (1-9), $\pm$30 mph (1-59), and $\pm$1 F-scale (1-9, 1-50, 1-71).

Table 1-4. Direct Evaluation Error Matrix

Conditional Probabilities, $P(I_i'|I_j)$, For 3σ Limit

True Tornado State	Classified Tornado Intensity State						
	I_0	I_1	I_2	I_3	I_4	I_5	I_6
I_0'	0.908400	0.079300	0.000033	0	0	0	0
I_1'	0.091598	0.839900	0.074897	0.000026	0	0	0
I_2'	0.000002	0.080798	0.850140	0.076334	0.000024	0	0
I_3'	0	0.000020	0.074927	0.847280	0.073506	0.000020	0
I_4'	0	0	0.000003	0.076357	0.852940	0.073526	0.000020
I_5'	0	0	0	0.000003	0.073500	0.852940	0.076340
I_6'	0	0	0	0	0.000030	0.073530	0.923640

Table 1-5. Combined Error Matrix

Conditional Probabilities, $P(I_i'|I_j)$, For 3σ Limit And $\alpha = 0.9$

True Tornado State	Classified Tornado Intensity State						
	I_0	I_1	I_2	I_3	I_4	I_5	I_6
I_0'	0.88077	0.07137	0.00003	0	0	0	0
I_1'	0.10729	0.75591	0.06741	0.00002	0	0	0
I_2'	0.00843	0.13593	0.76513	0.06870	0.00002	0	0
I_3'	0.00260	0.02441	0.13064	0.76255	0.06616	0.00002	0
I_4'	0.00063	0.00865	0.02457	0.13193	0.76765	0.06617	0.00002
I_5'	0.00023	0.00270	0.00848	0.02423	0.12936	0.76765	0.07634
I_6'	0.00005	0.00103	0.00374	0.01257	0.03682	0.16616	0.92364

Alternately, if the classification methodology is assumed to represent a perfect measurement system, the conditional probabilities would be unity along the diagonal and zero elsewhere. In this case, the posterior distribution would equal the prior or "as-classified" frequencies (if the random dispersion error is also assumed to be negligible). A combined error matrix is given in Table 1-5 which includes the direct evaluation error given in Table 1-4 and the random dispersion error computer from the shifted exponential distribution

$$f(U_{max}) = \lambda e^{-\lambda(U_{max}-U^{L}_{max})}, \quad U_{max} \geq U^{L}_{max} \tag{1.14}$$

Here U^{L}_{max} is the lower bound windspeed of the next intensity classification, and $\lambda = \frac{1}{U^{U}_{max}-U^{L}_{max}}$, where U^{U}_{max} is the upper bound of the next intensity classification. In this manner, 63% of the underclassified tornadoes due to dispersion error are assumed to be underestimated by one F-scale, approximately 25% by two F-scales, etc., the exact value depending upon the intensity being evaluated. The values in Table 1-5 are based upon the above model for dispersion error with weight factors of $\alpha = 0.9$ and $\beta = 0.1$. This implies that one tornado out of ten is assumed to be underclassified due to random dispersion error.

Using the above approach, a parametric evaluation of classification error is presented in Table 1-6. The posterior distribution $f(I')$ is calculated using the discrete form of Eq. 1.13 and is summarized by the probabilities $P(I'_i)$. The results indicate that in each of the NRC regions, the prior or as-classified tornado distribution underestimates the rare events ($\geq$ F4). Significantly, the less intense tornadoes (F0, F1, and F2) are not affected appreciably by potential classification error. This is true even for relatively high direct evaluation error ($\bar{U}_{max} + 2\sigma$ equals the midpoint of the next intensity range) combined with the assumption that one tornado out of five is underclassified due to random dispersion error (cf., cases c, g, k). However for the same parametric case, the more intense tornadoes, such as F5 in Region 1 and F4 in Regions 2 and 3 are underpredicted by factors 4.9, 4.6, and 5.6 respectively. Assuming that a more representative analysis of prediction error is given by the direct evaluation error in Table 1-4 combined with a 0.1 frequency of random dispersion error (cases e, i, m in Table 1-6) the same

Table 1-6. Posterior Distribution of Tornado Intensity

NRC Region	Case Description	I'_0	I'_1	I'_2	I'_3	I'_4	I'_5	$\geq I'_6$
1	(a) As classified, Johnson Distribution	0.2440	0.4240	0.2375	0.0735	0.0172	0.0032	0.0005
	(b) 2σ error, α=1, β=0	0.2725	0.3616	0.2433	0.0917	0.0247	0.0052	0.0010
	(c) 2σ error, α=0.8, β=0.2	0.2179	0.3202	0.2603	0.1264	0.0493	0.0157	0.0102
	(d) 3σ error, α=1, β=0	0.2553	0.3963	0.2418	0.0814	0.0205	0.0040	0.0007
	*(e) 3σ error, α=.9, β=0.1	0.2452	0.3627	0.2465	0.0992	0.0328	0.0097	0.0039
2	(f) As classified, Gamma Distribution	0.3559	0.3822	0.2008	0.0520	0.0080	0.0010	0.0001
	(g) 2σ error, α=0.8, β=0.2	0.2845	0.3245	0.2326	0.1043	0.0365	0.0107	0.0069
	(h) 3σ error, α=1, β=0	0.3537	0.3688	0.2050	0.0598	0.0110	0.0015	0.0002
	*(i) 3σ error, α=0.9, β=0.1	0.3407	0.3406	0.2122	0.0767	0.0215	0.0059	0.0024
3	(j) As classified, Lognormal Distribution	0.3336	0.4545	0.1710	0.0347	0.0054	0.0007	0.0001
	(k) 2σ error, α=0.8, β=0.2	0.2800	0.3521	0.2324	0.0901	0.0302	0.0090	0.0062
	(l) 3σ error, α=1, β=0	0.3391	0.4251	0.1847	0.0427	0.0073	0.0010	0.0001
	*(m) 3σ error, α=0.9, β=0.1	0.3263	0.3909	0.1978	0.0611	0.0171	0.0048	0.0020

Note: *Denotes posterior distribution used in this investigation.

underprediction factors are 3.0, 2.69, and 3.17. Thus, on the basis of this analysis, it appears that classification error is of the order of several hundred percent for the rare tornado events of interest and should be considered in a tornado risk assessment. In this investigation, the posterior distributions of tornado intensity given by cases e, i, and m in Table 1-6 will be utilized to reflect the uncertainty and potential error sources associated with F-scale assignment methodology. In a particular plant assessment, such regional characteristics as classification bias, population, and structure density could be considered in the above approach to derive a specific posterior distribution. In addition for Regions 2 and 3, the statistical uncertainty associated with the small data base could also be considered in an analysis of prediction error (6-24, 6-26).

1.3.5 Tornado Windspeed Correlation and Conversion

The preceding development of the tornado risk model has included the tornado strike model, the necessary input data and its prior analysis, the analysis of classification error, and the subsequent determination of the posterior distribution of tornado intensity. As a result of the indirect measurement system utilized in tornado intensity characterization, another major requirement is the transformation of F-scale intensity categories into actual tornado windspeeds. On the basis of the available data and recent windspeed analyses, modification to the original windspeed intensity ranges (1-9) is justified. In the following, tornado windspeed conversions are presented in the form of conditional density functions to reflect intensity variation along the track length, $f(I^*|I')$, windspeed transformation, $f(U_{max}|I^*)$, and the magnitude of the translational component, $f(U_T|U_{max})$.

1.3.5.1 Tornado Intensity Variation

Typical tornado life cycle characteristics, including variation of tornado strength or intensity near the ground surface are well recognized (e.g., 1-9, 1-55, 3-32, 3-60). Since F-scale classification is based upon the most intense damage evidence within the entire tornado track, consideration of

this aspect of the F-scale methodology in a risk assessment is warranted. Abbey's and Fujita's (1-50) work suggests that models which implicitly assume maximum intensity along the path tend to significantly overpredict tornado risks. In the utilization of intensity variation data in the risk model, consideration must be given to the tornado strike model as well as the geometry and size of the strike envelope relative to the tornado path. Obviously if the envelope corresponds to a significant portion of expected path lengths and event success is defined in terms of a point windspeed exceedance criteria, then consideration of intensity variation may not be important. However, for nuclear plant envelopes, with a maximum dimension generally less than one mile, and tornado tracks frequently exceeding 10 miles, consideration of intensity variation over one mile or greater intervals is appropriate. Because the events of interest are related to tornado missile impact phenomenon over relatively large areas (as compared to point windspeed exceedance events), consideration of lateral or path width intensity variation (cf. 1-16, 1-49, 1-65) is not possible. Thus, for the purpose of tornado missile risk assessment at nuclear facilities, the consideration of tornado intensity variation only in the path length direction and in intervals greater than one mile is applicable.

On the basis of the preceding discussion, the damage assessment and mapping of the tornadoes of April 3-4, 1974, by Fujita (1-75) provides a unique data base for evaluating tornado path length intensity variation. Each of the 148 tornadoes were assigned F scale intensity, F_j, over 2 to 3 mile intervals. Consequently, the normalized path lengths for each F_j intensity is evaluated by

$$P(I_i^* | I_j') = \begin{cases} \dfrac{\sum_m (F_i)_m}{\sum_{k=0}^{j} \sum_m (F_k)_m} & , i \leq j \\ 0 & , i > j \end{cases} \qquad (1.15)$$

where I_i^* denotes the local tornado intensity state (F_i), I_j' denotes the maximum or classified tornado state (F_j), and m is the summation index. The conditional probabilities computed by Eq. 1.15 are summarized by the tornado

intensity variation matrix in Table 1-7. The results indicate that only over a fraction of the path is a tornado at its maximum classified intensity, particularly for the more intense tornadoes. For example, on the basis of these statistics, F4 tornadoes exhibit F4 intensity along 23.8% of their path length, F3 intensity for 21.7% of their path length, etc. Until further or more comprehensive data is available, this analysis provides consistent probability estimates of tornado path length intensity variation. The implied assumptions of equal spacing of F-scale assessment and independent tornado sampling do not suggest any inherent unconservatism in the approach regarding utilization in a general risk assessment. However, to further evaluate the reasonableness of the results, Fujita's evaluations (1-9) of the life histories of the Dallas (F4) and Fargo (F5) tornadoes were also analyzed. The results indicate that the Dallas tornado was actually F4 for 6.2%, F3 for 12.5%, F2 for 15.6%, F1 for 34.4%, and F0 for 31.3% of its path length. The Fargo tornado was F5 for 4.8%, F4 for 11.1%, F3 for 15.9%, F2 for 15.9%, F1 for 15.9%, and F0 for 36.4% of its length. A comparison of these values to the I_4' and I_5' columns in Table 1-7 provides support for the conservatism of the April 3-4, 1974, tornado data analysis. Additionally, it should be emphasized that the 2 to 3 mile F-scale intervals are very conservative compared to typical plant strike envelopes. Finally, the F6 intensity in Table 1-7 represents the residual probability category (to assure density functions which sum to unity, as in Table 1-6) in which the conditional probabilities were synthesized from noted trends in the plots of the F5 and F4 categories.

The utilization of these results with the previous posterior analysis in the risk assessment is achieved by applying the total probability theorem. Simply, the conditional probabilities in Table 1-7 are combined with the posterior probabilities in Table 1-6 (cases e, i, & m for the 3 NRC regions) by

$$P(I_i^*) = \sum_j P(I_i^* | I_j') \; P(I_j') \qquad (1.16)$$

to yield the local tornado state posterior probabilities given in Table 1-8. To maintain the correct path length and width correlations to tornado intensity, Table 1-7 is used to determine the appropriate $f(L_t, W_t | I_j')$ for the

Table 1-7. Tornado Intensity Variation Matrix

Conditional Probabilities, $P(I_i^* | I_j')$

Local Tornado State	Maximum True Tornado State						
	I_0'	I_1'	I_2'	I_3'	I_4'	I_5'	$\geq I_6'$
I_0^*	1	0.551	0.216	0.087	0.122	0.123	0.100
I_1^*	0	0.449	0.352	0.243	0.158	0.108	0.125
I_2^*	0	0	0.432	0.318	0.265	0.169	0.175
I_3^*	0	0	0	0.352	0.217	0.246	0.175
I_4^*	0	0	0	0	0.238	0.169	0.200
I_5^*	0	0	0	0	0	0.185	0.100
I_6^*	0	0	0	0	0	0	0.125

Table 1-8. Local Tornado State Posterior Probabilities

Local Tornado State	NRC Region		
	1	2	3
I_0^*	0.5125	0.5845	0.5926
I_1^*	0.2805	0.2506	0.2635
I_2^*	0.1490	0.1231	0.1106
I_3^*	0.0451	0.0336	0.0267
I_4^*	0.0102	0.0066	0.0053
I_5^*	0.0022	0.0013^+	0.0011^+
$\geq I_6^*$	0.0005^+	0.0003^+	0.0002^+

Note: $^+$Denotes limiting risk events as noted in Section 1.3.5.2

distribution function sampling. This is achieved by normalizing each row in Table 1-7 and randomly sampling to find the j value for the particular tornado history. Thus, the prior, posterior, and tornado intensity variation analyses conveniently reduce to the utilization of Tables 1-7, 1-8, Figure 1-5, and Tables 5-1 through 5-6 in the simulation.

3.3.5.2 Windspeed Correlation

The damage correlation originally suggested for the F-scale windspeed ranges (1-9) was based upon the review of a number of ground and aerial photographs of tornado damage and previous engineering windspeed damage assessments. However, no comprehensive failure analysis of damage mechanisms was made specifically for the purposes of F-scale correlation. The damage specifications and aerial photographs presented as guidelines for F-scale classification (1-9) suggest that there is considerable uncertainty regarding windspeed correlation. In view of the windspeed analyses made since that time (1970), calibration of the F-scale damage categories to a new set of windspeed ranges is justified. In this section, a Bayesian inference scheme is utilized to update the original F-scale ranges and the use of upperbound or "limiting risk" tornado intensities is discussed.

Measurements of tornado wind velocity are basically limited to indirect estimates obtained from engineering damage analysis, photogrammetry, missiles, ground marks, and funnel shapes. For the purposes of assessing windspeed correlation to available damage statistics, engineering failure analysis must necessarily serve as the primary source of information. However, another consideration is that photogrammetry is perhaps the most accurate of the above techniques (e.g., 3-36, 1-66, 1-71) and thus should also be used to assess F-scale calibration where feasible. A basic difficulty is that only a relatively few engineering or photogrammetric analyses have been performed at tornado track locations where the F-scale assignments were also made. Further, the engineering analyses represent imperfect correlations since they generally represent lower bound estimates of windspeed. For photogrammetric correlation, the height at which the windspeeds can be calculated is generally above the level of residential construction (10'-30'), the frequent basis for F-scale

classification. These considerations suggest that the new windspeed correlation data is not of sufficient quality or quantity to completely ignore the originally proposed F-scale windspeeds, but rather should incorporate Fujita's ranges as a prior source of information.

On the basis of the above, windspeed correlation to the F-scale damage categories is achieved through Bayesian analysis (e.g., 6-24, 6-26, 6-27) of the windspeed variable and its model parameters. By combining the prior F-scale ranges of windspeed with a posterior distribution of the model's parameters, a compound distribution of windspeed is derived which includes both the fundamental uncertainty of windspeed correlation and the statistical uncertainty regarding the true values of the parameters of the model. This corresponds to the classical application of Bayesian formalism in which the form of the underlying probability distribution is assumed known but the parameters are not precisely known. Since the original F-scale windspeed ranges are bounded over small intervals and imply equally likely windspeed distribution within the interval, the prior inter F-scale windspeed density function, $f(U_{max}|I^*)$, is assumed uniform.

The parameter of the uniform distribution which is selected as the random variable to reflect the statistical uncertainty of windspeed correlation is the upper limit, b, of the distribution. The new information on b is expressed in the distribution f(b) which is processed with the prior or original correlation $f(U_{max}|I^*,b)$ by evaluating

$$f'(U_{max}|I^*) = \int_b f(U_{max}|I^*,b)\, f(b)\, db \qquad (1.17)$$

to yield the updated (Bayesian) distribution, $f'(U_{max}|I^*)$. On the basis of engineering analyses in a windspeed correlation study, the work reported in reference 1-56 is utilized to construct f(b). A series of structural failure calculations are presented for various building types and limiting windspeed bounds are defined for the Dames and Moore intensity classification scale. The intensity classification descriptions correspond closely to both the

Fujita (1-9) damage specifications and aerial photographic guidelines. Consequently, the failure analyses utilized in the specification of the Dames and Moore categories 1 through 6 basically represent new windspeed correlation data corresponding to b, the F-scale 0 through 5 upperbound windspeeds. Table 1-9 includes the original F-scale velocity ranges (column b) and the Dames and Moore velocity ranges (column c). Assuming f(b) is uniformly distributed between the Dames and Moore ranges, integration of Eq. 1.17 is straightforward and yields the Bayesian distributions which are uniform over the ranges given in column d. The generation of these updated windspeed ranges is achieved by sequentially integrating Eq. 1.17 for each F-scale intensity, beginning with F0, to solve for the new upperbound in each range. To assess the sensitivity of the posterior distribution to the form of f(b), the density function

$$f(b) = \frac{2}{(U-L)^2}(b-L), \quad L \leq b \leq U \tag{1.18}$$

(which conservatively specifies the maximum likelihood of b near U, the range upperbound, with linearly decreasing likelihood to zero at L, the range lowerbound) has also been evaluated. The results are given in column (e) of Table 1-9. To ensure consistent integral limits in the sequential numerical evaluation and conservative windspeed correlation, f(b) has an inter-scale lowerbound 10% greater than the next lower scale's upperbound. Each new distribution thus evaluated can be interpreted as the weighted average of all possible windspeed correlations, $f'(U_{max}|I^*,b)$, associated with the uncertainty on the parameter b.

The preceding analysis incorporates new windspeed correlation information to form posterior windspeed ranges for F-scale damage specification. Additional sources of recent windspeed correlation data, although not generated for the purpose of damage scale assessment, permit the evaluation of the distributions previously derived. Eagleman et al. (3-74) conducted experimental tests on twelve representative residence configurations to identify the one associated with maximum roof pressure loadings. Wind tunnel destructive testing

Table 1-9. F-Scale Windspeed Correlation

F-Scale (a)	Prior Windspeed Range (mph) (b)	D&M Windspeed Range (mph) (c)	Posterior Windspeed Range (mph) Uniform f(b) (d)	Linear f(b) (e)
0	40-72	50-90	40-65	40-73
1	72-112	80-120	65-96	73-103
2	112-157	100-150	96-114	103-135
3	157-206	120-180	114-139	135-168
4	206-260	150-225	139-181	168-209
5	260-318	*200-300+	181-241	209-277

NOTE: *318 is assumed as the finite upperbound for the D&M 6 intensity.

Table 1-10. Tornado Translation Model Parameters

Intensity Category	Truncated Normal Probability Model Parameters				
	Lowerbound (a) mph	Upperbound (b) mph	Mean (U_T) mph	Std. Dev (σ_{U_T}) mph	K
F0, F1	5	40	22.5	9	1.055
F2, F3	5	55	30	12	1.039
$\geq$ F4	5	70	40	15	1.034

was then performed on this configuration in a series of nine experiments to simulate construction variations. The results suggest that F3 to F4 damage can occur in the velocity range 125 to 190 mph. Although there are definite limitations to model testing, these experiments provide a degree of support for the windspeed correlation given in column (e) of Table 1-9. Mehta et al. (4-52) evaluated damaged structures at some 93 locations and concluded that no evidence exists which would indicate a value of near ground wind velocity greater than 200 mph for the May 11, 1970 Lubbock tornado. Since the Lubbock tornado was classified as F4, this further supports the windspeed ranges given in column (e) of Table 1-9. In an evaluation of the April 3-4, 1974 tornado outbreak, Mehta et al. (3-66) conclude that preliminary analyses of structural damage and missile incidents has not produced evidence of ground level windspeed exceeding 250 mph. Since several of the storms were assigned F5 intensity, this also supports the previously derived windspeed correlation.

The Xenia, Ohio tornado of April 3, 1974, provides unique F-scale windspeed correlation data since Abbey (1-72) mapped F-scale contours along the tornado damage path. In addition, the availability of both engineering and photogrammetric analyses permit further comparisons. Mehta (1-22) presents windspeed estimates for the Xenia High School area and subsequently (3-73) assesses the quality of these estimates. Three such estimates have good or acceptable credence levels for all factors: an 133 mph masonry chimney failure, an 159 mph monument collapse, and an 135 mph masonry wall failure. Abbey (1-72) classifies the area as F2-F3 damage. Comparison of aerial photographs (1-22, 3-66) with F-scale guidelines (1-9) suggest that F3 is the appropriate single classification. Considering Mehta's estimates on independent observations, a posterior distribution for the mean windspeed of F3 tornadoes can be found through application of Bayes theorem

$$f'(\bar{U}_{max}|U_1, U_2, \ldots U_n) = N\, L(\bar{U}_{max}|U_1, U_2, \ldots U_n)\, f(\bar{U}_{max}) \qquad (1.19)$$

where U_i constitutes the independent windspeed observations representing the new information, N is a normalizing constant, $L(\bar{U}_{max}|U_1, U_2, U_3) = \prod_{i=1}^{n} f(U_i|\bar{U}_{max})$

is the sample likelihood function, and $f(\bar{U}_{max})$ is the prior distribution of $\bar{U}_{max}$. To facilitate the assessment of Eq. 1.19 and to maintain consistency with the error analysis of Section 1.3.4, the F3 windspeeds are assumed to be normally distributed. Since the conjugate prior for the mean of a normal distribution (with σ known) is a normal distribution, the prior mean is assumed normally distributed with a mean equal to the midpoint of the original F3 range (181.5 mph). The prior standard deviation of the mean is conservatively assumed to be equal to the standard deviation of the F3 range since there is considerably more uncertainty in specifying the mean. Closed form evaluation of Eq. 1.19 is possible (6-24) and the results yield a posterior distribution of $\bar{U}_{max}$ for F'3 tornadoes which is normal with a mean equal to 152 mph. Thus on the basis of Mehta's windspeed estimates (1-22), the original mean windspeed of F3 damage is reduced about 16% from the prior value of 181.5 mph. This new mean compares favorably to the midpoint (151.5 mph) of the previously derived range given in column (e) of Table 1-9. A similar analysis using the maximum windspeed estimates derived from the photogrammetric analyses of Golden (1-66) and Fujita (3-48) has also been performed. Assuming that the two independently calculated windspeed maximums (255 mph and 220 mph) occurred in F5 zones, the posterior mean value F'5 windspeed is 255 mph from application of Eq. 1.19. This 12% reduction represents the updating of the prior value of 289 mph; it compares favorably to the F'5 range midpoint value of 245.5 mph given in column (e) of Table 1-9. Also, these photogrammetric results correspond to heights greater than 60 feet, which experience higher windspeeds than low profile structures generally used in damage assessments. In view of the above support of the Bayesian distribution summarized in column (e) of Table 1-9, this new windspeed correlation is proposed until further information becomes available.

Another major question related to windspeed correlation concerns the prediction of extreme events which have not been reported but whose likelihood of occurrence is required to meet the specified acceptable risk level. The prediction of such events (e.g., F'6 tornadoes in Region 1 or F'4 tornadoes in

Regions 2, 3) can be achieved from the proposed statistical model or from physical models which attempt to bound such characteristics. The general methodology previously developed is independent of the extent to which statistical or physical modeling considerations are employed to assign likelihoods to such events. In the assessment of tornado related risks at nuclear power plants, an acceptable probability of occurrence of 10^{-7}/year (2-6) requires that tornado intensities which correspond to conditional tornado strike probabilities up to 10^{-7}/year be considered. On the basis of the statistical data analysis, windspeed correlation, and recent windspeed estimates, near-ground (0-40 ft.) windspeeds of not more than 300 mph in Region 1, 225 mph in Region 2, and 200 mph in Region 3 are suggested as the upperbound limiting risk tornado intensities. These magnitudes are conservative considering: the respective values of 250 mph and 175 mph suggested by Kessler (1-64, 1-73); the 240-250 mph maximum discussed by Golden (1-66) on the basis of photogrammetric analyses; the 250 mph value suggested by Abbey (1-49); the 225 mph (no translation) discussed by Redman et al. (1-48); the 175-225 mph range proposed by Fujita (1-12) in an area corresponding to the NRC Regions 2, 3; the 200 mph suggested by Fujita (1-10) for the Los Alamos site; and the assessment of Mehta et al. (1-22) of 250-275 mph maximum. Thus, the tornado intensity windspeed correlation utilized in the risk examples in this investigation will incorporate the F-scale ranges given in column (e) of Table 1-9 and the limiting risk intensity ranges of 277-300 mph in Region 1, 168-225 mph in Region 2, and 168-200 in Region 3. As more data becomes available, new windspeed correlations to F-scale damage statistics and the possible reduction of the limiting risk tornado magnitudes may be feasible.

A final consideration of windspeed correlation involves the time period, or alternately distance, which is implied in the specification of maximum windspeeds. Fujita (1-9) states the basis for F-scale wind ranges is the fastest 1/4 mile wind, which corresponds to the mean wind for low speeds (F0, F1) and to the peak gust speed for higher winds. In the absence

of further data on tornado turbulence and gustiness, the windspeed correlation presented herein (fastest 1/4 mile wind) will be used as the tornadic forcing functions without further conversion.

1.3.5.3 Tornado Translation

The variation associated with the tornado translational velocity component is represented by the conditional density function, $f(U_T|U_{max})$. This recognizes the dependence of translational speed to the maximum tornado windspeed and facilitates the numerical risk assessment. The difference in these variables ($U_{max}-U_T$) is termed the rotational component, $U_{r\theta}$, which is characterized, along with the other internal tornado velocity components, by the vortex model discussed in subsequent sections.

Measurements of tornado translational velocity include those reported by Flora (1-5) and Melargno (3-36) which suggest a range of 5 to 70 mph with a mean value of 35 to 45 mph. Fujita reports a range of 15 to 62 mph with an average of 30 mph for seven tornado families (1-9) and proposed a U_T of 30 mph at the Los Alamos site (1-10). Golden (1-66) reports that the average translational velocity is between 33 to 45 mph with a maximum of 78 mph. The NRC Regulatory Guide 1.76 (1-20) specifies translational speed ranges of 5 to 70 mph in Region 1, 5 to 60 mph in Region 2, and 5 to 50 mph in Region 3. On the basis of this information, tornado translational velocity is modeled as a truncated normal distribution

$$f(U_T|U_{max}) = \begin{cases} 0 & , U_T<a \\ Kf^*(U_T|U_{max}), & a\leq U_T\leq b \\ 0 & , U_T>b \end{cases} \qquad (1.20)$$

where the normalizing constant $K = \frac{1}{F(b)-F(a)}$ and $f^*(U_T|U_{max})$ denotes the "non-truncated" distribution. The model parameters μ_{U_T}, σ_{U_T}, a, and b are given in

Table 1-10. Truncating the tails of the distribution ensures positive and reasonable translational speeds for all simulations. The standard deviations selected provide for a realistic frequency of tornadoes to have velocities near the bounds. The upper bounds reflect intensity dependence (by pairs of F-scale) similar to reference 1-20.

1.4 Review of Existing Tornado Models

A tornado wind model consists of the variation of the magnitude and direction of the wind velocity vector with respect to time and space. The wind velocity vector may be resolved into translational, tangential, radial, and vertical components. The resultant of the tangential and radial components is referred to as the rotational component. A wind model containing the above variables constitutes the minimum set of characteristics required for missile trajectory analysis. The term intensity, as employed here, corresponds to the maximum near-ground tornado windspeed (translational plus rotational components).

Tornado windfield models can basically be categorized as empirical, experimental, or theoretical derivations. The empirical models have relied heavily on Hoecker's observation and analysis of the 1957 Dallas tornado (1-1, 1-2). Experimental models are limited by the size of the flow fields and the artificial methods required in the tornado generation. However, they can be closely controlled and are useful in examining certain characteristics of the flow as well as testing tornado hypotheses. Theoretical treatments of tornado vortices are generally restricted to mathematical models of axisymmetric, laminar flows and are restricted by the simplifications required to obtain numerical solutions, particularly with regard to turbulence phenomena. The tornado models presented thus far have been deterministic in that the wind velocity components are invariant for a given intensity. No attempts have been made to recognize the fundamental or modeling uncertainties through probabilistic variable characterization.

1.4.1 Empirical Models and Significant Observations

A brief review of empirically based models as well as a summary of significant field observations, which may be pertinent to tornado missile trajectory modeling, are presented. Since the empirical tornado windfield models presented thus far largely utilize Hoecker's analysis of the 1957 Dallas tornado, limitations of this source are also noted.

1.4.1.1 The 1957 Dallas Tornado

From photogrammetric analysis of this tornado, Hoecker (1-1, 1-2) presents a family of isotachs as a function of height and radius from the center of the tornado. There are several points regarding the reliability of the analysis, including:

(1) The velocity distributions are composites of speeds from different times.

(2) The data points correspond to chance tracer particles and thus the highest speed measured was not necessarily the highest speed existing in the tornado.

(3) The relative velocity between the tracers and air was neglected (1-56).

(4) The pressure field of the Dallas tornado was obtained from the cyclostrophic wind equation. This is not applicable to the inflow region near the ground.

It can be seen that careful interpretation should be given when this data is used as a reference.

1.4.1.2 Empirically Based Models

Bates and Swanson (3-3) first utilized Hoecker's data in 1967 and were followed by Paddleford (3-4), Iotti (3-6), Lee (3-7, 3-11, 3-13), Huang (3-10, 3-14), TVA (3-8), and Duke Power (3-18). Lee's model (3-7) is the only one which utilizes a constant radius for the maximum tangential velocity and no radial velocity inside the core. Iotti (3-6) proposes that the tangential velocity component is a function of tornado translational velocity. This follows the idea presented by Suarez (3-9) that the radius in the cyclostrophic equation depends on the tornado translational velocity and time. Iotti's model appears to be the closest curve-fit to the Dallas tornado. A questionable aspect of each of the models involves the extrapolation of the Dallas windfield data to tornadoes of higher intensities. Many have scaled the data to 300 mph or higher. A major limitation of these models is the primary reliance on the results of the analysis of a single tornado.

1.4.1.3 Observations of Tornado Windfields

Scientific observation of tornadoes is difficult due to their rare and spatially random occurrence, brief duration, small horizontal extent, and highly destructive characteristics. Similarly, utilization of the field data is difficult because of the frequent piecewise nature of the information. Davies-Jones and Kessler (1-45) classify empirical sources as: (1) damage surveys, (2) direct passages over instruments, (3) photographic methods, (4) ground marks, (5) doppler radar, and (6) direct probing. Here, a few of the important tornado features assessed from observations are summarized.

In 1960, Fujita (1-3) presented a detailed analysis based upon observations of the Fargo tornadoes. The stages related to tornado life cycle were observed to be: (1) dropping stage, (2) rounded bottom stage, (3) shrinking stage, and (4) rope stage. Unfortunately, there was insufficient data to assess the relative time of each stage. Golden and Davies-Jones' (3-32) analysis of the Union City tornado suggest similar tornado life cycle characteristics.

The suction spot effect was described by Fujita et al. (1-3, 1-14) in 1967 and had also been observed by earlier investigators. The ground marks produced indicate that the convergence inside a tornado is concentrated at several spots which rotate around the traveling tornado center. These suction vortices have diameters up to approximately 50 ft and tangential speeds estimated from cycloidal suction marks range up to about 150 mph. Including the translational motion of the tornado the maximum speeds of the satellite vortices for the Palm Sunday tornadoes were estimated to be 200 mph. Another study of suction spots was made on the Lubbock Tornadoes in which a formula between the core diameter, traveling speed, funnel rotational speed and the distance between suction swaths was also proposed (1-13).

Fujita (1-11) proposed a mechanism of suction spots in which the flow around the vortex center tends to achieve a cyclostrophic balance when the suction vortex reaches a steady state. Agee, Church, Morris and Snow (1-55) studied the tornado outbreak of April 3, 1974 and suggest a revised form of Fujita's suction vortex model which includes: (1) vortex generation and acceleration on the left flank, (2) the attainment of maximum intensity at the rear, (3) weakening on the right flank, and (4) dissipation on the leading edge. A motion picture study also provided the first conclusive documentation of multiple suction vortices occurring within a parent vortex system. A maximum tangential velocity of 112 mph at the center of a suction vortex with respect to the center of the parent vortex was estimated. The suction swath noted in the Union City tornado (1-76) occurred in the late stages of the tornado and did not rotate around the core. Blechman's study (3-47) on the Wisconsin tornadoes also revealed multiple vortices in each funnel system, further substantiating the observations of Fujita and Agee. Vortex velocities were calculated in the range from 72 to 134 mph. When tornado translation and ambient wind was considered, the average wind velocity was 177 mph. The tornadoes underwent transitions from multiple vortices to a single vortex, which seemed to be related to increased ground roughness. This indicates that eddy viscosity may have a major role. The existence of suction vortices has also been interpreted to suggest a more locally intense tornado system than a single vortex configuration. The phenomenon of vortex splitting has been postulated to be a

function of the swirl ratio, which is defined by Davies-Jones (3-41) as the ratio of the tangential to vertical velocity. When the swirl ratio increases to a critical value, vortex splitting occurs. For higher values of the swirl ratio, multiple vortices are possible, occurring successively as two, three, and four vortices. The impact of these satellite vortex observations on tornado effects analysis has not fully been assessed. At the present time, no theoretical model has predicted or accounted for this feature. Iotti (3-6) has compared his model with the Fargo tornado which reportedly had suction vortices (1-43). Shanahan (3-67) incorporates a suction vortex into his combined Rankine vortex model.

Numerous other tornado windfield analyses and observations have been reported but are not discussed here. Some of the significant general features in terms of missile transport of risk assessment appear to be the observed life cycle characteristics and the potential for multiple vortex systems in the tornado flow field. Tornado intensity variation is considered directly in this investigation (cf. Section 1.3.5.1) and the potential for disorganized multi-vortex flows is considered indirectly in the missile transport model.

1.4.2 Experimental Models

Of the experimental investigations, Ward's work (3-27) may represent the closest simulation of real tornadoes. The multiple vortices observed in real tornadoes have also been confirmed in the laboratory by Ward. When the core diameter is greater than its height, a single vortex becomes unstable if the inflow angle is greater than a critical value. More vortices will form as the inflow angle is further increased. A laboratory model of the tornado-like vortex near the ground was developed and studied by Ying and Chang (3-33). They found that the radial velocity profile in the boundary layer was a reverse S-shaped profile and that the maximum inward velocity occurs very close to the ground. The tangential velocity started from zero at the ground and increased rapidly to a maximum, asymptotically approaching a constant value in the boundary layer.

The influence of ground roughness on tornadoes was studied experimentally by Dessens (3-39). He discovered that an increase of the vertical velocity in the vortex core was caused by a rough surface. In addition, the roughness could cause a vortex to decay which supports Blechman's observation (3-47) that multiple vortices could decay to single ones when roughness increases. These and other experimental results confirm certain observed features as well as those predicted by theoretical models and are useful in analyzing such phenomena under controlled conditions.

1.4.3 Theoretical Models

Theoretical treatments of vortex models generally have been limited to axisymmetric flows in incompressible fluids. Considerable uncertainty still remains concerning the realistic modeling of an intense tornado windfield, particularly with regard to the role that turbulence plays. The purpose of this review is to assess those theoretical considerations and the results of theoretical models which are significant in terms of tornadic missile transport.

1.4.3.1 Combined Rankine Vortex Model

This relatively simple model describes the tangential velocity fields of atmospheric vortices, and consists of a core of concentrated vorticity in an irrotational environment. Beeth and Hobbs (3-16) employed this type of vortex as their tornado windfield model. Basically it consists of a solid body motion inside of a finite radius and irrotational vortex motion outside of that radius. The investigators assume that the vertical and radial velocities are respectively 2/3 and 1/2 of the tangential velocity outside the core and zero inside the core. Sun et al. (1-54) employ a Rankine vortex model for wind loading design on structures. Simiu (3-68) also used this type of vortex in a tornado missile analysis. Dergarabedian and Fendell (3-19) employ this vortex model in their demonstration of velocity distribution for both one-cell and two-cell tornado structures and funnel-cloud shapes. Shanahan (3-67) utilizes this model

for the tangential windfield by determining the vertical windfield from the conservation of energy equation, and the radial windfield from the known vertical windfield and the principle of conservation of mass.

This type of vortex model is theoretically suitable to describe the tornado windfield in the inviscid region and thus most of the windfields derived from the boundary layer theory use it as the inviscid boundary condition. The utilization of a Rankine vortex in the near ground domain is not theoretically justified.

1.4.3.2 Boundary Layer and Other Theoretical Models

In a tornado missile investigation, Bhattacharyya et al. (3-12) first used a boundary layer model which was derived from the work of Wen (1-39) and some intermediate results of Kuo (1-31). Although this model is based upon laminar flow, the nonvanishing of the windspeeds at the ground implies a turbulent boundary layer. The model developed by the Jet Propulsion Laboratory (1-48) utilizes Carrier's work (3-23) and yields a wind definition derived from theoretical considerations that also relies on observational data for several assumptions. It was theoretically developed on the basis of a "worst case" tornado intensity corresponding to 225 mph. The tangential velocity profile is very similar to that of a combined Rankine vortex.

Kuo (1-31) developed a velocity distribution for a tornado windfield with an axisymmetric flow in the boundary layer of a maintained vortex. He solved the zeroth-order approximation of the axisymmetric boundary layer equations based on the assumption that the local boundary layer thickness is much smaller than the horizontal extent of the vortex. The upper boundary condition is imposed by a maintained Rankine vortex and the ground boundary conditions are no slip for laminar flow and a geophysical boundary condition assumed at the sublayer surface for turbulent flow. Hsu and Tesfamariam (3-44, 3-45) employ the same zeroeth-order approximation equations derived from the

axisymmetric boundary layer equations. In addition to these equations, two more equations were added to describe the turbulent transport processes. By solving these equations simultaneously, a four-cell vortex results. They conclude that the number of cells is proportional to the number of turbulence equations used. The oscillatory nature of the velocities near the vortex region is in agreement with Kuo's results.

Davies-Jones and Vickers (3-25) present a numerical model of axisymmetric thermal convection with swirl in a non-rotating cylinder with a height-to-radius ratio of order unity. The top and the rim are free boundaries, while either no-slip or the turbulent conditions used by Kuo are applied at the bottom. Chi and Jih (3-35) numerically solve the three-dimensional Navier-Stokes equations for laminar flow. The no-slip condition is applied at the ground surface and a two-dimensional Rankine vortex is maintained at the top of the boundary layer. The same oscillating nature of velocities as that found by Kuo and Hsu were also obtained.

Lewellen (3-60) has reviewed the development of theoretical models of the tornado vortex and divides the tornado windfield into four regions for comparison purposes. He concludes that a relatively consistent qualitative model of the flow in different regions of the tornado can be pieced together. The maximum velocities and sharpest pressure gradients occur in the corner flow region. The boundary layer approximation is invalid in this region and only the complete Navier-Stokes equations can be applied. In addition, the rate of turbulence appears to be critical in determining both the maximum velocities and the detailed structure of a tornado. Chi and Costopolus (3-80) developed a theoretical model utilizing the complete Navier-Stokes equations and a single equation turbulence model. They also simulated in the laboratory an intense atmospheric vortex near the ground. The results from theory and the experiments agree. According to Lewellen (3-60) this model should give more accurate data near the root of the tornado core since no boundary layer approximation is involved.

The wind velocity profiles developed from the above theoretical models are similar except for the JPL model (1-48) which does not exhibit oscillating characteristics. All the velocity profiles indicate that the reverse inward flow and oscillating characteristics disappear outside the tornado core. The boundary layer thickness grows as a function of radial distance from the tornado center and very rapidly near the center. The Hsu and Tesfamariam model exhibits four-cell characteristics with four regions of downward and upward flows. Chi and Costopolus have come up with a wind distribution more severe than any other tornado model.

1.5 Synthesized Tornado Windfield Model

As suggested in the previous section, a unified body of opinion does not exist regarding the detailed structure of tornado windfields. The significant variability of tornado events and the complexity of the processes implicit in tornado dynamics contribute to the uncertainty associated with scientific description of these phenomena. The progress that has been achieved in tornado modeling have naturally been aimed more at deducing basic flow characteristics (deterministically) than at assessing those flow features which may be important to the transport of missiles. The tornado wind model developed for use in this investigation departs from the conventional approaches in two important aspects: (1) it relies on probabilistic methodology to structure the fundamental and modeling uncertainties; and (2) it contains variable flow features which are significant in missile trajectory prediction. The major sources of uncertainty and important flow considerations (e.g., 3-60, 3-68) include: (1) turbulent flow characteristics, (2) suction vortex phenomena, (3) meridional flow pattern, (4) vertical variation of the radius of maximum tangential velocity, and (5) the ratio of the radial to tangential velocity components.

A primary influence on the assessment of these features is that conservative flow characteristics, in terms of missile transport, cannot generally be established *a priori*. Extreme variability in the aerodynamics of various missile types and in initial locations inhibit the use of introspection and

sensitivity analyses to specify deterministically the tornado flow characteristics which maximize a set of missile transport variables within some interval of uncertainty in the flow definition. Because of resulting limitations of any attempt to specify a "conservative" deterministic wind definition, tornadoes with variable wind flow are considered. In order to maintain relative model simplicity, several of these features are not included directly in the synthesized model but are considered indirectly in the missile transport model. Both a probabilistic and a deterministic model will be utilized in hypothetical case studies to assess the risk sensitivity to the wind definition. The windfield described in the following constitutes the probabilistic model; the JPL model (1-48) representing a deterministic approach will also be utilized.

1.5.1 Modeling Considerations

Observational and theoretical information indicates that the general flow in a tornado vortex is characterized by a tangential velocity component which rises rapidly as the radial distance from the center of the tornado increases (1-2, 3-33, 3-67, 1-48, 3-80), reaches a maximum at the edge of the core, and beyond that decays approximately inversely with radius. Vertically, the tangential velocity increases rapidly from the ground surface to the top of the sublayer and more slowly from there to the top of the boundary layer. This increase within the boundary layer may be monotonic (e.g., 1-48) or slightly oscillatory (e.g., 1-31, 3-79). Theoretical considerations suggest that the radial velocity is large and directed inward near the center of the tornado (3-80, 3-60). This inflow increases rapidly with height to a maximum and then decreases to the top of the boundary layer. Although some theoretical models indicate radial outflows at some elevations within the core (e.g., 1-31), all exhibit inflows near the ground where most of the missile transport will take place. The vertical velocity profile is not well established; however, considering continuity with the radial flow it is expected to decrease with radius (approaching zero outside the core) and generally increase with height to account for the cumulative updraft of the radial inflow. Figure 1-6 demonstrates these flow characteristics for a single cyclonic vortex.

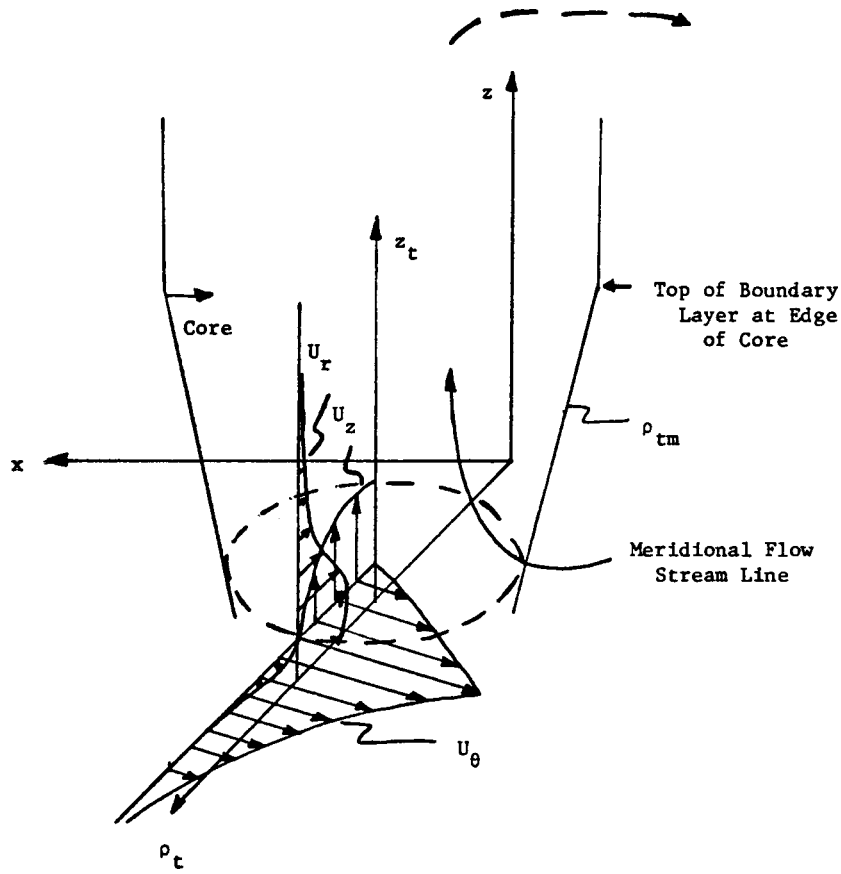

Figure 1-6. Characteristics of Cyclonic Tornado Flow

A wind model incorporating the basic flow features discussed above is synthesized for use as the energy source in the missile transport model. Velocity component profiles of previous deterministic models are assessed to determine the relative differences and possible bounding characteristics of the flow components. The elements of uncertainty are structured into the model through probabilistic variable characterization of the input variables. These random variables include the magnitude of the ratio factor of radial to tangential components (γ), the radius to the maximum tangential velocity (ρ_{tmo}) at a specified height (z_{tmo}), the linear variation of this radius with height as specified by the slope (S), and the ground roughness as specified by the reference boundary layer thickness (δ_o). Since the tornado classification

data implicitly reflects the intensity and size characteristics of multivortex systems, a single vortex with equivalent parameters provides an equivalent tornado path spatial distribution of the energy source. Rotational velocity profile geometry suggests that the mean windfield intensity of a single vortex model is comparable to that obtained from superimposing multivortex systems. In addition, the updraft vertical velocities can be derived from continuity considerations to provide uplifting capacity exceeding that which may be attributed to satellite suction vortices. In the absence of additional information regarding the dynamics of multivortex systems, a single vortex model is utilized. However, the random effects associated with flow turbulence, suction vortices, and "disorganized" three dimensional flows are simulated probabilistically in the missile transport model. Wind flows characterized by anticyclonic rotations are not considered because they are relatively rare (1-45) and should not affect the results of the risk analysis. The synthesized model has input variables (intensity and width) to ensure tornado scale compatibility with the tornado occurrence model in each tornado event assessment.

1.5.2 Variable Identification

The synthesized windfield model is presented utilizing the following definitions and conventions. Radial and vertical coordinates in the tornado frame are represented by ρ_t and z_t, respectively (see Figure 1-6); the origin of the tornado frame is at the center of the vortex and at the elevation of the origin of the plant reference frame. The radius of maximum tangential velocity is denoted ρ_{tm} and is allowed to vary linearly with height according to

$$\rho_{tm} = \begin{cases} \rho_{tmo} + S(z_t - z_{to}) & , z_t \leq \delta(\rho_t) \\ \\ \rho_{tmo} + S(\delta(\rho_t) - z_{to}) & , z_t > \delta(\rho_t) \end{cases} \tag{1.21}$$

where (ρ_{tmo}, z_{to}) is the point at which the reference rotational velocity $(U_{r\theta})_o$ is specified, S is the slope, and δ is the boundary layer thickness. Such a variation of ρ_{tm} with height has been observed (1-1) and, as noted by Simiu (3-68) and Costello (3-62), this feature is potentially significant in missile transport analysis. The local boundary layer thickness is modeled here as

$$\delta(\rho_t) = \begin{cases} \dfrac{5\delta_m - 2\delta_o}{3} + \dfrac{2(\delta_o - \delta_m)\rho_t}{3\rho_{tmo}} & , \ 0 < \rho_t \leq 2.5\rho_{tmo} \\ \\ \delta_o e^{-0.01(\rho_t/\rho_{tmo} - 2.5)} & , \ \rho_t > 2.5\rho_{tmo} \end{cases} \tag{1.22}$$

where δ_m is the boundary layer thickness at $\rho_t = \rho_{tmo}$ and δ_o is the maximum boundary layer thickness.

The radial, tangential, and vertical velocity components are represented as U_r, U_θ, U_z, respectively, while the rotational velocity is

$$U_{r\theta}(\rho_t, z_t) = [U_r^2(\rho_t, z_t) + U_\theta^2(\rho_t, z_t)]^{1/2} \tag{1.23}$$

A normalizing velocity, U_o, used to scale the components is defined by

$$U_o = \frac{(U_{r\theta})_o}{u_{r\theta}(\rho_{tmo}, z_{to})} \tag{1.24}$$

where $u_{r\theta}$ is the dimensionless rotational velocity. The use of U_o as a coefficient in the wind models ensures that the rotational velocity has the

desired magnitude, $(U_{r\theta})_o$, at (ρ_{tmo}, z_{to}). The parameter γ denotes the magnitude of the ratio of radial to tangential components at (ρ_{tmo}, z_{to}), i.e.,

$$\gamma = \left| \frac{U_r(\rho_{tmo}, z_{to})}{U_\theta(\rho_{tmo}, z_{to})} \right| \tag{1.25}$$

Tornado width and translational velocity are given by W_t and U_T, respectively. The boundaries of the tornado are defined by the locations at which the net horizontal velocity in the direction of U_T is v_b, the boundary velocity taken as 107 fps (73 mph, cf. Section 1.3.1). The radial and vertical coordinates of the left and right boundaries are $(\rho_{t\ell}, z_{to})$ and (ρ_{tr}, z_{to}), respectively.

1.5.3 Tangential Velocity

A comparison of several tangential velocity profiles is presented in Figure 1-7(a) and suggests relatively minor differences in the various models. The theoretically based profiles (1-48, 3-17, 3-44, 3-67, 3-80) are not for the same intensity tornado nor the same elevation and are thus useful only in the comparison of the relative shapes of the profiles. Hoecker's Dallas profile is the only empirical profile presented since most other empirically based models (3-3, 3-4, 3-6, 3-8, 3-10, 3-18) provide close curve fits to the Dallas tornado. It can be seen that a Rankine vortex type profile is characteristic of these tangential wind distributions with the exception of Hsu's profile (3-44), which gives two peaks resulting from his turbulence model of two equations. In general, these profiles suggest that a velocity distribution which permits variable ρ_{tmo} and rate of decay outside the core effectively bounds the basic tangential flow characteristics. The profile is thus synthesized with variable ρ_{tmo}, variable slope of ρ_{tm} (Section 1.5.2), and variable rate of decay consistent with the tornado width input.

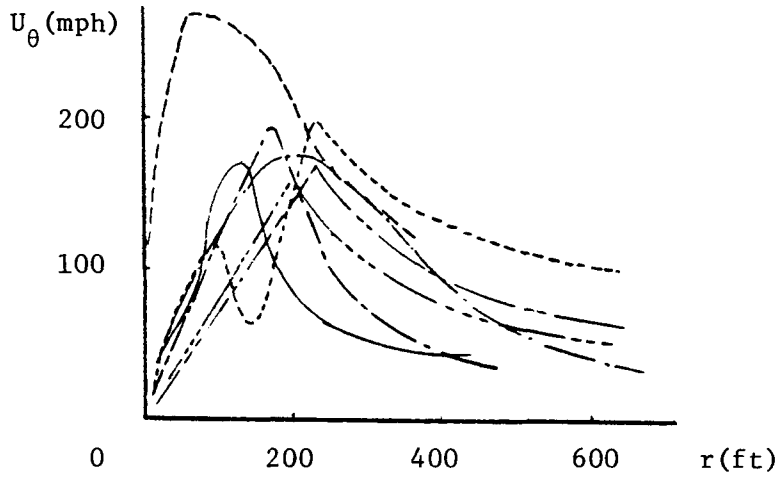

(a) Tangential Profiles at 150 ft. Elevation

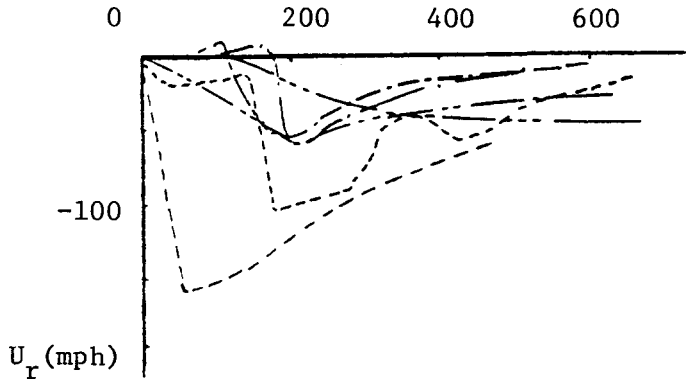

Legend

Chi (3-80) - - - - - - - - - -
Hsu (3-44) - - - - - - - - - - - - - -
WK (3-17) —·—·—·—·—
JPL (1-48) —··—··—··—
Shanahan (3-67)—···—···—
Kuo (1-31) —·—·—·—·—
Dallas (1-1)————————

(b) Radial Profiles at 40 ft. Elevation

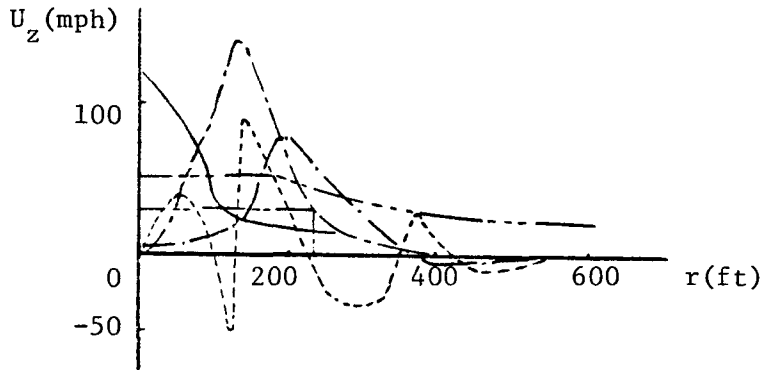

(c) Vertical Profiles at 50 ft. Elevation

Figure 1-8. Shape Comparison of Windfield Velocity Profiles

Utilizing Kuo's (1-31) work, the tangential velocity is modeled as

$$U_\theta(\rho_t, z_t) = U_o \frac{m(\rho_t)}{\rho_t} G(\rho_t, z_t) \tag{1.26}$$

in which

$$m(\rho_t) = \begin{cases} \rho_{tm}[1 - e^{-1.25643(\rho_t/\rho_{tm})^2}] & , \ 0 < \rho_t \leq \rho_{tm} \\ a\rho_t + b & , \ \rho_{tm} < \rho_t \leq \rho_{to} \\ 0 & , \ \rho_t > \rho_{to} \end{cases} \tag{1.27}$$

$$\rho_{to} = \begin{cases} -b/a, \ a < 0 \\ \\ \rightarrow \infty \ , \ a \geq 0 \end{cases} \tag{1.28}$$

$$G(\rho_t, z_t) = \begin{cases} 1 - e^{-\alpha(z_t+\zeta)/\delta(\rho_t)} & , \ z_t \leq \delta(\rho_t) \\ \\ 1 - e^{-\alpha(\delta(\rho_t)+\zeta)/\delta(\rho_t)} & , \ z_t > \delta(\rho_t) \end{cases} \tag{1.29}$$

and the parameters a and b are determined for a given tornado by the boundary specification, as will be shown in Section 1.5.6. In this formulation, U_θ

increases rapidly (concave downward) to a maximum at $\rho_t=\rho_{tm}$ and behaves as $1/\rho_t$ outside the core. The parameter "a" determines the asymptotic behavior of U_θ. For a>0, U_θ approaches a finite positive value; a=0 allows U_θ to approach zero; and for a<0, U_θ vanishes at $\rho_{to}=-b/a$. The vertical variation is specified by $G(\rho_t,z_t)$ which increases monotonically from the ground to the top of the boundary layer. This form for G is based on the first order solution of Kuo (1-31) for $\rho_t>\rho_{tm}$. The actual value of U_θ at the ground is determined by specification of the parameter ζ, which is an effective sublayer thickness. It is noted that increasing ζ has the effect of increasing the windfield near the ground, which favors missile injection. The parameter α adjusts the rate at which G increases with z_t. Values of ζ=20 ft. and α=10 have been found to give reasonable results and are used in all subsequent work.

1.5.4 Radial Velocity

A comparison of the form of several radial velocity profiles is presented in Figure 1-7(b). These models all exhibit an inverse flow, but with variable shapes and relative magnitudes. The ground surface topography and roughness influence the low level inverse flow characteristics. As noted by Simiu (3-68), the relative strength of the radial inflow significantly affects the maximum horizontal speeds attained by tornado missiles. Recognizing this importance and to account for the uncertainty in the specification of the relative magnitude of the radial velocity component, the ratio of radial to tangential velocity (γ) is characterized as a random variable. Since the conservatism of the actual shape of the profile cannot be readily established, a form similar to Chi's (3-80) is obtained by modeling Kuo's first order solution for $\rho_t>\rho_{tm}$ (1-31). Thus, the function for the radial component is

$$U_r(\rho_t,z_t) = \gamma' U_o \frac{m(\rho_t)}{\rho_t} F(\rho_t,z_t) \qquad (1.30)$$

where

$$\gamma' = \gamma \frac{U_\theta(\rho_{tmo}, z_{to})}{U_r'(\rho_{tmo}, z_{to})} = \gamma \frac{G(\rho_{tmo}, z_{to})}{F(\rho_{tmo}, z_{to})} \tag{1.31}$$

$$U_r'(\rho_t, z_t) = -U_r(\rho_t, z_t)/\gamma' = U_o \frac{m(\rho_t)}{\rho_t} F(\rho_t, z_t) \tag{1.32}$$

$$F(\rho_t, z_t) = \begin{cases} \dfrac{(z_t+\zeta)}{\delta(\rho_t)} e^{-\alpha(z_t+\zeta)/\delta(\rho_t)} & , \quad z_t \leq \delta(\rho_t) \\ \\ 0 & , \quad z_t > \delta(\rho_t) \end{cases} \tag{1.33}$$

The parameter γ' adjusts the ratio factor γ for the inherent ratio between radial and tangential models. It is noted that the radial velocity is also finite at the ground for nonzero ζ and that

$$\lim_{\rho_t \to 0} U_r(\rho_t, z_t) = 0 \tag{1.34}$$

which is required by physical arguments.

1.5.5 Vertical Velocity

A comparison of the vertical velocity profiles is presented in Figure 1-7(c) and suggests less agreement in the profile shape than either the tangential or the radial components. The plots support the concept of an

updraft inside the core, but with considerable disagreement as to the form of the updraft and its attenuation outside the core. This issue is resolved in the synthesized model by assuming meridional flow continuity. Thus the vertical component is generated from the continuity condition

$$-\frac{\partial}{\partial z_t} U_z(\rho_t, z_t) = \frac{\partial}{\partial \rho_t} U_r(\rho_t, z_t) + \frac{1}{\rho_t} U_r(\rho_t, z_t) \qquad (1.35)$$

Integrating both sides and neglecting the variation of ρ_{tm} with z_t, i.e., assuming $\rho_{tm} \tilde{=} \rho_{tmo}$, the following form for U_z is obtained,

$$U_z(\rho_t, z_t) = \frac{\gamma' U_o}{\rho_t} \left[\frac{dm(\rho_t)}{d\rho_t} H(\rho_t, z_t) + m(\rho_t) \frac{\partial H(\rho_t, z_t)}{\partial \rho_t} \right] \qquad (1.36)$$

where

$$H(\rho_t, z_t) = \frac{\delta(\rho_t)}{\alpha^2} e^{-\alpha\zeta/\delta(\rho_t)} \left\{ 1 + \frac{\alpha\zeta}{\delta(\rho_t)} - \left[1 + \frac{\alpha(z_t+\zeta)}{\delta(\rho_t)} \right] e^{-\alpha z_t/\delta(\rho_t)} \right\} \qquad (1.37)$$

and thus

$$\frac{\partial H(\rho_t, z_t)}{\partial \rho_t} = \frac{1}{\alpha^2} \frac{d\delta}{d\rho_t} e^{-\alpha\zeta/\delta(\rho_t)} \left\{ 1 + \frac{\alpha\zeta}{\delta(\rho_t)} + \left[\frac{\alpha\zeta}{\delta(\rho_t)}\right]^2 - \left[1 + \frac{\alpha(z_t+\zeta)}{\delta(\rho_t)} + \left[\frac{\alpha(z_t+\zeta)}{\delta(\rho_t)}\right]^2 \right] e^{-\alpha z_t/\delta(\rho_t)} \right\} \qquad (1.38)$$

Although no additional probabilistic elements have been utilized in the specification of U_z, variations in the previously introduced random variables, ρ_{tmo}, γ, δ_o, and S, provide for significant variations in vertical velocity profiles as noted subsequently.

1.5.6 Calculational Procedure and Sample Results

For this probabilistic model, the tornado windfield is defined by the parameters $(U_{r\theta})_o$, ρ_{tmo}, z_{to}, S, γ, δ_m, δ_o, W_t, and U_T. The dependent variables γ' and U_o are then calculated according to Eqs. 1.31 and 1.24 respectively, once the dimensionless velocities at (ρ_{tmo}, z_{to}) have been determined, e.g.,

$$u_{r\theta}(\rho_{tmo}, z_{to}) = m_o \left\{G^2(\rho_{tmo}, z_{to}) + [\gamma' F(\rho_{tmo}, z_{to})]^2\right\}^{1/2} \qquad (1.39)$$

In Eq. 1.39, m_o is a constant and is related to the tornado size variables by

$$a + \frac{b}{\rho_{tmo}} = \frac{m(\rho_{tmo})}{\rho_{tmo}} = 1 - e^{-1.25643} = m_o \qquad (1.40)$$

To ensure compatibility with the tornado width and intensity specifications, it is also necessary to find a, b, $\rho_{t\ell}$, and ρ_{tr} such that the following conditions (and Eq. 1.40) are satisfied:

$$R_r = \rho_{tr}\cos(\tan^{-1}\gamma) \qquad (1.41)$$

$$W_t = \rho_r + R_\ell \qquad (1.42)$$

$$U_{r\theta}(\rho_{tr}, z_{to}) = v_b - U_T \qquad (1.43)$$

and

$$[U_{r\theta}(R_\ell)\cos(\tan^{-1}\gamma) - U_T]^2 + [U_{r\theta}(R_\ell)\sin(\tan^{-1}\gamma)]^2 = v_b^2 \qquad (1.44)$$

This can be accomplished by an iterative procedure beginning with $R_\ell = \rho_{tmo}$ and calculating b from

$$b = \frac{\rho_{tr}\rho_{tmo}}{\rho_{tr}-\rho_{tmo}} \left[m_o - \frac{v_b - U_T}{U_o \{ [1-2e^{-\alpha(z_{to}+\zeta)/\delta(\rho_{tr})}]^2 + [\frac{\gamma'(z_{to}+\zeta)}{\delta(\rho_{tr})} e^{-2\alpha(z_{to}+\zeta)/\delta(\rho_{tr})}]^2 \}^{1/2}} \right] \tag{1.45}$$

Iteration continues until the following condition is satisfied

$$v_b - \varepsilon < \{ [U_{r\theta}(R_\ell)\cos(\tan^{-1}\gamma) - U_T]^2 + [U_{r\theta}(R_\ell)\sin(\tan^{-1}\gamma)]^2 \}^{1/2} < v_b + \varepsilon \tag{1.46}$$

where ε establishes the tolerance of the search. This procedure "fits" the model to the tornado occurrence data given, requiring the windfield to assume the proper magnitudes at the boundaries.

The tornado occurrence model specifies the three variables $(U_{r\theta})_o$, W_t, and U_T as sampled from the tornado data record. The height at which the reference intensity is specified, z_{to}, is taken as 20 feet. This is a representative mean value of the height of structures, trees, etc., associated with the damage descriptions of the F scale classification system (1-9). It should be noted that this does not state that the maximum velocity occurs at 20 ft. (cf. Fig. 1-9), only that the reference intensity of a given F scale tornado is attained by this elevation.

There is limited guidance on the proper choices for the boundary layer thicknesses δ_m and δ_o. JPL (1-48) uses an effective boundary layer of 1000 ft.; Kuo (1-31) shows a boundary layer which increases with ρ_t out to $\rho_t = 2.5\rho_{tmo}$, then slowly decreases, indicating that $\delta_m < \delta_o$. Moreover, δ_m is relatively insensitive to changes in the value of Kuo's surface stress variable (1-31),

whereas δ_o is not. The majority of the missile transport events are expected to occur at relatively low elevations (e.g., z_t<200 ft.) which will be considered to be entirely within the boundary layer. Based on these considerations, the value of δ_m will be assumed to be 400 ft. and δ_o will be considered to be uniformly distributed within the interval [400,500].

Values of γ reported in the literature range from effectively zero (i.e., negligible radial velocity) to about 0.6 (3-79). The tornadoes discussed by Simiu (3-68) have values ranging from 0 to 0.54; JPL's (1-48) standard tornado has a value $\gamma\tilde{=}0.5$ at $z_t=0$. The case $\gamma=0$ is not expected to yield higher mean values of maximum velocities as the missile is more quickly "centrifuged" from the whirling vortex (cf. 3-68). However, to provide for a representative range of radial velocities, γ is taken as uniformly distributed within the interval [0.1,0.6]. This provides an expected value of 0.35 and also permits relative extremes corresponding to small (3-74) and large (3-79) inflows.

Values of the slope (S) of the radius to the maximum tangential velocity have been suggested in the range 0 to 0.45 (1-30, 1-48, 3-3, 3-74). Bates and Swanson (3-3) refer to a value for the Dallas tornado of S=0.45 in the lowest 200 ft. Reference to Hoecker's paper (1-1) indicates that a value of 0.1 above 150 ft. is appropriate. Several investigators have used a cylindrical model above 200' and a Hoecker type model below 200' (3-4, 3-8, 3-18). To include the potential for both cylindrical and conical models, S is assumed to be uniformly distributed from 0 to 0.3 and to apply to all heights within the boundary layer.

The radial distance to the maximum tangential windspeed near the ground surface, ρ_{tmo}, has generally been considered to be in the 40 to 150 ft. range (1-1, 1-20, 3-4, 3-8). The JPL standard tornado has a 528-foot core and is a notable exception (1-48). Specification of ρ_{tmo} cannot be made independently of the width and translational velocity of the tornado. For the case

U_T=0, ρ_{tmo} must be less than $W_t/2$, or the core would exceed the 73 mph boundary. The effect of translation velocity is a significant loss of windfield symmetry such that $\rho_{t\ell} < \rho_{tr}$. Thus, another natural constraint is that $\rho_{tmo} < \rho_{t\ell}$. Also, it is noted that F5 tornadoes have reported widths that range over orders of magnitudes (e.g., from 168 feet to 16,368 feet) which further complicates the specification of ρ_{tmo}. Based upon geometrical considerations of tangential velocity profiles, the following characterization of ρ_{tmo} is utilized:

(1) Sample ρ_{tmo} from a linearly decreasing frequency density function in the range $[(\rho_{tmo})_L, (\rho_{tmo})_U]$ where $f(\rho_{tmo})_U = 0$.

(2) The bounds are defined by:

$$(\rho_{tmo})_L = \min \left\{ \begin{matrix} 0.1\ W_t \\ 100\ \text{ft.} \end{matrix} \right\}$$

$$(\rho_{tmo})_U = \min \left\{ \begin{matrix} 0.2\ W_t \\ 500\ \text{ft.} \end{matrix} \right\}$$

(3) If the sampled value, ρ^*_{tmo}, does not result in a feasible solution of Eqs. 1.40 through 1.46, reduce ρ^*_{tmo} as required for a solution in which $\rho_{t\ell} > \rho^*_{tmo}$.

This scheme provides for a probabilistic characterization of ρ_{tmo} consistent with suggested values (1-1, 1-20, 1-48, 3-4, 3-8) and avoids the situation in which ρ_{tmo} is so large that the windfield cannot assume the 73 mph level at the boundaries. For example, a tornado with W_t specified as 500' would have ρ_{tmo} bounds of [50',100'] and an expected value of 67'. The larger tornadoes with $W_t \geq 2500'$ would have ρ_{tmo} bounds of [100',500'] and an expected ρ_{tmo} equal to 233'.

Having specified the windfield equations and parameter ranges, some typical results are shown in order to demonstrate the model behavior. Radial, tangential, vertical, and rotational velocities are plotted in Figures 1-8 through 1-11 for the case $(U_{r\theta})_o$ = 406.27 fps, U_T = 7.33 fps, z_{to} = 20 ft., δ_o = 500 ft. with the remaining parameter values noted on the figures. The radial velocities given in Figure 1-8 demonstrate the variation in magnitude obtained for the stated conditions due to variation in the parameter γ. The effects of ground roughness and the extent of ground interaction are accounted for by allowing variation of the parameters γ and δ_o. It is noted that the vertical velocity component is also directly proportional to γ, so that significant variation of both radial and vertical magnitudes is possible, simulating gross ground interaction effects. The boundary layer thickness is also affected by ground conditions. The effect on vertical velocity of variation of δ_o from 400 ft. to 500 ft. is shown in Table 1-11. Note that smaller local boundary layer thicknesses generally result in smaller vertical velocities but that the effect is small. The vertical velocities at ρ_t=160 ft. differ even though the local boundary layer thicknesses are the same (δ=400 ft.) because the derivatives $d\delta/d\rho_t$ are different for the two cases. For the δ_o=400 ft. case, $d\delta/d\rho_t$=0; for δ_o=500 ft., $d\delta/d\rho_t$=0.42. Reference to Eqs. 1.36 and 1.38 demonstrates the dependence of vertical velocity on $d\delta/d\rho_t$.

Figures 1-8 and 1-9 indicate that radial, tangential, and hence rotational velocities are nonzero at z_t=0 and that rotational velocity is nearly constant with height above about 100 ft. Note that the boundary layer thickness is also plotted in Figure 1-9. The points of maximum tangential velocity in Figure 1-8 differ as a consequence of the use of S = 0.176 in the model. The two cases of infinite (Figures 1-8 and 1-9) and finite (Figure 1-11) radius to zero windfield (ρ_{to}) are demonstrated. Note that the vertical velocity in Figure 1-8 remains positive, though small, outside the core whereas in Figure 1-11 it becomes negative for large ρ_t. This is determined by the values of a and b which result from the boundary fitting process (note that a is positive in one case and negative in the other) since $dm/d\rho_t$ = a for large ρ_t.

Typical vertical variations of the three wind components are shown in Figure 1-10. It is noted that U_θ is not monotonically increasing with height for constant ρ_t. However, this is a consequence of the fact that this specific tornado is noncylindrical (S = 0.176); in fact, U_θ does monotonically increase with height for constant ρ_t/ρ_{tm}. All three components are constant above the boundary layer. The case of a narrow (W_t = 165 ft.), high intensity tornado is shown in Figure 1-11. Since the core region is small (ρ_{tmo} = 30 ft.), the vertical velocity is quite high inside the core as a result of applying the continuity relationship.

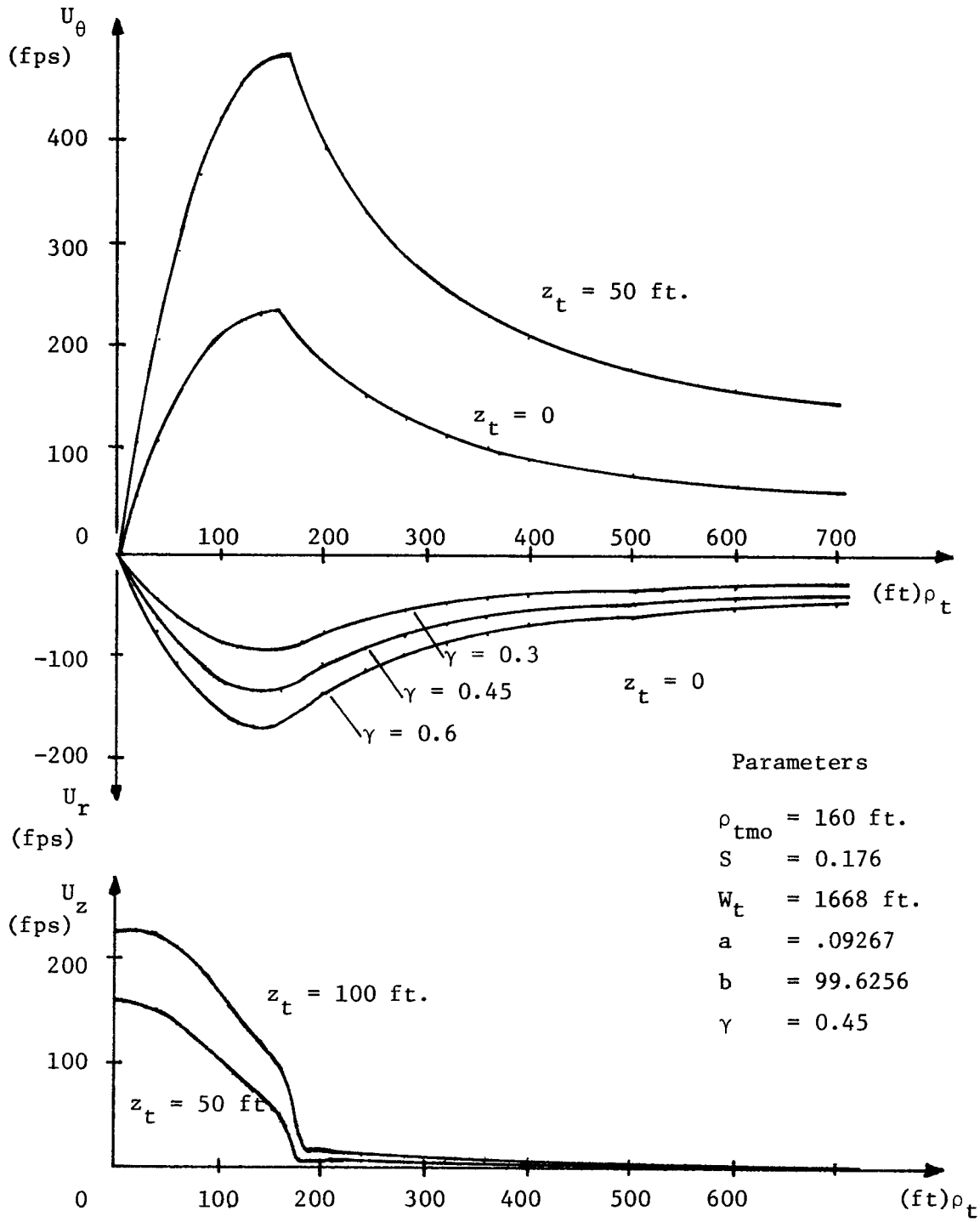

Figure 1-8. Synthesized Tangential, Radial, and Vertical Velocities as Functions of Radial Distance

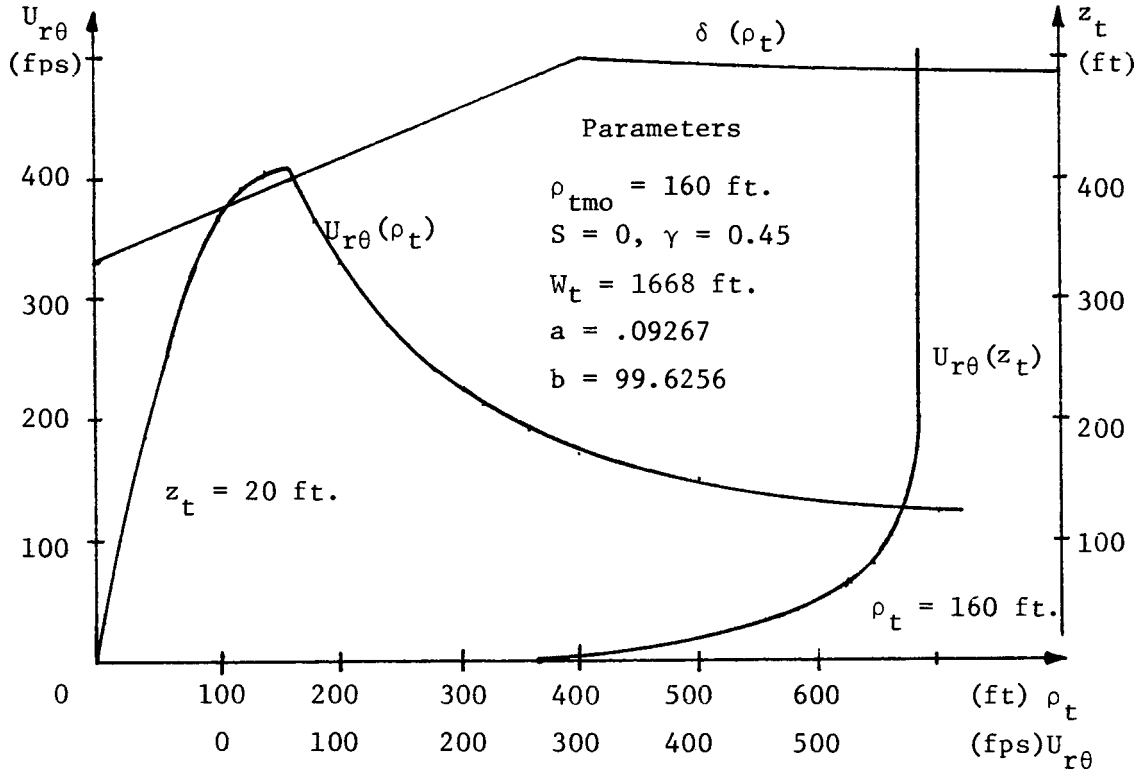

Figure 1-9. Synthesized Rotational Velocity and Boundary Layer Thickness

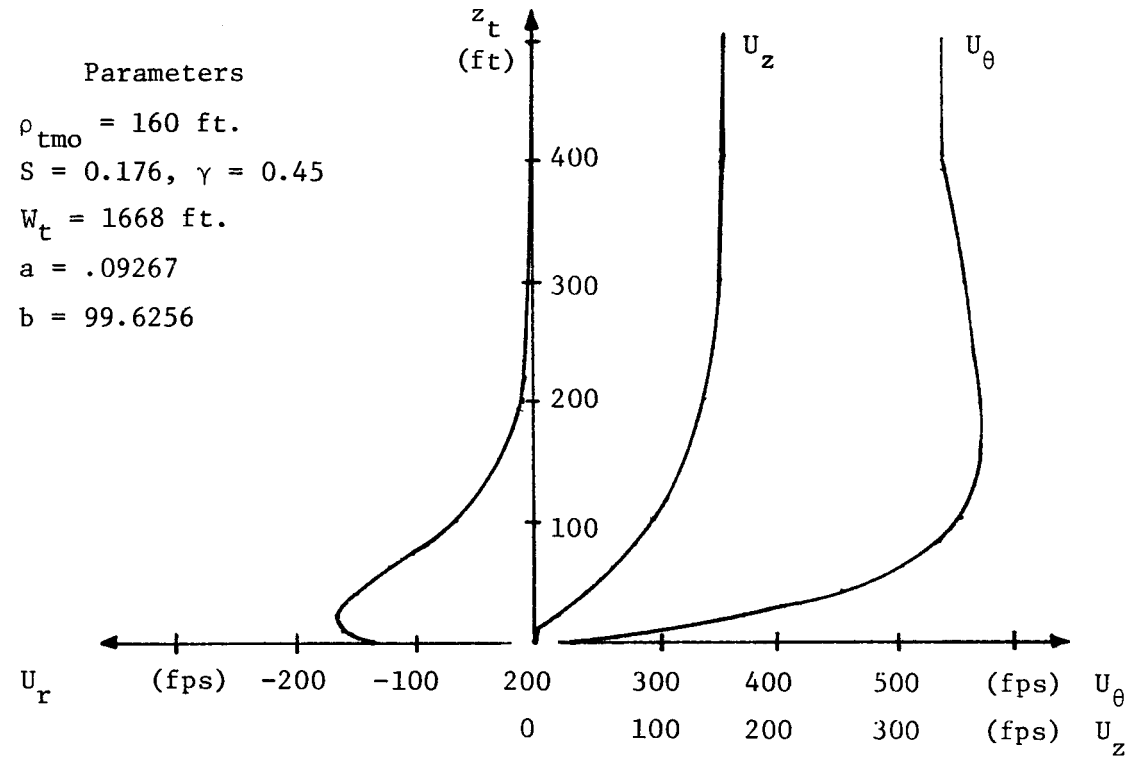

Figure 1-10. Synthesized Tangential, Radial, and Vertical Velocities as Functions of Height for ρ_t = 160 ft.

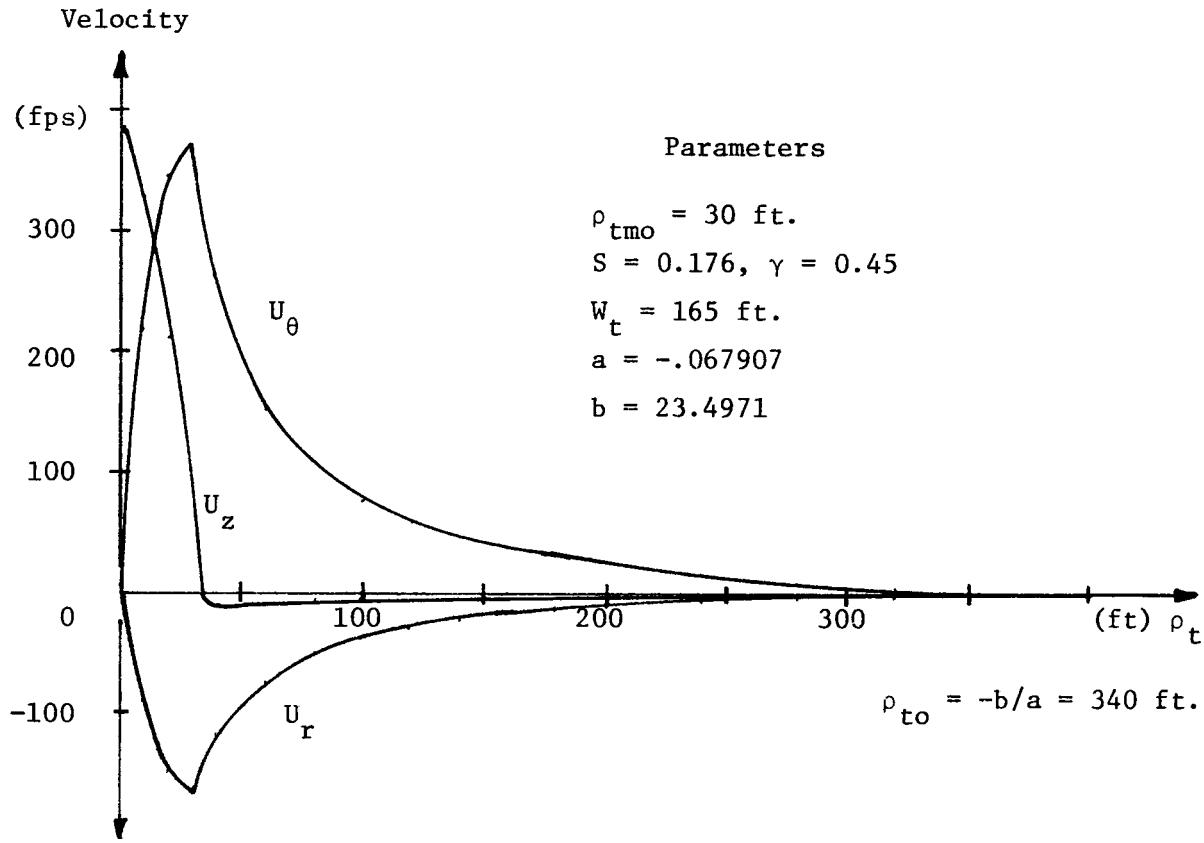

Figure 1-11. Synthesized Tangential, Radial, and Vertical Velocities for a Thin Tornado of Finite Extent

Table 1-11. Synthesized Vertical Velocities at z_t = 100 ft. for Different Boundary Layer Thicknesses

	δ_o = 400 ft.		δ_o = 500 ft.	
ρ_t (ft.)	δ (ρ_t) (ft.)	U_z (fps)	δ (ρ_t) (ft.)	U_z (fps)
10	400	258.88	337.5	231.76
20	400	255.68	341.7	232.12
40	400	243.27	350	226.82
80	400	199.37	366.7	195.40
160	400	89.94	400	97.72
320	400	3.71	466.7	8.53

APPENDIX 2

MISSILE CHARACTERIZATION METHODOLOGY

2.1 Introduction

The types of objects that have been observed to be displaced by tornadoes exhibit a wide range of physical characteristics. In addition to the debris commonly transported by any gale force wind, tornadic displacement of vehicles, railroad cars, storage tanks, equipment components, beams, pipes, roof sections, plates, trees, structural frames, etc., is also documented (e.g., 1-7, 1-42, 3-32, 3-65, 3-66, 3-67). The actual characteristics of the missiles that pose a safety threat to a particular environment depend upon the type of objects that are within the immediate region at the time of tornado incidence. At a typical nuclear power plant, the quantity and type of objects that could possibly become missiles as a result of a direct tornado strike vary significantly. In a risk assessment of the tornado missile hazard, the potential of these masses to be accelerated by the tornadic winds and thus to damage safety related components is recognized by characterizing these objects according to availability, transport, and barrier interaction properties. Such a missile characterization is complicated by the factors suggested above, namely:

(1) The variety in shape, size, material, composition, and availability modes form nearly continuous ranges of missile parameter characteristics.

(2) The missile distribution around a plant site is both dynamic and site dependent.

(3) The missiles which are actually generated during a tornado strike are dependent upon the characteristics of the tornado.

(4) Those characteristics which are favorable from an aerodynamic standpoint (e.g., low density, large exposed areas) are generally unfavorable in terms of maximizing barrier impact damage.

These factors have significant implications on any concept of missile identification and classification which is practically realizable in a data-based analysis. A major implication, in view of factors (1) and (4), is that a conservative missile characterization cannot be established a priori. This raises a basic question regarding the adequacy of the existing hypothetical missile spectrum (2-6) for utilization in a risk analysis. In addition, factor (2) suggests that the characterization methodology should be applicable to a variety of plant environments and related data sources. Since input from the tornado, trajectory, and barrier interaction models is required, the identification of the variables and subsequent determination of missile sets further suggests problem dimensionality as a fundamental difficulty. This multivariate aspect indicates that considerable simplifications and tradeoffs are necessary in both the analytical formulation and the data analysis. In this chapter, the methodological approach is developed, the proposed missile spectrum and availability modes are described, a probability model for data-based analysis is given, the results of the plant data acquisition surveys are summarized, and an analytical assessment of offsite missile significance is presented.

2.2 A Methodology for Characterizing Potential Missiles

Given the complicity of factors noted above which influence missile characterization, a methodology which relies on a continuous specification of missiles, including the correlation of the pertinent variables, is not feasible. An alternative approach is the consideration of a limited number of sets of missile types which approximates the actual missile distribution and related parameters. These sets should be inclusive in the sense that the range of missile characteristics can be covered through proper categorization and parameter selection. By tracking a well-chosen sample of the representative missiles, statistical estimates of tornado missile event probabilities can be obtained.

This approach naturally permits the exclusion of damage events below some defined lower bound hazard for which the spectrum of missile sets is not sufficiently inclusive. In particular, gale force debris need not be characterized if the events of interest exceed the damage potential of such missiles.

The NRC has defined a discrete set of representative missiles as a standard spectrum to form a conservative basis for plant design (1-47, 2-1, 2-6). These missiles are consistent with the types of objects found at nuclear plant sites. However, because the NRC spectrum has a limited range of missile flight parameters and was not developed for a probabilistic risk assessment, a methodology for characterizing potential missiles has been developed. The missile sets thus established are not significantly qualified by a priori assumptions of conservative missile characteristics. Risk assessments performed with a general missile set may aid the specification of design parameters for the limited spectrum.

The general procedure employed to characterize potential missiles in this investigation has included:

(1) Identification of the significant missile parameters.

(2) Reliance on empirical data bases to assess potential missile sources, characteristics, and frequencies.

(3) Establishment of a methodology for simplification and generalization of the observed characteristics based upon transport and barrier impact considerations.

(4) Formation of the basic missile sets for utilization in the risk case studies.

In the following, these steps are described in more detail.

2.2.1 Missile Definition and Classification

The set of parameters identified in a missile characterization scheme must specify the physical characteristics, location, restraints, and quantity distributions. The following list of parameters is suggested for the missile characterization:

(1) Shape
(2) Size (dimensions)
(3) Weight
(4) Material composition
(5) Location
(6) Availability
(7) Quantity

These parameters are self descriptive with the exception of missile availability, which refers to the missile's potential for injection into the tornado windfield and thus prescribes the initial conditions. The location, availability, and quantity parameters reflect the dynamic characteristics of potential missile sources.

With these identified variables, a simple process for evaluating and categorizing objects into missiles was devised utilizing the missile definitions given in ANSI N177 (2-5). The terminology is indicated in Figure 2-1. Any mass within some defined distance of the plant targets is considered a possible missile source. The governing parameters here are weight and location. If motion of the mass is not constrained, it is considered a potential missile. If the mass is constrained (earth founded), it is termed a structure missile source which can also become one or more potential missiles if the constraints fail. A potential missile which can be transported by the tornado is called a postulated missile. Those postulated missiles which could damage plant targets are called design missiles since they pose a potential threat to the plant safety. In this scheme, the small, light weight debris propelled by any gale force winds can be assumed to be incapable of damaging plant systems of interest and thus are

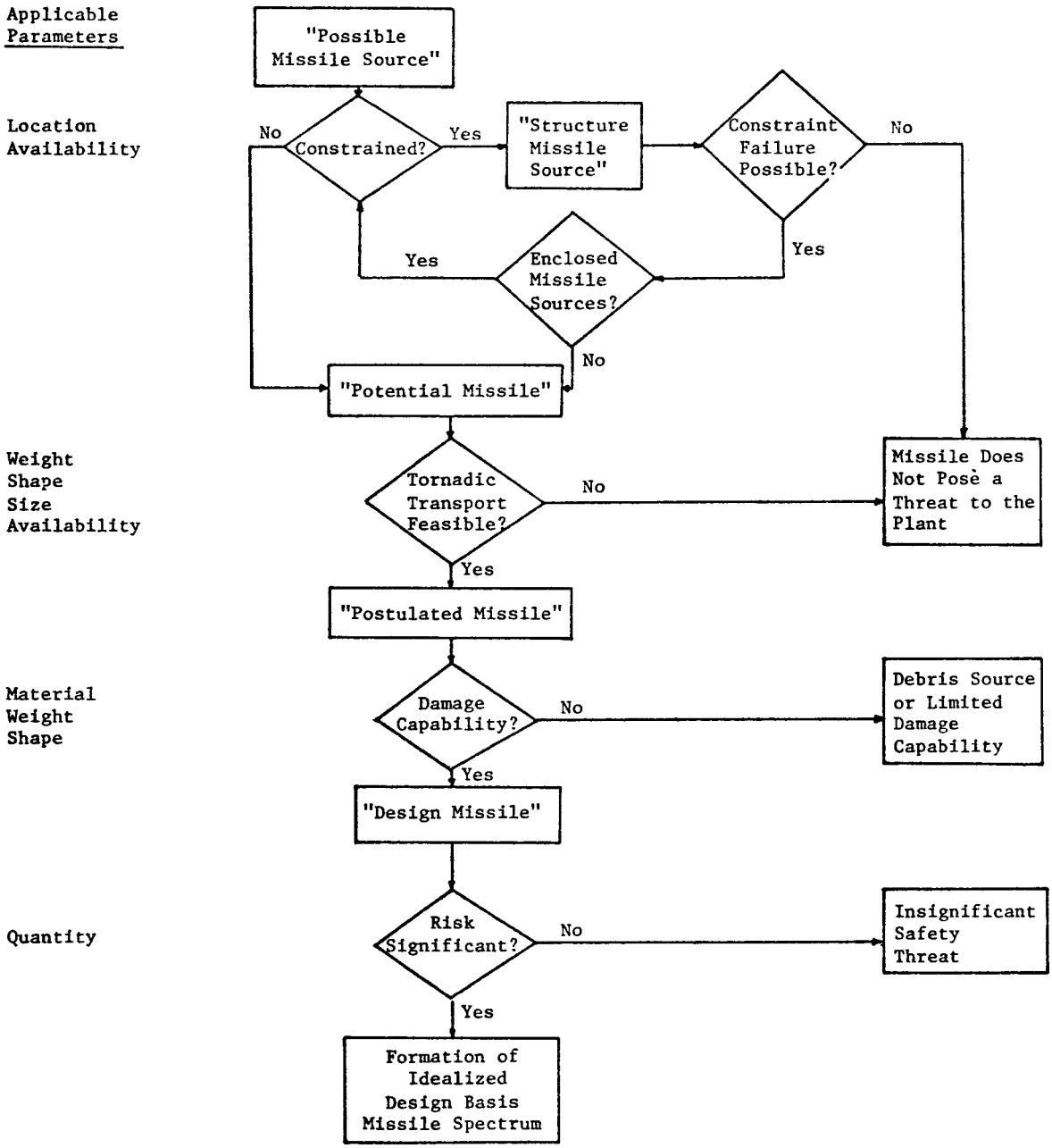

Figure 2-1. Missile Terminology

not considered as design missiles. In terms of these definitions, this missile characterization task reduces to deriving an appropriate set of design missiles for use in the simulation from among the possible missile sources which may exist. The determination of acceptable design parameters can then be assessed from a risk analysis.

The second phase of the missile characterization task involved the gathering of information about possible missile sources. The major source of information was obtained by on-site surveys of seven nuclear power plants in various stages of construction and operation as noted in Table 2-1. Information regarding the seven basic parameters discussed earlier was acquired from measurements, visual estimations, and photographs of possible missile sources within the plant boundary. Another source of information involved interviews with site construction managers to qualitatively assess material storage and construction site planning and scheduling.

The basic approach to missile characterization is outlined in Figure 2-2. The methodology relies on the specification of a mutually exclusive and collectively exhaustive set of missiles based upon aerodynamic, barrier impact, injection, and risk analysis considerations. The mapping of a potential missile into one of the sets is generally unambiguous, but not entirely unique. Each missile is characterized into a geometrical shape set which is defined by its three principal dimensions L (length), d (depth), and b (width) and its solidity ratio σ, defined as the ratio of solid to enclosed area (3-2). The ratio L/d is selected as the random variable in this missile shape characterization scheme. For aerodynamic characterization, given the basic shape and L/d, it is assumed that only the ratios σ and b/d are needed to completely define the missile. This implies that relative size is not important in terms of aerodynamic definition and also that any other dimensions of the basic shape are invariant.

The aerodynamic input to missile characterization involves the determination of the significance of σ and b/d variation in the trajectory analysis. On the basis of available data, a total of m basic sets are established as noted

Table 2-1. On-Site Missile Characterization Surveys

Plant Number	Type	Unit Number	Construction State
1	BWR	1	Final
		2	Operating
2	BWR	1	Operating
		2	Mid
3	PWR	1	Final
		2	Mid-Final
		3	Early
		4	Early
4	PWR	1	Mid
		2	Mid
5	PWR	1	Operating
		2	Operating
		3	Operating
6	PWR	1	Operating
7	PWR	1-4	Initial

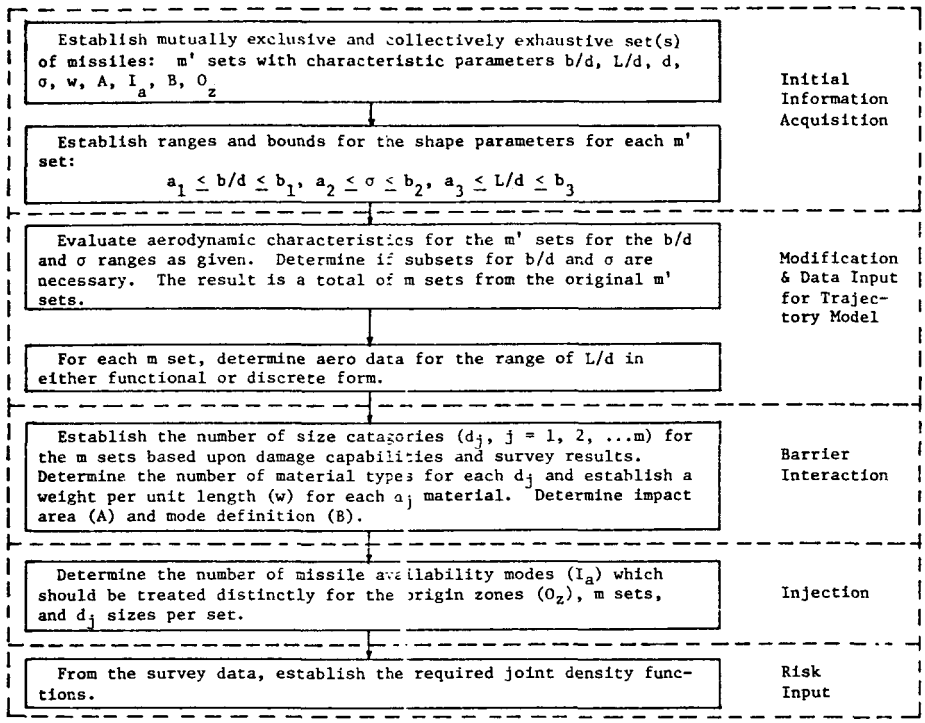

Figure 2-2. Missile Characterization Methodology

in Figure 2-2. Barrier impact parameters for a particular shape set are the value of d, the weight per unit length (w), material type, impact parameter mode (B), and the bounding values of impact areas $\{A\varepsilon(A_{min},A_{max})\}$. Thus, although a missile might be characterized aerodynamically as a wooden plate with certain L/d and b/d values, its impact parameters could characterize any protruding metal stiffener ribs. As depicted in Figure 2-2, the injection parameters (I_a = Availability Mode, O_z = Origin Zone) characterize the initial conditions and availability of the potential missile.

2.2.2 Missile Sets, Availability, and Impact Modes

On the basis of the methodology described in the preceding discussion, the mutually exclusive and collectively exhaustive sets of missile availability, aerodynamic, and damage characteristics are identified. In the following, a general characterization is presented although simplification of the sets can be made for particular case studies.

The aerodynamic missile characterization methodology is presented in Figure 2-3. Each potential missile is first categorized as prismatic (no cross section variation along its length) or nonprismatic. The prismatic shapes identified represent standard structural sections with appreciably different aerodynamic properties. On the basis of the plant surveys, it was found that the significant majority of the prismatic shapes were in the first five categories; i.e., tee and z sections were rare. Thus, for practical reasons, these latter two were eliminated as basic shapes and those reported in the survey were subsequently categorized among angle, channel and I sections. Nonprismatic objects constitute the more complex shapes for which there is generally very little aerodynamic data. The approach for these was to categorize them into one of the prismatic shapes unless there were both sufficient aerodynamic data and a significant number of the shapes to warrant a special classification. Thus, curved prismatic shapes were treated as linear prismatic; frames, trusses, or other structures whose solidity ratio (3-2, 3-77) was less than 0.5 were treated as porous shapes with rectangular cross sections; and the sectionally prismatic (miscellaneous) objects

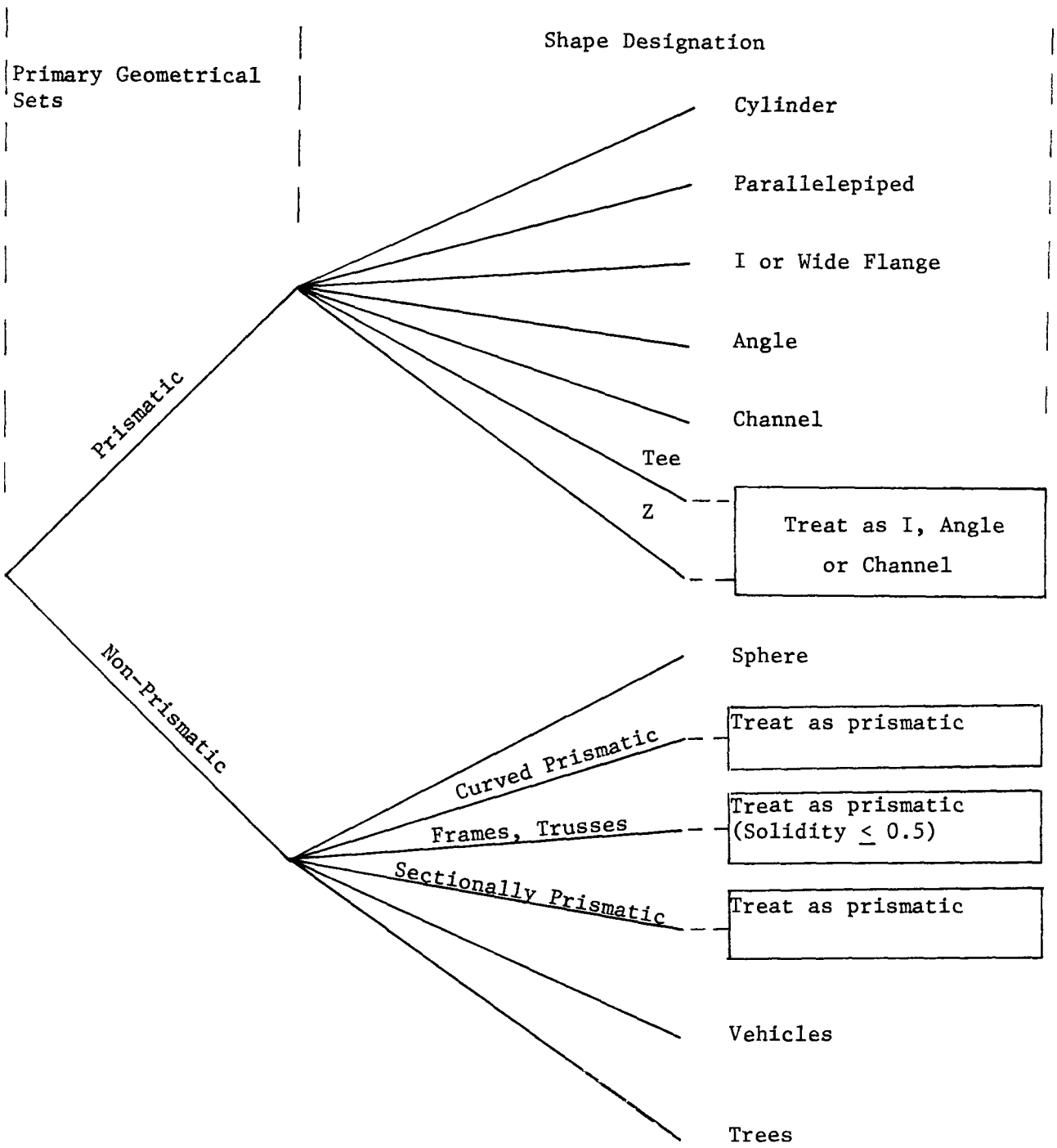

Figure 2-3. Aerodynamic Shape Characterization

were modeled into the most appropriate prismatic class. The availability of aerodynamic data for spheres and vehicles warranted retention of their basic shape designations. The flight characteristics of trees, which are structure missile sources in Figure 2-1, also suggest a separate category. Utilizing this procedure for aerodynamic shape characterization, the basic missile sets presented in Table 2-2 were formulated through evaluation of the missile survey data. Each aerodynamic shape designation was further subdivided according to cross-section b/d variation, barrier impact material, and shape (e.g. solid versus pipe effect), thus increasing the number of sets over that which would be necessary solely from aerodynamic considerations. For rectangular cross sections, four sets of b/d were considered for each b/d category with the exception of b/d = 1/4, for which case sufficient numbers of concrete panels were observed to warrant a special set. The structural shapes (I, angle, tee) were not given b/d variations since in general these are relatively small and comprehensive aerodynamic data is not available for such distinctions. Shapes which would be modeled aerodynamically as frames and trusses were grouped into two basic rectangular geometries as noted. The structural elements comprising frames are generally either cylindrical or structural (rectangular, angle, etc.) in cross-section and thus a further distinction was made both for aerodynamic and impact considerations.

Characterization of missile impact parameters for the basic missile sets in Table 2-2 was achieved by the parameters noted in Table 2-3. The corresponding minimum and maximum impact area for the applicable impact mode are recorded for each missile. In this approach, the missile damage characterization is considered independently of the aerodynamic characterization. Thus, a combination or unusually shaped missile can be conservatively and independently modeled from flight as well as barrier interaction standpoints.

On the basis of the site inspections, several availability modes for nonrestrained objects were identified. Five modes were considered sufficient to represent the range of initial conditions:

Table 2-2. Basic Missile Sets

Basic Aerodynamic Shape Set	General Description	Cross-Section b/d Variation	Impact Material	Final Set Number
Cylinder	Rod	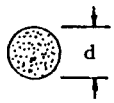	Steel	1
			Wood	2
	Pipe	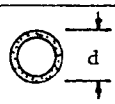	Steel	3
			Concrete	4
Rectangle	Box, Beam	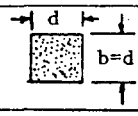	Steel	5
			Wood	6
		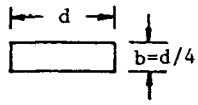	Steel	7
			Concrete	8
			Wood	9
	Plate	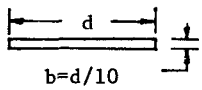	Steel	10
			Wood	11
		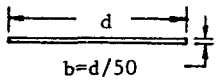	Steel	12
			Wood	13
I-Shape	Wide Flange	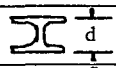	Steel	14
Angle	Angle	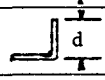	Steel	15
Channel	Channel		Steel	16
			Concrete	17
Frame, Truss	Pipe Frame	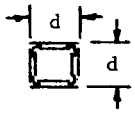	Steel	18
	Rect. Frame		Steel	19
	Rect. Frame		Wood	20
	Pipe Frame	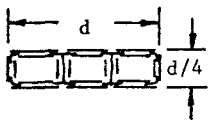	Steel	21
	Rect. Frame		Steel	22
	Rect. Frame		Wood	23
Sphere	Sphere		Steel	24
Vehicle	Auto, Trailer	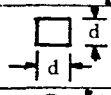	Steel	25
Tree	Tree		Wood	26

Table 2-3. Missile Impact Parameters

Impact Mode		Corresponding Impact Area	
Number	Designation	Minimum (A_{min})	Maximum (A_{max})
1	Linear Penetrator	Actual Cross-Section	Equivalent Circle or Enclosed Area
2	Body, Corner Impact	Minimum Face	Maximum Face
3	Body, Flat Impact	Minimum Projected	Maximum Projected
4	Planar, Edge Impact	Minimum Face	Maximum Face
5	Shape with Penetrator	Penetrator - Actual Cross Section	Penetrator - Equivalent Area

Table 2-4. Structure Missile Sources

Structure		Foundation	
Number	Type	Number	Type
1	Wood Frame	1	Post Embedment
2	Metal Frame	2	Slab Attachment
3	Metal Tower	3	Guy Cable
4	Trailer	4	None
5	Masonry		
6	Reinforced Concrete		

(1) Horizontal Storage - The components are stored with the major axis parallel to the ground surface. Contact forces exist in both vertical and lateral directions and only those elements in the top row are initially unrestrained.

(2) Vertical Storage - The components are stored with major axis perpendicular to the ground surface and lateral contact forces are present.

(3) Random Storage - The components are stored in various orientations and positions with significant contact and/or interlocking forces.

(4) Random Distribution - The objects exist separately with no appreciable lateral contact forces.

(5) Support Elements - The potential missiles serve as a structural support to other masses and rest on the ground surface but are not earth-founded.

For each of these modes, the minimum and maximum elevations above the ground plane to a missile or array surface are defined as Z_c, the clearance elevation, and Z_s, the stack elevation. For horizontal arrays, the proportion of the total number of missiles in the top row (A_h) was considered as well as the fraction of support elements not loaded. This specification of initial conditions according to these five modes and their associated parameters provides rough data for possible mechanistic modeling of missile injection.

The basic missile sets and impact modes previously discussed are also valid for structure missile sources which experience foundation or internal structural failures due to the tornadic induced forces. The missiles which

originate from structural failures are postulated from initial conditions which describe the structure type, size, materials, and construction details. Utilization of analytical failure models, empirical observations, and photographs of tornado damage can provide information useful in the transformation of structure missile sources into postulated missiles. Due to the inapplicability of the five availability modes presented above for structure missile sources, a separate availability mode is required. The types of structure missile sources and the categories of foundations observed in the surveys are presented in Table 2-4. In addition to this information, the principal dimensions and zone location of structures were also recorded. Because the major structure missile sources are nonengineered, no attempt has been made to document information regarding the individual structural details. The wide variability of construction practices would inhibit the use of such information except for the specific plant considered. The general data obtained should be useful in characterizing the numbers and sizes of the various structure missile source types to provide guidelines in hypothetical case studies. The structure missile sources were generally temporary construction buildings and included wood frames (warehouses, craft shops, concrete batch plants, etc.) and metal structures (pre-fab metal buildings, trailers, etc.). The permanent facilities, generally not designed for tornado loads, included transmission and switchyard structures, towers, and plant warehouses.

The photographs presented in Figure 2-4 provide examples of basic missile shapes and availability modes. Plates (a) and (b) of Figure 2-4 depict linear elements stored horizontally and planar elements stored in a vertical array, respectively. Plates (c) and (d) show the random array and random distribution availability modes, respectively. Plate (e) of Figure 4-4 is an example of timbers or wooden beams being used as support elements, a common practice (cf. plates (a), (b), (e), and (g)). Plate (f) is a photograph of one of the well-vented temporary structures found at a construction site. If the structure were to fail under the wind loading, it is likely

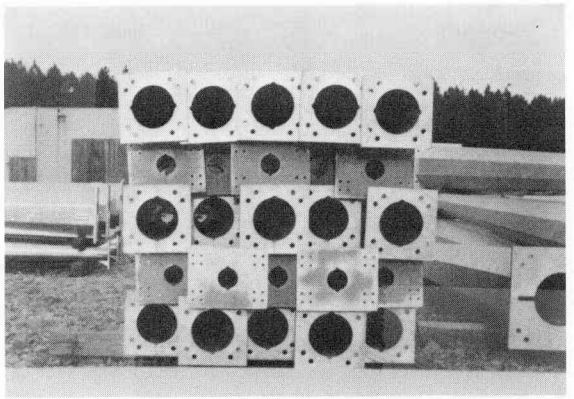

(a) Horizontal Array

(b) Vertical Array

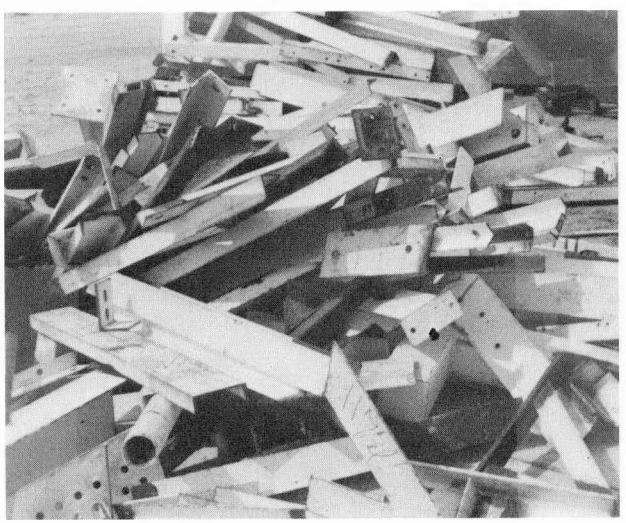

(c) Random Stack

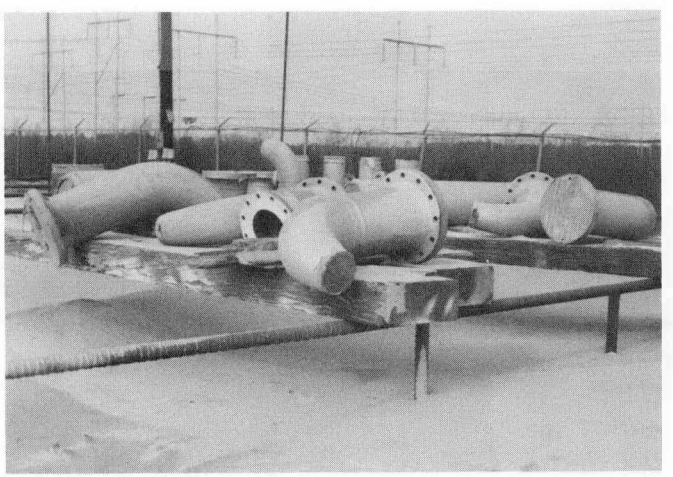

(d) Random Distribution

Figure 2-4. Examples of Missile Sources and Availability Modes

(e) Support Elements

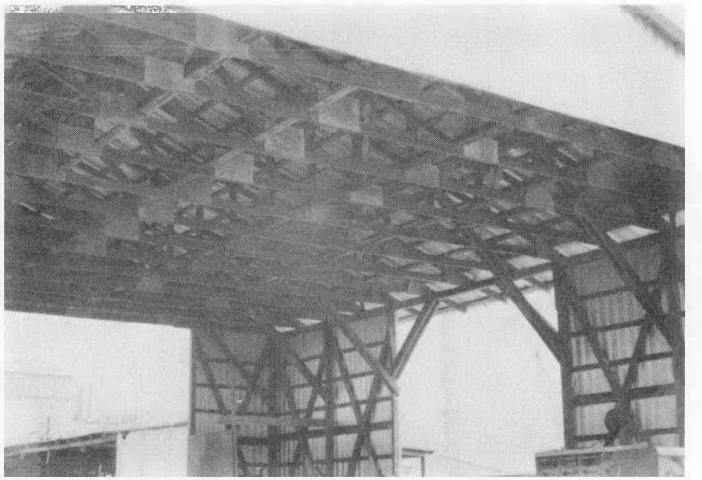

(f) Structure

(g) Linear Elements

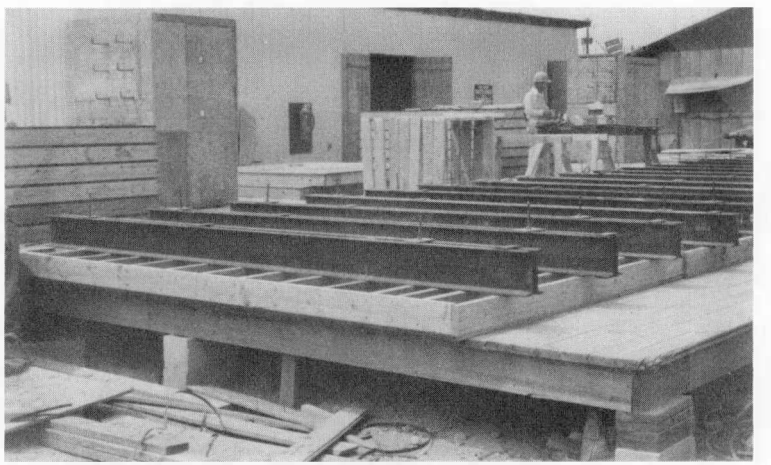

(h) Planar Element, with Penetrators

Figure 2-4 (Cont.). Examples of Missile Sources and Availability Modes

that some of the structural members would become missiles, especially if they remained attached to the roofing or siding. Plate (g) illustrates potential linear type penetrators and plate (h) shows a wood frame with wide-flange ribs. This formwork is typically found at most plants with on-site construction: it is modeled according to set 10 and impact mode 5 since the members likely to do damage are the protruding steel elements.

2.3 Probability Formulation, Data Summary, and Offsite Missiles

The variables that have been previously identified in the missile characterization methodology form a large multivariate data set. The information concerning these variables can be generally specified by the joint density function of a missile characterization vector, $\bar{M}$. This vector contains the variables defined in Section 2.2 plus one additional variable, t_m, which provides for the time function in the characterization

$$f(\bar{M}) = f(O_z, N, S, d, L, w, I_a, Z_c, Z_s, A_h, A_{min}, A_{max}, B, t_m) \qquad (2.1)$$

Consistent with the basic missile characterization approach, this expression can be considerably simplified by specifying unique missile sets, attributing probabilistic independence, and utilizing conditional density functions. In this section, a method for simplifying and analyzing the multivariate problem is discussed, the survey data is summarized as a guideline for specific case studies, and a criterion for offsite missile significance is presented.

2.3.1 Conditional Probability Model

A major simplification of Eq. 2.1 results if any time dependent characteristics are considered in a conditional framework. In the specification of missile descriptive variables, the time interval is less than the

design life, T, of the plant only if the plant model or event sequences are not appropriate for the entire time period. If this is the case, division of the plant real time history is simulated by separate risk assessments of different models. In the following, quantity and location variables are conditioned by t_m to indicate potential multiple time interval dependency in the simulation.

An additional simplification of Eq. 2.1 results if the quantity variable, N, is considered separately and independently from the other individual missile description variables. The specification of a total missile number (given a specified time interval), defines the missile sampling population and is thus analogous to the recursive probability models of repeated experiments. Given the separation of time interval and quantity variables from the single missile characterizing variables, further reduction of Eq. 2.1 follows from the categorization methodology. First, the missile set and origin zone variables are grouped and expressed in the conditional equivalent of Eq. 2.1 as

$$f_1(\bar{M}) = f(d,L,w,I_a,Z_c,Z_s,A_h,A_{min},A_{max},B|O_z,S)\ f(O_z,S|t_m) \qquad (2.2)$$

where $f_1(\bar{M})$ denotes a randomly selected single missile. This approach is analytically attractive since O_z and S are discrete variables according to the missile characterization methodology. Next, the missile sizing variate d is classified into discrete groups in order to facilitate the conditioning of the remaining variables.

$$f_1(\bar{M}) = f(L,w,I_a,Z_c,Z_s,A_h,A_{min},A_{max},B|d,O_z,S)\ f(d,O_z,S|t_m) \qquad (2.3)$$

For convenience, the missile length variable L is nondimensionalized by $\ell = L/d$. A major simplification is obtained by attributing independence between the barrier interaction variables and the availability variables.

$$f_1(\bar{M}) = f(\ell,w,A_{min},A_{max},B|d,O_z,S)\ f(I_a,Z_c,Z_s,A_h|d,O_z,S)\cdot$$

$$\cdot f(d,O_z,S|t_m) \qquad (2.4)$$

This assumption is reasonable since the availability mode variables and shape variables are not functionally dependent for a given missile aerodynamic set and size. Replacing the respective groups of barrier interaction and availability variables by vector equivalents, and $f(d,O_z,S|t_m)$ by its conditional equivalent, Eq. 2.4 becomes

$$f_1(\bar{M}) = f(\bar{B}|d,O_z,S)\ f(\bar{I}_a|d,O_z,S)\ f(d|O_z,S,t_m)\ f(S|O_z,t_m)\ f(O_z|t_m) \qquad (2.5)$$

In this form, the missile definition is given by the above density functions and N. For specific case studies, Eq. 2.5 may be further simplified if:

(1) $\bar{B}$ or d are zone independent for a given missile set; i.e., $f(d|O_z,S) = f(d|S)$.

(2) $\bar{I}_a$ is size independent for a given missile set; i.e., $f(\bar{I}_a|d,O_z,S) = f(\bar{I}_a|O_z,S)$.

(3) Weight and area variables are uniquely assigned for a given set and size; i.e., $f(\ell,w,A_{min},A_{max},B|d,O_z,S) = f(\ell,B|d,O_z,S)$ and $f(w) = w^*$, $f(A_{min}) = A^*_{min}$, $f(A_{max}) = A^*_{max}$.

Thus a simplification of the original Eq. 2.1 is suggested as

$$f_1(M) = f(\bar{B}|d,S)\ f(\bar{I}_a|O_z,S)\ f(d|S,t_m)\ f(S|O_z,t_m)\ f(O_z|t_m) \qquad (2.6)$$

utilizing N, w^*, A^*_{min}, and A^*_{max}.

2.3.2 Missile Data Summary

A summary of the missile data analysis utilizing the previous characterization methodology is presented in Appendix 6. This information, coupled with plant on-site inspection, should provide guidelines for particular tornado missile analyses. The scope of the data base which has been obtained through on-site surveys is illustrated in Table 6-1, which presents the field information obtained at one of the plants. Each entry in the table provides the information necessary to specify the missile characterization vector $\bar{M}$. In Table 6-2, the missile set distribution for each of the plants is summarized. The results indicate that several of the sets have a relatively small number of missiles; notably, sets 11, 17, 19, 20, 23, and 25 have less than 250 missiles for all the plants visited. Since the plants which form the data base cover the entire sequence of construction and operation activities (cf. Table 2-1), these results suggest that actual case studies can be simulated with less than the total number of basic missile sets. The missile set which has the greatest number of missiles is number one, largely a result of the on-site storage of reinforcing bars.

A summary of the missile size categories established for each missile set is presented in Table 6-3. These size categories were determined by examining the sorted data base for missile number distribution and logical "break" points in the data. For example, the first "d" size of set one includes all steel rods with diameters from zero to 1 inch, inclusive; the largest "d" size for set one includes steel cylinders with diameters greater than 20 inches. The mean depth, $\bar{d}$, presented for each group is presented as an input to aid the specification of missile size for each subset; it is generally near the upper bound of the interval as a result of the discretization process. As indicated in Figure 2-2, the characterization of barrier interaction variables involves the determination of impact area and weight relationships for a given size subset. The results of this analysis for A_{min} and w are also presented in Table 6-3. For each size subset, the minimum impact areas were evaluated to determine the need for area subsets.

If the variance and range of the data were sufficient, each size subset was divided into two area subsets. In particular, the established bound between these subsets was determined on the basis of data examination and the fact that a relatively small $\bar{A}_{min}$ for the first subset is conservative in terms of local damage assessment. The wide range in A_{min} largely results from the impact mode five categories, which considerably reduces A_{min} for a given size in a missile aerodynamic set. The mean weight per unit length is also presented for potential utilization in specific case studies. Examination of these results in Table 6-3 indicates that the parameters of previously identified potential tornado missiles (2-6) are bounded by the subset mean values of $\bar{d}$, $\bar{A}_{min}$, and $\bar{w}$. For example, the typical 12" pipe missile with w = 49.5 lb/ft would fall between the subset values of $\bar{d}$ = 10.68" ($\bar{w}$ = 45.78 lb/ft) and $\bar{d}$ = 20.52" ($\bar{w}$ = 58.47 lb/ft).

Since length is the continuous variable in the missile characterization methodology, several parameters obtained from the data analysis for each size subset are presented in Table 6-4: the minimum, maximum, mean, and variance of L/d. Appropriate probability distributions can be postulated for specific case studies. Although not presented in the table, the mean length ($\bar{L}$) for all missiles is 20.48 ft. Missile availability mode characteristics are summarized in Table 6-5. For the five availability modes presented in Section 2.2.2, the maximum storage height (Z_s) characteristics are identified. The most frequent availability mode for the various missile sets is type 1, horizontal array type storage. The data indicates that the maximum storage height for this availability mode is 20 ft. and the mean is calculated as 4.8 ft. for all missile sets. For the other modes, the maximum and mean values, respectively, are: vertical array - 30 ft. and 7.1 ft.; random array - 10 ft. and 5.2 ft.; random distribution - 155 ft. and 3.9 ft.; and support elements - 3 ft. and 0.8 ft. The high value of maximum storage height for the random distribution availability mode is a result of construction activity at high levels. It is noted that the mean value of maximum storage height for all non-structure missile sources is 4.7 ft. In Table 6-6, a brief summary of the numbers of temporary structures by plant is given. Wood frame structures, with minimal foundation design against uplifting forces, form a significant portion of these temporary structures; for metal frame

structures, slab foundations are common. Observations of tornado induced failures of the types of structures presented in Table 6-6 suggest that all of these non-engineered or pre-engineering buildings must be considered as a source of possible missiles (e.g., 3-66) for intense tornadoes. Such potential missiles are characterized into one or more of the basic sets; the initial conditions (restraining forces) can be conservatively specified in the methodology developed for missile injection (Section 3.4).

2.3.3 Off-Site Missile Assessment

To assess the significance of off-site missile sources and the potential for long range missile transport, a trajectory simulation study was performed. As part of a wind boundary study (refer to Section 3.3.5.3 for details), 1250 missiles were injected at random into high intensity tornadoes and their trajectories followed. The missiles were taken from sets 2, 9, 13, 14, and 26 and thus ranged from light plywood sheets to structural steel shapes. The average horizontal distances (and standard deviations) between injection and ground impact points traveled by all the missiles within a given set are presented in Table 3-6. The results indicate that missile transport greater than 1000 ft. (the mean plus two standard deviations) from the injection point is very unlikely; in fact, expected missile range is much smaller than 1000 ft. The maximum ranges achieved from among the 250 simulations of each missile are as follows: utility pole, 1650 ft.; wood beam, 1994 ft.; plywood sheet, 1201 ft.; wide flange beam, 1216 ft.; and tree, 733 ft. The fact that the maximum ranges for some of the heavier missiles exceed those for the light missiles is due to the spiral nature of the longer trajectories of the lighter missiles, which results in impact points closer to the injection points even though the total path length is larger. That increasing weight would result in trajectories with less horizontal curvature is an intuitive conclusion that is verified by this trajectory study. Consideration of the maximum ranges, the mean range distances (which are all less than 350 ft.), and the standard deviations indicates that missile sources which are greater than 1000 ft. from a critical component pose a small threat to the plant and those greater than 2000 ft. pose a negligible threat.

The implications for case study simulation are that missiles which are in excess of 2000 ft. from any safety related component need not be considered. Similarly, missiles greater than 1000 ft. are not expected to contribute significantly to the risk in most cases. It is recognized, however, that a few missiles with favorable injections and random trajectories can travel very large distances, as has been demonstrated in the literature (e.g., 1-5). Thus, missiles which are between 1000 and 2000 ft. from the target area will be considered in the case studies. The treatment of off-site missiles thus reduces to the following. If the site boundary is everywhere greater than 2000 ft. from the closest target, direct flight of the off-site missiles is neglected. If the boundary is within 2000 ft. of some targets, the boundary is considered to exist at 2000 ft. and a distribution of missiles is postulated, simulating off-site missiles. These are then injected and flown as on-site missiles.

APPENDIX 3

MISSILE AERODYNAMICS, INJECTION, AND TRAJECTORY ANALYSIS

3.1 Introduction

The transport of missiles by tornado induced forces constitutes a complex physical process which is characterized by a paucity of observational data. The most common evidence of missile transport is simply the resultant displacement of objects with presumed known initial locations (e.g., 1-5, 1-7, 1-13, 1-22, 3-67). These observations, including the related impact embedments and/or missile-ground contact marks, do not provide the inclusive data base necessary for a primarily empirically derived missile transport model. However, they do provide useful benchmarks for comparative purposes and suggest several general characteristics of the transport phenomenon. Perhaps the most significant conclusion which can be inferred from this type of observational data is that the processes of missile generation (production) and transport produce highly variable trajectory end point results. This is particularly true for missile transport in the ground surface injection domain where flow turbulence and missile interference density are the greatest. The fact that identical objects having similar initial conditions exhibit significantly different terminal conditions suggests that the variations can be assumed to result from contributing probabilistic mechanisms. This conclusion is qualitatively supported by photogrammetric evidence, which constitutes a second type of observational data. The time history of cloud debris and small tracer objects suggests erratic trajectory patterns. However, there is an apparent total lack of eyewitness photography which documents the trajectory history of potentially damaging missiles of the type discussed in Appendix 2. Faced with these shortcomings of the available missile transport data and observed transport variability, probabilistic analytical modeling of missile injection and trajectory phenomenon is applicable.

Analytical prediction of the flight paths of tornado generated missiles requires knowledge of the tornadic forcing functions, the missile aerodynamic coefficients, the initial conditions, and the governing dynamic and kinematic relations. Because of the complexity of the tornado missile

transport process, considerable modeling uncertainty exists in several of these areas. This modeling uncertainty, coupled with the fundamental uncertainty discussed above, naturally affect the injection and trajectory sophistication suitable for the transport simulation. The models developed for this investigation represent an attempt to structure the contributing sources of modeling uncertainty and inherent variability.

3.2 Review of Previous Work

The tornado missile trajectory analyses presented to date have typically treated the problem deterministically for worst case conditions. An exception to this is Iotti's (3-6) treatment of drag coefficients. Following is a literature summary and brief analysis of the major aspects of missile transport which are significant from both modeling and risk analysis standpoints.

3.2.1 Tornado Movement

The tornado windfield is generally assumed to move with a constant translatory velocity U_T (3-6, 3-8, 3-9, 3-10, 3-14, 3-17, 3-18, 3-68) although Lee (3-7) assumes the tornado to be stationary. Some of those who refer to a translatory windfield appear not to actually include U_T in their analysis (cf., 3-8, 3-9, 3-18). The translational velocity of the tornado should be included in the wind velocity description to obtain the correct inertial trajectory.

3.2.2 Missile Constraints and Initial Condition

There are at least three basically different modes by which a potential missile may become airborne. The object could experience lift-off either from its original position or as a displaced ground missile. This mode is generally referred to as aerodynamic injection. Parts of buildings may also become airborne due to high winds or explosion of the buildings caused by the rapid pressure reduction within the tornado vortex. This is

termed explosive injection. The third basic mode is ramp injection which implies horizontal motion followed by either deflection upward into the windfield or falling off of an elevated position.

The study reported in (3-12, 3-17) proposes a mechanistic treatment in which the missile motion is assumed to be governed by the equations of motion from the instant of lift-off. Most other investigations (1-36, 3-4, 3-7, 3-8, 3-14, 3-18) have followed the suggestion of Bates and Swanson (3-3) in which the flight motion is divided into an injection stage and a flight stage. During the injection stage, lift or pressure forces are modeled as impulsive forces that only act in the vertical direction. At the end of this stage, which lasts from 0.1 to 0.2 second, the missile is at an elevation termed the injection height. At this height, the equations of motion govern the remainder of the flight. Lee (3-7) further tried to test for suspensibility of the missile.

The initial condition of motion where trajectory calculations begin is a significant source of uncertainty because of the inherent modeling difficulties. Both drag and lift forces are amplified when a missile is near the ground plane, and purely aerodynamic launching cannot be evaluated by a trajectory model. However, all missiles are obviously not launched from a smooth "runway." Ground-based obstacles will randomize the missile ground motion and the launch point, as well as the actual occurrence of lift-off. This ground interaction as well as potential interference with other missiles can significantly affect the trajectory and thus the estimation of subsequent event probabilities.

3.2.3 Missile Trajectory Models

The size and shape of a missile affect the degree of complexity of the system of dynamic and kinematic equations of motion required to accurately simulate the trajectory. The simplist form of dynamic equations of motion are those that are used to describe the motion of a mass particle, and these are

either in the form of the force equations ($\bar{f} = m\bar{a}$) or the angular momentum equations ($\bar{G} = \dot{\bar{h}}$). When solved as an initial value problem with the necessary kinematic equations of motion, the position (x,y,z) of the mass particle could be predicted at any given time to a degree of accuracy dependent on the accuracy of the forcing function, $\bar{f}$. Such a trajectory model is called a three degree-of-freedom model (3-D model). The 3-D models ignore the angular motion about the mass center entirely and assume that only the drag force (f_D) is acting through the mass center and in the direction of the wind-missile relative velocity. Such models do not consider lift (f_L) and side (f_S) forces.

In contrast to the relative ease in tracking a mass particle, both the force and angular momentum equations, in addition to other kinematic equations, are required to solve the initial value problem associated with the motion of a rigid body. Such a six degree-of-freedom trajectory model (6-D model) can be used to predict both the position of the mass center and the angular displacements relative to it.

Considerations which have apparently influenced the choice of trajectory models include the availability of the necessary aerodynamic coefficients, the characteristics of the missile trajectory which are determined to be important, and the utility and ease of model development. For the purpose of evaluating missile velocity design bases at nuclear power plants, previous investigators have primarily utilized the 3-D model. The implied assumption is that it provides conservative estimates of maximum missile velocities if conservative drag coefficients and optimum placement of the missiles are employed.

The only 6-D model which has been applied to tornado missile trajectory analysis was recently developed by JPL (1-48). Due to difficulties in obtaining aerodynamic coefficients, the preliminary report included trajectory studies for only cylindrical missiles with length to diameter ratios

of about 31. Their results indicate that in some cases the 3-D simulation using a random tumbling drag coefficient for high fineness ratio (L/d ≃ 31), cylinders potentially underestimates velocity and trajectory range when compared with the 6-D simulation. Their comments imply that the above trajectory simplification is probably adequate for low fineness ratio bodies (L/d ≃ 1), but the L/d limit of applicability for three-degree simplification is unclear. Generalized treatment of 6-D models can be found in the literature (e.g., 3-69).

3.2.4 Missile Aerodynamic Characterization

Regardless of the missiles considered, aerodynamic characterization depends on the degree of sophistication used in the trajectory simulation. If a 3-D ballistic model is used, missile characterization can be accomplished with the quantity known as a flight parameter (C_DA/W) or the reciprocal, ballistic coefficient (W/C_DA). If the missile is assumed to tumble during flight, the flight parameter is modified accordingly. When 6-D models are considered, additional aerodynamic terms must be accounted for, such as lift and side forces as well as aerodynamic moments.

The acceleration due to drag that a missile modeled as a particle experiences is proportional to the flight parameter. Due to a lack of experimental verification of actual missile flight, the choice of this parameter has been a major source of uncertainty. Several authors have derived tumbling drag coefficients (C_{Dt}), which are intended to account for random tumbling by averaging over missile orientation. This quantity represents a mathematical expectation which depends both on the form of the drag coefficient as a function of missile attitude and on the averaging process (e.g., the assumed probability distribution on missile attitude). Some of the early attempts at developing tumbling coefficients, such as the derivations by Bates and Swanson (3-3) for cylinders and rectangular parallelepipeds, lack mathematical rigor. The recent derivation by JPL (1-48) for cylindrical missiles does not agree with that in the present work; see Appendix C.1, which follows an approach for axially symmetric satellites (3-86). Apart from the question of how it is derived is the manner in which the tumbling coefficient is used.

Several investigators (3-4, 3-7, 3-18) have adopted the assumption of using the C_{Dt} and setting $A = A_m$, where A_m is the maximum projected area. Others (3-6, 3-8) solve for cases under this assumption, but also include a random tumbling flight mode. The work reported in 1-36 and 3-10 utilize a mean effective area $A_e \equiv \frac{2A_m}{\pi}$ as a compromise. References 3-11 and 3-17 both use $A = A_m$ with a Reynolds number dependent drag coefficient. Iotti (3-6) develops probabilistic distributions of missile velocities from arguments based on the random drag coefficients. Reference 3-84 reports experimental and analytical work concerning autorotation modes of slender bodies.

The aerodynamic characteristics required for 6-D trajectory analysis include drag, lift, and side force coefficients as a function of missile attitude relative to the wind. In addition, pitching moment and damping coefficients as a function of missile attitude and attitude rates are needed for the rotational equations. For most missile shapes found in the vicinity of nuclear power plants, this full aerodynamic definition is not available. The experimental work at JPL (1-48, 3-75) will provide 6-D data for certain cylindrical, rectangular, and vehicular shapes.

3.2.5 Flow Related Phenomena

There are several flow related phenomena peculiar to tornadoes which affect the external forcing function acting on a missile. These include:

1) Flow entrained particle effect on tornado intensity and missile forcing function.

2) Flow turbulence intensity distribution within the tornado.

3) The missile forcing function related to the inertial acceleration of the local flow field.

Reference 3-52 mentions a potentially important contribution of entrained particles on tornado intensity. The energy required to accelerate a significant mass of dust and water particles is obtained from the flow field which thus reduces the field strength. One effect of the suspended dust and debris particles on missile trajectory is the increased density of the accelerating fluid. Physical modeling of this process is complicated since the energy transfer from the tornado flow field to the entrained particles is fluid dynamic, but the energy transfer from entrained particles to the missile is the result of impulsive type collisions. Evaluation of this effect requires quantitative data on particle availability, high density particle entrainment, and two phase gas-solid flow. In absence of further information, a constant increase in the ambient air density will be assumed in this investigation to simulate particle entrainment.

Flow field turbulence intensity in tornadoes is currently being investigated (e.g., 3-40, 3-57). As suggested by the frequent irregular appearance of the tornado cloud, strong turbulence may significantly affect tornado dynamics (1-62). Recordings of tornado gustiness are limited and only a few wind traces are available (1-14). Turbulence affects missile acceleration because the local dynamic pressure, which is the basis for all aerodynamic forces, will fluctuate due to the local turbulence intensity. During initial missile motion, turbulence intensity has a smaller effect since the wind-missile relative velocity is at a maximum. However, as the missile accelerates and approaches the local wind speed, the unsteady velocity fluctuations due to turbulence could become the same order of magnitude or even larger than the steady component. This tends to randomize the resultant aerodynamic forces and moments in direction and magnitude. Thus, even an aerodynamically stable shape could respond randomly to such a forcing function. It should be noted that non-tornadic vertical wind shear turbulence can have intensities as high as 20% (3-82). To properly account for the turbulence effect on the aerodynamic forces and moments, accurate turbulence intensity maps in the flow field are required. Since this data is not currently available, this phenomenon will be accounted for indirectly by assuming random missile orientation during flight.

Another effect on the missile forcing function is the result of apparent flow field acceleration as the missile moves through the turbulent field. The inertia forces due to tornado flow field acceleration have been studied by Wen (1-39) and Sarpkaya (3-58) and are apparently significant. This phenomenon is not considered in the current study because of the problem complexity and the required flow inertial coefficients for the potential missiles (bluff bodies) in a tornado vortex do not exist.

3.3 Missile Trajectory Methodology

As noted previously, the two basic missile motion models which have been utilized in trajectory analyses require significantly different quantities of aerodynamic data input. Equally important in terms of simulation practicality are the increased computational requirements of the 6-D model above the ballistic 3-D model. In this section, the basis and methodology of an alternative probabilistic trajectory model are discussed and results are presented.

3.3.1 Probabilistic Trajectory Considerations

The determination of the trajectory of a tornado generated missile requires, as a minimum:

(1) The tornadic aerodynamic forcing functions.

(2) The dynamic and kinematic relations comprising the trajectory model.

(3) Quantitative characterization of the aerodynamic coefficients (near ground and freestream).

(4) Specification of the initial conditions, constraints, and release mechanisms.

Based upon the preceding discussion, there are significant sources of both fundamental and modeling uncertainty regarding the first, third, and fourth requirements. Thus, it does not appear that a deterministic trajectory model, regardless of its sophistication, can provide a realistic assessment of tornado missile risks. However, if only one trajectory characteristic (e.g., maximum missile velocity) is of interest, a simple 3-D ballistic model may be sufficient. This philosophy has been implied in the majority of the tornado missile analyses to date.

A major requirement in the risk assessment is that the potential range, height, and lateral scatter of the missiles be reflected in the trajectory model. These characteristics are important since missile origin location relative to critical target location significantly influences impact probability. Structure shadowing is a major consideration and its influence on the risk at a particular plant can be assessed accurately only if an unbiased trajectory model (e.g., a biased trajectory model might not recognize lift or side forces) is utilized. Thus, the utilization of a 3-D ballistic model in this study does not appear to be justifiable.

Based upon the above, 6-D missile simulation appears to be desirable; however, consideration of the first and third requirements suggests several shortcomings for a 6-D deterministic trajectory analysis. As discussed in Sections 1.4 and 3.2.5, turbulence is inherent in tornadic wind definition and results in local random changes in wind velocity and direction. These, in turn, can cause the missile attitude to vary randomly from that which might be predicted by mean flow 6-D motion. As noted by Costello (3-62), fixed attitude flight is improbable for bluff bodies even in a steady flow field. It is entirely possible that sufficient turbulence intensity exists to cause the random or disorganized flow fluctuations to dominate missile behavior. This argument becomes more plausible if one recognizes the fact that the majority of missile flight is within the turbulent boundary layer. Thus, it is possible that the trajectories predicted by a 6-D model may in fact be less representative of actual missile response in

a turbulent tornadic wind than a model which in some way recognizes this probabilistic mechanism. The potential for "random walk" of missiles has been discussed earlier (3-3) and the authors included a 33% gust component in the wind model. Others (e.g., 1-54) have used gust components as high as unity in tornado effects analysis.

In view of this turbulence consideration, the randomization inherent in the initial phase (injection) of the missile trajectory, the data requirements and increased computational requirements of a 6-D model, the inadequacies of the ballistic 3-D models, a modified 3-D random missile orientation model has been developed for this study. In this model, missile rigid body orientation is specified by two random vectors and drag, lift, and side forces are included. The kinematic relations developed allow for random tornado touchdown points and approach angles relative to the plant.

3.3.2 Random Missile Orientation Model

The inclusion of drag, lift, and side components in the aerodynamic force specification requires rigid body missile orientation definition. The missile centerline orientation is defined by two randomly determined angles (ψ,ϕ) which are measured from a (u,v,w) coordinate system as defined in Figure 3-1(b). The relative velocity vector defines the $\hat{v}$ direction while $\hat{u} = (\hat{v} \times \hat{k})/|\hat{v} \times \hat{k}|$ and $\hat{w} = (\hat{u} \times \hat{v})$. Once the missile orientation is established for a time step, wind axis unit vectors are determined by forming the vector cross product of the missile centerline position unit vector $(\hat{MCL})$ with the relative velocity vector $(\hat{v})$ to establish the pitch axis $(\hat{P})$. The missile diameter unit vector $(\hat{MD})$ is rotated through a randomly selected angle (δ) from the pitch axis. The relative velocity unit vector $(\hat{v})$ is then combined with the pitch axis $(\hat{P})$ in a vector cross product to establish the lift unit vector $(\hat{L})$. This approach defines the wind axis $(\hat{v}, \hat{P}, \text{and } \hat{L})$ for each time step which provides the respective directions for the three aerodynamic force components: drag, side, and lift. This approach provides an aerodynamic force that is properly oriented for the missile attitude.

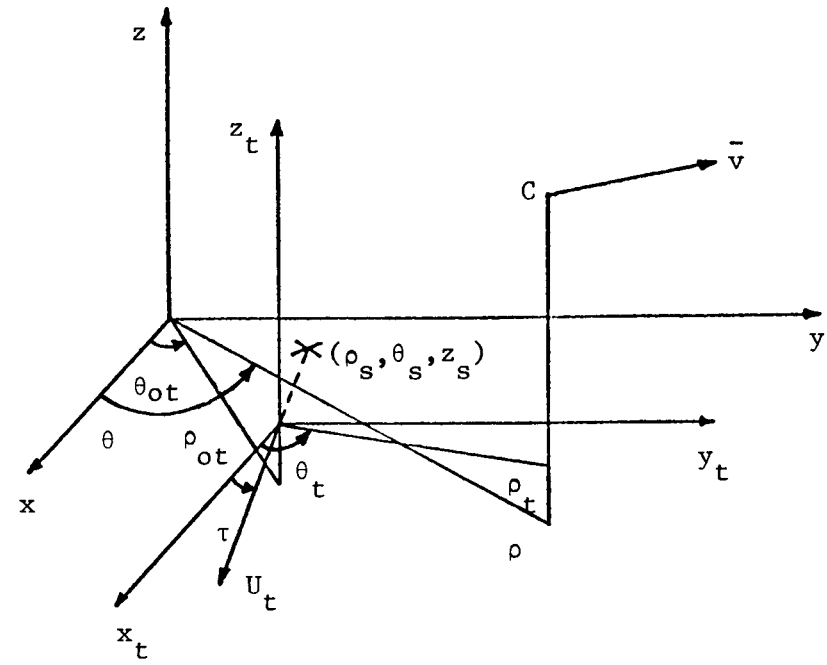

(a) Plant and Tornado Frames

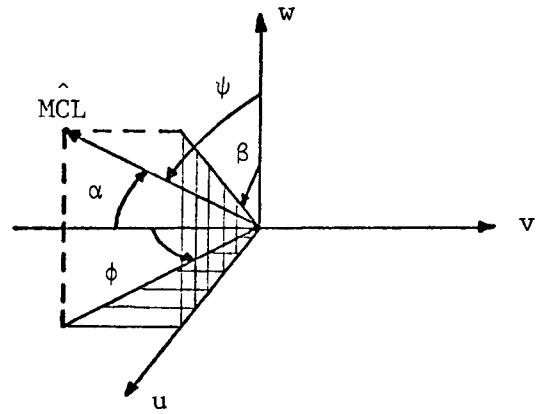

(b) $\hat{MCL}$ Specification

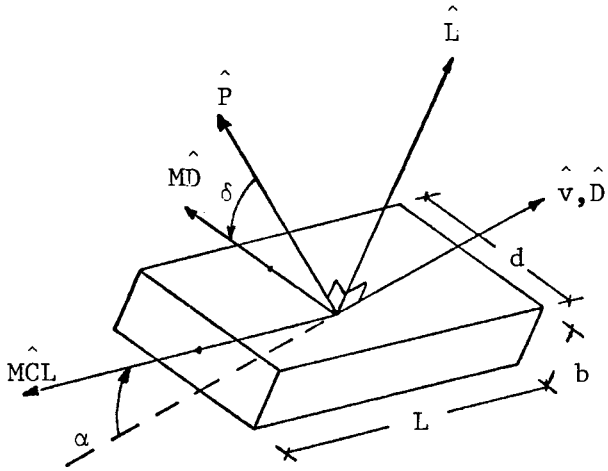

(c) Wind Frame and Missile Orientation

Figure 3-1. Coordinate Systems and Missile Specification

The magnitudes of the three translational forces are taken as proportional to the three static aerodynamic coefficients (C_D,C_S, and C_L), which may each be functions of total wind angle of attack (α) and roll angle (δ). These angles (α,δ) are both shown in Figure 3-1(c). The missile angles, and hence vectors $\hat{MCL}$ and $\hat{MD}$, are updated (selected at random) at selected intervals according to

$$\begin{aligned} \psi &= \text{Cos}^{-1}(1 - 2\xi_1) \quad , \quad 0 < \psi \leq \pi \\ \phi &= \pi(2\xi_2 - 1) \quad , \quad -\pi \leq \phi < \pi \\ \alpha &= \text{Cos}^{-1}(\text{Sin } \psi \text{ Cos } \phi) \quad , \quad 0 < \alpha \leq \pi \\ \delta &= 2\pi\xi_3 \quad , \quad 0 < \delta \leq 2\pi \end{aligned} \tag{3.1}$$

where ξ_1, ξ_2, and ξ_3 are random numbers selected from a uniform distribution on the unit interval. The time between missile orientation updates is termed the update period, and its reciprocal, update frequency. The angles are used as input to the aerodynamic coefficient determination. Once the three coefficients are determined, they are combined with the dynamic pressure, reference area, and the three appropriate wind axis unit vectors to form the total aerodynamic force for a single time step, as discussed in the following subsection.

3.3.3 Dynamic and Kinematic Relationships

For a given plant site, an appropriate location is chosen to situate a right hand cartesian frame (F_p) such that the axes are preferably parallel or perpendicular to major safety related plant structures. Since the tornado windfield covers only a small portion of the Earth and the missiles are expected to travel at subsonic speed, it is reasonable to assume the Earth to be locally flat and that the Earth's rotation can be neglected. The reference frame F_p and any other reference frame that is either fixed or in uniform motion relative to F_p is therefore inertial. Figure 3-1 shows this reference frame F_p along with other reference frames

that will be used in the development of the model. Whenever necessary, appropriate subscripts will be used to distinguish variables in one frame from another.

As indicated in Figure 3-1(a), the tornado is assumed to touch down at point $S(\rho_s,\theta_s,z_s)$, the centerline of the path of the tornado will intersect the x_p-axis at an approach angle (τ), and this angle is measured positive counterclockwise from the positive x_p-axis. To correctly set up the kinematic equations, an additional parallel cartesian frame (F_t) is used. This F_t frame has its origin $O_t(\rho_{ot},\theta_{ot},z_{ot})$ attached to the center of the tornado windfield and moving along with it at a uniform speed of U_T. Associated with each of these reference frames are two corresponding cylindrical frames F_{pc} and F_{tc}. The mass center of the tornado-generated missile is tracked relative to the plant cylindrical frame, F_{pc}, according to the dynamic equations of motion, which take the form

$$\begin{bmatrix} f_r \\ f_\theta \\ f_z \end{bmatrix} - mg \begin{bmatrix} 0 \\ 0 \\ 1 \end{bmatrix} = m \begin{bmatrix} \frac{dV_r}{dt} - \frac{V_\theta^2}{\rho} \\ \frac{dV_\theta}{dt} + \frac{V_r V_\theta}{\rho} \\ \frac{dV_z}{dt} \end{bmatrix} \tag{3.2}$$

and, from kinematic considerations

$$\begin{bmatrix} V_r \\ V_\theta \\ V_z \end{bmatrix} = \begin{bmatrix} \dot{\rho} \\ \rho\dot{\theta} \\ \dot{z} \end{bmatrix} \tag{3.3}$$

Here, the aerodynamic forces are taken as proportional to the square of the wind-missile velocity ($\bar{v}$). The random orientation model includes drag, lift, and side forces

$$\begin{bmatrix} f_D \\ f_L \\ f_S \end{bmatrix} = \frac{\rho_a A v^2}{2} \begin{bmatrix} C_D \\ C_L \\ C_S \end{bmatrix} \tag{3.4}$$

and then transforms these to the F_p system according to

$$\begin{bmatrix} f_r \\ f_\theta \\ f_z \end{bmatrix} = \begin{bmatrix} \frac{v_r}{v} & L_r & P_r \\ \frac{v_\theta}{v} & L_\theta & P_\theta \\ \frac{v_z}{v} & L_z & P_z \end{bmatrix} \begin{bmatrix} f_D \\ f_L \\ f_S \end{bmatrix} \tag{3.5}$$

where L_i and P_i represent components of the lift and pitch unit vectors, respectively, in the i-direction. Details of the derivation of the equations of motion are presented in Appendix 7.

In either the ballistic or random orientation forms, these equations compose a set of six coupled, nonlinear, ordinary differential equations which define an initial value problem given the prescribed initial conditions. Two methods of solution have been utilized. One is a simple fourth-order Runge Kutta method and the other is an integration code developed by L. F. Shampine et al. (3-76). Shampine's method is a modified divided difference form of the Adams PECE formulas with local extrapolation which adjusts the integration order and time step size to obtain a solution that is within prescribed local

error bounds. It offers a good compromise between accuracy and run time (cf. 3-87) and appears most suitable for the probabilistic trajectory model used in the study.

3.3.4 Missile Flight Models & Aerodynamic Data

The eight aerodynamic shape sets which form the missile spectrum have been previously identified in Table 3-2. With the exception of spheres and vehicles, each of the geometrical subsets presented in Section 3.2.2.2 requires the specification of only L/d for a complete aerodynamic coefficient definition. Spheres and vehicles are considered as singularly defined shapes. Thus, L/d is considered as the continuous variate in the flight model characterization, and d is the characteristic sizing variable.

Review of existing data reveals that complete aerodynamic characteristics for the potential missile array do not exist (cf. 1-53). Thus, an analytical approach is employed to predict the aerodynamic translational forces within the trajectory program. Cross flow theory has been investigated for this purpose and is utilized extensively in the following development. It has been successfully used to develop the wind axis aerodynamic forces as a function of angle of attack for slender cylinders knowing only the drag force coefficients for the body in normal flow to the major body axes (3-78). The basic theory assumes the superposition of two flows perpendicular to the missile axis (axial and cross flow) in which the magnitude of the mutually orthoginal flows is determined vectorially knowing freestream velocity and angle of attack. The only forces acting on the missile are drag forces that are parallel to each flow direction and are proportional to the directional dynamic pressure. For circular cylinders (aerodynamic shape set 1), the resulting expressions can be easily derived and are presented in Table 3-1.

Table 3-1. Aerodynamic Force Coefficients

Entry	Missile Type	Set No.	Aerodynamic Coefficient Formulas[a]	C_{D_a}	C_{D_b}	C_{D_d}	Finite Span Correction Factor, K_i
1	Rod	1,2	$C_D = \frac{\pi}{4}\frac{d}{L} K_1 C_{Da} \lvert\cos^3\alpha\rvert + K_2 C_{Db} \sin^3\alpha$ $C_L = -\frac{\pi}{4}\frac{d}{L} K_1 C_{Da} \cos\alpha \lvert\cos\alpha\rvert \sin\alpha$ $+K_2 C_{Db} \sin^2\alpha \cos\alpha$ $C_S = 0$	1.16, $L/d \leq 1$ $0.84+0.32e^{-2(L/d-1)}$, $L/d \in [1,4)$ $0.79+0.0125L/d$, $L/d \geq 4$ (see Figure 3-6)	1.2	-	$K_1 = 1$ $K_2 = 0.59+0.41e^{-20d/L}$
2	Pipe	3,4	Same as for Entry 1	0.65 times C_{D_a} for Entry 1, since $C_D(d_i/d_o) \leq 0.8 \approx 1.16$ (see Figure 3-7)	1.2	-	Same as for Entry 1
3	Box b=d	5,6	$C_D = \frac{b}{L} K_1 C_{Da} \lvert\cos^3\alpha\rvert$ $+K_2 C_{Db} \lvert\cos\delta \sin\alpha\rvert^P \lvert\cos\delta\rvert \sin\alpha$ $+\frac{b}{d} K_3 C_{Dd} \lvert\sin^3\delta\rvert \sin^3\alpha$ $C_L = -\frac{b}{L} K_1 C_{Da} \cos\alpha \lvert\cos\alpha\rvert \sin\alpha$ $+K_2 C_{Db} \lvert\cos\delta \sin\alpha\rvert^P \lvert\cos\delta\rvert \cos\alpha$ $+\frac{b}{d} K_3 C_{Dd} \lvert\sin^3\delta\rvert \sin^2\alpha \cos\alpha$ $C_S = K_2 C_{Db} \cos\delta \lvert\cos\delta\rvert^{P-1} \sin\delta \sin^P\alpha$ $-\frac{b}{d} K_3 C_{Dd} \sin\delta \lvert\sin\delta\rvert \cos\delta \sin^2\alpha$	2.05, $L/b \leq 3$ $0.84+1.21e^{-2(L/b-3)}$, $L/b \in (3,4)$ $0.95+0.0125L/b$, $L/b \geq 4$ (see Figure 3-8)	2.05	2.05	$K_1 = 0.59+0.41e^{-20b/d}$ $K_2 = 0.59+0.41e^{-20d/L}$ $K_3 = 0.59+0.41e^{-20b/L}$
4	Beam b=d/4	7,8,9	Same as for Entry 3	Same as for Entry 3	2.0	1.0	Same as for Entry 3
5	Plate b=d/10	10,11	Same as for Entry 3	Same as for Entry 3	2.0	1.075	Same as for Entry 3
6	Plate b=d/50	12,13	Same as for Entry 3	Same as for Entry 3	2.0	1.575	Same as for Entry 3

Table 3-1. Aerodynamic Force Coefficients (continued)

7	Wide Flange	14	Same as for Entry 3	0.15	1.60	δ	1.9	Same as for Entry 3
8	Angle Section	15	$C_D = 0.2 \frac{d}{L} K_1 C_{Da} \lvert\cos^3\alpha\rvert$	1.0	1.8-2.57δ	$[0,\frac{\pi}{4})$	-2.1+5.09δ	Same as for Entry 3
			$+K_2 C_{Db} \cos\delta \sin^3\alpha$		-2.3+1.66δ	$[\frac{\pi}{4},\frac{\pi}{2})$	1.8+0.13δ	
			$+K_3 C_{Dd} \sin\delta \sin^3\alpha$		3.7-2.16δ	$[\frac{\pi}{2},\frac{3\pi}{4})$	3.2-0.76δ	
			$C_L = -0.2 \frac{d}{L} K_1 C_{Da} \cos\alpha \lvert\cos\alpha\rvert \sin\alpha$		0.4-0.76δ	$[\frac{3\pi}{4},\pi)$	6.5-2.16δ	
			$+K_2 C_{Db} \cos\delta \sin^2\alpha \cos\alpha$		-2.4+0.13δ	$[\pi,\frac{5\pi}{4})$	-5.5+1.66δ	
			$+K_3 C_{Dd} \sin\delta \sin^2\alpha \cos\alpha$		-21.9+5.09δ	$[\frac{5\pi}{4},\frac{3\pi}{2})$	15.-3.57δ	
			$C_S = K_2 C_{Db} \sin\delta \sin^2\alpha - K_3 C_{Dd} \cos\delta \sin^2\alpha$		3.9-0.38δ	$[\frac{3\pi}{2},\frac{2\pi}{4})$	-1.8	
					1.8	$[\frac{7\pi}{4},2\pi)$	0.3-0.38δ	
9	Channel Section	16,17	Same as for Entry 3	0.5	2.05, $\delta \leq \frac{\pi}{2}$, $\delta > \frac{3\pi}{2}$ 1.8, $\frac{\pi}{2} < \delta \leq \frac{3\pi}{2}$		0.6	Same as for Entry 3
10	Frame b=d	18, 19,20	Same as for Entry 3	.4 times C_{D_a} for Entry 3, since K_σ [a] 0.4 for $\sigma = 0.5$ (see Figure 3-4)	0.41		0.41	Same as for Entry 3
11	Frame b=d/10	21, 22,23	Same as for Entry 3	Same as for Entry 10	0.40		0.215	Same as for Entry 3
12	Sphere	24	$C_D = 0.47$ $C_L = 0$ $C_S = 0$	-	-		-	-
13	Vehicle	25	Same as for Entry 3	1.0125	2.05		2.05	Same as for Entry 3
14	Tree	26	$C_D = 0.80$ $C_L = 0$ $C_S = 0$	-	-		-	-

[a] $P(b/d) = 0.5+0.15b/d+1.35(b/d)^2$

For other shapes, flow field similarity in the cross flow regime as the angle of attack changes is the major requirement for the cross flow theory to be applicable (3-78). Using this fact, it is possible to expect extension of the theory to any body that might exhibit this characteristic. These include sharp edged beams with rectangular or "I" cross sections where the sharp edges force boundary layer separation at a fixed point and therefore produce similar potential cross flow fields for all angles of attack. In principle, this concept allows the generation of lift, drag, and side forces for certain sharp edged planar symmetric sections if the drag coefficients are known for flow impacting normal to the three major faces of each shape. The derivation of the necessary expressions for a sharp edged shape with length, L, greater than the depth, d, which is greater than the width, b, follows. The missile orientation relative to the flow is shown on Figure 3-2. The theory develops the wind axis aerodynamic force coefficients by vectorially separating the flow field into three components each perpendicular to the major faces of the body. When the flow is normal to a symmetric body face, drag in the direction of velocity is the only aerodynamic force generated. Therefore, the body has three forces acting normal to the three major body faces which can be vectorially separated into the wind axis to develop the lift, drag, and side forces as a function of angle of attack, α, and roll angle, δ. Using Figure 3-2 for reference, the three wind axis force equations are written as

$$
\begin{aligned}
f_D &= dL\, C_D(\rho_a/2)v^2 = D_a\, \mathrm{Cos}\alpha + D_c\, \mathrm{Sin}\alpha \\
f_L &= dL\, C_L(\rho_a/2)v^2 = -D_a\, \mathrm{Sin}\alpha + D_c\, \mathrm{Cos}\alpha \\
f_S &= dL\, C_S(\rho_a/2)v^2 = D_b\, \mathrm{Sin}\delta - D_d\, \mathrm{Cos}\delta
\end{aligned}
\tag{3.6}
$$

Using the vector components in the cross flow plane, the cross flow drag D_c can be expressed in terms of the drag normal to the lateral faces.

$$
D_c = dL\, C_{D_b}(\rho_a/2)v_b^2\, \mathrm{Cos}\delta + bL\, C_{D_d}(\rho_a/2)v_d^2\, \mathrm{Sin}\delta \tag{3.7}
$$

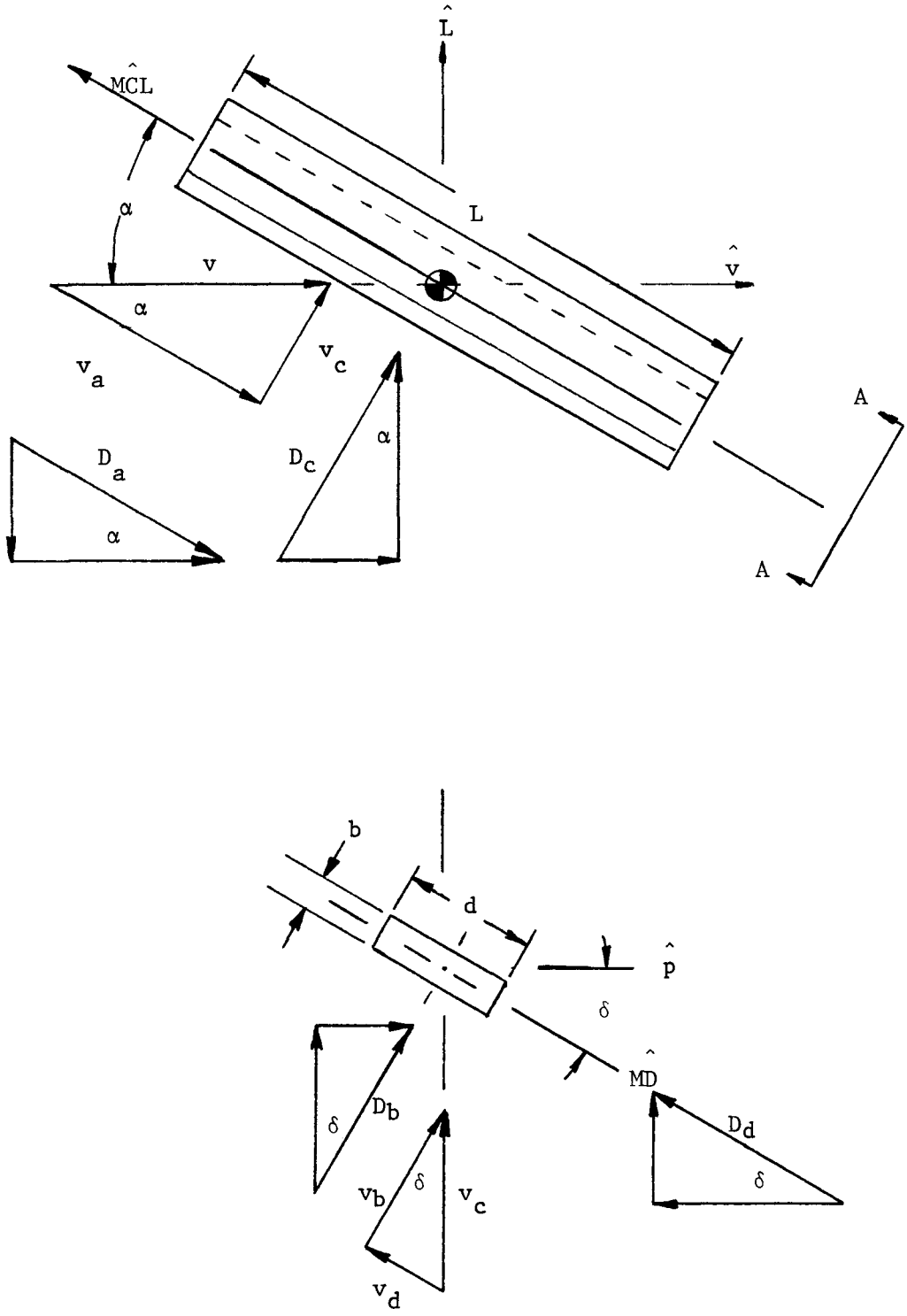

SECTION A-A

Figure 3-2. Missile Orientation and Flow Field Components Used With Cross Flow Theory

Combining Eq. 3.7 with the trigonometric identities $[(v_c/v)^2 = \mathrm{Sin}^2\alpha$, etc.] and substituting into Eq. 3.6 the three wind axis aerodynamic force coefficients can be expressed as functions of the drag coefficients for normal flow to the three major body faces, the wind angle of attack, and the body roll angle.

$$C_D = (b/L)C_{D_a}|\mathrm{Cos}^3\alpha| + C_{D_b}|\mathrm{Cos}^3\delta|\mathrm{Sin}^3\alpha + (b/d)\,C_{D_d}|\mathrm{Sin}^3\delta|\mathrm{Sin}^3\alpha$$

$$C_L = -(b/L)C_{D_a}\,\mathrm{Cos}\alpha|\mathrm{Cos}\alpha|\mathrm{Sin}\alpha + C_{D_b}|\mathrm{Cos}^3\delta|\mathrm{Sin}^2\alpha\,\mathrm{Cos}\alpha + (b/d)\,C_{D_d}|\mathrm{Sin}^3\delta|\mathrm{Sin}^2\alpha\,\mathrm{Cos}\alpha \qquad (3.8)$$

$$C_S = C_{D_b}\,\mathrm{Cos}\delta|\mathrm{Cos}\delta|\mathrm{Sin}\delta\,\mathrm{Sin}^2\alpha - (b/d)\,C_{D_d}\,\mathrm{Sin}\delta|\mathrm{Sin}\delta|\mathrm{Cos}\delta\,\mathrm{Sin}^2\alpha$$

A comparison of the above equations with a specific shape from recent wind tunnel data (3-75) suggests a discrepancy regarding the power of the cosine and sine functions used with the drag component normal to the maximum missile surface (d x L) or what is defined as the drag in the "b" direction (refer to Figure 3-2). A review of wind tunnel data on flat plate normal force coefficients (3-78) reveals a variation proportional to the square root of the sine of the attitude angle instead of the theoretical cross flow power of two. However, additional data in the same reference indicates that the normal force coefficient variation varies as the square of the sine of the attitude angle when the plate thickness equals or exceeds the plate width. Sufficient wind tunnel data is available (e.g., 3-75, 3-78) to develop the following empirical equation for a modified exponent used in cross flow theory for rectangular beams.

$$P(b/d) = 1.35(b/d)^2 + 0.15(b/d) + 0.5 \qquad (3.9)$$

where P is the power of certain sine and cosine function that correct for the local dynamic pressure normal to the major missile face, and b and d are defined previously. The equations with the above modification are presented in Table 3-1 under rectangular box sections.

A final consideration in the cross flow equations is the near-ground effect on the drag, lift, and side force coefficients due to the distortion of the flow field near the ground plane. Experimental data (3-75, 3-78) indicates that the drag modification is usually an increase over the free stream value for three dimensional (non-planar) shapes but can be a reduction for bluff shapes such as thin vertical plates. Since many missiles in this study are non-planar, only drag increases will be conservatively considered. The ground effect on lift and side force is a function of attitude, shape and distance above the ground. The approach here is to use a modification factor that is only a function of the nondimensional height because the additional effort to make the correction a function of attitude and shape does not seem to be a warranted refinement in view of the uncertainties involved and the lack of refinement in interfacing models (such as local ground elevation variations). This approach implies that all missiles will be predominatly oriented in a favorable flight attitude near the ground and thus results in a conservative forcing function. The near ground correction factors for drag, lift, and side force are presented on Figure 3-3 and were obtained from reference 3-78.

The determination of the proper normal flow drag coefficients for the various missile shapes is the final input to the aerodynamic characterization. Experimental data is available to characterize these parameters (3-2, 3-5, 3-72). Those flow characteristics which are considered in this investigation regarding drag coefficient specification include Reynolds number effect, tip losses, and missile face porosity. All drag coefficients used in this study are assumed to be invariant with Reynolds number for the following reasons. First, most of the missiles are in the fully turbulent Reynolds number regime only during the initial phase of the trajectory. Once the missile begins to move with the wind, the relative velocity decreases and the relative Reynolds number drops back below transition. Therefore, constant drag coefficients related to the pretransition Reynolds number range will be

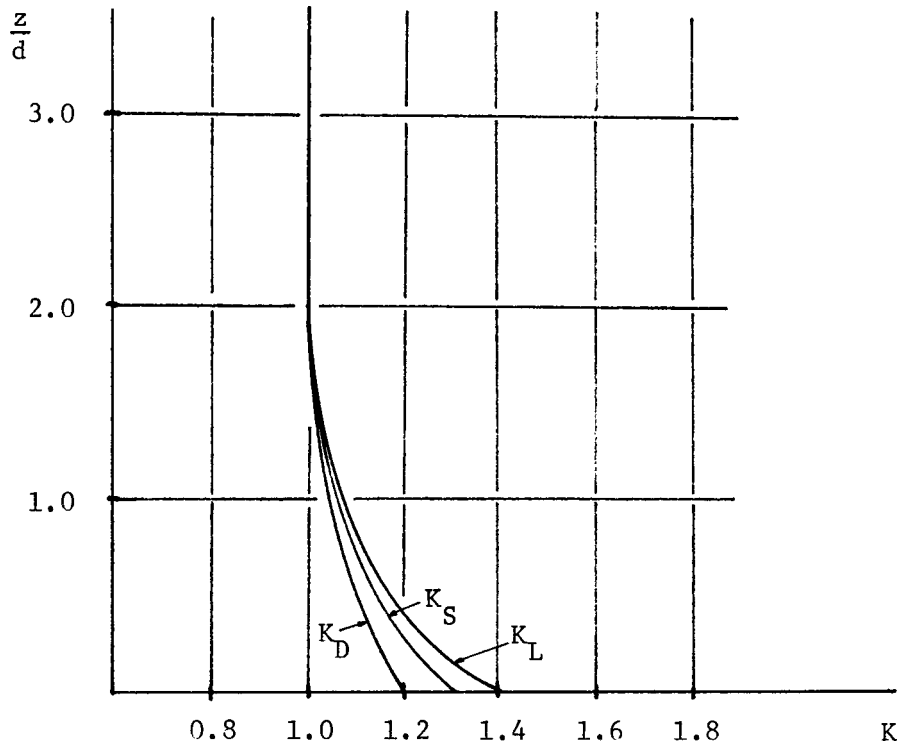

Figure 3-3. Near-Ground Corrections for Drag, Lift, and Side Forces

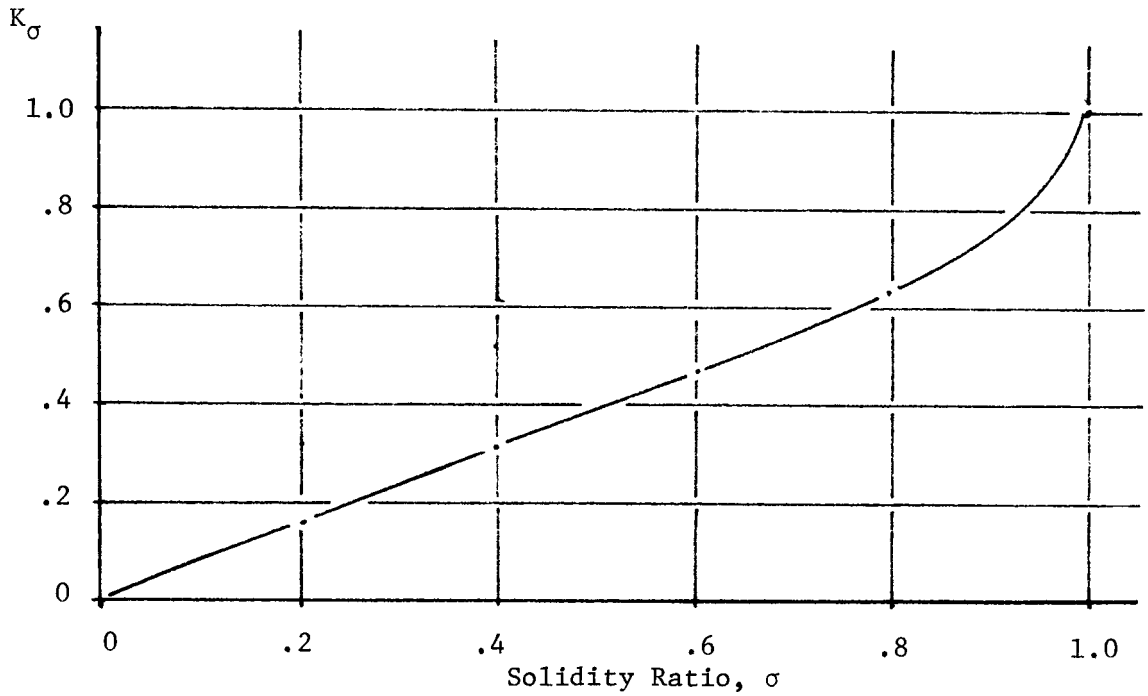

Figure 3-4. Porosity Correction Factor

considered. Second, most pipes, poles, and beams located near power plants predominantly have rough surfaces and therefore any fully turbulent flow regime drag coefficient would approach the pretransition value mentioned previously. Finally, the sharp edged beams will force boundary layer separation at a fixed point of the edge and tend to offset the potential flow field modification associated with boundary layer transition. Thus, Reynolds number effect will be conservatively neglected in this study on the basis of utility.

Since all the missiles have finite dimensions, a tip loss correction is required for all drag coefficients. The following curve-fit equation corrects infinite span drag coefficients for cylinders and bluff shapes and was obtained from data presented in reference 3-78

$$C_{D_{\substack{\text{Finite}\\\text{Span}}}} = C_{D_{\substack{\text{Infinite}\\\text{Span}}}} \left[0.59 + .41\, e^{-20(h/s)}\right] \qquad (3.10)$$

where h is the minor face dimension on the beam surface facing the flow and s is the major face dimension on the beam surface facing the flow. This tip loss correction is employed on all drag coefficients used in the cross flow equations except the axial coefficient on circular cylinders. This particular coefficient is corrected in the original data source.

The drag coefficients for the faces of composite beams are developed knowing the solidity ratio, σ, of the beam. The approach is to develop the drag coefficients for a solid beam, then correct each drag coefficient for its solidity ratio in a direction normal to the beam face using Figure 3-4. This allows for the treatment of composite beams which have different solidity ratios normal to the three major faces. However, in the simplified missile set treatment outlined in Appendix 2, objects are categorized into sets with solidity ratios of either 0.5 for relatively porous objects or 1 for relatively solid objects.

The previous discussion has dealt with centerline symmetric cylinders and planar symmetric beams. There are four missile sets that do not fit these requirements. These are vehicles, approximate spheres, trees, and angle shapes.

Vehicles are approximated by a rectangular beam with dimension 4'x5'x20'. Missiles that are roughly shaped as spheres are flown as a ballistic point mass with no lift or side forces. Trees are modeled as ballistic darts with no lift or side forces since those generated by trunk failures represent a very stable shape with rapid aerodynamic damping. This means the tree would fly with the canopy forward during the acceleration phase, swing around and damp out quickly with the trunk forward during the deceleration phase. This behavior can be approximated by a ballistic point mass.

The remaining missile category is the angle cross-section, which cannot be simulated using the standard cross flow discussed previously because it generates a side force as well as drag when the flow is normal to an angle face. The cross flow equations are modified and the drag coefficients obtained from experimental data (3-72) in order for these missiles to be properly simulated in the trajectory model. The modified equations are presented on Table 3-1 and the drag coefficients are presented on Figure 3-5.

A summary of the previous discussion is presented on Table 3-1. It contains the equations and the method for developing each required drag coefficient so proper aerodynamic forces can be developed for each type of missile to be considered in this study. Figure 3-6 provides the axial drag coefficients for cylinders. The axial drag coefficient for pipes as a function of inside to outside diameter ratio is given in Figure 3-7. Figure 3-8 provides the infinite span drag coefficients for each face of the rectangular beams as a function of cross flow dimension ratioed to beam thickness.

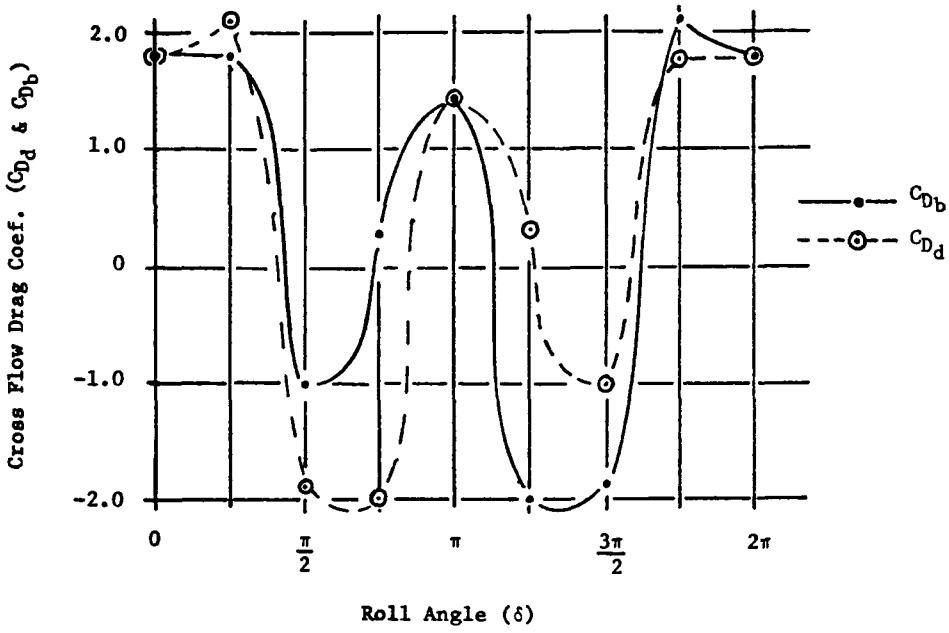

Figure 3-5. Cross Flow Coefficients for Angle Section

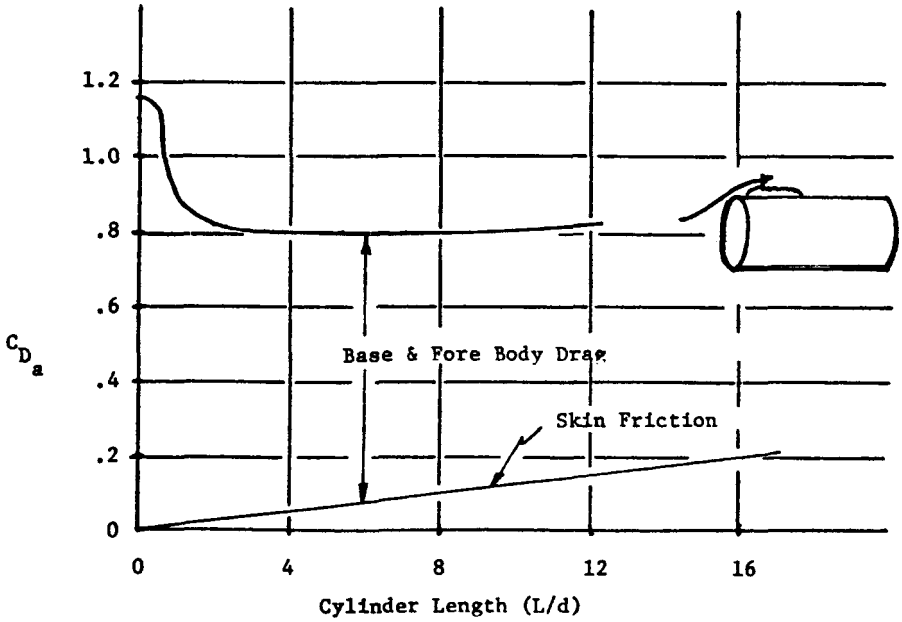

Figure 3-6. Axial Drag Coefficient for Solid Cylinders

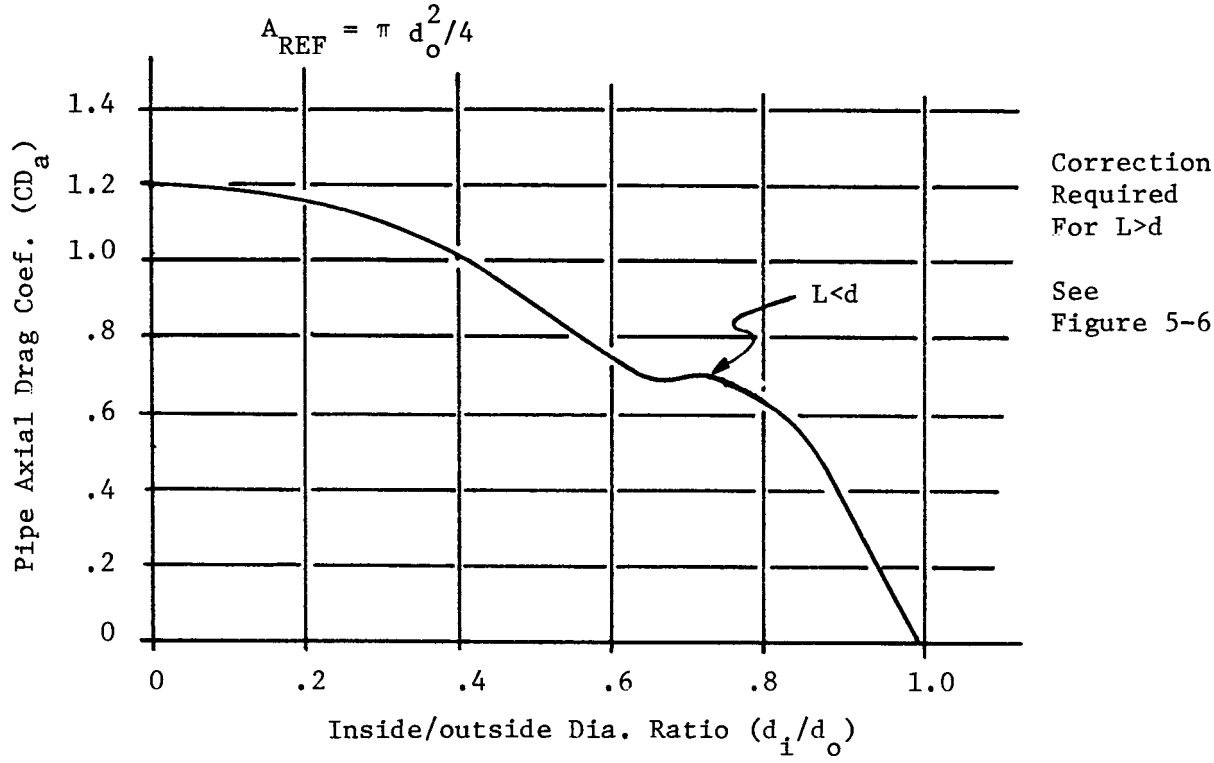

Figure 3-7. Axial Drag Coefficient for Pipes (Ref. 3-78)

Using the preceeding methodology, it is possible to develop the required wind axis aerodynamic force coefficients as a function of attitude for missile shapes varying from solid circular cylinders to rectangular trusses if the drag coefficients for flow perpendicular to the major missile axes are known. Comparison with experimental data (3-81) is presented in Figure 3-9 and indicates reasonable agreement for the probabilistic simulation.

3.3.5 Trajectory Model Verification and Results

The random orientation trajectory model computer program has been developed such that it can operate in any of three modes: 3-D ballistic; random orientation, drag force only (random drag); or random orientation, with drag, lift, and side forces (full random). This approach has facilitated model verification and hypothesis testing although only one mode (full random) will be employed in the simulation studies for the reasons described in the previous sections. In particular, verification of the

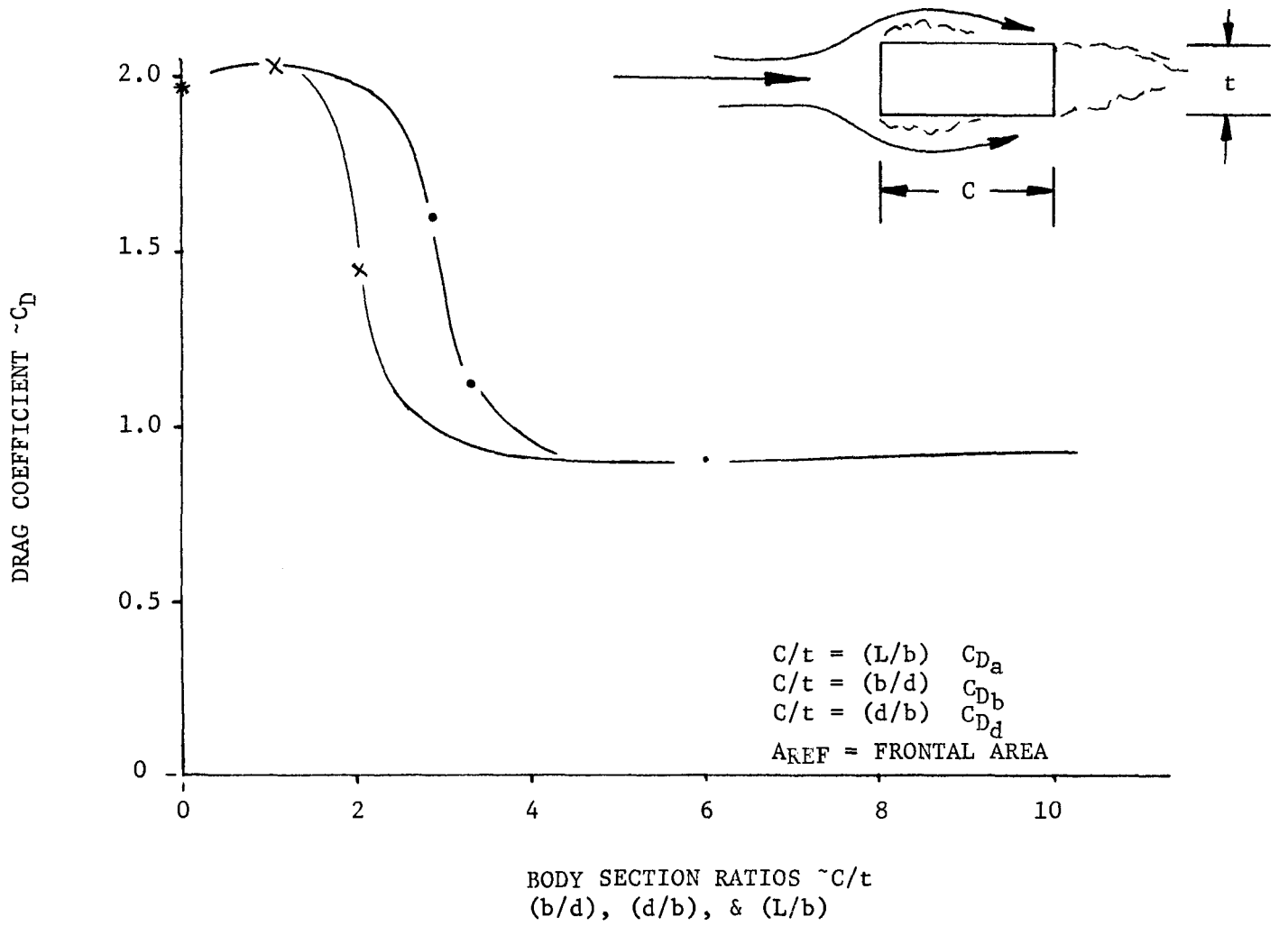

Figure 3-8. Drag Coefficients on Sharp Edged Beams in Normal Flow (Ref. 3-78)

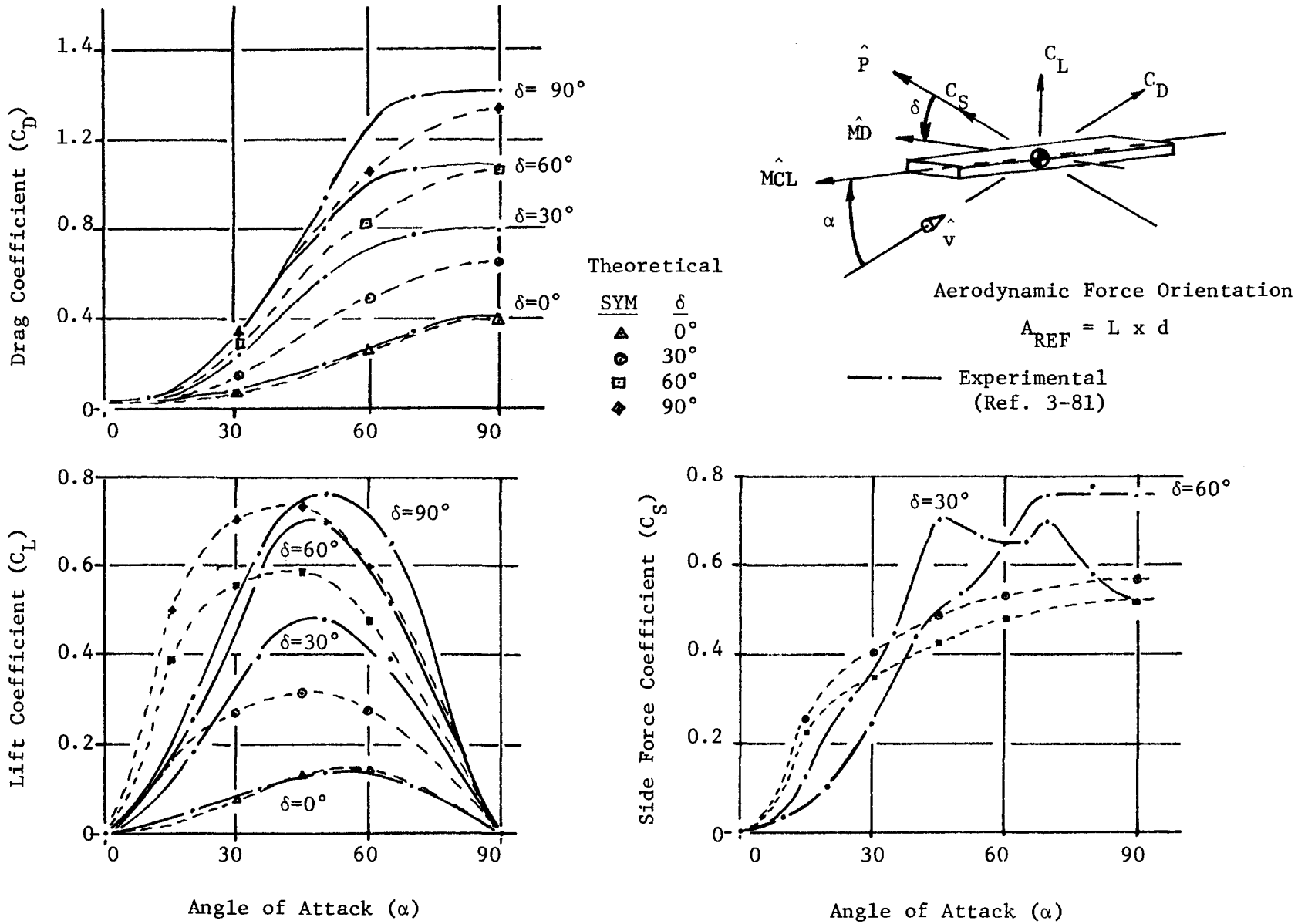

Figure 3-9. Comparison of Wind Axis Coefficients Using Cross Flow Theory to Wind Tunnel Data for a 4" x 12" x 144" Beam

3-D ballistic mode has been achieved by comparison of results with the independent calculation of the trajectory of a falling object in a uniform, planar windfield, with the sample problem presented by NBS (3-68), and with several of the ballistic random tumbling mode cases reported by JPL (1-48). There are no comparable random orientation models to test against directly, so a series of tests was devised to indicate the validity and applicability of these models and the correctness of the programming. These tests include:

(1) Comparison of the random drag model at various update frequencies with 3-D ballistic results.

(2) Comparison of the full random and random drag models at a similar update frequency.

(3) Comparison of the full random model at various update frequencies to the JPL 6-D model.

Additionally, a study was made to assess missile trajectory characteristics in conjunction with the tornado strike model (Section 1.3.1) and the offsite missile threat (Section 2.2.3). The remainder of this section presents the results of these tests and model hypotheses.

3.3.5.1 Random Drag Model

An expected feature of the random drag model is that it should duplicate the corresponding ballistic case if the update frequency is zero since, by never updating orientation, a fixed-attitude trajectory is obtained. Further, by varying the initial orientation, the range of ballistic trajectories (from minimum to maximum drag coefficient) are predicted. Another expected feature of the random drag model is that at the opposite extreme of high update frequency the trajectory should approach, in the limit, the ballistic random tumbling mode trajectory.

To assess these hypotheses, the random drag tests presented in Table 3-2 were conducted using the JPL windfield model (1-48) acting on the standard utility pole missile. The results are summarized in Table 3-2 and verify the expected features of this model. Comparison of cases 1 and 2 indicates that the zero update frequency random drag model is equivalent to a ballistic (fixed-attitude) model. Demonstration that the random drag model tends to converge to the ballistic random tumbling mode case as update frequency is increased is achieved by comparison of cases 3 through 6 with case 7.

Hence, the random drag trajectory mode of the random orientation model has the following features:

(a) For high update frequency, the trajectories closely approximate the random tumbling mode ballistic trajectory and the variance is small.

(b) For more moderate update frequency, the trajectory pattern spreads and is characterized by a larger variance.

(c) For sufficiently low update frequency, a maximum spread among the trajectories is obtained, corresponding to the range of ballistic 3-D fixed-attitude trajectories for random initial orientations.

This is significant in that it affords excellent control of the extent of variation of the random trajectory model from a deterministic model.

3.3.5.2 Full Random Model

The full random model was compared to the random drag model in order to investigate the effects of the addition of lift and side forces. It is frequently argued, with respect to the use of random tumbling mode coefficients, that lift and side forces will tend to have negligible net effect because the

Table 3-2. Comparison of Ballistic 3-D and Random Drag Models

Case No.	Number of Trials (n)	Mode	Initial Orientation	Update Freq. (Hz)	Ground Impact Point[a] $\hat{x}$	Ground Impact Point[a] $\hat{y}$	$\hat{D}$[b] (ft)	$\hat{V}_H$[c] (fps)	$\hat{V}_z$[d] (fps)
1	1	Ballistic 3-D	Max C_D	-	76.8	30.5	82.6	115.6	- 31.4
2	1	Random Drag	Max C_D	0	76.8	30.5	82.6	115.6	- 31.4
3	50	Random Drag	Random	1	51.3	19.9	55.1	80.7	- 32.7
							(26.4)[e]	(31.9)	(1.1)
4	50	Random Drag	Random	2	50.5	19.5	54.1	78.0	- 33.0
								(22.4)	(0.9)
5	50	Random Drag	Random	10	49.8	19.1	53.4	80.2	- 32.8
							(8.7)	(8.3)	(0.4)
6	50	Random Drag	Random	100	49.0	18.8	52.5	79.7	- 32.7
							(2.9)	(3.4)	(0.2)
7	1	Ballistic 3-D	RTM C_D	-	48.7	18.7	52.2	79.7	- 32.7

Notes: (a) For multiple trial runs the impact point is the centroid of the impact pattern.

(b) $\hat{D} = \frac{1}{n} \sum_{i=1}^{n} [x_i^2 - y_i^2]^{1/2}$.

(c) $\hat{V}_H = \frac{1}{n} \sum_{i=1}^{n} [(V_r)_i^2 + (V_\theta)_i^2]^{1/2}$.

(d) $\hat{V}_z = \frac{1}{n} \sum_{i=1}^{n} (V_z)_i$.

(e) Numbers in parentheses are standard deviations.

directions in which these forces act will vary, and thus cancel out, as the missile randomly tumbles. This argument is not supported by the results of this study using the JPL wind model and utility pole missile. Only drag and lift are considered here since cylindrical missiles do not experience side forces. In Table 3-3 random drag and full random impact results of 50 trials each are shown. Both random modes employed an update frequency of two Hz. Not only is the variance larger in the full random case, but the trajectories tend to be longer. Hence, the 3-D random orientation model, with lift and side forces included, is considered to be the most appropriate model for the probabilistic simulation analysis. It is noted that the full random model exhibits the same type of behavior with update frequency as the random drag model, but has larger variances and different impact points.

The recently developed 6-D model by JPL (1-48) permits comparison of "controlled" rotational rigid body flight with the full random 3-D model in a laminar tornadic field. Comparison of a series of cases with different update frequencies with 50 6-D trajectories for the utility pole missile is presented in Table 3-4. It is noted that trajectory horizontal path length tends to increase with decreasing update frequency and that the random model results tend to change little beyond an update frequency of one Hz. In Fig. 3-10, the impact positions of the 50 trials at the one Hz. update frequency are illustrated with those corresponding to the 50 6-D trajectories. Among the 6-D trajectories there are a few unusually long ones, two covering horizontal distances of 805.4 and 612.0 ft. These missiles remained airborne on the order of 4.8 - 5.8 sec. and result from chance favorable initial orientations and slow tumbling during flight. It is postulated that the randomizing effects (such as tornado turbulence, flow modifications, and missile interactions) would tend to enhance missile tumbling, having the net effect of shortening these trajectories. It is interesting to note that if the single longest trajectory is ignored, the mean range ($\hat{D}$ in Table 3-4) is 93.5 ft. It is also noted that the full random model is capable of generating very long trajectories, if very low update frequencies are employed. For instance, ten missiles were flown from an initially favorable orientation at an update frequency of 0.2 Hz and resulted in an average horizontal distance travelled of 723.3 ft. Based on the preceding results and considerations, an update frequency of one Hz is selected for use in the simulation model.

Table 3-3. Comparison of Random Drag and Full Random Models[a]

Case No.	Number of trials (n)	Mode	Ground Impact Point x (ft)	Ground Impact Point y (ft)	$\hat{V}_H$ (fps)	$\hat{V}_Z$ (fps)
1	50	Random Drag (2 Hz)	50.5	19.5	78.0 (22.4)	- 33.0 (0.9)
2	50	Full Random (2 Hz)	60.7	26.2	83.8 (28.6)	- 35.5 (7.0)

[a]Notes: a-e of Table 3-2 apply.

Table 3-4. Comparison of Full Random and 6-D Models[a]

Case No.	Number of trials (n)	Mode	Update Frequency (Hz)	Ground Impact Point x (ft)	Ground Impact Point y (ft)	$\hat{D}$ (ft)	$\hat{V}_H$ (fps)	$\hat{V}_Z$ (fps)
1	50	Full Random	5	48.1	18.9	52.8 (28.1)	76.0 (18.8)	- 33.5 (4.9)
2	50	Full Random	2	64.5	28.4	72.4 (58.5)	87.9 (34.2)	- 36.2 (6.8)
3	50	Full Random	1.25	71.1	27.9	80.5 (65.0)	85.9 (34.3)	- 36.0 (7.6)
4	50	Full Random	1.0	81.1	31.9	91.8 (72.3)	91.8 (32.8)	- 37.0 (8.8)
5	50	Full Random	0.667	81.2	38.2	93.1 (92.1)	88.4 (46.5)	- 36.3 (7.4)
6	50	6-D	-	98.4	32.5	107.7 (147.5)	102.7 (45.2)	- 36.8 (8.6)

Notes: [a]Notes a-e of Table 3-2 apply.

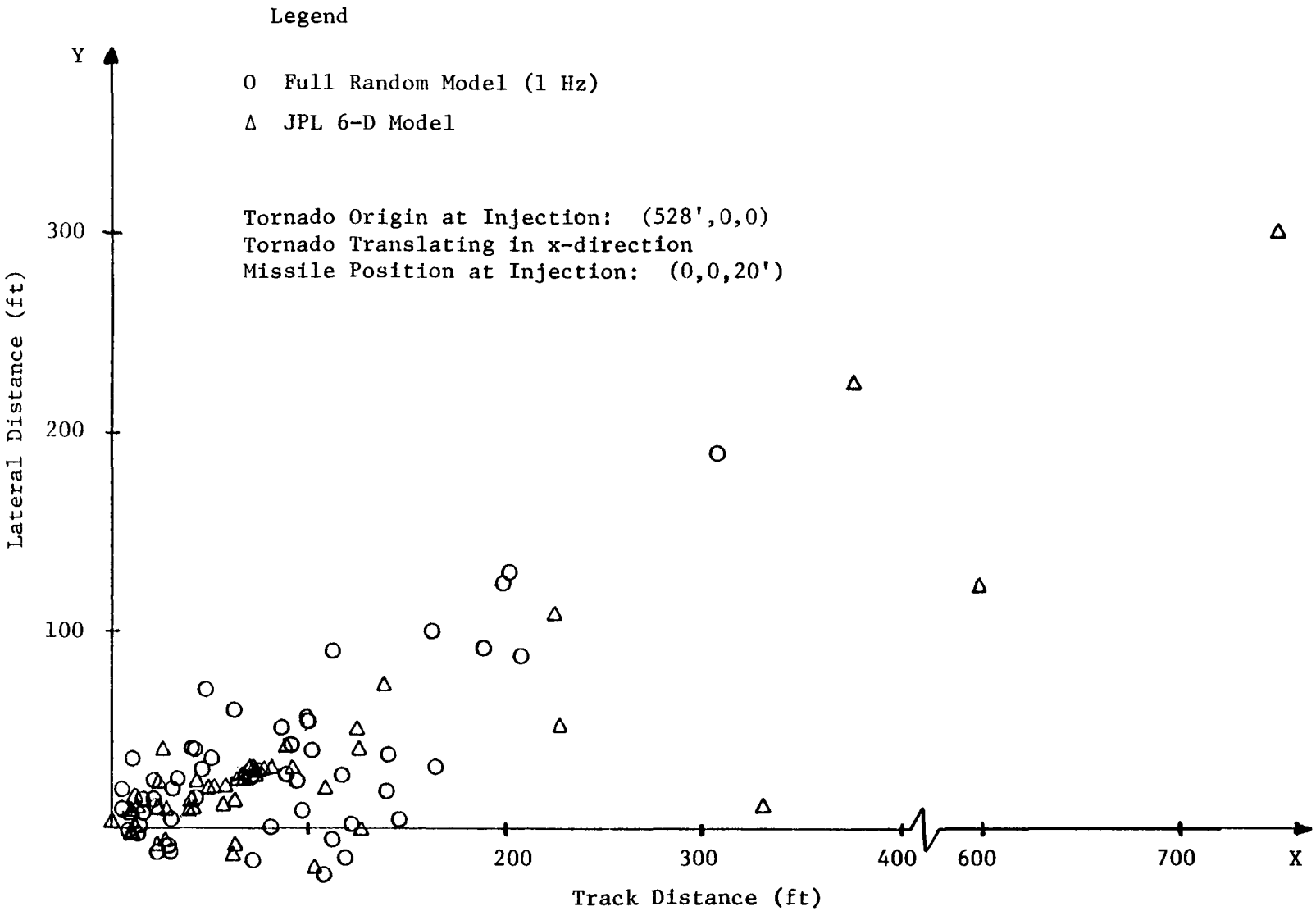

Figure 3-10. Scatter Diagram of Impact Points of Utility Pole Missiles

As evident from Figure 3-10, it provides adequate lateral scatter, and considering flow turbulence and multivortex phenomena which tend to randomize rotation, the 3-D random orientation model at one Hz is an appropriate probabilistic simulation of rigid body flight in a tornadic environment.

3.3.5.3 Missile Impact Boundary and Range Study

Using the full random trajectory model (with one Hz update frequency), missile trajectories were computed to assess the adequacy of the tornado strike model and the significance of offsite missiles. The missiles utilized in this parametric study are described in Table 3-5 and generally have favorable aerodynamic characteristics which should maximize range. One heavy metal shape was considered in order to simulate a dominating centrifuge effect from the vortex (cf. 3-85). It is reasonable to expect that the tendency to expel missiles through the wind boundary would increase as translational velocity and tornado width decrease and as tornado intensity increases, since at the extreme of monodirectional flow (translational velocity only) and/or infinite width, the missile expulsion rate would be a minimum. An F5 tornado intensity of 282 mph (cf. Table 1-9, column e) was conservatively assumed with the minimum and maximum translational velocities of 5 and 70 mph (cf. Table 1-10). The FPP data record analysis (Section 1.3.3) suggests that most F5 tornadoes have widths (W_t) between 176 and 556 yards (P_w=3) or between 56 and 176 yards (P_w=2). Hence, widths corresponding to the midpoints of these two intervals were considered.

The study was conducted in three stages. In the first stage, fifty missiles from each of the five missile sets were flown in each of the first four tornadoes of Table 3-5, for a total sample of 1000 missile trajectories, using the JPL wind model. It is noted that these tornado widths used with the JPL wind model result in very large updrafts in the central core. Thus, missiles injected within ρ_{tm} of the tornado center experience conservatively high aerodynamic forces. The missiles were injected with random initial orientations and at random positions within the volume described by vertical planes at the right and left 73 mph boundaries, the ground plane and 100 ft.

Table 3-5. Missile and Tornado Descriptions for the Boundary Study

(a) Missiles

Number	Missile Set	Missile	L/b	d/b	Area (ft^2)	Weight (lb)
1	2	Utility Pole	30	1	30	950
2	9	Beam or Box	20	4	80	1600
3	13	Plywood Sheet	96	50	32	100
4	14	Wide Flange	24	1.2	20	1160
5	26	Tree	20	1	300*	600

(b) Tornadoes

Number	Maximum Velocity (fps)	U_T (fps)	$V_{r\theta}^{max}$ (fps)	Width (feet)
1	413.6	102.67	310.93	1098
2	413.6	102.67	310.93	348
3	413.6	7.33	406.27	1098
4	413.6	7.33	406.27	348
5	306.53	7.33	299.20	108

*The area is based on an assumed spherical canopy of about 19.6 ft. diameter.

elevation planes, and vertical planes located $W_t/2$ ahead of and behind the tornado center. Of the 1000 trajectories, only 57 transcended the 73 mph wind boundary planes and of these, 45 involved the tornadoes translating at 5 mph, supporting our hypothesis and influencing the subsequent tests.

Based upon these results, the second part of the study was limited to the two slowly translating F5 tornadoes, numbers 3 and 4 of Table 3-5(b), utilizing the synthesized tornado windfield model. One hundred missiles from each of the five sets were flown in each tornado for another sample of 1000

missile trajectories. These were injected randomly as in the first stage. The results, summarized in Table 3-6, indicate that 138 missiles were expelled beyond the 73 mph wind boundary planes. It is noted that:

(a) Only 33 missiles were ejected from the wider (1098 ft.) tornado, the other 106 from the thin (348 ft.) tornado.

(b) The ejected missiles were predominantly the plywood sheets and trees which are relatively "light" missiles. Of the 138 ejected missiles, 23 were injected within 50 ft. of the wind boundary, most at sufficient elevations that they were essentially carried out while dropping from their injected positions. It seems unlikely that many of these missiles would actually be injected at these elevated positions in this region of the windfield.

(c) The average horizontal distances traveled by the plywood sheets and the trees were comparable, but the variance was much smaller for the trees. This was expected since the tree shape is considered to have constant aerodynamic coefficients, but the coefficients vary significantly with orientation for the plywood sheet. This effect led to almost twice as many plywood sheets being ejected as trees.

Based on the results of these first two studies, involving 2000 missile transport simulations, it can be concluded that the 73 mph wind boundary employed in the tornado strike model bounds the statistically significant impact region for tornadoes with widths greater than 1000 ft. Since the percentage (7%) of the missiles that impacted outside the boundary is based upon "favorable" missiles, injection, and tornado translation speed, the actual contribution is much less considering the conservatism of the study. However, for the 348 ft., high intensity tornado, approximately 20% of the missiles injected from 0 to 100 ft. impact outside the 73 mph wind boundary.

Table 3-6. Missile Transport Simulation Results

Missile No.	Tornado No.	$\hat{D}$(a) (ft)	$\hat{V}$(b) (ft)	Number of Trajectories	Number Transcending Wind Boundary Planes
1	3	101.2 (258.6)(c)	71.7 (39.5)	100	2
	4	61.4 (155.6)	65.9 (32.7)	100	5
	5	84.7 (234.2)	60.3 (38.9)	50	9
2	3	169.8 (370.0)	87.0 (49.3)	100	7
	4	235.2 (376.9)	95.4 (50.2)	100	21
	5	148.9 (290.0)	72.4 (41.4)	50	18
3	3	321.2 (341.0)	125.8 (59.0)	100	17
	4	266.6 (221.2)	106.2 (75.8)	100	44
	5	228.8 (200.0)	91.8 (35.5)	50	34
4	3	50.4 (153.3)	60.1 (34.0)	100	1
	4	76.6 (190.5)	64.7 (36.9)	100	8
	5	30.0 (59.4)	51.4 (24.9)	50	6
5	3	325.3 (203.2)	106.4 (26.9)	100	6
	4	213.1 (118.8)	87.0 (279.4)	100	27
	5	200.0 (115.5)	63.2 (70.3)	50	37
Totals:	Stage 2			1000	138
	Stage 3			500	104

NOTES:

(a)$\hat{D}$ is the average horizontal distance traveled.

(b)$\hat{V}$ is the average missile impact velocity.

(c)Numbers in parentheses are standard deviations.

To further investigate this effect, the third stage of this study was conducted in which fifty missiles from each set were injected into the windfield of tornado 5 (from Table 3-5), which represents a very thin (midrange of P_w=1), high intensity F4 tornado. The synthesized windfield model was used and the missiles were again injected at random locations. For this extreme case, 104 of the 250 missile trajectories exceeded the 73 mph wind boundaries (see Table 3-6). This suggests that an effective tornado width for intense tornadoes (F4, F5) which have widths less than 1000 ft. is needed for the tornado strike probability calculation. Analysis of the missile impact distribution suggests an effective width (W_{te}) modification as

$$W_{te} = 440 + 0.56W_t \ , \ W_t < 1000 \text{ ft.} \qquad (3.11)$$

The coefficients were determined such that the coordinates (W_t,W_{te}) assumed the values (1000, 1000) and (108, 500), the latter point representing the width for which 8% of the missiles from the third stage of the study escaped. Considering the conservatism in selecting the parameters for this study, the expected number of missile impacts outside W_e defined by Eq. 3.11 is much less. It should be noted that the tornado width, W_t, used in the computation of the windfield remains unchanged.

3.4 Missile Injection Methodology

The missile trajectory methodology discussed previously is appropriate for missiles in free flight subjected to gravitational and aerodynamic accelerations. In general, the initial acceleration of a stationary object by tornadic winds requires that certain restraining forces be overcome before motion is possible. In addition to gravity forces, these restraints can consist of structural, frictional, or interlocking mechanisms which tend to resist motion. They are important in characterizing the initial release conditions of the object relative to the moving tornado. The determination of the initial motion of the missile and its release mechanism constitutes the missile injection analysis. The physical environment of the injection region is considerably

more complex than that associated with free stream missile transport. The general characteristics of this domain (ground surface, elevated structure, etc.) in the immediate vicinity of a nuclear power plant suggest that:

(1) Flow field turbulence and flow interference modification are considerably increased over free flight flow.

(2) The presence of potential sources of missile interaction, such as ground surface perturbations, other missiles, and small structures, contributes to the randomization of injection domain transport.

(3) The restraining mechanisms, including both initial restraint conditions as well as subsequent "trapping" or wedging restraints, exhibit considerable variability in type, location, and magnitude.

Each of these general hypotheses regarding the transport environment in the injection domain contributes to the statistical variability and complexity of missile injection events. Mechanistic deterministic modeling is thus not feasible for missile injection and a probabilistic approach is adopted. In recognition of this injection modeling difficulty and uncertainty described above, three fundamental questions must be considered in the development of an analytical missile injection methodology:

(1) How are the initial conditions defining missile location and orientation modified by potential missile interactions and debris source effects?

(2) What type of missile restraints and release mechanisms are applicable considering the complex injection domain environment?

(3) How are ground interactions modeled in the injection sequence?

The first question recognizes the potential for missile collisions, possible instability of storage modes, and debris source impact. The injection methodology must reflect these simultaneous effects by effectively transforming the initial value missile availability conditions into equivalent injection conditions. Consideration of missile retraints such as the weight and interlocking effects of other potential missiles or structural mechanisms is implied in the second question. Injection of missiles in the near ground domain also suggests a potential for ground interactions during the early phase of transport. Thus, the third question addresses issues of ground ricochet and missile termination. The injection methodology developed below relies on probabilistic characterization of the initial conditions and optimization of restraint forces to conservatively simulate initial release conditions and missile transport within the injection domain. The mechanistic treatment allows for the inclusion of both vertical and horizontal restraints and considers tornado translatory effects.

3.4.1 Injection Domain Variables and Missile Release Criterion

As illustrated in Figure 3-11, the injection domain is the region in which the missile is generated. Since most potential missile sources are at or near the ground surface, the injection domain extends laterally over the ground surface and roughly parallel to the ground/structure profile. For the purposes of analytical modeling, it is useful to define a missile transport probability event space in which the missile either: (1) remains entirely in the injection domain, or (2) successfully escapes the injection domain into the trajectory domain. As suggested in Figure 3-11, there are a number of possible event sequences which comprise this mutually exclusive probability event space. Potential missile m_i could interfere with missile m_j and terminate within the injection domain as depicted in event a. It could have unfavorable aerodynamic orientation and fall (event b) or become blocked by another object (event f), both resulting in transport termination within the injection domain. Alternately, missile m_i could experience favorable wind gusts and accelerate vertically (event c), be subjected to a favorable missile collision (event d), or experience a ramp

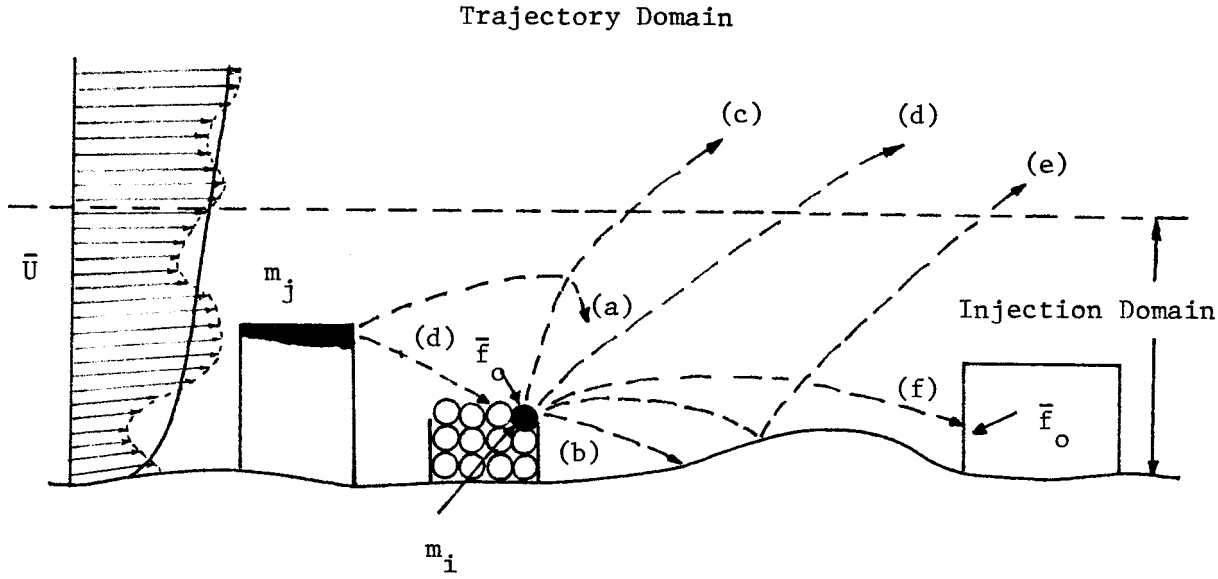

Figure 3-11. Hypothetical Injection Domain Events

injection (event e) and thereby escape the injection domain. These hypothetical event sequences imply that missile transport within the injection domain is significantly complex and involves a multitude of nonaerodynamic probabilistic event sequences. In terms of hazard assessment, the frequency of successful injection is directly related to the missile risk to plant safety components.

The methodology developed to simulate missile transport in the injection domain relies on probabilistic characterization of variables which specify the initial release conditions. Missile injection location in the horizontal plane within the specified origin zone (refer to Appendix 2) is assumed to be randomly distributed consistent with plant modeling and missile characterization methodology. This reflects the natural distribution of potential missiles and the effects of injection domain transport, similar to events a, b, and f in Figure 3-11, which tends to randomize missile location within the zone.

Missile injection elevation is an important variable since the height above the ground "datum" affects the chances for favorable trajectories and introduces potential energy of position. Missiles located at the top of a storage mode are much more likely to be injected than those on the ground surface. Considering the potential for multiple missile interference and debris source impacts, all missiles are conservatively assumed to be injected at the top elevation of that storage mode. For example, in Figure 3-11, all 12 missiles in the horizontal array are considered to be on the top row in the analysis of injection height statistics. The variable which has been identified as Z_s in Chapter 4 is thus utilized; this assumption ensures conservative exposure to favorable wind forces in the injection methodology. Missile orientation relative to the tornado windfield is possibly the most critical factor regarding successful missile escape from the injection domain. The initial orientation, as specified by the availability mode, provides information regarding the orientation of the $\hat{MCL}$ axis. For example, approximately 70% of the potential missiles in plant surveys described in Appendix 2 were observed to be stored with the $\hat{MCL}$ axis horizontal. If this initial condition is utilized, a minimum of the missiles would be injected due to the small lift forces generated for most of the potential shapes (e.g., cylinders and parallelpipeds). Simulation studies of injection indicate that such orientations result in the missile generally falling from the injection height Z_s. Another consideration in the specification of initial orientation is the fact that debris impact, storage characteristics, and ground interference tend to randomize the orientation of the missile. Vertical "lift-off" without rotation or contact with other objects is highly unlikely for the potential missile sets identified in Appendix 2. Thus, on the basis of the effects which tend to randomize missile orientation during the injection sequence and the unfavorable horizontal mode of the major missile sources, uniformly random spatial orientation is utilized. This assumption explicitly recognizes the characteristics of injection domain transport discussed previously; coupled with the placement of the missile at the

maximum storage height, it provides a conservative specification of initial missile spatial conditions. Finally, the near ground effect on aerodynamic coefficients (cf. Figure 3-3) is applied to a height of at least 5 ft. regardless of the magnitude of the missile diameter, d. This conservative modification recognizes the potential for near uniform missile storage heights ($\bar{Z}_s$ = 4.7 ft.) which may tend to provide an elevated "near-ground" effect.

For a particular missile position and orientation, motion is achieved when the restraining forces acting on the object are exceeded. The characterization of these restraints is specified by the random variable $\bar{f}_0$, as depicted in Figure 3-11. By postulating frequency distributions of $\bar{f}_0$, conditions which depict the original missile availability modes, subsequent wedging forces, missile weight, and friction forces can be considered in this approach. The effects of potential missile interactions and multiple missile contact forces suggest that $\bar{f}_0$ is at least partially dependent upon the events of separate missiles. This raises questions of missile dependence in the injection methodology and suggests that conservative models must be utilized in this part of the risk analysis because of the infeasibility of modeling correlated missile injection. In view of all these injection domain event possibilities, characterization of restraining force on the basis of mechanistic modeling is infeasible. The approach adopted here is to specify restraining force over a range which tends to optimize missile transport. Minimum restraint specification is not necessarily conservative since the missile may tend to fall before the maximum tornadic forces have arrived; whereas maximum restraint specification will result in many objects which do not displace at all. The question of optimum $\bar{f}_0$ specification is discussed in Section 3.4.4 and the results of a simulation study of variable restraining force are presented.

The initial velocities of the missiles in the injection domain are assumed to be zero. This follows the concept of optimizing the restraint force to account for the effects of missile collisions and debris impact which are assumed to break restraints and dislodge "trapped" objects. The likelihood

of imparting net favorable kinetic energy from one missile to another is considered to be unlikely and not an explicit modeling requirement of the initial release condition. Since in a missile-missile collision the energy lost by one body represents the maximum that can be transmitted to another, the use of a zero initial injection velocity is also consistent with this tradeoff.

Missiles generated from structural failures in the injection domain (m_j in Figure 3-11) also constitute a threat. As noted in Appendix 2, a number of non-tornado proof structures can exist in the vicinity of nuclear power plants, especially those undergoing construction activity. Damage to such structures with subsequent missile generation is well documented in the literature with photographic evidence (e.g., 3-51, 3-65, 3-66, 3-73). The injection domain variables described previously are also appropriate for structurally restrained missile sources. The main difficulty involves the prediction of the failure response mechanism and the subsequent missile characteristics of the failed elements. Photographs of structures that have been affected by tornadoes indicate a significant amount of structural debris remains in the immediate vicinity of the structure (e.g., 1-9, 4-52). Cases of structural missile sources being transported several hundred feet are also documented (e.g., 3-67). The complexity of structural response prediction to tornadic loads, the variation in construction practice, and the lack of detailed drawings of non-engineering structures imply that a simplified conservative characterization of structure missile sources is appropriate. The approach adopted here involves the conservative specification of missile parameters (numbers, set type, etc.) for all structure missile sources. The predefined missiles are then considered in the same manner as nonstructurally restrained missiles. The injection release point is consistent with the structure origin zone and height; the restraining force characterization is similarly optimized for missile transport considerations. This scheme is consistent with the probabilistic injection sequence and conservatively assumes failure of all non-tornado proof systems.

Utilizing the preceeding variables to specify the initial release conditions, a missile release criterion of first calculated exceedance of the restraining force is selected. That is, given the missile location and orientation, the missile is released to the trajectory model at a position where the calculated aerodynamic forces exceed the restraining force $\bar{f}_0^*$, where the asterisk denotes a particular sampled value from the appropriate density function $f(\bar{f}_0)$. This criterion ensures that the tornado is sufficiently close to the missile such that horizontal or vertical motion is imminent. Subsequent motion, which may involve ground collisions and ricochet, is evaluated by the random orientation transport model. In conjunction with the optimal specification of $\bar{f}_0$, this criterion provides for realistically conservative initialization of injection domain transport.

3.4.2 Envelope of Injection and Injection Zone

The potential for initial motion of an object in the injection domain is governed by the injection variables discussed previously and the relative tornado position and strength. In Figure 3-12, a tornado with direction defined by the angle τ is approaching a missile located at point m. The object displaces when the release criterion is met; this presumably occurs when the center of the tornado has moved from the assumed touchdown point S to the injection point I. If the direction of this tornado is maintained but its touchdown point is allowed to vary laterally, a set of such injection points is formed. This set will form a closed curve (or curves) called the envelope of injection. The region enclosed by the envelope is defined as the injection zone; for given $\bar{f}_0^*$, the tornado wind force can inject the missile only if the tornado origin (O_t) is within this zone. The zone

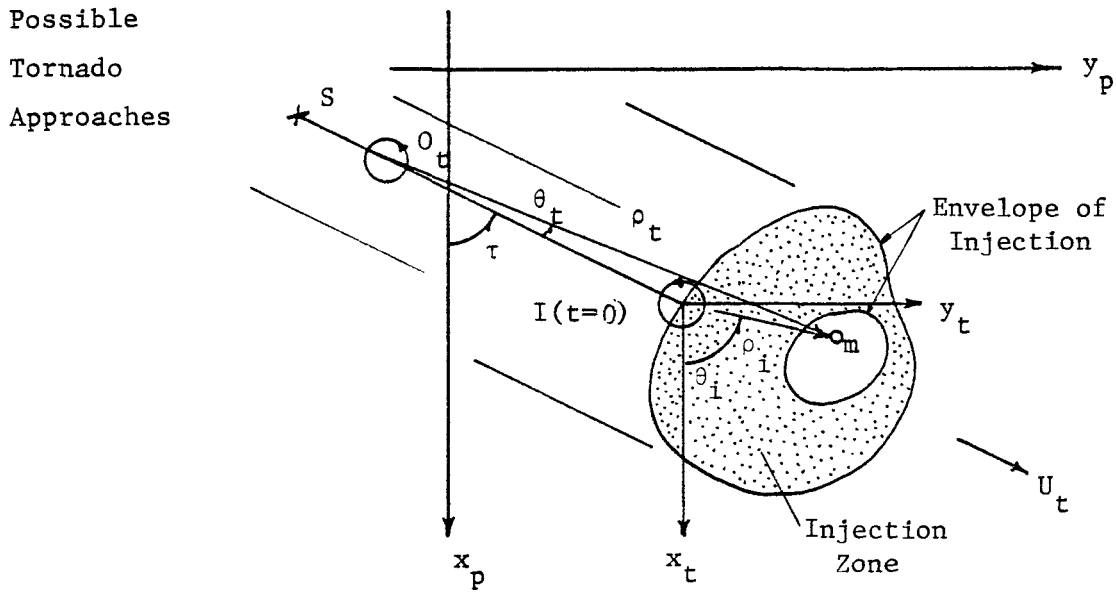

Figure 3-12. Envelope Of Injection and Injection Zone

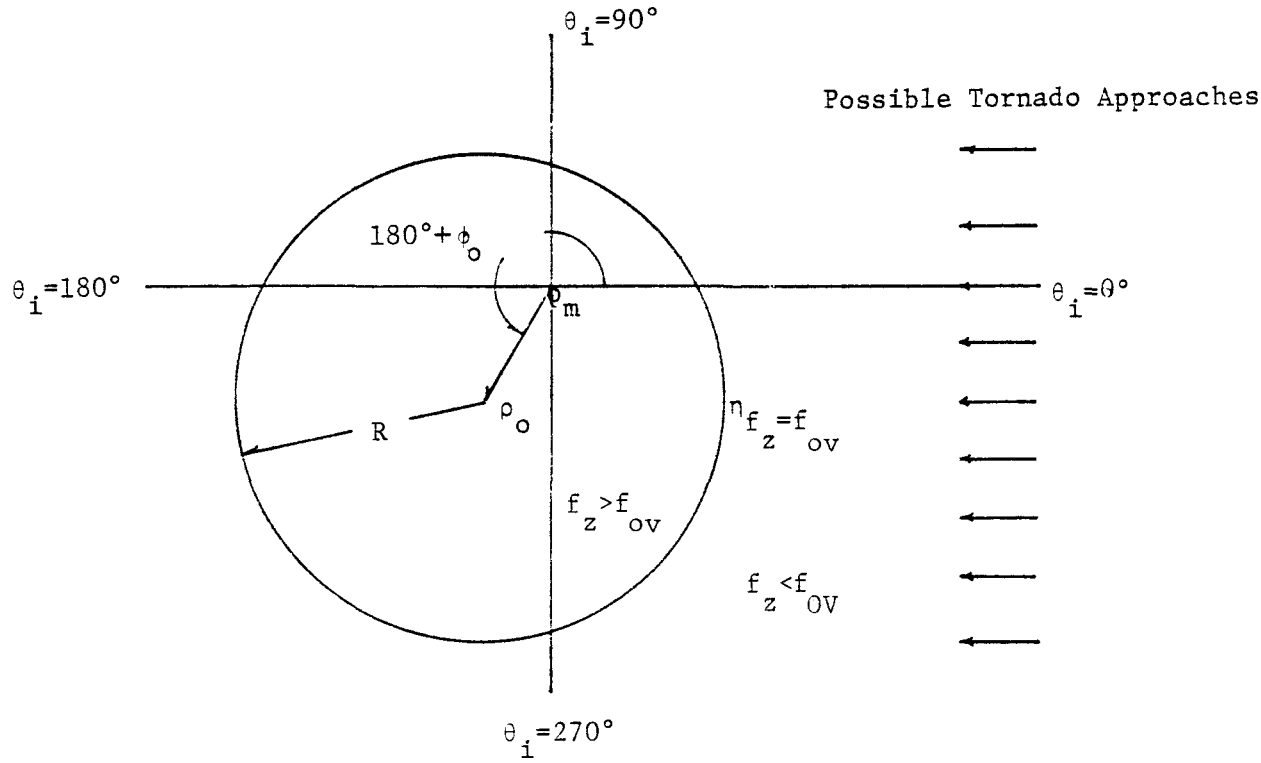

Figure 3-13. Injection Circle

can be singly or doubly connected depending on the missile orientation and characteristics, tornado description, and the value of $\bar{f}_0^*$. A doubly connected injection zone is shown in Figure 3-12.

With the tornado center at the injection point I and the missile at the polar coordinates (ρ_i, θ_i, z_0) relative to F_t, the injection criterion implies that

$$\bar{f} \geq \bar{f}_0^* \tag{3.12}$$

where $\bar{f}$ is the aerodynamic force. In this investigation, this release criterion is simplified by specifying that the missile restraints consist of two resultant forces, f_{OV} and f_{OH}, which represent the restraints in the vertical and horizontal directions. It is then assumed that release occurs when either

$$[f_R^2 + f_T^2]^{1/2} \geq f_{OH}^* \tag{3.13}$$

or

$$f_Z \geq f_{OV}^* \tag{3.14}$$

are satisfied. In the above, f_R, f_T, and f_Z are the F_{pc} components of the aerodynamic force. The decoupling of the restraining forces is conservative since it does not require that both restraints be exceeded. In addition, it simplifies the $\bar{f}_0$ specification consistent with the concept of optimizing $\bar{f}_0$ for maximum missile transport.

3.4.3 Mathematical Solutions of Injection Envelopes and Profiles

An analytical solution to the injection envelope has been obtained for a hypothetical missile with a uniform flight parameter subjected to the JPL windfield (1-48). The resulting equation governing the vertical injection envelope is

$$\rho_i^2 - 2\rho_o \text{Cos}(180° + \phi_o - \theta_i)\rho_i + \rho_i + \rho_o^2 = R^2 \tag{3.15}$$

where ρ_o, ϕ_o, and R are functions that are dependent on the windfield definition, flight parameter, and vertical constraint f_{OV}. Eq. 3.15 indicates that the vertical injection envelope of the hypothetical missile is a displaced circle of radius R with its center located at (ρ_o, 180° + ϕ_o, z_o) as shown in Figure 3-13. The displacement demonstrates the effects of the tornado translation speed U_T and the counter-clockwise rotation of the windfield.

For the general case of wind direction dependent missile coefficients, a numerical solution is required. Using the JPL wind model with a 242 mph rotational velocity, 40 mph transalation speed, and a radius to maximum rotational speed of 158.4 ft., solutions were generated for a beam shaped missile with geometry ratio L:d:b=20:4:1 (missile sets 7, 8, and 9). The missile, resting on its long edge, was placed at 0, $\pm \frac{r_m}{3}$, $\pm \frac{2r_m}{3}$, $\pm r_m$, and $\frac{4r_m}{3}$ offsets relative to the tornado traveling along the x-direction. Figure 3-14 depicts the horizontal aerodynamic force distribution for three lateral offset positions, namely for the zero, + r_m, and - r_m offset cases. All show double spikes, but they are not of equal value, and this is clearly due to the rotational nature of the wind, the translational movement, and the inward radial flow towards the tornado center. From these force distributions, a family of horizontal injection envelopes were generated and are shown in Figure 3-15 for horizontal contraints varying from 200-lb to 3000-lb. That the injection zone for small contraints is either clustered near the missile or far from the missile is consistent with the nature of the windfield. The displacement of the 3000-lb or larger injection zones as the tornado approaches the missile should also be noted and is due to the relation between translational and radial velocities. Injection envelopes and zones for the vertical contraints could be obtained in a similar manner, but due to the orientation of this particular missile and the wind model used, the vertical aerodynamic force was found to be small.

3.4.4 Specification of Restraining Force

To assess the characterization of missile restraints and the effect of injection domain interactions, a simulation study was performed. Using the first four missiles identified in Table 3-5 (utility pole, wood box, wood

sheet, and wide flange beam) and the standard 12 in. pipe missile, transport ranges and impact velocities were evaluated in conjunction with the first calculated exceedance criterion. Tornado number 1 in Table 3-5 with the mean translational velocity of 58.67 fps was employed in the simulations. A ground impact trajectory termination criterion for missiles which are falling (and not rising during the injection process) was employed in the study. Discussion of missile-ground interaction and the relationship of missile injection modeling and missile termination criteria is given in Section 4.4.2.

The force distribution presented in Figure 3-14 is characteristic of the "time-history" effect resulting from the translating tornado and suggests the difficulty in specifying missile restraints. For example, the specification of a horizontal restraint of 1000 lb. for the case of zero offset would result in a release when the tornado center is some 250 ft. from the missile. The resulting trajectory is likely to be much shorter than that associated with injection near the maximum wind speeds; if the missile were to stick in the gound or become "trapped" in the injection domain, the transport event could be potentially terminated. On the other hand, if the horizontal restraint is equivalent to 2500 lb., the missile would release very near to r_{max} (150 ft.) and the subsequent trajectory would generally have greater range and impact velocity. However, the specification of a 2500 lb. restraint would result in the missile not being picked up at all for the + r_m offset case. Thus, the tradeoff in terms of optimization of the restraint force involves maximizing transport at the expense of increasing the number of unsuccessful restraint exceedances.

The results given in Table 3-7 of the sensitivity study on horizontal restraint force confirm the above hypothesis of missile injection. In this study, the missiles were injected uniformly over the Z_s range from 0 to 20 ft. within the 73 mph wind boundaries. For the total attempted 6665 missile injections, the number of unsuccessful attempts increased as the horizontal restraining force is increased. For the heavier missiles (wide flange and pipe) the number of unsuccessful trials begins to dominate the results as the horizontal restraint approaches 5W, where W is the missile weight.

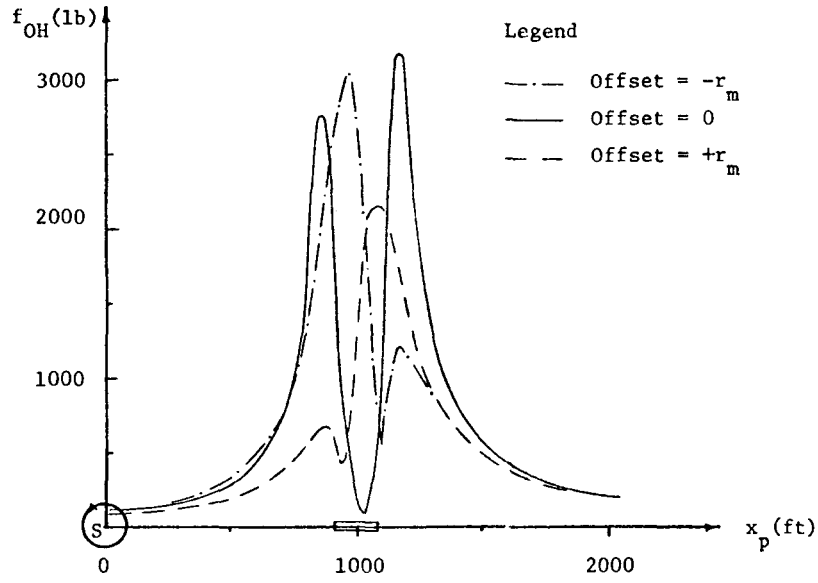

Figure 3-14. Force Distribution For Board Missile

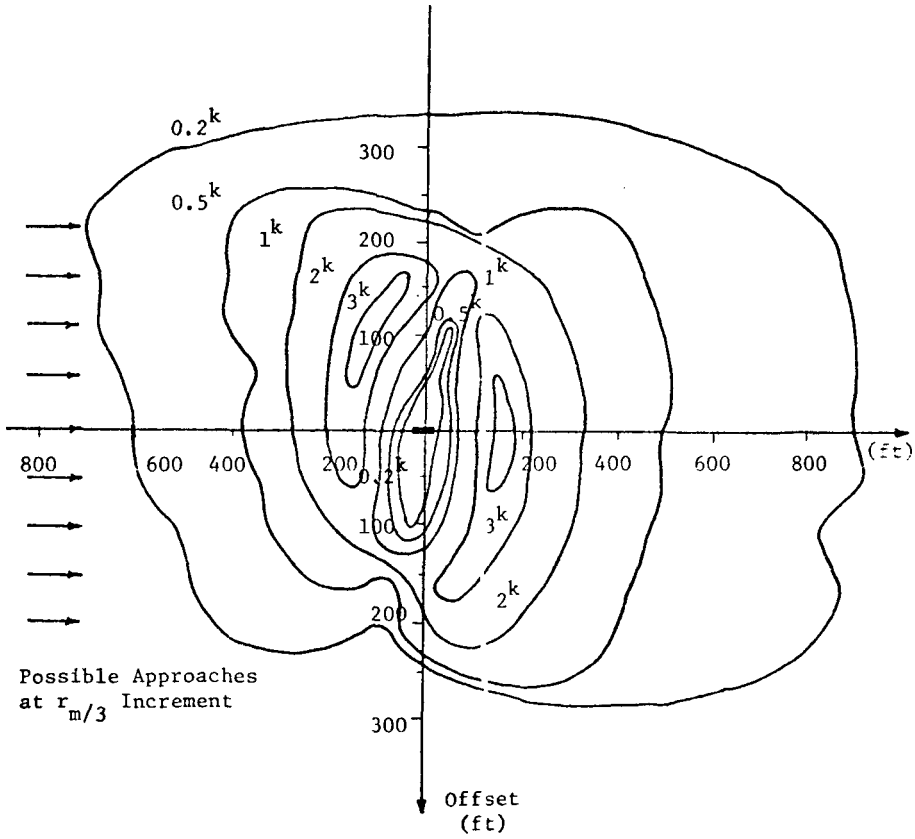

Figure 3-15. Injection Envelopes For Board Missile

Table 3-7. Restraining Force Simulation Results

Missile Type	Horizontal Restraint f_{OH}	Transport Range Conditional $\hat{D}$ (ft)	Transport Range Unconditional $\hat{D}$ (ft)	Impact Velocity $\bar{V}_i$ (fps)	Initial Successes	Number of Trials Unsuccessful Restraint Exceedances	Total	Percent Successful Injection
Utility Pole	0.5W	2.72	2.72	18.15	50	0	50	100
	W	6.77	6.77	23.16	50	0	50	100
	2W	19.05	8.50	39.71	50	62	112	45
	5W	146.22	19.73	105.35	100	641	741	13
Box	W	112.70	77.19	41.03	50	23	73	68
	2W	176.55	88.28	44.40	100	100	200	50
	5W	273.80	99.93	106.96	100	174	274	36
Sheet	W	23.65	23.65	29.44	50	0	50	100
	2W	45.65	44.75	39.33	50	1	51	98
	5W	67.69	59.38	65.19	100	14	114	88
Wide Flange	W	8.45	3.28	24.32	50	79	129	39
	2W	29.36	7.73	46.15	50	140	190	26
	5W	128.10	4.16	84.96	50	1489	1539	3
Pipe	0.5W	2.68	1.49	18.05	50	40	90	56
	W	5.14	2.01	22.51	50	78	128	39
	2W	24.09	3.51	42.17	50	293	343	15
	5W	113.40	2.24	92.86	50	2481	2531	2
Totals					1050	5615	6665	

For example, out of a total of 2531 trials for the pipe, only 50 successes were obtained. The study indicates that the mean range and impact velocity of the initial trajectory increases with increasing restraint. In all cases, the conditional range until initial ground impact ($\hat{D}$) and the impact velocity ($\hat{V}_i$) increase as f_{OH} is varied from W to 5W. Use of f_{OH} = 0.5W was also investigated for the two cylindrical missiles to simulate rolling friction (2-9) and the results follow the same pattern as previously indicated. For the purpose of specifying optimal horizontal restraint forces, the mean unconditional ranges presented in Table 3-7 are useful. These values are based upon the total number of attempted injections and thus provide a measure of optimality. For the heavier missiles, the unconditional mean transport range ($\hat{D}$) peaks within the range of f_{OH} = [W,5W]. For the lighter missiles, the restraints are exceeded even at f_{OH} = 5W and thus the total range increases with increasing f_{OH}. However, since horizontal restraints in excess of 5W are not expected for the majority of availability modes and the unconditional ranges of the heavier missiles (with better damage capability) peak for $f_{OH} < 5W$, the range [W,5W] is suggested as the bounds for optimal f_{OH} specification. This range provides for wide limits in the percentage of successful injections as noted in the last column of Table 3-7.

In this investigation, the vertical restraining force is conservatively specified as the missile weight. The use of vertical restraining forces in excess of missile weight is not justified considering the potential for injection domain interactions which may tend to displace or break vertical restraints. In addition, the use of $f_{OV} > W$ would not appreciably affect the results for the cases of $f_{OH} \leq 2W$ since horizontal exceedance generally occurs first. For example, in the case of f_{OH} = W, only 0, 4, 5, 2, and 0 histories out of the total number of trials for the utility pole, box, sheet, wide flange, and pipe, respectively, experienced vertical restraint exceedance first. For the cases of high horizontal restraints (e.g., f_{OH} = 5W) the number of unsuccessful trials significantly affects the unconditional ranges and the use of a higher vertical restraint would reduce the values further.

APPENDIX 4
MISSILE IMPACT METHODOLOGY

4.1 Introduction

The final event in a tornado missile event sequence involves the collision of the missile with the ground surface, a structure, a safety-related barrier, or another object. In a risk analysis, two questions concerning the impact event are pertinent. Does the missile still pose a threat to other components after the impact and, if the barrier is safety related, has the specified damage criterion been exceeded? The complex phenomenology of impact dynamics, the observed scatter in military ballistics tests under controlled conditions, and the virtual absence of oblique impact data for potential tornado generated missiles suggest that a combination of empirical, analytical, and probabilistic models are appropriate for the development of a general missile impact methodology. The major components of the impact assessment include the specification of damage criteria for reinforced concrete and structural steel barriers, the analysis of oblique and noncollinear impact orientation, the evaluation of existing damage models utilizing the recent impact test data, and the formulation of missile continuation criteria following an impact event. Since damage to a structure is the final event in that particular tornado missile-structure sequence, analytically derived expected values provide a basis for model development of damage assessment. Consequently, in the methodology development, the probabilistic inputs to the damage models are evaluated for the purpose of obtaining expected value approximations. Missile continuation events, such as ricochet, are probabilistically characterized since they define a new event sequence. A missile termination criterion based upon a sequence of ground impacts is established.

4.2 A General Basis for Missile Impact Assessment

The assessment of component damage and the possibility of missile continuation following an impact can be categorized in an event space defined by four mutually exclusive and collectively exhaustive compound events:

(1) (Structural Damage) $\sqcap$ (Missile(s) Continuation)

(2) (Structural Damage) $\sqcap$ (Missile Termination)

(3) (No Structural Damage) $\sqcap$ (Missile(s) Continuation)

(4) (No Structural Damage) $\sqcap$ (Missile Termination)

The basis for assessing which of these four event sequences occurs or the relative likelihoods of occurrence constitutes the missile impact methodology. For given tornado missile parameters, structure characteristics, and damage criteria, the most influential factors in the evaluation are the relative orientations of the missile axis and the velocity vector at impact. A normal impact with a collinear missile axis will most likely result in either event sequence 2 or 4, whereas a significantly oblique impact will ricochet without damaging the structure (event sequence 3). Thus, the prediction of damage and missile continuation likelihoods for oblique and noncollinear impacts are a major consideration in a generalized impact methodology.

Current design procedures for protection against missile impact effects conservatively specify the normal collinear missile orientation (4-57) and recent tornado missile impact tests (4-38, 4-55, 4-65) have simulated this case. Consequently, the methodology formulation for oblique and non-collinear impact must rely upon analytical modeling and available military data sources. Since the available damage analyses also assume normal collinear impact, the formulation for general impact conditions is developed externally to the specific model. In this section, characteristics of the missile impact event are summarized, a method for evaluating oblique noncollinear impacts is presented, and the significance of "offset" missile hits are analyzed.

4.2.1 Missile Impact Characteristics

An impact event denotes the collision of a translating and/or rotating mass with another body; it occurs in a small time interval, during which the two bodies exert on each other relatively large forces. For given missile and

velocity vector orientation, the impact load transient is a function of the inertial and stiffness properties of the missile and the structure. Two principal modes of damage to the structure can result from this load: local effects and overall structural response. Local damage includes the effects at the impact location and may consist of such phenomena as penetration, perforation, scabbing (backface material ejection), spalling, and punching shear. Due to the complex processes contributing to the transient stress state, the assessment of local effects is based upon empirically derived relationships. Local effects are largely independent of the dynamic characteristics of the structure, whereas the overall response is primarily controlled by such properties. The overall response mode includes flexure and reaction shear in regions other than the impact location. The prediction of the dynamic structural response is generally based upon an energy or momentum balance or the derivation of the impact forcing function. Currently, for tornado generated missiles the control of local effects is typically the dominating design consideration and generally ensures satisfactory overall response.

In addition to the types of damage which can result from the collision, the initial conditions which describe the missile impact event form a basis for categorizing impact phenomena. As noted previously, missile orientation and velocity direction significantly influence which impact event sequence will occur for a given missile-structure combination. For missiles whose length is significantly greater than depth (e.g., $L/d \geq 4$), a particle model is not appropriate and it is necessary to consider the direction of the missile axis ($\hat{MCL}$) as well as the velocity vector ($\bar{V}_i$) relative to the surface. The geometry of the impact conditions is given in Figure 4-1 in which the Z_s axis represents the outward normal to the surface. The angle θ measures the obliquity from the surface normal to the velocity vector of the center of mass of the missile; γ defines the angle of yaw and is a measure of the collinearity of the impact; and β is the angle from Z_s to the $\hat{MCL}$. Thus by definition, $\theta = 0$ for normal impacts and $\gamma = 0$ for collinear impacts. The range of variation of these impact variables is given by $\theta \in [0, \frac{\pi}{2}]$ and $\gamma \in [0, \pi]$. In a

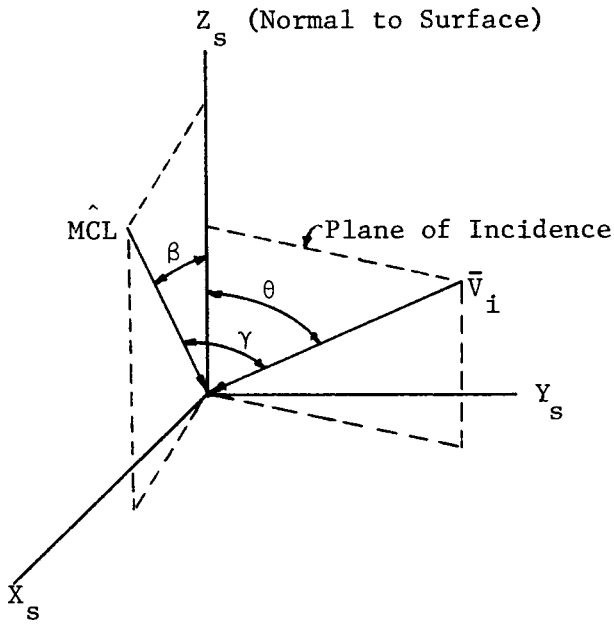

Figure 4-1. Missile Impact Geometry

risk assessment of tornado missile effects, limitation of the analysis to the conventionally postulated normal collinear case is inconsistent with the probabilistic formalism.

4.2.2 Oblique Noncollinear Impact Model

The significance of oblique impact in significantly reducing missile damage potential has been established in ordnance experiments. Reported military impact tests clearly indicate that obliquity tends to reduce penetration depth measured perpendicular to the target face. A tabulation summary presented in reference 4-23 for projectiles impacting reinforced concrete indicates that at 35° obliquity the normal component of the penetration depth is less than 50% of that corresponding to the equivalent normal impact case. It has also been observed that the random variations for oblique impacts are larger than those for normal impact (4-23). The effect of yaw is not well established, but it is expected to reduce the damage over that from collinear impact. Even for oblique collinear impact, no generally

applicable empirical formula has been derived. The problem is significantly more complex than normal collinear impact because of the presence of transverse forces and the onset of missile rotation. Missile rotation at the instant of impact should also tend to reduce damage potential.

Methods for evaluating oblique impact have generally been limited to the collinear case for which two basic approaches have been suggested. One procedure involves the transformation of the impact velocity V_i to an equivalent velocity V_i' as the input to the damage model. Since the component of the missile's momentum which is normal to the impacted surface is proportional to $\text{Cos}\theta$, several analyses (4-31, 4-40, 4-49) have utilized $V_i' = V_i\text{Cos}\theta$. Similarly, the missile's kinetic energy is proportional to V_i^2 and thus if damage is related to missile energy (e.g., 4-55), then $V_i' = V_i\text{Cos}^2\theta$ could also be employed (4-40). The second basic approach is simply to compute the oblique penetration path length, assuming no deviation from θ, and determine the normal penetration depth by $z' = z\text{Cos}\theta$ (e.g., 4-13, 4-22) or $z' = z'\text{Cos}^2\theta$ (5-7), where z is calculated utilizing V_i. Depending upon the damage equation selected, one or more of these techniques may provide the best fit to the available military test data. For example, consider the recent 45° oblique impact by a 12 in. pipe missile conducted by Sandia Laboratories (4-65). Utilizing the modified NDRC equation (4-57), the predicted normal penetration depths are 4.00 in., 2.83 in., 4.14 in., and 2.93 in. for the $z' = z\text{Cos}\theta$, $z' = z\text{Cos}^2\theta$, $V' = V\text{Cos}\theta$, and $V' = V\text{Cos}^2\theta$ approaches, respectively. Comparing these to the actual depth of 4.30 in. suggests that the $V' = V\text{Cos}\theta$ correction may be the most accurate for this missile-target combination. It should be noted that for similar tornado generated missiles in which the NDRC equation is applied, this approach is easily demonstrated to be the most conservative.

An analytical evaluation of the general case of oblique noncollinear impact based upon the LaGrange dynamical equations of motion has been presented by Beeth and Hobbs (3-16). Expressions are conservatively derived which give the normal and transverse components of the impulse the missile imparts to the target surface for the generalized coordinates θ and β (refer to Fig. 4-1).

The missile is assumed to rotate only in the plane of incidence and thus the condition $\beta = \theta$ defines oblique collinear impact. Assuming structure damage is proportional to the normal component of impulse, the following expression is obtained

$$V_i' = V_i[(1 - \frac{3}{4}\,\mathrm{Sin}^2\beta)\,\mathrm{Cos}\theta + \frac{3}{4}\,\mathrm{Sin}\beta\,\mathrm{Cos}\beta\,\mathrm{Sin}\theta] \qquad (4.1)$$

$$= V_i g(\theta,\beta)$$

Equation 4.1 reduces to $V' = V\mathrm{Cos}\theta$ for the collinear case and thus agrees with the frequently suggested approach for oblique collinear impact. In the above expression, the value of β which maximizes $g(\theta,\beta)$ for a given value of θ is determined from classical optimization techniques to be

$$\beta^* = \frac{1}{2}\theta \qquad (4.2)$$

and the resulting maximum is

$$g(\theta,\beta^*) = 1 - \frac{5}{4}\,\mathrm{Sin}^2\,\frac{\theta}{2} \qquad (4.3)$$

Thus, for a 30° oblique impact, the maximum normal impulse is achieved when the $\hat{\mathrm{MCL}}$ is 15° from the normal and equals 0.916 of the normal collinear impulse. It is slightly larger than the impulse of the 30° oblique collinear impact (0.866) which is given by the $\mathrm{Cos}\theta$ modification. This is illustrated by Fig. 4-2 in which comparisons of several $g(\theta,\beta)$ functions to the $\mathrm{Cos}\theta$ and $\mathrm{Cos}^2\theta$ corrections are presented. This model thus predicts higher maximum values of V' than that given by the other methods to evaluate oblique impact.

To investigate the total effect of angle of yaw variations, mathematical expectations of $g(\theta,\beta)$ have been numerically evaluated. The results are also indicated in Fig. 4-2 for two expected value calculations in which β was varied over the complete range of missile impact $[-\frac{\pi}{2}, \frac{\pi}{2}]$. The expectation identified as $E[g(\theta|\beta_{PL})]$ is based upon equally likely missile orientation in the plane of incidence. The curve denoted as $E[g(\theta|\beta)]$ assumes equally likely missile

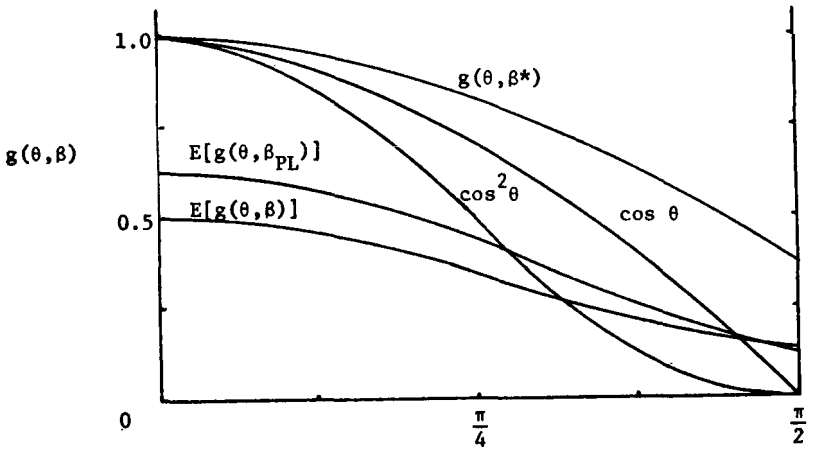

Figure 4-2. Equivalent Velocity Relationships

direction in spherical space; as anticipated, its values are lower than the planar expectations. Both of these curves indicate that the net effect of yaw is a considerable reduction over the maximum impulse at all obliquity angles. Comparison of the Cosθ correction to the expected value curves of Eq. 4.1 indicates that for obliquities less than 80°, the average effect of yaw is a significant reduction in the equivalent normal impact velocity. For the spatial orientation analysis, $E[g(\theta|\beta)]$, the effect of yaw is basically a $\frac{1}{2}$Cosθ reduction up to obliquities of 55°. On the basis of this analysis, the utilization of the theoretically derived equivalent velocity expressed by Eq. 4.1 is selected for this investigation. It provides a consistent analytical approach to oblique noncollinear impact and reduces to the generally employed Cosθ correction for oblique collinear impact; in addition, the expected values for general space orientation are in consonance with engineering judgement. Table 4-1 summarizes several of the results of this evaluation; an important conclusion is that the expectation over the complete ranges of both θ and β results in an equivalent velocity which is 28% of the normal collinear case. Thus, structural design loading conditions which assume a normal collinear missile impact velocity of magnitude $|V_i|$, have a nominal factor of safety of approximately 3.55 over the expected value equivalent velocity V_i'. The probability distribution function of $g(\theta,\beta)$ presented in Fig. 4-4

provides a further quantitative measure of the equivalent velocity impact likelihoods. It is noted that for a random impact there is only a 0.01 probability that $g(\theta,\beta)$ will exceed 0.89 and the chance of exceeding $0.96|V_i|$ is 0.001. For convenience, probabilities of exceeding several values of $g(\theta,\beta)$ are summarized in Table 4-2. By using Fig. 4-4 or Table 4-2, it is possible to determine the equivalent velocity reduction from $|V_i|$ for a specified design risk level.

4.2.3 Consideration of Finite Missile Size

Since the missile transport model tracks the center of mass of the missile, there are several considerations regarding the non-particle nature of real missiles in the impact methodology. The fact that the missile has some finite size implies a potential for impact although the trajectory of the missile center of mass does not intersect a surface of the target. As noted in the preceding section, such noncollinear orientations can result in significant impact loads. A simple analysis of the event depicted in Fig. 4-3(a) was conducted to determine the likelihood of such impacts. For $\theta \in [-\frac{\pi}{2},0]$, missile impact on surface AB is possible if $\bar{V}_i$ passes through the offset region, O_r, whose radius is equal to one half the missile length (L/2). Assuming fixed orientation during the time interval the missile center of mass is between points Q and Q', it can be shown that the probability of impact, $P(H_c)$, for equally likely $\hat{MCL}$ directions in spherical space is simply

$$P(H_c) = 1 - \frac{2c}{L} \quad , \quad 0 \leq c \leq \frac{L}{2} \tag{4.4}$$

where c is the perpendicular distance from $\bar{V}_i$ to point B. For $c \leq 0$, the missile must impact the surface and $P(H_0) = 1$, whereas for $c \geq \frac{L}{2}$, $P(H_{L/2}) = 0$. Assuming that the distance c of the trajectories which pass through this region are uniformly distributed $[0,\frac{L}{2}]$, the expected value of the offset hit probability equals 0.5. One method to consider such offset impacts would be to extend target areas past their actual dimensions and define successful impact as intersection of the velocity vector itself with this modified surface.

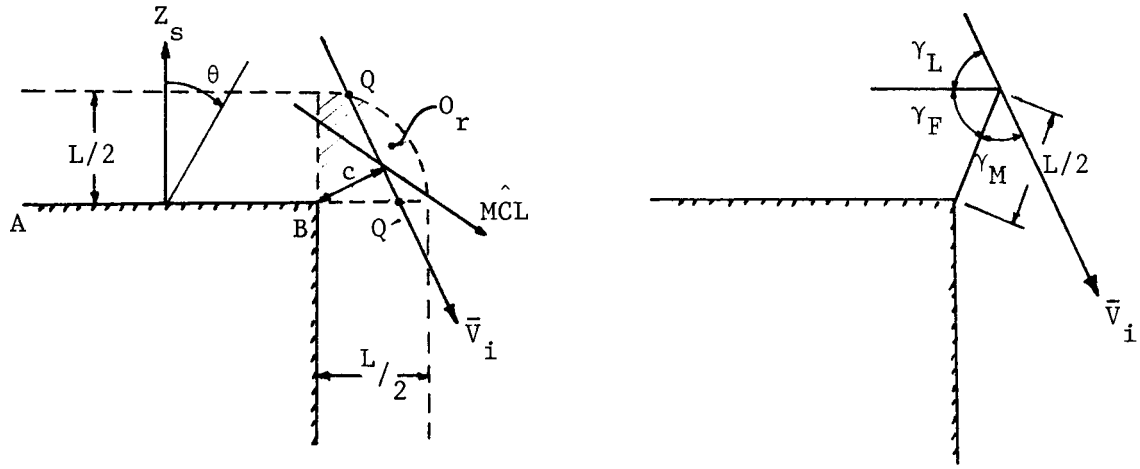

(a) Offset Zone (b) Angle Definition

Figure 4-3. Offset Missile Impact

Table 4-1. Special Case Summary for Oblique Impact

θ	β	$g(\theta,\beta)$	$E(g(\theta,\beta))$	$E[g(\theta,\beta)_{PL}]$
0	0	1	-	-
$[0, \frac{\pi}{2}]$	0	$\cos\theta$	0.500	0.637
$[0, \frac{\pi}{2}]$	θ	$\cos\theta$	0.500	0.637
$[0, \frac{\pi}{2}]$	$\beta^* = \frac{\theta}{2}$	$1 - \frac{5}{4}\sin^2\frac{\theta}{2}$	0.688	0.773
0	$[-\frac{\pi}{2}, \frac{\pi}{2}]$	$1 - \frac{3}{4}\sin^2\beta$	0.500	0.625
$[0, \frac{\pi}{2}]$	$[-\frac{\pi}{2}, \frac{\pi}{2}]$	Eq. 4.1	0.282	0.340

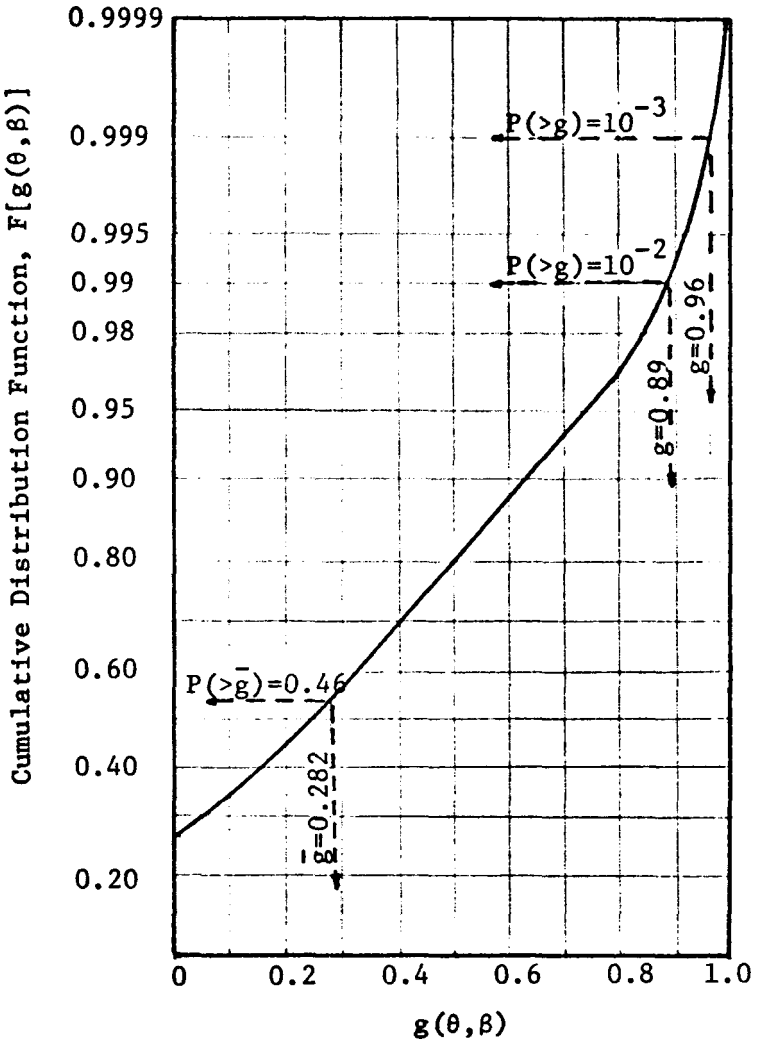

Figure 4-4. Probability Distribution Function of $g(\theta,\beta)$

Table 4-2. Equivalent Velocity Coefficient Exceedance Probabilities

$g(\theta,\beta)$	0.999	0.99	0.95	0.9	0.5
$P[g>g(\theta,\beta)]$	5.78×10^{-7}	1.07×10^{-4}	2.02×10^{-3}	7.97×10^{-3}	2.14×10^{-1}

4.3 Missile-Structure Interaction Models

The criterion adopted for damage success and the impact characteristics of the missile and target are the primary inputs to the missile-structure interaction analysis. Alternative local damage criteria include, in order of increasing conservatism: safety component damage as a result of missile impact, barrier perforation, barrier backface scabbing, barrier penetration or cracking, and frontface contact. Thus, if barrier or component frontface contact events can be demonstrated to be "rare" events, a more refined damage criterion is not necessary. However, for sizeable structures, such frontface contact events may occur relatively frequently given a tornado strike and a more realistic damage criterion is warranted. Thus, in this investigation, damage event success will include barrier or component contact in addition to a conventional safety based criterion of damage. Consistent with current barrier design procedures (4-7), backface scabbing of reinforced concrete barriers and perforation of steel barriers will be utilized. The potential for overall structural response damage is not assumed to be the primary design consideration. Consequently, the design parameters relating to overall response failure are delegated to the role of decision variables independent of the local effects analysis to determine barrier thickness. However, in order to facilitate input load characterization for an overall response analysis, frequency distributions of input force and energy parameters will be constructed. Considering the complexity of overall response analysis and the fact that local effects frequently govern the barrier design process, this approach is reasonable for a simulation analysis. Since the missile-structure interaction models that are applicable to tornado missiles assume normal impact condition, utilization of Eq. 4.1 provides the necessary velocity component input to the missile-structure interaction assessment.

4.3.1 Local Effects Analysis in Reinforced Concrete

Available models for predicting local damage effects in reinforced concrete barriers have generally been developed from ordnance applications. Although some of the formulas have a partial theoretical basis, they are

primarily empirically derived from tests involving nondeformable ogival-shaped projectiles. The frequently employed models include the modified National Defense Research Committee (NDRC) formula (4-23), the Modified Petry formula (4-11, 4-13, 4-18), the Army Corps of Engineers formula (4-14), the Ballistic Research Laboratory expression (4-14), and the Amman and Whitney formula (4-61). Numerous reviews and comparisons of these formulas in nuclear safety applications have been made (4-40, 4-46, 4-70, 5-7) with arguments being offered for the use of one or the other. Recently, utilization (4-46, 4-57, 4-65) of the modified NDRC expression suggests its acceptance as the most reliable expression for predicting damage due to steel missiles in the velocity range associated with tornado or turbine missiles. The recent experimental tests for reinforced concrete barriers (4-38, 4-55, 4-65) provide a basis for assessing the accuracy of penetration models for potential tornado missiles. Comparison of the predicted penetration, perforation, and scabbing thicknesses with the actual data supports the utilization of the NDRC formula over the other models listed above (4-46, 4-57). In addition to these models, empirical relationships to predict backface scabbing for potential tornado missiles have been proposed by Rotz (4-38) on the basis of a series of impact tests (4-37). The formulas for pipe and rod missiles which were developed provide close fits to the data and offer a possible alternative approach to the use of the NDRC model for predicting scabbing threshold. Thus, from the array of possible local damage models, the modified NDRC and Rotz formulas are considered as potential choices for utilization. In the following, the prediction accuracy, the effect of statistical strength variations in concrete barrier design, and applicability to other shapes and missile types are briefly considered for both models.

4.3.1.1 Tornado Missile Impact Data Base

Missile penetration in reinforced concrete has been extensively studied in military applications; experimentation dates back to the nineteenth century. A major characteristic of terminal ballistics is that even under well controlled conditions, the data is significantly scattered for the

transition and hypervelocity impact regimes. Recently, a series of low-speed impact tests for potential tornado generated missiles have been completed (4-38, 4-55, 4-65). These results also indicate the existence of "noise" in the penetration events for similar conditions; however, the prediction error associated with the threshold scabbing event is relatively small.

A total of 28 impact experiments involving 1 in. steel rods (8 tests), 8 in steel slugs (8 tests), 8 in. steel pipe (9 tests), and 8 in. wood poles (3 tests) were conducted for Bechtel Corporation (4-37, 4-38). The concrete panels ranged from 3 to 24 in. thickness and tests were conducted for both midspan and quarter point impact for the 8 in. missile tests. No significant difference in the resulting damage was noted for this variation in impact location. In general, the steel pipes produced less scabbing damage than the steel slugs although the pipes penetrated deeper. From these results, a total of eight tests are associated with producing threshold backface scabbing. These are noted in Table 4-3 (numbers 1-8) and were characterized by Rotz (4-38) as producing either "light" or "incipient" scabbing damage. The ratios of observed penetration depth (z) to missile diameter (d) and scabbing thickness (s) to missile diameter are also noted in the table.

A series of full scale impact tests have recently been completed by Sandia Laboratories (4-65) for EPRI. Of the eighteen tests on 12, 18, and 24 in. panels, two involved 13 in. utility poles, two utilized 1 in. rebars, one employed a 3 in. pipe and the remaining thirteen used a 12 in. pipe as the tornado missiles. Of these tests, a total of four experienced backface flaking and are thus conservatively considered as threshold scabbing (See Table 4-3). All of the tests were conducted for normal collinear impact with the exception of one 45° oblique collinear impact (4-65).

A one-quarter scale test program was performed for Stone and Webster (4-55) for several missile types and barrier designs. A total of 48 tests agaist 22 panels utilized steel pipes (36 tests), steel slugs (8 tests), and wood poles (4 tests). The results suggest that pipe wall thickness is an

Table 4-3. Threshold Scabbing Data and Predicted Values

Obs. No.	Missile Type	Reference No.	Reference Test	Penetration Obs. $\frac{x}{d}$	Penetration NDRC Predicted[a] Prior $(\frac{x}{d})_N$	Penetration NDRC Predicted[a] Posterior $(\frac{x}{d})''_N$	Scabbing Obs. $\frac{s}{d}$	Scabbing Rotz Predicted[b] Prior $(\frac{s}{d})_R$	Scabbing Rotz Predicted[b] Posterior $(\frac{s}{d})''_R$	Scabbing NDRC Predicted[a] Prior $(\frac{s}{d})_N$	Scabbing NDRC Predicted[a] Posterior $(\frac{s}{d})''_{N_e}$
1	1" Rod	4-38	2	1.60	1.84	1.75	6.0	6.77	6.29	4.62	4.50
2	1" Rod	4-38	8	1.23	1.410	1.34	6.0	6.30	5.86	4.03	3.97
3	8" Slug	4-38	18F	0.375	0.518	0.493	2.25	2.20	2.05	2.73	2.66
4	8" Slug	4-38	12F	0.25	0.920	0.875	3.0	3.17	2.95	3.37	3.31
5	8" Pipe	4-38	16F	0.50	0.494	0.470	1.5	1.58	1.55	2.67	1.77
6	8" Pipe	4-38	6F	0.925	0.754	0.717	2.25	2.22	2.17	3.15	2.26
7	8" Pipe	4-38	8F	1.00	1.09	1.04	3.0	2.98	2.91	3.60	2.87
8	8" Pipe	4-38	9F	1.19	1.13	1.07	3.0	3.14	3.07	3.66	2.95
9	12" Pipe	4-65	"Flaking"	0.342	0.448	0.426	1.5	1.58	1.55	2.45	1.63
10	12" Pipe	4-65	"Flaking"	0.442	0.436	0.415	1.5	1.56	1.52	2.48	1.61
11	12" Pipe	4-65	"Flaking"	0.292	0.294	0.280	1.5	1.26	1.23	1.89	1.33
12	12" Pipe	4-65	"Flaking"	0.325	0.289	0.275	1.5	1.23	1.20	1.86	1.32
13	3" Pipe	4-55	17	0.067	0.361	0.344	2.0	2.29	2.13	2.20	2.12
14	3.5" Pipe	4-55	21	0.429	0.404	0.384	1.71	1.62	1.58	2.37	1.52
15	3" Pipe	4-55	22	0.500	0.595	0.567	2.0	2.15	2.10	2.92	1.87
16	3" Pipe	4-55	24	0.123	0.465	0.442	2.0	2.36	2.20	2.58	2.51
17	3" Pipe	4-55	30	0.623	0.615	0.585	2.0	2.27	2.21	2.95	1.92
18	1.75" Pipe	4-55	40	1.08	1.456	1.38	3.43	4.39	4.29	4.10	3.59
19	3" Pipe	4-55	41	0.67	0.438	0.416	1.5	1.90	1.85	2.49	1.53
20	3" Slug	4-55	42	0.333	0.261	0.248	1.5	1.90	1.76	1.72	1.65
21	3.5" Pipe	4-55	43	0.257	0.288	0.274	1.29	1.36	1.32	1.86	1.30

Notes: (a) N subscript denotes modified NDRC formula; N_e subscript denotes equivalent missile diameter utilized.

(b) R subscript denotes Rotz formula.

important missile characteristic with regard to scabbing damage. Nine of these results are interpreted in this analysis as corresponding to threshold scabbing. Those tests in which scab particles traveled less than one foot from the barriers are assumed to be the velocities associated with scabbing initiation. For penetration depth, the larger of the neck depth and the depth to solid plug ("c" and "d" dimensions, respectively, in Fig. 2.4.1 of reference 4-55) is utilized as the observed value summarized in Table 4-3.

4.3.1.2 Damage Models with Bayesian Estimators

The previous data summary provides a direct means of assessing the accuracy of the Rotz scabbing formulas and the modified NDRC expressions in predicting tornado missile damage. The predicted scabbing thickness for pipes is derived by Rotz (4-38) as

$$s = K_1 \frac{W^{0.4} V_i'^{0.65}}{f_c'^{0.5} d^{0.2}} \tag{4.6}$$

where W = missile weight (lbs), V_i' = equivalent impact velocity (fps), f_c' = concrete compressive strength (psi), d = missile diameter (in), K_1 = 5.42 (empirical constant), and s = concrete thickness for scabbing threshold (in). For solid steel missiles, the suggested relationship is

$$s = K_2 \frac{W^{0.4} V_i'^{0.5}}{f_c'^{0.5} d^{0.2}} \tag{4.7}$$

where K_2 = 15.5. Using these expressions, the predicted values of s/d for the 21 threshold scabbing tests have been calculated and are presented as the Rotz prior values in Table 4-3. Graphical illustration of the accuracy of these models is presented in Figure 4-5(a). As noted, predicted s/d values which are larger than the observed values (and thus fall below the

line) are unconservative. A classical statistical analysis of this prediction error suggests that the values of predicted scabbing thickness are slightly unconservative when the additional thirteen tests (not used in Rotz's development) are considered. To rationally incorporate this additional data, a Bayesian analysis, which relates the posterior distribution to the prior distribution and the sample-likelihood function, has been performed. Utilizing the "new" impact test results (4-55, 4-65), the posterior estimate of the mean values of K_1 and K_2 in Eqs. 4.6 and 4.7 are thus obtained through application of Eq. 3.20. It is assumed that K_1 and K_2 are normally distributed and that the prior distribution of the mean is also normally distributed with prior means μ'_{K_1}=5.42 and μ'_{K_2}=15.5. The ratio of the standard deviation σ_K to the prior mean standard deviation σ'_μ is taken as two. This assumption is not particularly critical since the results vary only slightly for the expected range of $\frac{\sigma_K}{\sigma'_\mu}$. For K_1, the new data indicates that $\bar{K}_1$=5.26 from a sample of 10; for K_2, the tests suggest $\bar{K}_2$=12.97 for the three additional impacts. Utilizing these new sample results and the assumptions of normality, solutions of Eq. 1.19 yield posterior estimates of the mean of K_1 and K_2 as μ''_{K_1}=5.30 and μ''_{K_2}=14.42. Thus, the new data base provides an updating of the prior parameters which decreases the predicted scabbing thickness by 2.2% and 7.0%, respectively, for the pipe and rod formulas. A graphical comparison of observed versus predicted values using the posterior means for K_1 and K_2 is presented in Figure 4-5(b). Since this updating eliminates the slight potential for unconservatism and yields results which are comparable to the expected values, the above values of K_1 and K_2 are suggested in the use of Eqs. 4.6 and 4.7.

The modified NDRC formula for penetration depth (z) in reinforced concrete is given by

$$z = \begin{cases} [4K_bK_mWd(\frac{V'_i}{1000d})^{1.8}]^{0.5} & , \ \frac{z}{d} \leq 2.0 \\ \\ K_bK_m(\frac{V'_i}{1000d})^{1.8} + d & , \ \frac{z}{d} \geq 2.0 \end{cases} \tag{4.8}$$

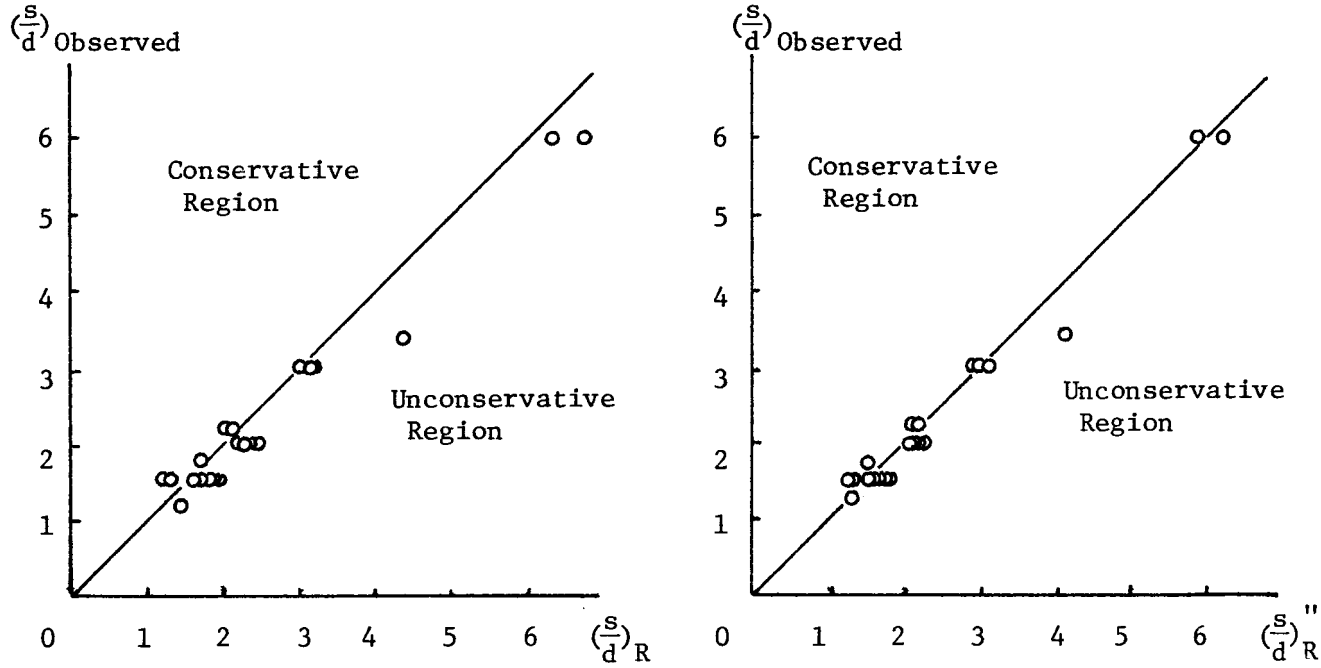

(a) Prior K_1 and K_2 Parameters

(b) Bayesian K_1 and K_2 Estimators

Figure 4-5. Comparison of Rotz's Model with Test Data

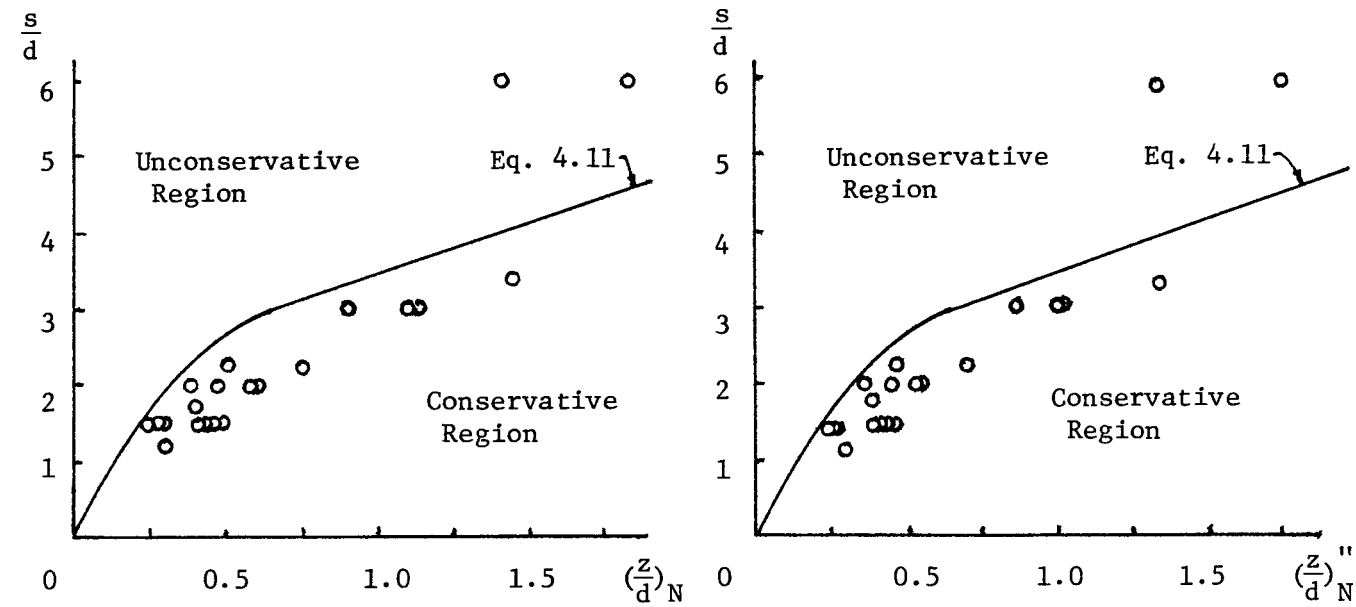

(a) Prior K_{b_1} Parameter

(b) Bayesian K_{b_1} Estimator

Figure 4-6. Comparison of NDRC Formula with Test Data

where K_m is the missile shape factor and is suggested as (4-46, 4-57)

$$K_m = \begin{cases} 0.72, \text{ Flat nosed bodies} \\ 0.84, \text{ Blunt nosed bodies} \\ 1.00, \text{ Average bullet nose (spherical end)} \\ 1.14, \text{ Very sharp nose} \end{cases} \tag{4.9}$$

and K_b is the concrete penetrability factor as given by

$$K_b = \frac{K_{b_1}}{\sqrt{f'_c}} \tag{4.10}$$

where K_{b_1}=180 (4-13, 4-46). The scabbing thickness (s) is related to penetration depth and missile diameter by

$$\frac{s}{d} = \begin{cases} 7.91\left(\frac{z}{d}\right) - 5.06\left(\frac{z}{d}\right)^2 , & \frac{z}{d} \leq 0.65 \\ \\ 2.12 + 1.36\left(\frac{z}{d}\right) , & 0.65 \leq \frac{z}{d} \leq 11.75 \end{cases} \tag{4.11}$$

as suggested by Kennedy (4-46). The relative accuracy of the NDRC model compared to the existing data is summarized in Table 4-3 and illustrated in Figure 4-6(a). The results suggest that the modified NDRC model is a very conservative predictor of scabbing thickness. Of the 21 tests, the NDRC formulas would have predicted scabbing for all except two tests, the 1" rods corresponding to s/d = 6. In order to modify the NDRC formula for tornado missile analysis on the basis of this recent series of tests, a Bayesian estimator for K_{b_1} was determined. The prior mean of K_{b_1} is assumed to be 180, as suggested by Kennedy (4-13, 4-69). From the 21 tests which produced scabbing, the sample estimate of $\hat{K}_{b_1}$ is 159.9. Assuming a normal

distribution for K_{b_1} and a conjugate normal distribution for the mean of K_{b_1}, the posterior mean of K_{b_1} is determined as $\mu''_{K_{b_1}} = 163$. In this analysis, the ratio of the standard deviations of the distribution ($\sigma_{K_{b_1}}$) to the mean (σ'_{μ}) is two. The resulting scabbing thickness values as a function of ($\frac{z''}{d}$) compare more favorably with the actual data as summarized in Table 4-3 and Figure 4-6(b). Thus, the Bayesian estimator $K''_{b_1} = 163$ is suggested for utilization in place of the prior value of 180.

In the previous use of the modified NDRC formula, the actual diameter for pipe missiles was employed and the results suggest that even the updated scabbing predictions are overly conservative. An alternate method was investigated in an attempt to yield a model which predicted the expected value for scabbing thickness. This approach employs the use of an equivalent diameter (d_e) for the hollow pipes defined simply as

$$d_e = 2\left(\frac{A}{\pi}\right)^{0.5} \tag{4.12}$$

where A is the actual missile contact area. The selection of the appropriate penetration equation (Eq. 4.8) is given by $\frac{z''}{d}$ and the scabbing formula choice (Eq. 4.11) is controlled by $\frac{z''_e}{d_e}$ where z''_e is the equivalent penetration depth using $K_{b_1} = 163$. For the pipe data in Table 4-3, the first of Eqs. 4.8 is applicable; the equivalent diameter scabbing relationship for this equation can be derived as

$$\frac{s}{d} = \begin{cases} 7.91\left(\frac{z}{d}\right)\left(\frac{d}{d_e}\right)^{0.4} - 5.06\left(\frac{z}{d}\right)\left(\frac{z}{d_e}\right)\left(\frac{d}{d_e}\right)^{0.8}, & \frac{z_e}{d_e} \leq 0.65 \\ 2.12\left(\frac{d_e}{d}\right) + 1.36\left(\frac{z}{d}\right)\left(\frac{d}{d_e}\right)^{0.4}, & \frac{z_e}{d_e} > 0.65 \end{cases} \tag{4.13}$$

Utilizing the posterior estimate of K_{b_1}, this equivalent diameter approach for pipes accurately predicts scabbing thicknesses as noted in Figure 4-7. The predicted values now are reasonable representations of an expected value model since they all do not fall below the observed data points. The linear relationship corresponds to the mean value of $\frac{d_e}{d}$ for the pipe impact tests. In summary, this analysis suggests that the use of the Bayesian estimator in the modified NDRC equations reasonably predicts the expected value result when coupled with the equivalent diameter approach for hollow pipes.

4.3.1.3 Model Utilization

The previous modifications to the Rotz and NDRC Equations provide a basis for predicting mean value scabbing thicknesses for the cylindrical missiles tested. The consideration of other missile shapes and materials and the significance of actual versus design target material strengths are considered here and approaches are suggested for model utilization.

In addition to the empirical concrete penetration constants (K_b), another variable which characterizes the reinforced concrete design resistance for impactive loads in the preceding equations is the compressive strength, f'_c. Design codes for reinforced concrete structures require field testing to ensure concrete compressive strength equal to or greater than that utilized in the design calculations (4-57). Thus, an expected value analysis for local damage should also reflect the expected statistical strength increase resulting from the code requirements. An illustration of this increase is seen in the recent Sandia missile impact tests (4-65) in which 3000 psi design mix had an actual mean strength of 3818 psi and a standard deviation of 409 psi. This is consistent with data reported by Neville (4-58) which suggests that for very good mix control, the minimum strength is of the order of 75% of the mean strength. It should also be noted that the barriers may have several years to cure (thus increasing f'_c) before commencement of reactor operation. To assess the significance of the as-built strength increase over

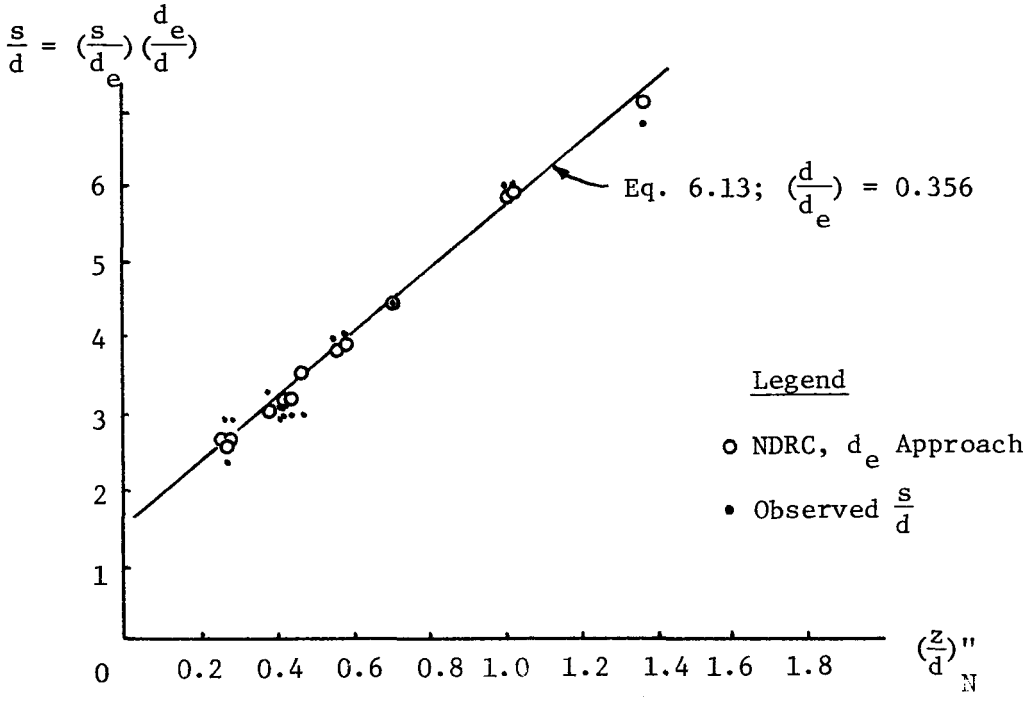

Figure 4-7. Equivalent Diameter Scabbing Predictions Compared to Test Data

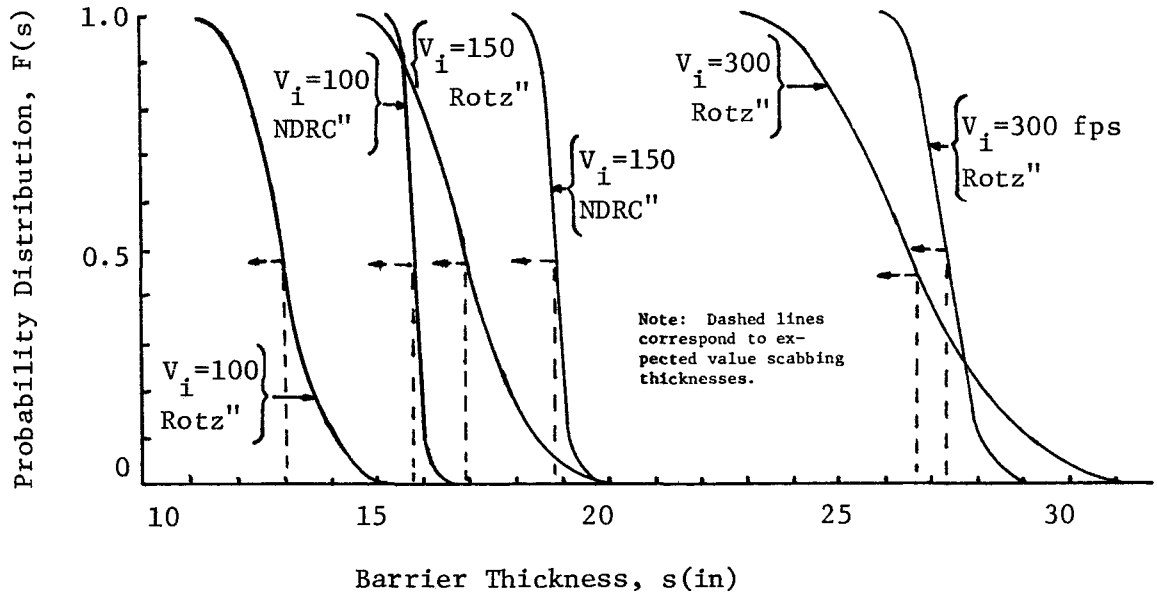

Figure 4-8. Derived Scabbing Thickness Distributions for 12" Pipe Missile with Concrete Strength = $N(4895,(600)^2)$

nominal design strength, probability distributions of scabbing thickness were derived for the Rotz and NDRC formulations (with updated Bayesian estimators) from assumed distributions of concrete strength. A concrete design strength of 4000 psi and the field mix standard deviation of 600 psi were utilized. Application of the ACI minimum strength requirements suggests an expected as-built strength of 4895 psi and a coefficient of variation equal to 12%. This is comparable to reported nuclear plant cylinder tests with a coefficient of variation equal to 11% and a standard deviation of approximately 500 psi (4-66). Assuming that concrete strengths are normally distributed (4-58), distributions of scabbing thickness were obtained from numerical integration of the transformed function (e.g., 6-28). The results are illustrated in Figure 4-8 for the standard 12 in. pipe missile impacting at 100, 150, and 300 fps. As noted, the derived probability distributions for the Rotz formula have a much wider range than the NDRC expression as a result of variation in concrete strength. The figure illustrates that the distribution functions are skewed to the right, a result of the scabbing function transformation for the normally distributed concrete strength. The significance of the strength variability can be assessed by comparing the expected value scabbing thickness to that obtained from using the nominal design strength, f'_c = 4000 psi. The mathematical expectations of these derived distributions were evaluated numerically and the results are summarized in Table 4-4. They indicate that the significance of actual concrete strength variation above the design value is not significant for the NDRC formula; only a two to three percent reduction in scabbing thickness results. The Rotz formula is slightly more sensitive to concrete strength variation and a nine to ten percent reduction in scabbing thickness is obtained. Thus, on the basis of this analysis for typical design conditions, actual strength exceedance over design strength is only moderately significant. Still, it is suggested that both models be modified by a scabbing thickness reduction factor (R_s) for use in an expected value risk analysis. These factors are estimated by R_s = 0.9 for Rotz's model and R_s = 0.97 for the NDRC model. Table 4-4 also indicates that the modified NDRC equation (using the equivalent pipe diameter) predicts slightly greater scabbing thicknesses in the

Table 4-4. Effect of Concrete Strength Variation

Impact Velocity (fps)	Scabbing Thickness[a] (in) 4000 psi Design Strength NDRC	Rotz	Expected Strength, N(4895,600) NDRC	Rotz
100	16.22	14.33	15.90 (.980)[b]	13.04 (.910)
150	19.34	18.67	18.87 (.976)	16.98 (.909)
300	28.18	29.26	27.30 (.969)	26.61 (.909)

NOTES: (a) For Standard 12" Pipe Missile.

(b) Numbers in parentheses are ratios (R_s) of expected value scabbing thickness to nominal design thickness.

velocity range of interest. Both models, with the updated parameter estimates, are reasonable choices for predicting local damage effects in reinforced concrete. However, since the NDRC formula has a partial theoretical basis and is more conservative in the low velocity region, it is utilized in this investigation with the updated parameters derived previously.

Although steel missile impacts on reinforced concrete are by far the greatest threat to the plant, the potential for impact by missiles of other material types must also be considered. The missile sets identified in Table 2-2 indicate that wood and concrete objects are also potential missiles at nuclear power plants. These materials are much more deformable than steel and have a tendency to shatter or collapse at impact, significantly reducing the damaging potential. However, because of the reduced density, they also have more favorable aerodynamic characteristics and thus could

contribute to the damage risk. Kennedy (4-69) estimates that a missile which shatters (but does not collapse) at impact, has a perforation thickness which is approximately 70% of that corresponding to a similar nondeformable missile. For high velocity projectiles, reference 4-61 suggests the following missile deformability factors (K_d) based on relative metal hardness: armor-piercing steel, K_d=1.0; mild steel, K_d=0.70; lead, K_d=0.50; aluminum, K_d=0.25. In the recent series of impact tests, the wood missiles produced no damage in the Bechtel tests (4-38) for 8 in. poles impacting 12 and 24 in. panels at 300 to 490 fps; impacts of 4 x 12 in. wood beams on 16 in. panels produced no damage at 352 and 280 fps (4-2); no damage was noted in the full scale utility pole test (205 fps) performed by Stephenson for EPRI (4-65); no backface scabbing was noted in model tests performed by Baker et al. (4-62); backface scabbing was noted in the quarter-scale Stone & Webster utility pole tests (4-55) only for two repeated shots which impacted a previously damaged area. In the absence of successful scabbing tests by wood on undamaged reinforced concrete panels, a simplified conservative analysis is made to estimate K_d for wood. Using the two Stone & Webster tests and the single EPRI test in which cracking was noted, estimates of K_{dw} are calculated as 0.17, 0.27, and 0.19. Since these are each upperbound estimates which did not actually cause scabbing as a result of a single impact, the smallest value (K_{dw}=0.17) is suggested as a conservative missile deformability factor.

The final missile-target material combination for a concrete barrier is the case of concrete or masonry missiles. Because of the small numbers of such potential missiles compared to the wood and metal sources (cf. Appendix 6), this case is expected to contribute negligibly to the damage risk. For generality, however, a reduction factor for concrete missiles (K_{dc}) is postulated as 0.5. This value is estimated from relative penetration coefficient values from the classical Robins-Euler formula (4-22). It is noted that these deformability factors are simple, conservative estimates and that the effects resulting from both wood and concrete impacts could be more accurately assessed using "soft" missile impact analysis techniques (4-46, 4-57).

A final consideration in the model utilization is the determination of an equivalent missile diameter for noncircular missiles. Utilization of an equivalent diameter (Eq. 4.12) based upon the projected frontal area has been suggested by several investigators (4-4, 4-46, 4-49, 4-57, 5-15). Since this method has been demonstrated to provide conservative results using the NDRC model for the circular pipe missile, it will also be utilized for the other missile sets. The impact area variable appropriate for this technique was obtained in the missile characterization study (A_{min}) as identified in Appendix 2.

4.3.2 Local Effects Analysis for Steel Targets

The second material classification group of possible targets is steel and may include piping, equipment components, pressure vessels, and barrier plates. The majority of the impact tests, particularly in the military domain, have involved small diameter steel rods or projectiles impacting relatively thin steel plates (4-23). However, test data is also available for wood poles (4-62), concrete rods (4-64), and steel disk fragments (4-29). The damage criterion that has been conventionally employed in the steel target formula development is perforation, which is also utilized in this investigation since it is consistent with regulatory guidelines (4-7).

Current procedures for estimating perforation thickness of steel barriers by steel missiles generally utilize the Ballistic Research Laboratory (BRL) formula (4-9, 4-14), the Stanford equation (4-14, 4-64), or the Hagg-Sankey model (4-29). Several comparisons of these alternative formulas have been made and each has been recommended for nuclear plant missile applications. Rotz (4-49) and Linderman et al. (4-4) suggest use of the BRL equation; the ASCE Committee on Nuclear Structures and Materials (4-57) recommends the Stanford equation as modified by Amirikian (4-11); and Johnson (4-70) suggests use of the Hagg-Sankey model for turbine missile fragments. Recent regulatory criteria provide acceptance of the BRL formula with a 1.2

factor of safety for tornado missiles. In view of the utility of the BRL formula, it is selected for use in this study and is presented as

$$e = \frac{W^{0.67} V_i^{1.33}}{10788 d_e K_b^{1.33}} \tag{4.14}$$

where K_b is the steel target penetration constant, normally taken as unity. The equivalent missile diameter is determined from Eq. 4.12 for non-circular and/or nonsolid missiles. As new tornado missile data becomes available, updated estimators of Eq. 4.14, or an alternative model, may be justified.

For reinforced concrete missiles impacting steel barriers, the Stanford data suggest a significant reduction in penetration capability. A simple approximation of the reduction factor for concrete missiles (K_{dc}) to be applied to Eq. 4.14 is suggested as

$$K_{dc} = \begin{cases} 0.5 - 0.0011 \dfrac{WV_i^2}{2gd}, & \dfrac{WV_i^2}{2gd} \leq 250 \text{ lbs} \\ 0.23, & \dfrac{WV_i^2}{2gd} > 250 \text{ lbs} \end{cases} \tag{4.15}$$

This expression provides for reductions between 0.5 and 0.23 in the low energy range for a given missile and for constant reduction of 0.23 above the transition. This reduction is consistent with the data reported in Figure 6.97 of reference 4-64.

Wilson et al. (4-62) conducted a series of 56 model tests of wood poles impacting sheet steel targets. Impact velocities were sought which produced threshold of perforation for each missile-target combination.

The authors applied an energy method based upon the deformed structure shape and derived the following perforation equation

$$\frac{\rho_m V_i'^2}{\sigma_y} = 1.751\left(\frac{e}{d}\right)\left(\frac{L}{d}\right)^{-1} + 144.2\left(\frac{e}{d}\right)^2\left(\frac{L}{d}\right)^{-1} \qquad (4.16)$$

where ρ_m = missile density and σ_y = yield stress of steel target. The coefficients were derived empirically from the wood pole impact tests and a plot of the data indicates excellent agreement. Replacing d by d_e in Eq. 4.16 and solving for perforation thickness yields

$$e = .005d_e\left[-1.21 + \left(1.46 + 1.92\,\frac{\rho_m L V_i'^2}{\sigma_y d_e}\right)^{0.5}\right] \qquad (4.17)$$

which is utilized for wood missiles impacting steel targets in this investigation. As a result of the large number of tests which this formulation is based upon, Eq. 4.17 is considered a better model for wood missiles than the reduction factors (K_d) previously employed.

4.3.3 Overall Response and Integrated Damage Methodology

Overall dynamic structural response, such as flexure and reaction shear, does not control the design of most tornado missile barriers. However, this cannot be established a priori in a risk analysis since the impacting velocity distributions of the various types of missiles is not known and the controlling response mode is highly dependent on these values. As noted previously, the barrier design parameters for dynamic response analysis are not considered directly in this investigation; however, simplified input which may be useful in characterizing an impulsive load is generated. In the following, the integrated damage assessment methodology, including consideration for overall response analysis, is presented.

4.3.3.1 Overall Response Considerations

Overall response analysis for impact loads is generally based upon either an energy/momentum balance or the derivation of the load forcing function. For the purpose of classifying the analytical methods, it is convenient to distinguish "soft" from "hard" missile impacts (4-46). Soft impact is characterized by significant local deformation of the missile or the target in the impact region; the stiffness properties of the missile or target are used to develop an impulsive load time history. A hard impact results in negligible local deformation; energy and momentum balance techniques are used to determine the maximum response (4-57). Response analyses for hard impacts are conservative since any energy absorption through local deformation is neglected. The consideration of overall structural response in a risk analysis must be limited to a simplified summary of loading information which may be useful input to the available analytical techniques, including dynamic and nonlinear analysis.

The first distinction in the overall response loading assessment is made by missile material type (steel, concrete, and wood) and target (steel, concrete) combination. Of these three material types, the steel missiles are the only group which are not expected to deform extensively at impact with concrete or steel barriers. The exception to this is the vehicle shape which will be conservatively assumed to be the only soft missile out of 15 steel missile sets (Refer to Table 2-2). Thus, wood, concrete, and vehicle impacts are considered as soft in which an overall response analysis technique which takes into effect missile deformability is appropriate (cf. Linderman (4-4), Riera (4-34), Rice (4-44), etc.). For these missiles, joint probability distributions of impacting velocity and mass will be constructed by missile material type to provide input for this type of analysis.

The potential for overall response damage to steel missile impacts will be evaluated by either a simplified soft target (rather than soft missile) or a hard impact method depending on the amount of target penetration. The

analysis of soft target impact follows the approach originally suggested by Williamson and Alvy (4-56); the exact form utilized follows the modification proposed by the ASCE Committee on Nuclear Structures and Materials (4-57). The basic concept is that the work done by the missile as it penetrates the barrier equals the initial kinetic energy. Assuming that the velocity varies linearly to zero as a function of time during penetration, the impact force is given simply as

$$F_i = \frac{WV_i^2}{2gz} \tag{4.18}$$

and the time of the impulse (t_i) is

$$t_i = \frac{2z}{V_i} \tag{4.19}$$

The joint distribution of these variables, $f(F_i,t_i)$, provides the necessary probabilistic loading input to design the structure for the resulting rectangular impulsive load. Following the suggestion in Reference 4-57, a predicted penetration depth greater than 15% of the target thickness (t_b) is considered sufficient to use this soft target technique. If the predicted penetration depth is sufficient to cause local damage (scabbing), then the above analysis for overall response is not enacted. Conversely, if the predicted penetration depth is less than 15% for steel missiles, then a hard impact analysis is considered appropriate.

A conservative simplified analysis of hard missile impact can be based upon conservation of energy and momentum (4-47) with assumptions regarding the barrier effective mass (M_b) and coefficient of restitution (e_r). Using the principle of conservation of momentum and the coefficient of restitution, the velocities of barrier (V_b) and missile (V_m) after impact are respectively

$$V_b = V_i' \frac{1 + e_r}{\frac{M_b}{m} + 1} \tag{4.20}$$

and

$$V_m = V_i' \frac{\frac{m}{M_b} - e_r}{\frac{m}{M_b} + 1} \tag{4.21}$$

The energy absorption capacity of the target must thus exceed

$$KE_b \geq \begin{cases} \frac{1}{2} M_b V_b^2 & , \frac{m}{M_b} \leq e \\ \\ \frac{1}{2} M_b V_b^2 + \frac{1}{2} m V_m^2 & , \frac{m}{M_b} > e \end{cases} \tag{4.22}$$

In this energy balance, it is conservative to use a lower bound of M_b determined from the target material with the effective missile diameter d_e. In the absense of experimental data for the basic missile shapes, the coefficient of restitution is taken as unity. In addition to this analysis for hard steel missile impacts, joint probability distributions of m and V_i also will be developed.

4.3.3.2 Integrated Damage Methodology

The missile structure interaction models previously discussed have been suggested for use with the basic missile sets presented in Appendix 2. The missile descriptive variables which are utilized in the damage assessment

include m, W, L, A_{min}, d, and S. With the missile impact velocity and orientation known at impact, Eq. 4.1 provides the normalized impact velocity component for "slender" missiles with $L \geq 4d$. For body type missiles, defined as shapes with $L < 4d$, collinear impact is conservatively assumed. The damage models which are utilized for specific missile target combinations have been identified; the integrated methodology is summarized in Figure 4-9. The prediction of local damage for given barrier properties has been emphasized although simple loading information for use in overall response analysis can also be extracted from a risk analysis. Naturally, for unprotected components or targets which are rarely impacted, the damage criterion that missile contact is equivalent to failure, may be appropriate.

4.4 Missile Continuation and Termination Events

The potential for missile continuation following a ground surface or barrier interaction is the second event of interest in the impact event sequence discussed in Section 4.2. For a given impact, the missile either perforates, sticks, rebounds, or ricochets off the surface. Missile termination occurs if the missile actually sticks in the target or ground surface; rebound from a normal impact, rocochet from an oblique impact, or complete barrier perforation with residual velocity all constitute events in which the missile's initial kinetic energy has not been totally absorbed. For practical purposes, missile continuation following most impact events is not expected to be a significant contribution to the damage risk. However, for a general assessment of missile continuation events and missile termination, it is convenient to consider structure or barrier interactions separately from ground interaction. Structure impacts involve questions of damage, as well as missile continuation, in which the missile potential energy above the ground "datum" after impact may pose a threat to other systems. Ground interactions represent potential loss of all kinetic energy as well as the loss of all potential energy of position and thus constitute the logical termination event. In the following, missile continuation methodology for structural interactions and an assessment of missile termination for ground interactions are presented.

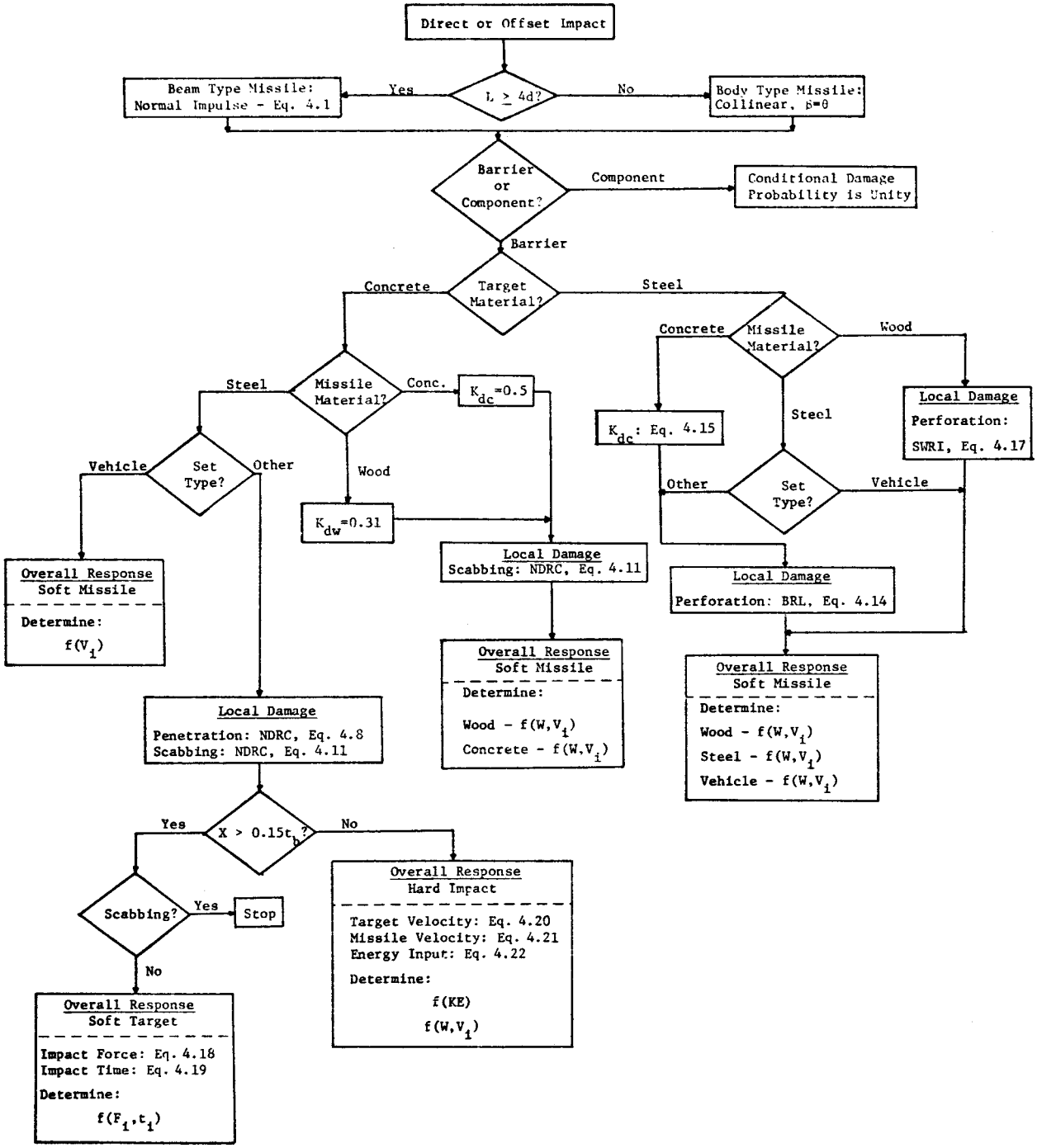

Figure 4-9. Missile Impact Methodology

4.4.1 Missile-Structure Continuations

Potential missile continuation events for structure interactions can be conveniently illustrated by ballistic limit curves (4-23). A typical relationship for a thin slab concrete barrier is indicated in Figure 4-10. It is noted that the perforation, sticking, and scabbing limit curves cross the zero obliquity axis normally. Also, for a given obliquity, perforation also requires a higher velocity than sticking or scabbing; however, the relative location of the sticking and scabbing curves may interchange depending upon slab thickness. Ricochet will occur for a given impact velocity when the obliquity becomes great enough; the ricochet limit increases sharply with obliquity. Although perforation and ricochet cannot, by definition, occur simultaneously, Figure 4-10 indicates that it is possible for both scabbing and ricochet to occur. Military tests suggest that the ricochet limit is a function of missile nose shape, length, and concrete strength.

The available impact data for identified tornado generated missiles does not permit the development of such sticking and ricochet limit curves. However, for the conservative backface scabbing (concrete) and threshold perforation (steel) criterion of damage, the majority of missile continuation events are not expected to contribute significantly to the risk of externally generated missiles. The hypothetical missile impact events presented in Figure 4-11 suggests the relative unimportance of most continuation sequences. A plan view of hypothetical missile impact sequences on vertical walls is illustrated in part (a); missile trajectory (i) perforates the barrier; missile path (j), a highly oblique ricochet from wall AB, impacts wall BC in a near normal intersection; missile path (k) ricochets from wall AB and impacts BC at a significantly oblique angle; missile rebound (l) does not stick or perforate AB and travels toward wall CD. Of these possible sequences, path j is the only continuation event of practical importance since the energy loss on AA is minimal and the subsequent hit on AB is a near normal $\bar{V}_i$. Perforation (event i) results in a damage probability of unity from the conservative damage criteria and the sequence is terminated; path k is not a significant

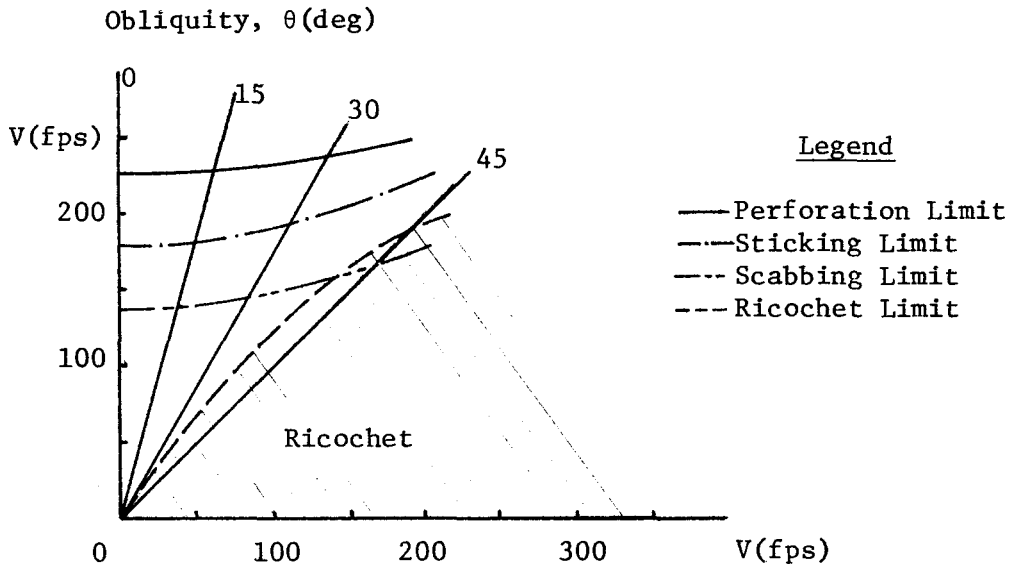

Figure 4-10. Ballistic Limit Curves for Concrete Barrier

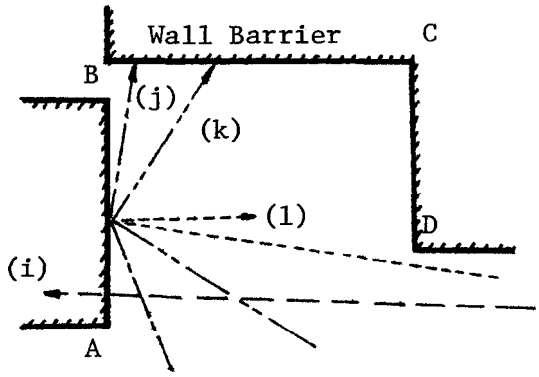

(a) Horizontal Plan

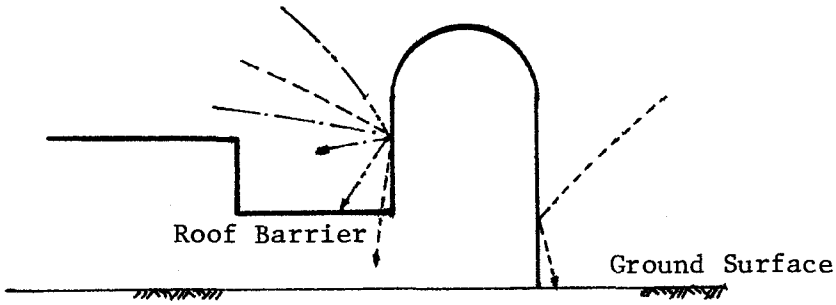

(b) Vertical Plane

Figure 4-11. Hypothetical Missile Continuation Events

continuation threat due to the two consecutive oblique impacts and energy loss sustained on wall AA; low rebound velocities of recent test data from normal impacts (4-37) support the hypothesis that path 1 is an unlikely threat to barrier CD. Consequently, for vertical barriers, highly oblique missile ricochet appears to be the most significant missile continuation event. The vast majority of the ricochets will not subsequently impact vertical walls as a result of the typical rectangular plant layout geometry. In Figure 4-11(b), possible trajectory paths in a vertical plane are illustrated. Missile continuation is important in this case by virture of the missile potential energy. In particular, if there are safety related components below the impact point, gravity, even without tornado energy sources, ensures a damage potential. Oblique ricochets with potential for subsequent normal roof impacts pose the greatest threat.

Based upon these considerations, a conservative criterion for missile ricochet would be one which permitted continuation for all non-perforation events and which favors oblique angles. In the absence of experimental data for the shapes of interest (particularly large L/d missiles) and considering the likelihood of noncollinear rotating missile impact, probabilistic characterization of missile ricochet direction is appropriate. A simple analytical solution of oblique central impact for smooth, frictionless bodies gives the angle of ricochet as

$$\alpha = \tan^{-1}(-\frac{1}{e}\tan\theta) \tag{4.23}$$

which reduces to $\alpha=\theta$ for the perfectly elastic case (e=1). Figure 4-12 indicates that the ricochet angle α increases as e reduces; the maximum deviation from the $\alpha=\theta$ case occurs at

$$\theta = \text{Cos}^{-1}(\frac{e-1}{e^2-1})^{1/2} \tag{4.24}$$

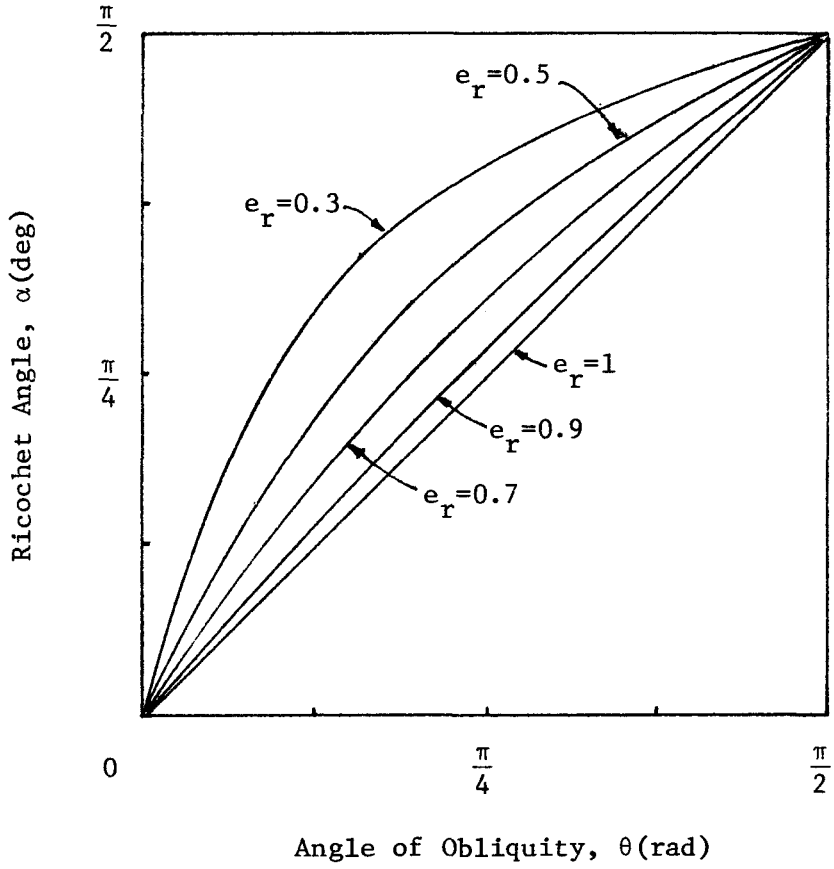

Figure 4-12. Ricochet Angle Function for Various e_r

Thus, this idealized analysis indicates that impacts which are nonelastic may experience greater obliquity in the ricochet angle. The above considerations suggest that $(\theta, \frac{\pi}{2})$ probability density function bounds for α are reasonable and should provide a conservative ricochet direction characterization. Considering this result, the expected nonelastic type impacts and the conservatism of an oblique bias in ricochet, the uniform interval $\alpha=\theta$ to $\alpha=\frac{\pi}{2}$ is suggested for the ricochet direction probability density function. Although large L/d missiles may actually rebound, rather than ricochet for oblique impact, this characterization is considered conservative for the aforementioned reasons. In this approach, coplanarity with the surface normal is assumed.

In view of the expected small risk contribution of a missile causing damage as a result of impacting more than one barrier, the magnitude of the missile ricochet velocity (V_m) is estimated from a simple energy balance

$$V_m = (\bar{V}_i^2 - V_i'^2)^{1/2} \tag{4.25}$$

With this magnitude and the previous characterization of ricochet angle, missile impact ricochets can be simulated.

4.4.2 Ground Interaction and Missile Termination

A missile interaction with the ground surface could result in a semi-elastic type ricochet, a plastic impact in which the missile is still available for regeneration, or loss of availability because of missile impact damage or a sticking position resulting in insurmountable restraining forces. Which of these events occurs is not dependent upon the missile and ground surface characteristics but also whether the interaction occurs during the injection phase or after the peak trajectory. Since most missiles originate in the near ground injection domain, ground interactions (due to rigid body rotations, tumbling, and rolling) would be expected during the early response to the translating tornado. This type of ground interaction is considered in the injection model in several ways: (1) the initial orientation of the rigid body is assumed to be random, (2) the missiles are assumed to have random (x, y) position within an origin zone, (3) the missile are independent and the initial elevation of all the missiles in an origin zone is specified in terms of the maximum storage heights, and (4) missile injection is not terminated if ground interaction occurs while the center of mass of the missile has an upward velocity. Thus, the injection methodology accounts for ground interactions in injection domain transport and provides favorable chances for each object to be displaced.

Ground interaction after the peak trajectory is attained is expected to result in missile termination by virture of missile impact damage, earth pentration, and/or a possible windfield expulsion as a result of the transport. Consequently, consistent with the favorable injection methodology, a missile

termination criterion of ground impact is suggested. For generality, the TORMIS code has the capability to simulate ground-type ricochets prior to missile history termination. A simulation study as performed to assess the possibility of multiple favorable missile trajectories and to quantify the transport ranges for multiple ground interactions. Elastic (ricochet) and plastic (regeneration) interactions were simulated. The elastic impact model assumed a coefficient of restitution of 0.5; considering the highly penetrable characteristics of the ground (e.g., 4-1), the specification of a rebound velocity equal to 50% of the impact velocity is considered an upperbound of ground impact elasticity. The ricochet angle (α), was biased normally to ensure conservatism in a manner similar to the oblique bias adopted for structure interactions. The sampled range for α was $[0,\theta]$ assuming a uniform distribution. In the plastic impact model, the missile was assumed to stick but remain available for subsequent reinjection if the initial restraining forces were again exceeded.

The results for five successive impacts are summarized in Table 4-5 for the same initial release conditions of the restraining force study reported in Section 3.4.4. The notation $\bar{D}_{i-j}$ describes the mean transport range from the i^{th} to j^{th} impact points. From these results, it can be concluded that the role of ground interaction in missile transport is significantly dependent upon the elasticity assumed. For the heavier metal missiles (most effective penetrators) in which plastic type ground interactions would dominate, the transport ranges are less than several hundred feet. In addition, for these missiles regeneration appears unlikely after the first impact. Secondly, examination of actual ricochet sequences for the elastic model indicates that once a missile is successfully injected and attains a significant velocity, its transport displacement and new tornado position generally result in insignificant ricochets. This is noted in Figure 4-13 for the utility pole missile described in Table 3-5. In these histories, as well as others examined, once a favorable trajectory is achieved, subsequent ricochets do not generally result in significant range cumulation. Frequently, the missile is behind the translating tornado (example "b" in Figure 4-13) and/or in the region of small wind forces (example "a" in Figure 4-13). Thus the termination criterion of initial ground impact coupled with an injection scheme which tends to maximize the chance for missile transport is suggested. For generality, the TORMIS code was developed such that any number of ground ricochets can be simulated in specific case studies.

Table 4-5. Ground Interaction Simulation Results

Missile Type	Horizontal Restraint f_{OH}	Transport Range: Ground Ricochet $\bar{D}_{0-1}$ (ft)	$\bar{D}_{1-2}$ (ft)	$\bar{D}_{2-3}$ (ft)	$\bar{D}_{3-4}$ (ft)	$\bar{D}_{4-5}$ (ft)	$\bar{D}_{0-5}$ (ft)	Transport Range: Missile Regeneration $\bar{D}_{0-1}$ (ft)	$\bar{D}_{1-2}$ (ft)	$\bar{D}_{2-3}$ (ft)	$\bar{D}_{3-4}$ (ft)	$\bar{D}_{4-5}$ (ft)	$\bar{D}_{0-5}$ (ft)
Utility Pole	W	6.77	18.17	28.22	62.24	35.36	119.75	7.16	2.54	7.43	0.93	15.64	33.11
	5W	182.73	244.59	128.43	113.45	90.79	631.84	177.45	16.06	24.31	53.20	0	216.90
Box	W	112.70	83.35	73.99	200.92	196.38	596.87	131.49	44.12	19.09	51.06	43.62	276.59
	5W	419.20	365.38	167.75	75.57	57.78	890.33	349.22	302.85	29.17	54.26	0	673.63
Sheet	W	23.65	29.63	95.42	58.34	87.85	235.06	30.26	18.22	22.24	39.05	37.58	117.52
	5W	91.98	227.86	223.48	191.54	212.81	608.35	68.46	146.76	71.14	84.31	86.76	374.62
Wide Flange	W	8.44	20.33	39.26	31.79	34.98	115.85	23.51	0	0	0	0.73	24.24
	5W	128.10	121.34	90.22	69.17	40.85	372.53	123.63	32.42	0	0	0	126.21
Pipe	W	5.14	49.6	22.5	15.8	41.6	105.14	9.14	0	0	0	0	9.14
	5W	113.40	147.90	182.40	170.80	78.4	582.46	89.09	1.72	0	0	0	89.77

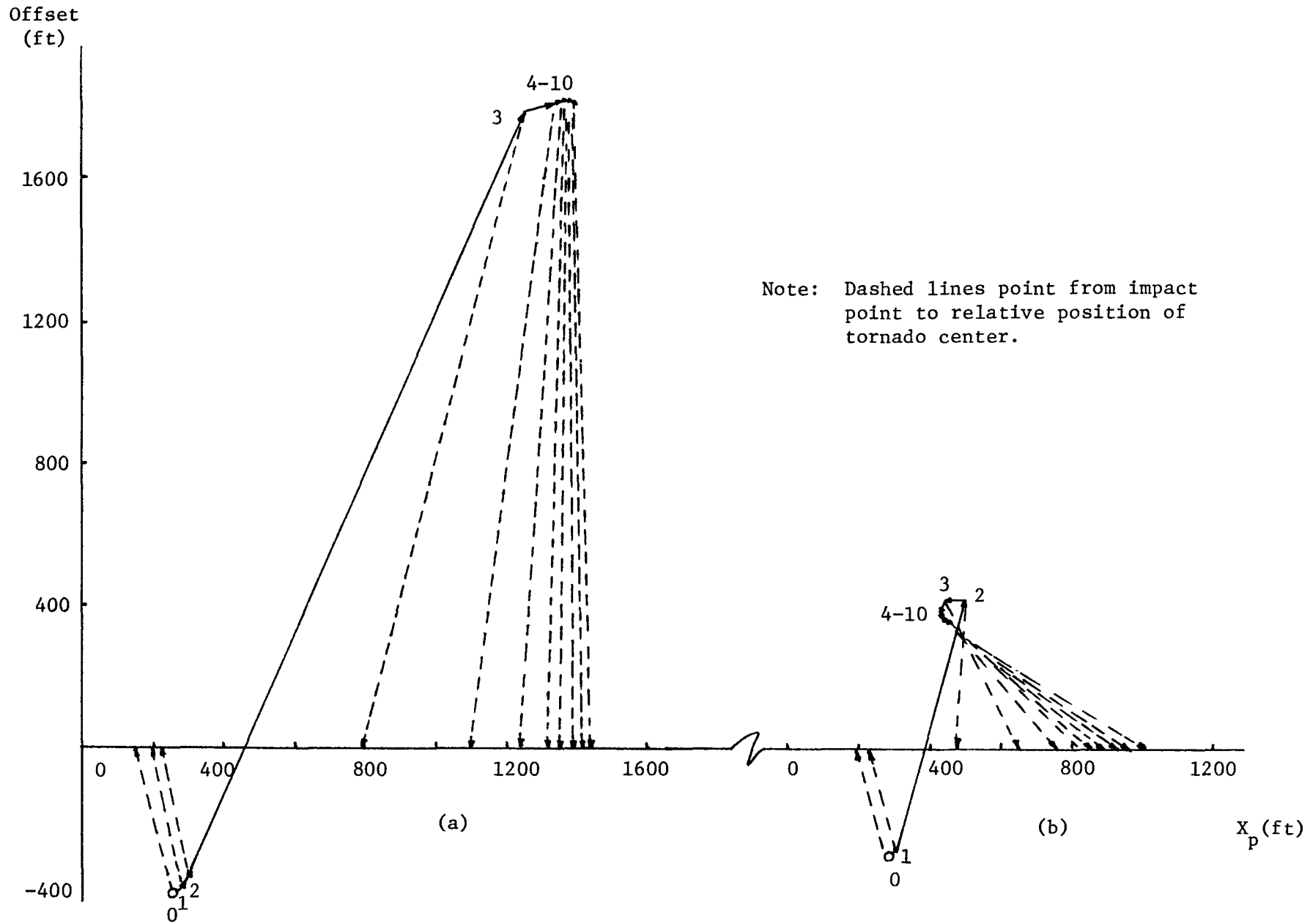

Figure 4-13. Trajectory Ranges for Ten Consecutive Ground Ricochets for Utility Pole Missile

APPENDIX 5

TORNADO DATA CHARACTERISTICS

5.1 Classification Tables

Classification of the 1971 - 1975 FPP data record is presented in tabular form in Tables 5-1, 5-2, and 5-3 for NRC Regions I, II, and III, respectively. The blank designation under direction indicates that direction of the tornado was not noted in the available statistics.

5.2 Path Length and Width Frequency Charts

Relative frequency contours of path length and width for each tornado intensity are presented in Figures 5-1 through 5-14 for NRC Regions I, II, and III. The positive correlation of the path variables to tornado intensity is indicated by the shift in the contours diagonally to the right for increasing F scale intensity.

Table 5-1. 1971-1975 FPP Data for NRC Region I

Direction	Intensity (F-Scale)	Path Length (P_L)	Path Width (P_W)	Frequency
BLANK	0	0	0	524
BLANK	0	0	1	158
BLANK	0	0	2	23
BLANK	0	0	3	6
BLANK	0	1	0	5
BLANK	0	1	1	23
BLANK	0	1	2	9
BLANK	0	1	3	4
BLANK	0	1	4	1
BLANK	0	2	2	1
BLANK	0	3	0	2
BLANK	0	3	4	1
BLANK	1	0	0	258
BLANK	1	0	1	382
BLANK	1	0	2	78
BLANK	1	0	3	20
BLANK	1	1	0	10
BLANK	1	1	1	113
BLANK	1	1	2	64
BLANK	1	1	3	21
BLANK	1	1	4	4
BLANK	1	2	1	1
BLANK	1	2	2	5
BLANK	1	2	3	2
BLANK	1	3	2	1
BLANK	1	3	3	2
BLANK	2	0	0	54
BLANK	2	0	1	115
BLANK	2	0	2	42
BLANK	2	0	3	10
BLANK	2	0	4	2
BLANK	2	1	0	3
BLANK	2	1	1	46
BLANK	2	1	2	42
BLANK	2	1	3	21
BLANK	2	1	4	3
BLANK	2	2	0	1
BLANK	2	2	1	2
BLANK	2	2	2	5
BLANK	2	3	1	4
BLANK	2	3	2	1
BLANK	2	3	3	1
BLANK	3	0	0	4
BLANK	3	0	1	16
BLANK	3	0	2	5
BLANK	3	0	3	1
BLANK	3	1	0	1
BLANK	3	1	1	8
BLANK	3	1	2	4
BLANK	3	1	3	5
BLANK	3	2	1	1
BLANK	3	2	2	5
BLANK	3	2	3	1
BLANK	3	2	4	1
BLANK	3	3	3	1
BLANK	4	0	1	3
BLANK	4	0	2	1
BLANK	4	0	3	1
BLANK	4	4	3	1
E	0	0	0	34
E	0	0	1	22
E	0	0	2	2
E	0	1	0	5
E	0	1	1	7
E	0	2	0	1
E	0	2	1	3
E	0	2	2	1
E	0	2	3	1
E	0	3	0	3
E	0	3	1	1
E	0	3	2	1
E	1	0	0	18

Table 5-1. 1971-1975 FPP Data for NRC Region I (Continued)

Direction	Intensity (F-Scale)	Path Length (P_L)	Path Width (P_W)	Frequency
E	1	0	1	31
E	1	0	2	10
E	1	0	3	1
E	1	1	0	8
E	1	1	1	52
E	1	1	2	23
E	1	1	3	10
E	1	1	4	1
E	1	2	0	3
E	1	2	1	15
E	1	2	2	18
E	1	2	3	4
E	1	2	4	1
E	1	3	1	20
E	1	3	2	11
E	1	3	3	6
E	1	4	1	3
E	1	4	2	2
E	1	4	3	1
E	2	0	0	4
E	2	0	1	9
E	2	0	2	9
E	2	0	3	2
E	2	0	4	1
E	2	1	0	3
E	2	1	1	19
E	2	1	2	19
E	2	1	3	9
E	2	2	1	10
E	2	2	2	16
E	2	2	3	5
E	2	2	4	1
E	2	3	1	5
E	2	3	2	9
E	2	3	3	10
E	2	3	4	4
E	2	4	1	1
E	2	4	2	1
E	3	0	0	1
E	3	0	1	2
E	3	0	2	1
E	3	0	3	1
E	3	1	1	1
E	3	1	2	3
E	3	1	3	1
E	3	1	4	1
E	3	2	1	5
E	3	2	2	6
E	3	2	3	8
E	3	2	4	1
E	3	3	0	1
E	3	3	1	3
E	3	3	2	5
E	3	3	3	9
E	3	3	5	3
E	3	4	1	1
E	3	4	3	6
E	3	4	4	2
E	4	1	3	1
E	4	2	2	3
E	4	2	3	1
E	4	3	2	1
E	4	3	3	2
E	4	3	4	2
E	4	4	2	1
E	5	3	2	1
E	5	4	4	1
NE	0	0	0	57
NE	0	0	1	16
NE	0	0	2	7
NE	0	0	3	3
NE	0	1	0	7

Table 5-1. 1971-1975 FPP Data for NRC Region I (Continued)

Direction	Intensity (F-Scale)	Path Length (P_L)	Path Width (P_W)	Frequency
NE	0	1	1	11
NE	0	1	2	6
NE	0	1	3	1
NE	0	1	4	2
NE	0	2	0	6
NE	0	2	1	9
NE	0	2	2	5
NE	0	2	3	3
NE	0	3	0	1
NE	0	3	1	2
NE	0	3	2	1
NE	0	3	3	1
NE	0	4	0	2
NE	0	4	1	1
NE	0	5	0	1
NE	1	0	0	29
NE	1	0	1	39
NE	1	0	2	30
NE	1	0	3	3
NE	1	1	0	10
NE	1	1	1	80
NE	1	1	2	35
NE	1	1	3	30
NE	1	1	4	2
NE	1	2	0	7
NE	1	2	1	60
NE	1	2	2	36
NE	1	2	3	15
NE	1	2	4	5
NE	1	3	0	6
NE	1	3	1	25
NE	1	3	2	28
NE	1	3	3	18
NE	1	3	4	3
NE	1	3	5	1
NE	1	4	0	3
NE	1	4	1	4
NE	1	4	2	6
NE	1	4	3	2
NE	1	5	1	2
NE	2	0	0	13
NE	2	0	1	29
NE	2	0	2	19
NE	2	0	3	6
NE	2	1	0	1
NE	2	1	1	37
NE	2	1	2	51
NE	2	1	3	34
NE	2	1	4	4
NE	2	2	0	6
NE	2	2	1	43
NE	2	2	2	58
NE	2	2	3	26
NE	2	2	4	1
NE	2	2	5	1
NE	2	3	0	3
NE	2	3	1	12
NE	2	3	2	28
NE	2	3	3	37
NE	2	3	4	4
NE	2	4	1	4
NE	2	4	2	7
NE	2	4	3	4
NE	2	4	5	2
NE	2	5	2	1
NE	2	5	3	1
NE	3	0	0	2
NE	3	0	1	4
NE	3	0	2	2
NE	3	0	3	2
NE	3	1	0	1
NE	3	1	1	6

Table 5-1. 1971-1975 FPP Data for NRC Region I (Continued)

Direction	Intensity (F-Scale)	Path Length (P_L)	Path Width (P_W)	Frequency
NE	3	1	2	10
NE	3	1	3	15
NE	3	2	0	1
NE	3	2	1	5
NE	3	2	2	17
NE	3	2	3	15
NE	3	2	4	3
NE	3	3	0	2
NE	3	3	1	5
NE	3	3	2	16
NE	3	3	3	32
NE	3	3	4	10
NE	3	4	2	7
NE	3	4	3	6
NE	3	4	4	5
NE	3	4	5	1
NE	3	5	2	2
NE	4	1	2	2
NE	4	1	3	3
NE	4	2	3	2
NE	4	2	4	2
NE	4	3	2	8
NE	4	3	3	10
NE	4	3	4	6
NE	4	3	5	2
NE	4	4	0	1
NE	4	4	2	1
NE	4	4	3	4
NE	4	4	4	6
NE	4	4	5	1
NE	4	5	0	1
NE	4	5	3	1
NE	4	5	4	2
NE	5	3	2	1
NE	5	4	3	2
NE	5	4	4	1
NE	5	4	5	1
NE	5	5	3	1
N	0	0	0	8
N	0	0	1	5
N	0	1	0	1
N	0	1	1	4
N	0	2	0	1
N	0	2	1	1
N	0	2	2	1
N	0	2	3	1
N	0	3	0	1
N	0	3	1	3
N	0	3	2	1
N	1	0	0	4
N	1	0	1	14
N	1	0	2	4
N	1	1	0	1
N	1	1	1	8
N	1	1	2	3
N	1	1	3	2
N	1	2	1	10
N	1	2	2	3
N	1	2	3	4
N	1	3	1	1
N	1	3	2	2
N	1	3	3	1
N	2	0	0	3
N	2	0	1	2
N	2	0	2	3
N	2	1	0	1
N	2	1	1	12
N	2	1	2	7
N	2	1	3	2
N	2	1	4	1
N	2	2	1	3
N	2	2	2	8

Table 5-1. 1971-1975 FPP Data for NRC Region I (Continued)

Direction	Intensity (F-Scale)	Path Length (P_L)	Path Width (P_W)	Frequency
N	2	2	3	2
N	2	3	1	3
N	2	3	2	3
N	2	3	3	3
N	2	3	5	1
N	2	4	1	2
N	3	0	0	1
N	3	1	1	2
N	3	1	3	2
N	3	2	1	1
N	3	2	2	5
N	3	2	3	3
N	3	3	1	2
N	3	3	2	8
N	3	3	3	1
N	3	3	4	2
N	3	3	5	2
N	4	0	3	1
N	4	1	3	1
N	4	1	4	1
N	4	2	1	1
N	4	2	3	1
N	4	3	2	2
N	4	3	3	3
N	4	3	4	2
N	4	3	5	1
N	4	4	4	1
N	5	3	3	1
NW	0	0	0	3
NW	0	0	1	1
NW	0	1	1	2
NW	0	1	2	1
NW	0	2	2	1
NW	0	3	0	1
NW	0	3	3	2
NW	1	0	0	7
NW	1	0	1	5
NW	1	1	0	1
NW	1	1	1	2
NW	1	1	2	3
NW	1	1	3	1
NW	1	2	1	2
NW	1	2	3	1
NW	1	3	1	1
NW	1	3	2	1
NW	1	3	3	1
NW	1	3	4	1
NW	2	0	1	1
NW	2	1	1	2
NW	2	1	2	1
NW	2	2	3	1
NW	2	3	1	1
NW	2	3	2	1
NW	3	0	3	1
NW	3	1	2	1
NW	3	2	3	1
W	0	0	0	3
W	0	1	1	1
W	1	0	1	1
W	1	1	1	1
W	1	1	2	1
W	2	0	0	1
W	2	1	1	1
W	2	2	2	1
W	3	1	2	1
SW	0	1	1	1
SW	0	1	2	1
SW	1	0	0	4
SW	1	0	1	2
SW	1	0	2	1
SW	1	1	1	4
SW	1	1	2	1

Table 5-1. 1971-1975 FPP Data for NRC Region I (Continued)

Direction	Intensity (F-Scale)	Path Length (P_L)	Path Width (P_W)	Frequency
SW	1	2	1	2
SW	1	3	0	1
SW	1	3	1	1
SW	2	1	2	1
S	0	0	0	4
S	0	0	1	2
S	0	1	1	1
S	0	3	5	1
S	0	4	1	1
S	1	0	0	2
S	1	0	1	2
S	1	1	0	1
S	1	1	1	2
S	1	2	1	1
S	1	2	2	2
S	2	0	0	3
S	2	0	2	1
S	2	1	1	2
S	2	1	3	1
S	2	2	1	1
S	2	2	2	1
S	2	3	2	1
S	2	3	3	1
S	3	1	2	1
S	3	3	3	2
S	4	2	4	1
S	4	4	3	1
SE	0	0	0	16
SE	0	0	1	5
SE	0	1	0	1
SE	0	1	1	8
SE	0	1	2	1
SE	0	2	1	4
SE	0	2	3	1
SE	0	3	0	1
SE	0	3	1	1
SE	1	0	0	7
SE	1	0	1	23
SE	1	0	2	6
SE	1	1	0	1
SE	1	1	1	21
SE	1	1	2	9
SE	1	1	3	4
SE	1	1	4	1
SE	1	2	0	1
SE	1	2	1	20
SE	1	2	2	7
SE	1	2	3	5
SE	1	3	0	2
SE	1	3	1	5
SE	1	3	2	6
SE	1	3	3	2
SE	1	3	4	2
SE	1	4	1	2
SE	2	0	0	1
SE	2	0	1	10
SE	2	0	2	3
SE	2	0	3	4
SE	2	1	1	3
SE	2	1	2	4
SE	2	1	3	8
SE	2	2	0	1
SE	2	2	1	6
SE	2	2	2	7
SE	2	2	3	3
SE	2	3	1	5
SE	2	3	2	7
SE	2	3	3	2
SE	2	3	4	1
SE	2	4	2	1
SE	2	4	3	2
SE	3	1	1	3

Table 5-1. 1971-1975 FPP Data for NRC Region I (Continued)

Direction	Intensity (F-Scale)	Path Length (P_L)	Path Width (P_W)	Frequency
SE	3	1	3	1
SE	3	2	1	1
SE	3	2	2	2
SE	3	2	3	2
SE	3	3	2	1
SE	3	3	3	2
SE	3	4	3	2
SE	4	1	3	2
SE	4	2	2	2
SE	4	2	3	2
SE	4	3	0	1
SE	4	3	3	2
SE	4	3	4	1
SE	5	3	2	1

Table 5-2. 1971-1975 FPP Data for NRC Region II

Direction	Intensity (F-Scale)	Path Length (P_L)	Path Width (P_W)	Frequency
BLANK	0	0	0	11
BLANK	0	0	1	5
BLANK	0	0	3	1
BLANK	1	0	0	3
BLANK	1	0	1	1
BLANK	1	0	2	1
BLANK	1	0	3	1
BLANK	1	1	1	2
BLANK	2	0	0	1
BLANK	2	0	1	1
BLANK	2	1	2	1
BLANK	2	1	4	1
BLANK	3	1	3	1
E	0	0	0	1
E	1	0	0	1
E	1	0	1	1
E	1	1	1	1
E	2	1	2	1
E	2	1	4	1
E	2	2	2	1
E	3	0	4	1
NE	0	0	0	1
NE	0	0	1	1
NE	1	0	1	1
NE	1	2	2	1
NE	2	1	2	1
NE	2	2	2	1
NE	2	2	3	1
NE	3	3	2	2
N	0	1	1	1
N	0	2	0	1
N	0	2	1	1
N	1	1	1	1
N	2	2	4	1
NW	1	1	1	1
NW	2	1	1	1
W	0	1	1	1
SW	1	0	0	1
SE	1	0	1	1

Table 5-3. 1971-1975 FPP Data for NRC Region III

Direction	Intensity (F-Scale)	Path Length (P_L)	Path Width (P_W)	Frequency
BLANK	0	0	0	6
BLANK	0	0	1	2
BLANK	0	0	2	1
BLANK	0	1	1	1
BLANK	1	0	0	6
BLANK	1	0	1	1
BLANK	1	0	2	2
BLANK	1	1	1	2
BLANK	1	3	2	1
BLANK	2	0	1	1
BLANK	2	0	3	1
E	1	2	2	1
NE	0	0	0	1
NE	1	0	0	1
NE	1	1	5	1
NE	2	0	2	1
NE	3	2	2	1
N	3	2	2	1
NW	1	1	2	1
W	2	0	0	1
SW	1	1	2	1
SE	0	0	0	1
SE	1	1	0	1

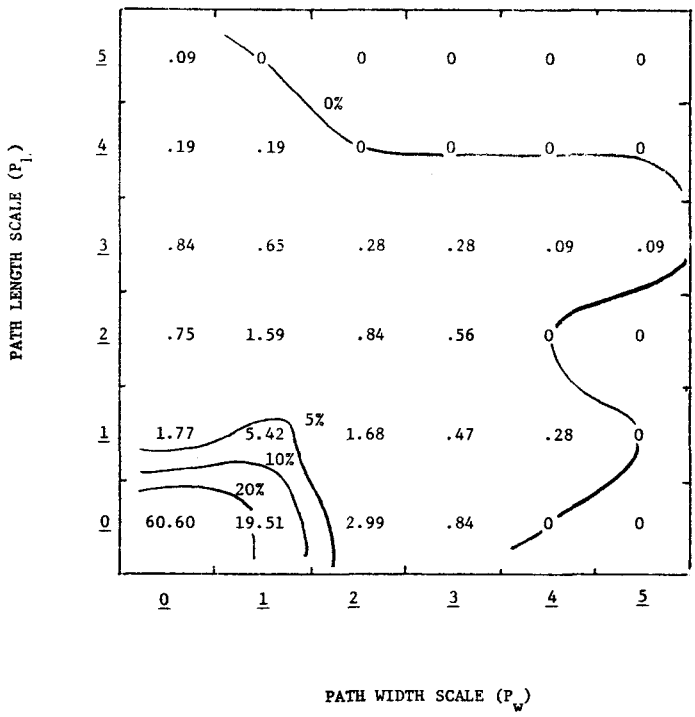

Figure 5-1. Path Length and Width Frequency Contours for F0 Tornadoes in Region I

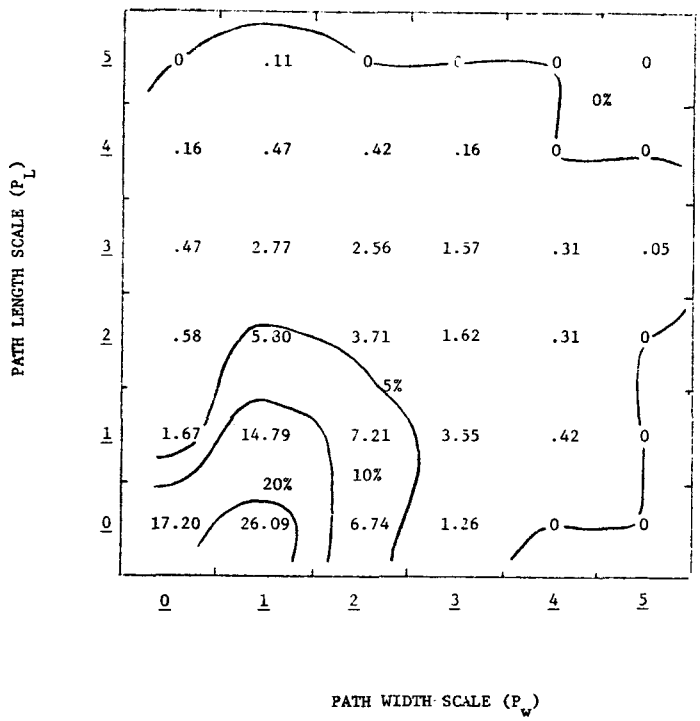

Figure 5-2. Path Length and Width Frequency Contours for F1 Tornadoes in Region I

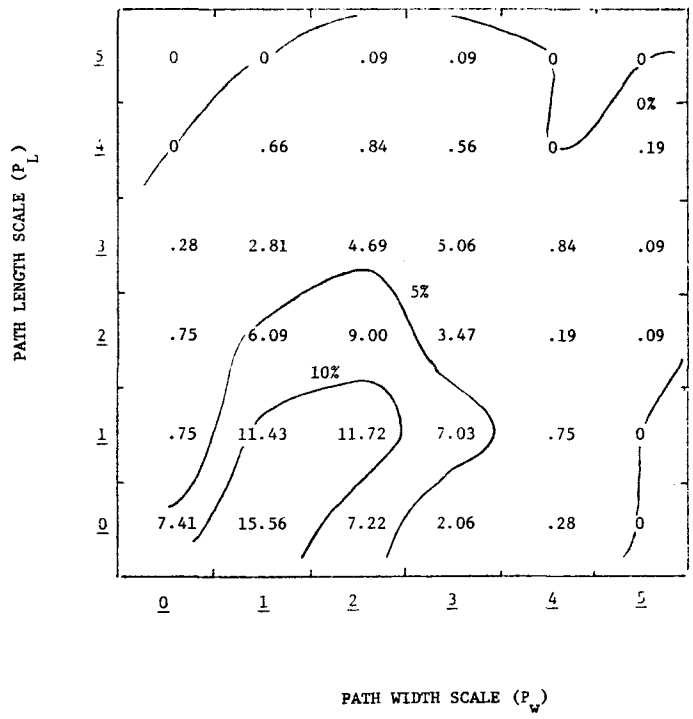

Figure 5-3. Path Length and Width Frequency Contours for F2 Tornadoes in Region I

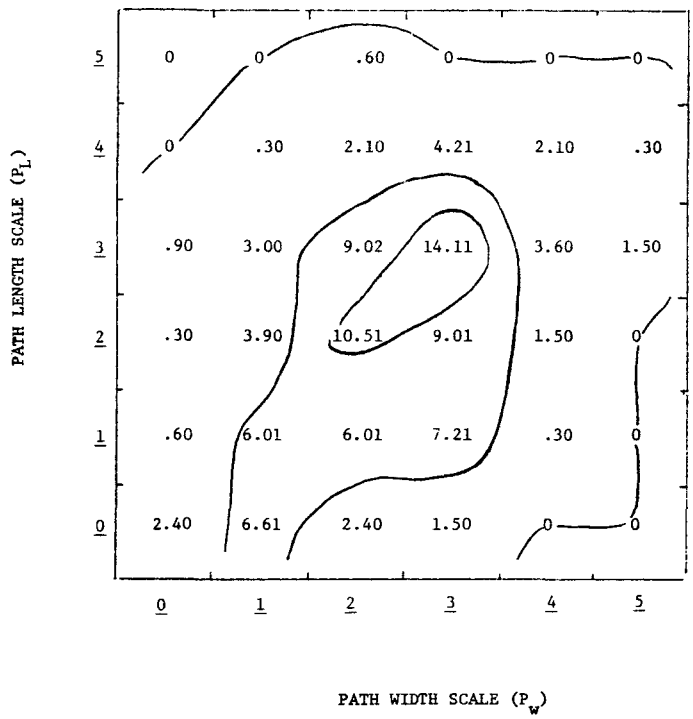

Figure 5-4. Path Length and Width Frequency Contours for F3 Tornadoes in Region I

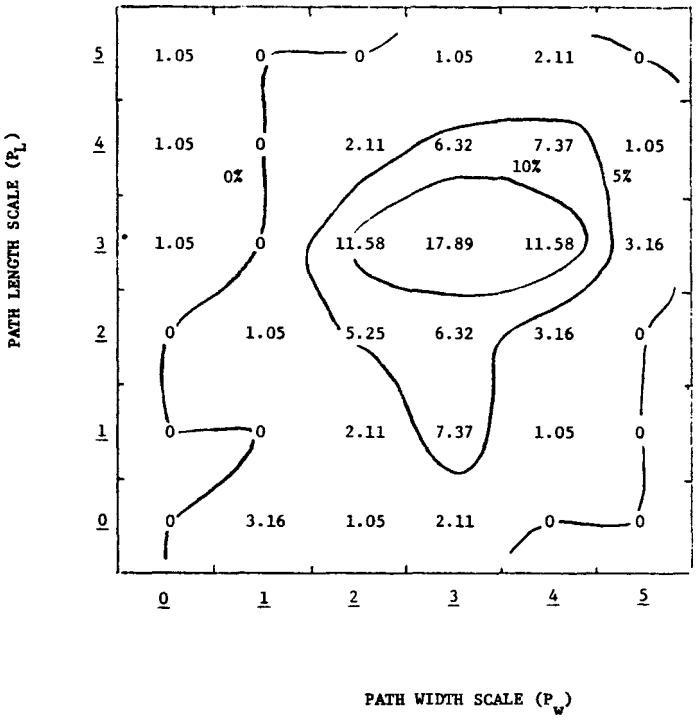

Figure 5-5. Path Length and Width Frequency Contours for F4 Tornadoes in Region I

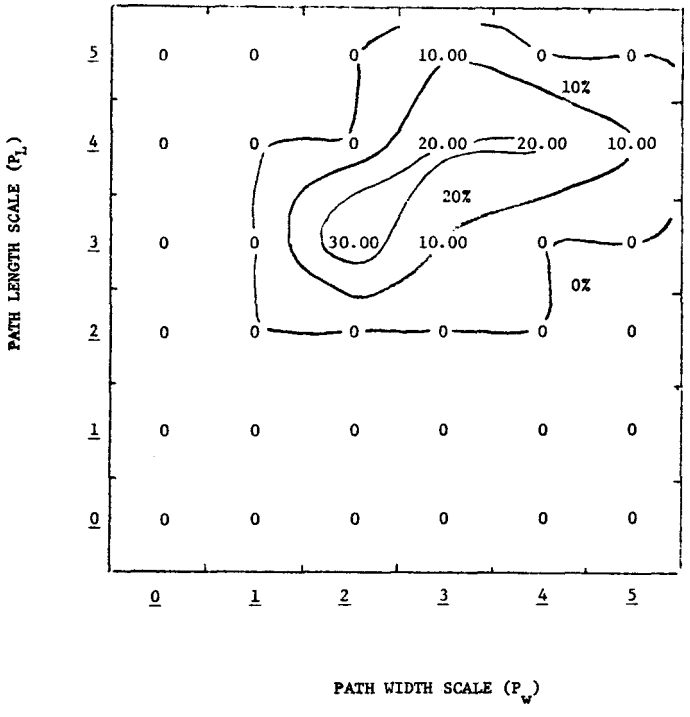

Figure 5-6. Path Length and Width Frequency Contours for F5 Tornadoes in Region I

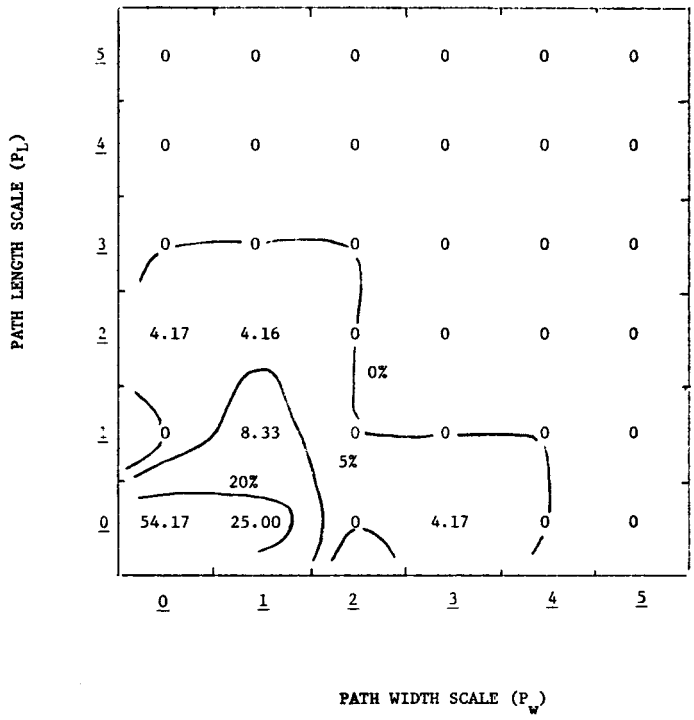

Figure 5-7. Path Length and Width Frequency Contours for F0 Tornadoes in Region II.

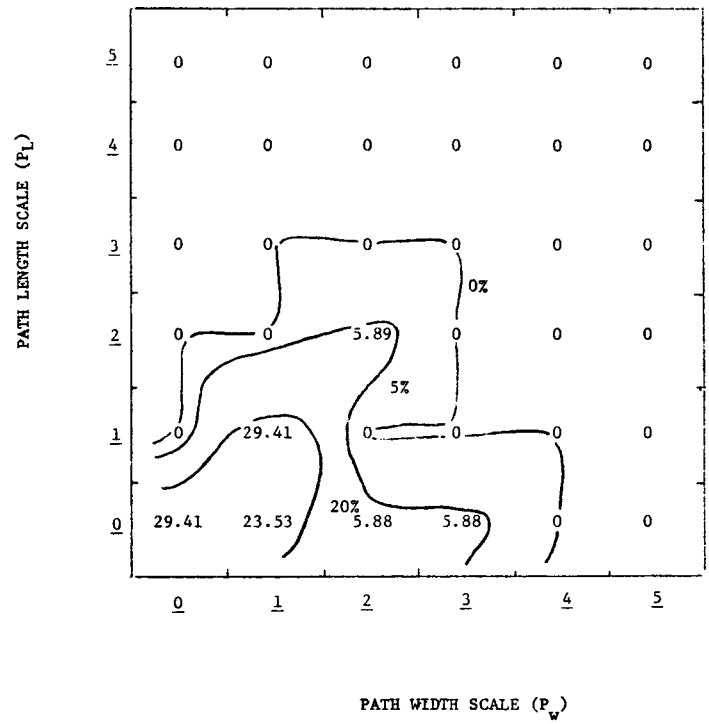

Figure 5-8. Path Length and Width Frequency Contours for F1 Tornadoes in Region II

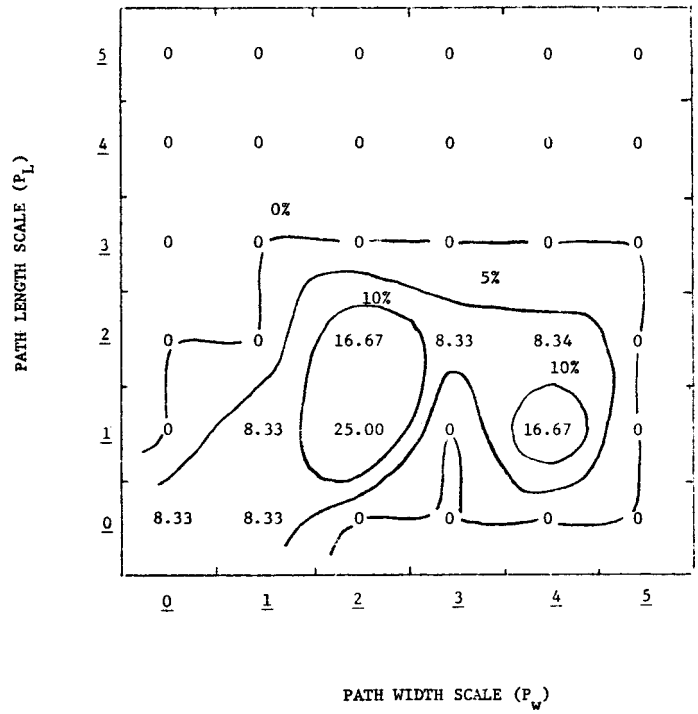

Figure 5-9. Path Length and Width Frequency Contours for F2 Tornadoes in Region II

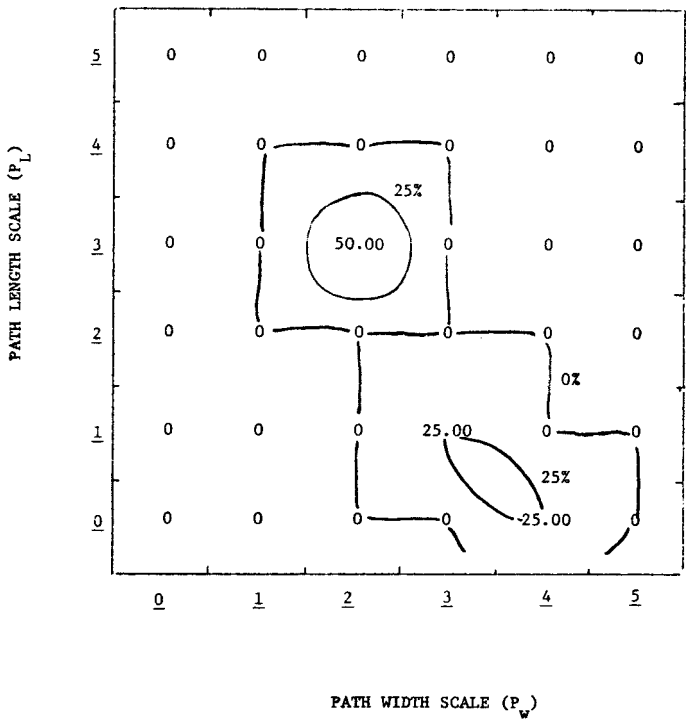

Figure 5-10. Path Length and Width Frequency Contours for F3 Tornadoes in Region II

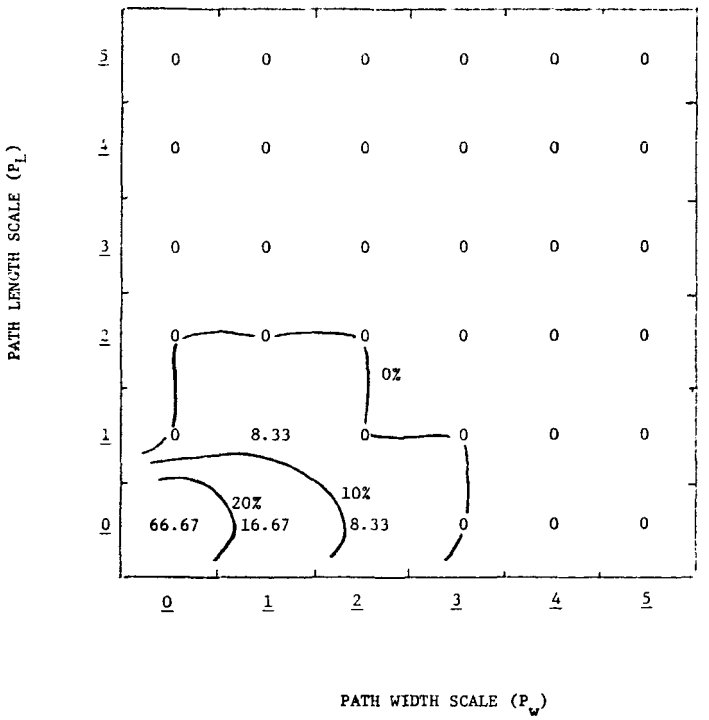

Figure 5-11. Path Length and Width Frequency Contours for F0 Tornadoes in Region III

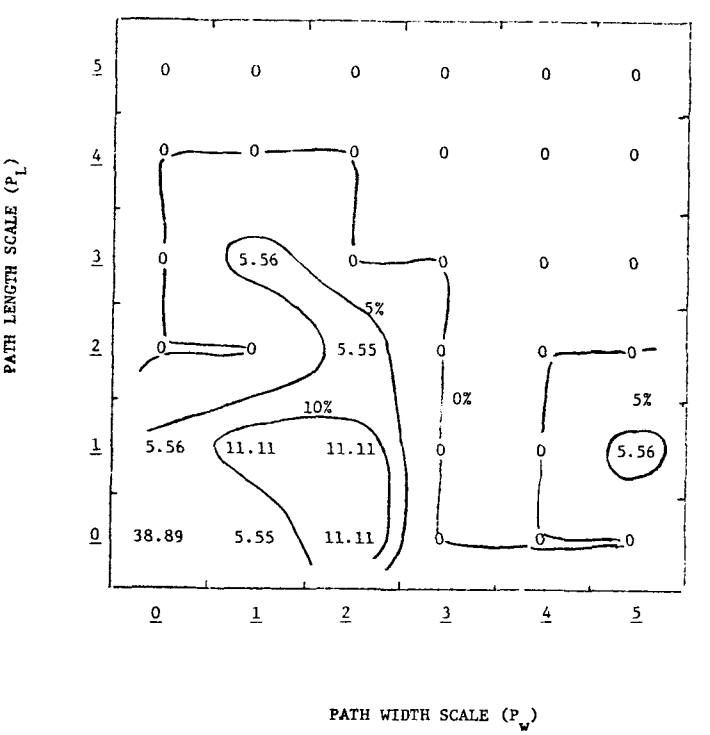

Figure 5-12. Path Length and Width Frequency Contours for F1 Tornadoes in Region III

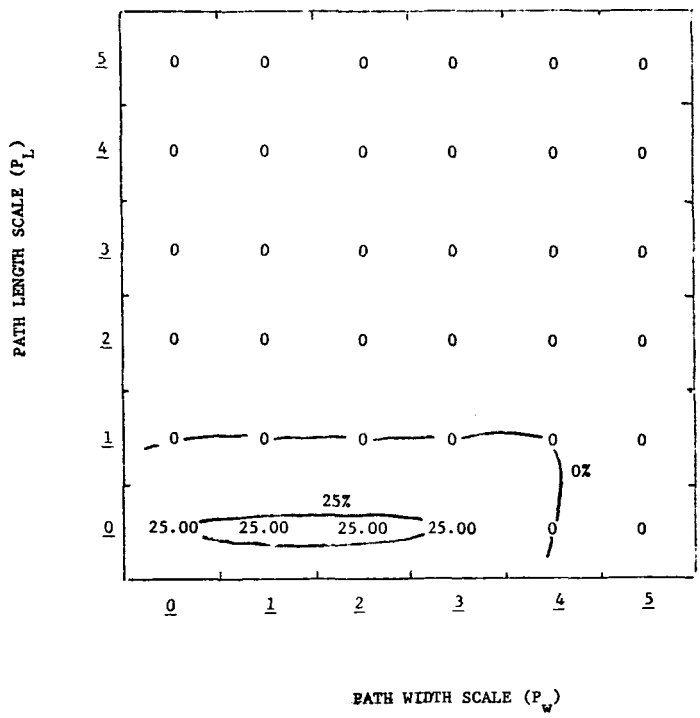

Figure 5-13. Path Length and Width Frequency Contours for F2 Tornadoes in Region III

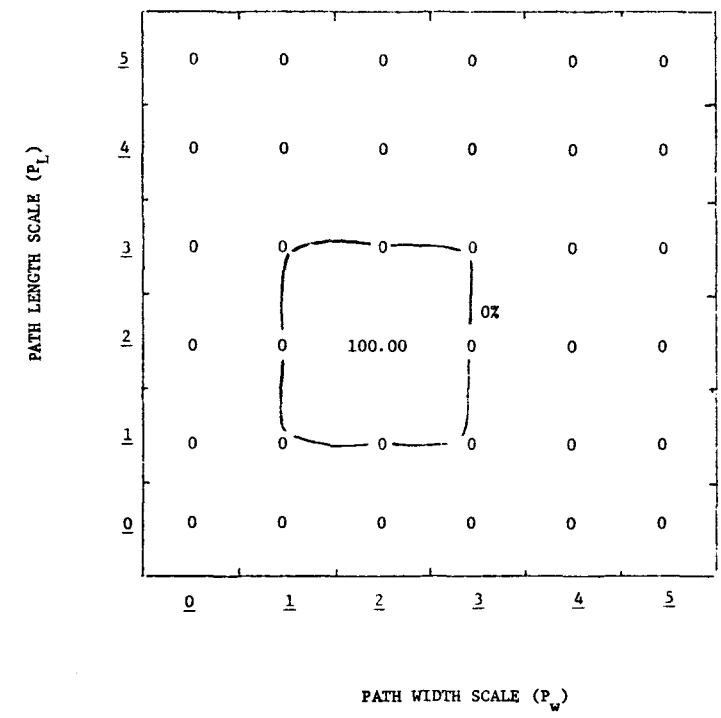

Figure 5-14. Path Length and Width Frequency Contours for F3 Tornadoes in Region III

APPENDIX 6

MISSILE CHARACTERIZATION DATA

The results of the missile characterization survey, methodology application, and data analysis is summarized in Tables 6-1 through 6-6. The notation is described in Appendix 2; note that the numbers identifying the origin zone (column 1) refer to the location of the object as depicted on a master plan view of the plant vicinity. In addition, it should be noted that the parameter A_h has two interpretations: for horizontal arrays (availability mode 1), A_h refers to the percentage of objects in the top row and for support elements (availability mode 5), A_h is the percentage of elements which are unloaded; for all other availability modes, the parameter is undefined and a zero is indicated.

Table 6-1. Missile Characterization Survey for a Particular Plant

Origin Zone	Number of Missiles	Missile Set	d (in)	L (ft)	Wt/L (lb/ft)	Availability Mode	Z_c (in)	Z_s (in)	A_h (%)	A_{min} (in^2)	A_{max} (ft^2)	Impact Mode
1	6	6	48.0	9.0	82.0	4	0	36	0	624.00	36.00	2
1	12	3	2.9	12.0	5.8	3	0	36	0	1.70	0.01	1
1	85	6	12.0	15.0	400.0	5	0	12	10	144.00	1.00	1
1	125	2	12.0	14.0	31.4	5	0	12	50	113.00	0.78	1
1	33	2	10.0	25.0	21.8	4	0	10	0	79.00	0.55	1
1	25	4	12.0	3.0	78.7	1	12	60	25	138.00	0.96	1
1	220	1	20.0	4.0	10.0	4	0	48	0	318.00	6.60	3
1	20	6	12.0	8.0	40.0	3	0	24	0	144.00	1.00	1
1	400	2	48.0	2.0	160.0	3	0	120	0	144.00	12.00	3
1	2	7	66.0	8.0	550.0	1	6	36	50	17.00	0.20	5
1	300	3	16.0	1.5	73.3	4	0	24	0	21.00	0.15	1
1	12	25	60.0	20.0	266.7	4	12	60	0	2880.00	100.00	3
1	1	11	72.0	15.0	200.0	4	24	33	0	192.00	90.00	4
1	100	15	6.0	10.0	28.7	4	12	18	0	8.40	0.06	1
1	125	16	6.0	10.0	13.0	4	12	18	0	3.80	0.03	1
1	100	3	10.0	4.0	54.8	4	12	22	0	16.10	0.11	1
1	20	12	12.0	10.0	15.3	4	12	13	0	4.50	10.00	4
1	20	1	1.0	10.0	26.7	1	4	12	15	0.79	0.01	1
1	100	3	1.9	4.5	3.6	4	12	14	0	1.10	0.01	1
1	5	19	48.0	4.0	141.0	4	0	48	0	608.00	4.90	2
1	9	20	48.0	6.0	50.0	4	0	36	0	1728.00	24.00	2
1	200	5	36.0	8.0	112.5	1	12	120	30	40.50	6.00	5
1	25	12	72.0	20.0	367.5	2	12	84	0	18.00	120.00	4
1	150	1	1.4	40.0	5.3	1	4	12	15	1.56	0.01	1
1	2	5	72.0	8.0	225.0	4	0	72	0	384.00	2.60	5
1	1	12	96.0	20.0	306.3	4	48	49	0	36.00	160.00	4
1	1	21	60.0	16.0	65.6	5	12	72	25	144.00	1.78	5
1	150	14	12.0	15.0	190.0	4	12	24	0	55.90	0.39	1
1	300	7	4.0	15.0	13.6	1	12	14	50	4.00	0.03	1
1	20	2	36.0	1.5	120.0	4	0	36	0	108.00	7.10	3
1	24	3	36.0	6.0	143.0	4	0	36	0	42.00	0.29	1
1	175	14	6.0	15.0	25.0	4	12	18	0	7.35	0.05	1
1	5	18	36.0	4.0	48.2	4	0	36	0	192.00	2.70	5
1	100	3	4.0	10.0	9.1	1	12	24	30	2.68	0.02	1
1	50	3	10.0	15.0	40.5	1	0	48	25	11.90	0.08	1
1	290	3	20.0	25.0	104.0	4	12	32	0	30.60	0.21	1
1	50	15	4.0	12.0	18.5	3	0	36	0	5.40	0.04	1
1	30	2	12.0	20.0	31.4	4	0	12	0	113.00	0.78	1
1	700	9	2.0	12.0	6.7	3	0	60	0	24.00	0.17	1
1	8	9	60.0	20.0	200.0	1	0	96	12	720.00	40.00	4
1	20	9	15.0	20.0	25.0	5	0	6	50	90.00	0.63	1
1	25	9	15.0	20.0	25.0	1	0	36	16	90.00	0.63	1
1	300	14	8.0	6.0	28.0	3	0	48	0	8.20	0.06	1
1	100	15	8.0	6.0	56.9	3	0	48	0	16.70	0.12	1
1	100	16	8.0	6.0	19.0	3	0	48	0	5.51	0.04	1
1	60	14	14.0	12.0	136.0	1	12	36	30	40.00	0.28	1
1	40	16	10.0	15.0	30.0	1	12	36	30	8.82	0.06	1
1	1	7	72.0	12.0	209.9	4	24	54	0	3.17	0.09	5
1	221	3	8.0	10.0	28.6	1	12	48	20	8.40	0.06	1
1	402	3	12.0	10.0	49.6	1	12	36	30	14.60	0.10	1
1	200	3	18.0	6.0	93.5	1	12	48	50	27.50	0.19	1
1	12	3	36.0	15.0	360.0	1	60	132	50	105.00	0.73	1
2	1	6	46.0	4.0	62.0	4	0	48	0	16.00	16.00	2
2	17	1	20.0	4.0	10.0	4	0	48	0	318.00	6.60	3
2	2	6	96.0	8.0	36.0	4	0	96	0	16.00	32.00	2
2	1	5	84.0	8.0	113.0	4	0	12	0	40.00	56.00	4
2	20	2	95.0	5.0	280.0	4	0	95	0	570.00	49.00	3
2	80	11	29.0	10.0	26.0	1	0	84	25	609.00	4.23	1
2	78	11	43.0	14.0	35.0	1	0	84	25	688.00	4.78	1
2	1	18	72.0	7.0	215.0	4	0	84	0	4.00	0.09	5
3	5	5	48.0	9.0	74.0	4	0	36	0	624.00	36.00	2
3	50	1	1.0	10.0	2.7	4	0	24	0	0.78	0.01	1
3	90	14	6.0	7.0	25.0	3	0	36	0	8.00	0.06	1
3	80	16	6.0	10.0	15.0	3	0	36	0	5.00	0.03	1
3	3	6	8.0	9.0	18.0	4	0	9	0	64.00	0.44	1

Table 6-1. Missile Characterization Survey (Con'd)

Origin Zone	Number of Missiles	Missile Set	d (in)	L (ft)	Wt/L (lb/ft)	Availability Mode	Z_c (in)	Z_s (in)	A_h (%)	A_{min} (in^2)	A_{max} (ft^2)	Impact Mode
3	30	13	48.0	8.0	13.0	4	0	12	0	48.00	32.00	4
3	30	18	18.0	9.0	14.0	2	0	36	0	1.50	0.02	5
3	215	5	48.0	5.0	50.0	1	0	72	50	1728.00	20.00	2
3	160	1	20.0	4.0	10.0	4	0	48	0	318.00	6.60	3
3	225	3	4.0	5.0	11.0	1	36	72	25	3.20	0.02	1
3	150	3	2.0	12.0	5.0	1	0	72	25	1.50	0.01	1
3	390	15	5.0	12.0	12.0	1	0	36	40	3.60	0.02	1
3	330	16	6.0	12.0	16.0	1	0	36	40	4.80	0.03	1
3	112	7	48.0	10.0	16.0	1	0	24	5	6.00	40.00	2
3	1000	16	3.0	20.0	9.0	1	0	48	25	2.60	0.02	1
3	800	15	3.0	20.0	7.0	1	0	48	25	2.10	0.01	1
3	86	3	5.0	20.0	20.0	1	0	24	20	6.10	0.04	1
3	11	1	40.0	6.5	106.0	4	0	78	0	1256.00	8.72	1
3	14	6	13.0	14.0	47.0	4	0	13	0	169.00	1.17	1
3	20	3	12.0	5.0	78.0	4	24	40	0	17.00	0.12	1
3	40	2	14.0	15.0	43.0	4	0	14	0	153.00	1.06	1
3	1	12	96.0	15.0	572.0	4	0	12	0	20.00	0.76	5
3	20	3	12.0	15.0	65.0	4	12	24	0	19.00	0.13	1
3	20	15	8.0	10.0	40.0	4	36	48	0	12.00	0.08	1
3	30	14	12.0	12.0	58.0	4	12	24	0	17.00	0.12	1
3	36	6	17.0	15.0	57.0	1	0	12	0	204.00	1.42	1
3	10	7	48.0	9.0	141.0	4	6	30	0	1152.00	36.00	2
4	6	18	72.0	7.0	57.0	4	0	72	0	4.00	0.14	5
4	288	3	6.0	8.0	9.0	1	0	72	25	3.10	0.02	1
4	2	11	72.0	15.0	200.0	4	24	33	0	192.00	9.00	4
4	1400	3	3.0	12.0	3.8	1	0	48	30	2.20	0.02	1
4	23	1	20.0	4.0	10.0	4	0	48	0	318.00	6.60	3
4	44	6	48.0	12.0	42.0	4	0	48	0	1728.00	48.00	2
6	20	25	60.0	20.0	200.0	40	120	600	0	28800.00	750.00	3
4	30	3	12.0	20.0	65.0	4	0	12	0	19.20	0.13	1
4	36	1	12.0	5.0	55.0	4	0	60	0	16.00	0.11	1
4	5	6	50.0	5.0	70.0	4	0	36	0	1800.00	20.00	2
4	15	25	60.0	20.0	200.0	0	4001	2006	0	288.00	100.00	3
6	25	13	72.0	8.0	40.0	4	0	48	0	144.00	48.00	4
6	2	11	72.0	15.0	167.0	4	24	33	0	192.00	9.00	4
6	40	1	20.0	4.0	10.0	4	0	48	0	318.00	6.60	3
6	35	1	12.0	5.0	55.0	2	0	60	0	16.00	0.11	1
6	10	6	36.0	8.0	38.0	4	0	36	0	1728.00	24.00	2
10	41	1	20.0	4.0	10.0	4	0	48	0	318.00	6.60	3
10	500	3	4.0	10.0	11.0	1	36	72	25	3.20	0.02	1
10	500	15	3.0	12.0	8.0	1	30	72	20	2.70	0.02	1
10	4	6	36.0	6.0	42.0	4	0	36	0	1728.00	18.00	2
10	4	18	72.0	7.0	57.0	4	0	72	0	4.30	0.09	5
10	1	7	36.0	4.0	103.0	4	0	24	0	864.00	12.00	2
10	464	25	60.0	20.0	200.0	4	12	60	0	2880.00	100.00	3
11	22	1	20.0	4.0	10.0	4	0	48	0	318.00	6.60	3
11	16	2	48.0	2.0	160.0	4	0	48	0	144.00	12.00	3
11	15	6	60.0	6.0	67.0	4	0	60	0	3600.00	30.00	2
11	10	11	96.0	8.0	36.0	4	0	96	0	16.00	32.00	2
11	1000	3	6.0	20.0	19.0	1	0	36	25	5.60	0.04	1
11	1	11	72.0	15.0	167.0	4	24	33	0	192.00	1.33	1
11	200	14	18.0	20.0	85.0	1	4	72	35	25.00	0.17	1
11	400	15	6.0	12.0	37.0	1	4	72	25	11.00	0.08	1
11	400	16	8.0	15.0	19.0	1	4	36	30	5.50	0.04	1
11	50	12	72.0	10.0	195.0	2	0	72	0	72.00	60.00	4
11	100	14	12.0	20.0	58.0	4	0	72	0	17.00	0.12	1
11	25	3	12.0	15.0	49.0	4	0	48	0	14.00	0.10	1
11	100	1	12.0	5.0	55.0	4	0	60	0	16.00	0.11	1
11	200	3	3.0	20.0	7.6	1	0	72	25	2.20	0.02	1
11	20	6	8.0	12.0	18.0	4	0	8	0	64.00	0.44	1
11	300	3	18.0	6.0	93.5	4	0	36	0	27.00	0.19	1
11	10	25	60.0	20.0	200.0	4	12	60	0	2880.00	100.00	3
11	20	12	72.0	10.0	245.0	2	0	72	0	72.00	60.00	4
11	7	2	36.0	1.5	120.0	4	0	36	0	108.00	7.10	3

Table 6-1. Missile Characterization Survey (Con'd)

Origin Zone	Number of Missiles	Missile Set	d (in)	L (ft)	Wt/L (lb/ft)	Availability Mode	Z_c (in)	Z_s (in)	A_h (%)	A_{min} (in^2)	A_{max} (ft^2)	Impact Mode
12	171	25	60.0	20.0	200.0	4	12	60	0	2880.00	100.00	3
14	9	1	3.0	5.0	24.0	1	0	23	20	7.00	0.05	1
14	3	6	28.0	6.0	50.0	4	0	28	0	644.00	14.00	2
14	100	3	4.0	5.0	5.4	1	0	36	20	3.10	0.02	1
14	16	3	3.0	12.0	3.8	3	0	6	0	2.20	0.02	1
14	670	2	48.0	2.5	160.0	4	0	48	0	144.00	12.00	3
14	590	2	36.0	1.5	120.0	4	0	36	0	108.00	7.00	3
14	42	2	60.0	3.0	200.0	4	0	60	0	300.00	20.00	3
14	42	2	80.0	4.0	240.0	4	0	80	0	480.00	35.00	3
14	5	2	95.0	5.0	280.0	4	0	95	0	570.00	49.00	3
14	9	11	48.0	7.0	10.0	4	0	12	0	36.00	28.00	4
14	74	1	20.0	4.0	10.0	4	0	48	0	318.00	6.60	3
14	875	1	1.0	8.0	2.7	1	0	24	30	0.78	0.01	1
14	28	6	6.0	12.0	10.0	4	0	0	12	36.00	0.25	1
14	1	18	48.0	10.0	40.0	4	0	72	0	3.10	0.09	5
14	19	1	12.0	5.0	55.0	4	0	60	0	16.00	0.11	1
14	6	12	21.0	15.0	35.0	4	0	4	6	10.00	28.00	4
14	138	3	5.0	6.0	7.3	1	0	40	20	4.30	0.03	1
14	12	3	2.0	21.0	1.9	4	4	12	0	1.07	0.01	1
14	190	15	6.0	8.0	37.4	4	0	36	0	11.00	0.08	1
14	2	18	24.0	4.0	28.5	4	0	48	0	2.23	0.05	5
14	5	14	6.0	6.0	16.0	4	0	12	0	4.70	0.03	1
14	586	3	6.0	10.0	9.4	1	0	96	33	5.60	0.04	1
14	2050	3	4.0	10.0	10.8	3	0	48	0	3.20	0.02	1
14	800	3	4.0	8.0	10.8	3	36	48	0	3.20	0.02	1
14	1	9	72.0	15.0	150.0	4	24	36	0	72.00	90.00	2
14	9	17	37.0	5.0	228.0	1	0	72	25	219.00	9.00	2
14	220	8	12.0	3.0	31.0	1	0	72	15	30.00	3.00	2
14	1	19	96.0	50.0	250.0	4	0	108	0	200.00	5.00	5
14	61	15	2.0	16.0	4.7	4	0	36	0	1.36	0.01	1

Table 6-2. Missile Set Distribution by Plant

Set Number	Plant Number 1	2	3	4	5	6	7	Total
1	1,902	19,430	117,107	19,559	2,959	390	2,800	164,147
2	2,040	1,209	2,904	49	90	61	100	6,453
3	9,757	18,740	27,286	15,931	2,268	540	0	74,522
4	25	0	190	0	0	0	700	915
5	423	605	42	1,209	23	106	50	2,458
6	296	4,034	10,196	6,139	461	1,250	140	22,516
7	314	1,650	100	0	0	4	0	2,068
8	220	62	0	186	0	6	0	474
9	754	3,262	1,004	3,762	0	131	0	8,913
10	0	1,521	4,584	4,560	0	0	0	10,665
11	183	43	6	3	0	0	0	235
12	235	395	1,328	1,228	140	112	408	3,846
13	55	490	20	184	0	0	0	749
14	1,110	2,845	1,885	3,907	1,002	8	280	11,037
15	2,611	5,640	4,140	2,622	1,602	0	0	16,615
16	2,075	3,768	1,670	2,453	235	13	0	10,214
17	9	0	0	97	0	0	0	106
18	49	17	14	258	1	0	10	349
19	6	0	143	44	19	7	0	219
20	9	188	31	1	0	1	0	230
21	1	29	9,788	1,250	194	118	0	11,380
22	0	227	2,894	114	19	0	0	3,254
23	0	3	0	4	1	0	0	8
24	0	0	0	0	0	23	0	23
25	692	1,527	990	1,140	280	148	50	4,827
Total	22,766	65,685	186,322	64,700	9,294	2,918	4,538	356,223

Table 6-3. Missile Size and Impact Area Subsets

Missile Set	Subset Range d(in)	$\bar{d}$ (in)	Subset Range A_{min}(in^2)	A_{min} Subset Bounds (in^2)	$\bar{A}_{min}$ (in)	$\bar{w}$ (lb/ft)	Number	Relative Set Freq. (%)
1	(0,1]	1.00	[0.2,0.79]	≤0.5	0.25	0.88	1,070	0.65
				>0.5	0.78	2.70	95,515	58.19
	(1,2]	1.65	[1.56,3.14]	≤1.6	1.56	5.30	37,810	23.03
				>1.6	3.15	8.74	25,062	15.27
	(2,12]	10.02	[7,16]	≤12	9.45	38.64	891	0.54
				>12	16.00	55.00	883	0.54
	(12,20]	19.98	[7,318]	>0	311.60	23.55	2,794	1.70
	>20	57.64	[457,7238]	>0	978.10	128.20	127	0.08
							164,152	100.00
2	(0,13]	12.27	[79,133]	>0	118.00	40.49	551	8.54
	(13,17]	16.87	[153,227]	>0	223.70	62.12	906	14.04
	(17,48]	42.21	[108,144]	>0	126.60	140.70	2,985	46.26
	>48	66.72	[300,570]	>0	359.90	213.60	2,011	31.16
							6,453	100.00
3	(0,3]	2.34	[0.49,2.3]	≤1.7	1.06	1.86	19,162	25.71
				>1.7	2.22	4.44	11,083	14.87
	(3,6]	5.14	[2.68,6.1]	≤3.5	3.17	9.47	12,958	17.39
				>3.5	5.55	26.99	17,133	22.99
	(6,12]	10.68	[8.4,19.2]	≤12	10.35	35.40	3,146	4.22
				>12	15.07	45.78	3,752	5.04
	(12,24]	20.52	[21,192]	≤22	17.77	58.47	1,686	2.26
				>22	41.42	134.71	5,016	6.73
	>24	34.35	[42,238]	>0	104.50	311.00	586	0.79
							74,522	100.00
4	>0	16.60	[34,138]	>0	54.55	51.05	915	100.00
5	(0,24]	19.93	[37,240]	≤110	57.93	100.30	592	24.08
				>110	232.40	160.30	795	32.34
	(24,48]	38.40	[40,4608]	≤48	40.50	112.50	200	8.14
				>48	943.00	327.20	695	28.28
	>48	94.81	[40,6048]	≤48	386.70	452.20	6	0.24
				>48	3,573.40	638.80	170	6.92
							2,458	100.00
6	(0,6]	4.44	[16,36]	≤17	16.00	4.39	8,433	37.45
				>17	36.00	10.00	2,323	10.32
	(6,12]	10.36	[49,144]	≤100	63.04	17.78	4,890	21.72
				>100	14.40	40.25	6,413	28.48
	>12	39.51	[144,4465]	>0	1,482.20	111.90	457	2.03
							22,516	100.00
7	(0,4]	4.00	[4,4]	>0	4.00	13.60	1,950	94.29
	>4	27.46	[17,1152]	≤20	12.39	436.60	3	0.15
				>20	236.30	42.64	115	5.56
							2,068	100.00
8	>0	21.30	[30,2880]	>0	107.30	92.69	474	100.00
9	(0,12]	7.60	[16,24]	>0	16.97	5.38	7,832	87.87
	>12	24.38	[5,720]	≤10	7.37	7.72	9	0.10
				>10	152.70	22.10	1,072	12.03
							8,913	100.00
10	(0,24]	24.00	[2,60]	≤10	6.00	20.40	590	5.53
				>10	50.40	30.40	6,010	56.35
	(24,72]	39.87	[24,432]	≤36	34.57	27.66	3,365	31.55
				>36	371.80	115.20	332	3.11
	>72	157.70	[8,960]	≤33	32.16	487.40	230	2.16
				>33	437.30	563.20	138	1.30
							10,665	100.00
11	>0	50.39	[16,688]	≤38	25.47	23.68	19	8.09
				>38	602.00	57.23	216	91.91
							235	100.00

Table 6-3. Missile Size and Impact Area Subsets (Con'd)

Missile Set	Subset Range d(in)	$\bar{d}$ (in)	Subset Range A_{min} (in^2)	A_{min} Subset Bounds (in^2)	$\bar{A}_{min}$ (in)	$\bar{w}$ (lb/ft)	Number	Relative Set Freq. (%)
12	(0,36]	34.92	[4.5,36]	≤10	8.80	30.26	546	14.20
				>10	27.53	93.58	894	23.24
	(36,72]	51.34	[3.4,168]	≤12	10.35	38.84	521	13.55
				>12	64.67	110.20	931	24.20
	>72	110.35	[16,240]	≤24	21.79	129.60	83	2.16
				>24	96.30	401.30	871	22.65
							3,846	100.00
13	(0,48]	48.00	[32,96]	>0	50.74	15.02	333	44.46
	>48	96.26	[88,672]	>0	177.60	68.30	416	55.54
							749	100.00
14	(0,6]	5.06	[3.8,8]	>0	4.37	15.20	5,680	51.46
	(6,12]	11.29	[3.8,55]	≤10	8.16	27.87	454	4.11
				>10	18.11	61.48	3,640	32.98
	>12	21.24	[8,132]	>0	33.47	113.90	1,263	11.45
							11,037	100.00
15	>0	5.27	[1.36,45]	≤6	2.38	7.98	5,011	30.16
				>6	11.25	38.08	11,604	69.84
							16,615	100.00
16	(0,8]	5.11	[1.7,5.5]	>0	3.49	11.88	8,840	86.55
	(8,20]	11.62	[8.8,9.9]	>0	8.81	30.01	1,253	12.27
	>20	99.97	[17.6,1680]	≤20	16.29	722.80	32	0.31
				>20	439.40	860.00	89	0.87
							10,214	100.00
17	>0	22.61	[36,984]	>0	213.80	204.00	106	100.00
18	>0	46.48	[1.5,864]	≤15	4.63	44.02	321	91.98
				>15	557.00	76.11	28	8.02
							349	100.00
19	>0	67.07	[10,15000]	≤20	15.70	88.67	64	29.22
				>20	3,817.50	171.60	155	70.78
							219	100.00
20	>0	69.18	[64,8640]	≤65	64.00	49.78	27	11.74
				>65	1,207.30	77.55	203	88.26
							230	100.00
21	(0,54]	53.69	[1.6,4.0]	>0	1.61	13.95	10,825	95.12
	>54	95.05	[0.4,144]	>0	5.28	41.80	555	4.88
							11,380	100.00
22	(0,48]	43.31	[1.36,384]	≤10	2.22	12.37	2,455	75.45
				>10	144.40	40.57	620	19.05
	>48	97.41	[9.4,9216]	≤20	11.00	47.23	68	2.09
				>20	1,720.20	168.30	111	3.41
							3,254	100.00
23	>0	168.00	[32,1296]	>0	240.00	35.35	8	100.00
24	>0	10.44	[6,40]	>0	107.10	60.87	23	100.00
25	>0	60.00	[60,72]	>0	2,876.80	200.20	4,827	100.00

Table 6-4. Missile Length Characteristics

Missile Set	Size Subset Rage d(in)	ℓ Parameters Minimum Observed	Maximum Observed	$\bar{\ell}$	$\sigma(\ell)$
1	(0,1]	60.00	960.00	292.68	117.12
	(1,2]	3.00	400.00	251.28	122.64
	(2,12]	5.00	160.00	28.56	42.84
	(12,20]	2.33	6.00	2.76	1.08
	>20	0.50	7.50	1.92	1.80
2	(0,13]	12.86	46.15	22.08	8.64
	(13,17]	14.12	45.88	25.80	14.04
	(17,48]	0.50	0.63	0.60	0.12
	>48	0.50	0.63	0.60	0.04
3	(0,3]	24.00	288.00	62.52	32.76
	(3,6]	6.00	60.00	35.88	11.52
	(6,12]	3.00	48.00	18.43	13.42
	(12,24]	0.50	33.75	6.82	6.31
	>24	1.00	13.33	7.05	2.89
4	> 0	3.00	15.00	5.05	3.29
5	(0,24]	1.00	240.00	12.42	36.65
	(24,48]	1.00	11.43	3.32	2.58
	>48	1.00	3.57	1.94	0.80
6	(0,6]	15.00	45.00	34.71	8.87
	(6,12]	6.00	36.00	18.76	7.68
	>12	0.83	13.33	3.56	3.11
7	(0,4]	36.00	45.00	44.77	1.42
	> 4	1.33	2.50	2.13	0.24
8	> 0	1.00	15.00	4.88	4.43
9	(0,12]	10.80	72.00	29.65	14.09
	>12	2.00	16.00	5.40	2.24
10	(0,24]	1.50	60.00	7.21	10.82
	(24,72]	1.00	5.50	1.77	0.40
	>72	1.00	2.00	1.49	0.33
11	>0	1.00	4.14	3.24	1.16
12	(0,36]	1.00	1.00	2.60	1.99
	(36,72]	1.00	5.00	1.86	0.75
	>72	1.00	3.11	2.12	0.36
13	(0,48]	2.00	2.00	2.00	0.00
	>48	1.33	5.00	3.06	1.70
14	(0,6]	12.00	90.00	50.12	16.91
	(6,12]	8.00	60.00	16.47	8.13
	>12	0.50	26.67	12.32	2.91
15	(0,6]	0.39	108.00	50.05	19.70
16	(0,8]	9.00	80.00	45.58	20.91
	(8,20]	10.00	30.00	15.85	7.21
	>20	0.12	1.50	1.66	3.81
17	> 0	1.33	8.00	4.88	2.98
18	> 0	1.17	13.26	3.82	2.08
19	> 0	0.34	18.75	4.26	3.04
20	> 0	1.00	5.25	2.85	1.43
21	(0,54]	1.11	6.00	1.17	0.53
	>54	1.00	3.20	1.92	0.26
22	(0,48]	1.00	7.50	1.91	1.76
	>48	1.00	5.00	2.65	1.68
23	> 0	1.00	2.50	1.44	0.42
24	> 0	1.00	1.00	1.03	0.07
25	> 0	1.00	4.00	4.00	0.07

Table 6-5. Missile Availability Mode Characteristics

Missile Set Number	Availability Mode	Number	Relative Frequency (%)	Z_s Parameters (in)			
				Minimum Observed	Maximum Observed	$\bar{Z}_s$	$\sigma(Z_s)$
1	1	138,888	84.61	12	96	40.62	17.45
	2	713	0.43	36	96	63.55	16.22
	3	6,000	3.66	24	60	52.00	60.66
	4	18,546	11.30	6	144	43.10	27.22
	5	-	-	-	-	-	-
		164,147	100.00				
2	1	275	4.26	48	108	73.96	17.84
	2	10	0.16	360	360	360.00	0.00
	3	450	6.97	48	120	112.00	22.63
	4	5,097	78.99	12	95	51.22	19.60
	5	621	9.62	12	24	17.33	56.81
		6,453	100.00				
3	1	61,701	82.80	12	144	85.33	31.80
	2	4	0.01	48	48	48.00	0.00
	3	8,231	11.04	6	144	70.36	34.96
	4	4,510	6.05	12	96	30.67	12.02
	5	76	0.10	12	12	12.00	0.00
		74,522	100.00				
4	1	915	100.00	48	100	88.11	21.54
	2	-	-	-	-	-	-
	3	-	-	-	-	-	-
	4	-	-	-	-	-	-
	5	-	-	-	-	-	-
		915	100.00				
5	1	2,093	85.15	24	144	101.11	38.69
	2	-	-	-	-	-	-
	3	-	-	-	-	-	-
	4	365	14.85	12	1200	88.21	149.45
	5	-	-	-	-	-	-
		2,458	100.00				
6	1	9,707	43.11	12	144	108.45	35.10
	2	100	0.44	144	144	144.00	0.00
	3	1,800	8.00	24	72	42.87	11.60
	4	3,926	17.44	0	96	15.35	11.82
	5	6,983	31.01	4	36	9.28	3.21
		22,516	100.00				
7	1	1,982	95.84	30	50	36.16	9.57
	2	-	-	-	-	-	-
	3	-	-	-	-	-	-
	4	86	4.16	24	60	47.88	7.40
	5	-	-	-	-	-	-
		2,068	100.00				
8	1	474	100.00	60	200	70.00	15.54
	2	-	-	-	-	-	-
	3	-	-	-	-	-	-
	4	-	-	-	-	-	-
	5	-	-	-	-	-	-
		474	100.00				
9	1	7,551	84.72	24	144	94.10	46.57
	2	-	-	-	-	-	-
	3	700	7.85	60	60	60.00	0.00
	4	130	1.46	12	1196	930.25	485.75
	5	532	5.97	2	10	5.26	3.14
		8,913	100.00				
10	1	10,603	99.42	24	180	72.08	25.36
	2	-	-	-	-	-	-
	3	-	-	-	-	-	-
	4	62	0.58	24	1284	150.39	371.24
	5	-	-	-	-	-	-
		10,665	100.00				
11	1	183	77.87	72	84	82.36	4.12
	2	-	-	-	-	-	-
	3	18	7.66	70	70	70.00	0.00
	4	34	14.47	12	96	45.97	33.40
	5	-	-	-	-	-	-
		235	100.00				
12	1	2,548	66.60	15	84	55.16	18.27
	2	902	23.58	48	144	102.44	29.30
	3	98	2.56	12	36	28.16	11.26
	4	278	7.26	4	132	34.94	17.40
	5	-	-	-	-	-	-
		3,826	100.00				

Table 6-5. Missile Availability Mode Characteristics (continued)

13	1	280	37.38	36	120	90.00	40.25
	2	-	-	-	-	-	-
	3	-	-	-	-	-	-
	4	469	62.62	8	48	11.64	9.34
	5	-	-	-	-	-	-
		749	100.00				
14	1	7,402	67.07	20	120	34.09	21.02
	2	290	2.63	30	120	116.90	16.42
	3	1,482	13.43	36	84	46.59	4.15
	4	1,863	16.87	12	1196	40.64	120.96
	5	-	-	-	-	-	-
		11,037	100.00				
15	1	13,940	83.90	24	96	43.25	19.46
	2	-	-	-	-	-	-
	3	1,300	7.82	36	48	47.08	3.20
	4	1,375	8.28	12	84	26.55	10.95
	5	-	-	-	-	-	-
		16,615	100.00				
16	1	9,459	93.49	12	180	37.96	22.83
	2	-	-	-	-	-	-
	3	280	2.74	36	48	40.29	5.75
	4	385	3.77	18	144	32.21	27.37
	5	-	-	-	-	-	-
		10,214	100.00				
17	1	89	83.96	24	72	35.60	13.40
	2	-	-	-	-	-	-
	3	-	-	-	-	-	-
	4	17	16.04	90	90	90.00	0.00
	5	-	-	-	-	-	-
		106	100.00				
18	1	267	76.50	40	120	117.30	14.44
	2	30	8.60	36	36	36.00	0.00
	3	-	-	-	-	-	-
	4	52	14.90	24	84	61.08	16.68
	5	-	-	-	-	-	-
		349	100.00				
19	1	99	45.21	24	144	120.73	24.82
	2	-	-	-	-	-	-
	3	-	-	-	-	-	-
	4	120	54.79	24	1860	129.30	293.99
	5	-	-	-	-	-	-
		219	100.00				
20	1	58	25.22	120	120	120.00	0.00
	2	-	-	-	-	-	-
	3	-	-	-	-	-	-
	4	172	74.78	24	240	81.90	39.39
	5	-	-	-	-	-	-
		230	100.00				
21	1	2,495	22.04	24	240	70.33	42.71
	2	7,533	66.55	54	84	83.92	1.42
	3	300	2.65	60	60	60.00	0.00
	4	991	8.75	24	600	109.25	94.13
	5	1	0.01	60	72	72.00	0.00
		11,320	100.00				
22	1	1,010	31.04	15	144	66.24	26.95
	2	30	.92	72	72	72.00	0.00
	3	2,173	66.78	72	96	95.97	0.89
	4	41	1.26	48	1212	643.32	555.20
	5	-	-	-	-	-	-
		3,254	100.00				
23	1	-	-	-	-	-	-
	2	-	-	-	-	-	-
	3	-	-	-	-	-	-
	4	8	100.00	8	300	130.00	118.15
	5	-	-	-	-	-	-
		8	100.00				
24	1	-	-	-	-	-	-
	2	-	-	-	-	-	-
	3	-	-	-	-	-	-
	4	23	100.00	18	40	20.87	7.41
	5	-	-	-	-	-	-
		23	100.00				
25	1	-	-	-	-	-	-
	2	-	-	-	-	-	-
	3	-	-	-	-	-	-
	4	4,827	100.00	58	84	60.02	0.71
	5	-	-	-	-	-	-
		4,827	100.00				

Table 6-6. Temporary Structure Missile Source Distribution by Plant

Plant Number	Wood Frame Foundation Type 1	2	3	4	Metal Frame Foundation Type 1	2	3	4	Metal Tower	Trailer	Masonry	Totals
1	9	2	29	20	10	6	0	1	1	20	2	100
2	16	14	7	50	5	32	0	0	5	21	1	151
3	1	10	0	63	3	12	21	0	0	35	2	147
4	2	3	5	9	8	33	0	0	3	2	3	68
5	0	20	0	0	0	8	0	0	2	1	0	31
6	0	0	0	0	0	13	0	0	1	0	4	18
Totals	28	49	41	142	26	104	21	1	12	79	12	515

APPENDIX 7

TUMBLING COEFFICIENT AND TRAJECTORY EQUATIONS

7.1 Random Tumbling Mode Drag Coefficient for Cylinders

The general expression for the mathematical expectation of the aerodynamic drag function is given by

$$\bar{C}_d = \int_0^{\pi} \int_0^{2\pi} \int_0^{2\pi} C_d(\alpha,\beta,\delta) \quad f(\alpha,\beta,\delta) d\delta d\beta d\alpha \tag{7.1}$$

where $\bar{C}_d$ is the expected value, α is the angle of attack, β is an azimuthal angle, and δ is the roll angle, as shown in Figure 3-1. The joint probability density function $f(\alpha,\beta,\delta)$ defines the missile orientation likelihood and thus expresses the missile tumbling characterization. For the standard assumption of uniformly random spatial orientation, the joint density function is

$$f(\alpha,\beta,\delta) = \frac{1}{8\pi^2} \quad \text{Sin } \alpha \tag{7.2}$$

The drag coefficient of a cylinder was given in Appendix 3 as

$$C_d(\alpha,\beta,\delta) = C_d(\alpha) = C_{dc} \text{ Sin}^3 \alpha + \frac{\pi d}{4L} \left|\text{Cos}^3 \alpha\right| \tag{7.3}$$

Substituting Equations 7.2 and 7.3 into Equation 7.1 yields

$$\bar{C}_d = \frac{1}{2} \left[C_{dc} \int_0^{\pi} \text{Sin}^4 \alpha d\alpha + \frac{\pi d}{4L} \int_0^{\pi} \left|\text{Cos}^3 \alpha\right| \text{Sin } \alpha \, d\alpha \right] \tag{7.4}$$

Noting that

$$\int_0^{\pi} \text{Sin}^4 \alpha \, d\alpha = \frac{3\pi}{8} \tag{7.5}$$

and

$$\int_0^{\pi} |\mathrm{Cos}^3 \alpha| \mathrm{Sin}\ \alpha\ d\alpha = 2 \int_0^{\pi/2} \mathrm{Cos}^3 \alpha\ \mathrm{Sin}\ \alpha\ d\alpha = \frac{1}{2} \tag{7.6}$$

the random tumbling mode drag coefficient becomes

$$\bar{C}_d = \frac{1}{4} \left[\frac{3\pi}{4} C_{dc} + \frac{\pi d}{4L} C_{da} \right] \tag{7.7}$$

This expression yields a significantly higher expected value than some previous published results, e.g., Bates and Swanson (3-3) and JPL (1-48). However, Bates and Swanson used a drag coefficient whose terms varied as $\mathrm{Sin}^2 \alpha$ and $\mathrm{Cos}^2 \alpha$ instead of the cubes of these quantities, and their averaging process is questionable. JPL employed a formulation similar to that given by Equation 7.1 but apparently evaluated one of the integrals improperly. Evaluation of this same integral by composite numerical quadrature has duplicated the expectation given in Equation 7.7 to four decimal places.

7.2 Equations of Motion

Relative to the reference frames F_p, F_{pc}, and F_{tc} (see Figure 3.1), the position of the mass center C of the missile is expressed as

$$\bar{R} = x\hat{i} + y\hat{j} + z\hat{k} \tag{7.8}$$

$$= \rho\hat{r} + z\hat{k} + \theta\hat{\theta} \tag{7.9}$$

$$\bar{R}_t = \rho_t \hat{r}_t + z_t \hat{k}_t + \theta_t \hat{\theta}_t \tag{7.10}$$

where the subscript p has been dropped for convenience.

At time t, the center of the tornado moves from S to O_t, and relative to F_{pc} it is located at

$$\rho_{ot} = \left[(\rho_s \text{Cos}\theta_s + U_T t \text{Cos}\tau)^2 + (\rho_s \text{Sin}\theta_s + U_T t \text{Sin}\tau)^2\right]^{1/2} \tag{7.11}$$

$$\theta_{ot} = \text{Tan}^{-1}\left[\frac{\rho_s \text{Sin}\theta_s + U_T t \text{Sin}\tau}{\rho_s \text{Cos}\theta_s + U_T t \text{Cos}\tau}\right] \tag{7.12}$$

$$z_{ot} = z_s \tag{7.13}$$

The position of the point C in F_{tc} and F_{pc} is related by

$$\rho_t = \left[\rho^2 - 2\rho\rho_{ot}\text{Cos}(\theta-\theta_{ot}) + \rho_{ot}^2\right]^{1/2} \tag{7.14}$$

$$\theta_t = \text{Tan}^{-1}\left[\frac{\rho\text{Sin}\theta - \rho_{ot}\text{Sin}\theta_{ot}}{\rho\text{Cos}\theta - \rho_{ot}\text{Cos}\theta_{ot}}\right] \tag{7.15}$$

$$z_t = z \tag{7.16}$$

where the position (ρ,θ,z) in F_{pc} and (x,y,z) in F_p is given by the standard cylindrical-cartesian transformation.

As discussed earlier, the aerodynamic force $\bar{f}$ is postulated to be proportional to the relative velocity between the inertial wind velocity ($\bar{U}$) and the inertial missile velocity ($\bar{V}$), it is therefore essential to derive an expression for this velocity $\bar{v}$.

From the windfield definition, the wind velocity relative to F_{tc} is normally given in components parallel to F_{tc} as

$$\bar{u}_{tc} = \bar{u}_{tc}(\rho_t, \theta_t, z_t) = \begin{bmatrix} u_{rt} \\ u_{\theta t} \\ u_{zt} \end{bmatrix} \tag{7.17}$$

and these are related to the components of $\bar{u}$ in F_{pc} as follows

$$\bar{u}_{pc} = \begin{bmatrix} u_r \\ u_\theta \\ u_z \end{bmatrix} = \begin{bmatrix} u_{rt}\text{Cos}(\theta_t - \theta_p) - u_{\theta t}\text{Sin}(\theta_t - \theta_p) \\ u_{rt}\text{Sin}(\theta_t - \theta_p) - u_{\theta t}\text{Cos}(\theta_t - \theta_p) \\ u_{zt} \end{bmatrix} \tag{7.18}$$

Also, since the inertial translatory wind velocity ($\bar{U}_T$) has components in F_{pc} as

$$\bar{U}_{T_{pc}} = \begin{bmatrix} U_T\text{Cos}(\theta_p - \tau) \\ -U_T\text{Sin}(\theta_p - \tau) \\ 0 \end{bmatrix} \tag{7.19}$$

the wind-missile relative velocity $\bar{v}$ in components parallel to F_{pc} is

$$\bar{v}_{pc} = \bar{u}_{pc} + \bar{U}_{T_{pc}} - \bar{V}_{pc} = \begin{bmatrix} v_r \\ v_\theta \\ v_z \end{bmatrix} \tag{7.20}$$

and

$$v = \left(v_r^{\,2} + v_\theta^{\,2} + v_z^{\,2} \right)^{1/2} \tag{7.21}$$

where $\bar{V}$ is the inertial velocity of the missile mass center C at time t.

This inertial velocity of C expressed in components parallel to F_p is

$$\bar{V}_p = \begin{bmatrix} V_x \\ V_y \\ V_z \end{bmatrix} = \begin{bmatrix} \dot{x} \\ \dot{y} \\ \dot{z} \end{bmatrix} = \begin{bmatrix} \dot{\rho}Cos\theta - \rho\dot{\theta}Sin\theta \\ \dot{\rho}Sin\theta + \rho\dot{\theta}Cos \\ \dot{z} \end{bmatrix} \tag{7.22}$$

and

$$\bar{V}_{pc} = \begin{bmatrix} V_r \\ V_\theta \\ V_z \end{bmatrix} = \begin{bmatrix} \dot{\rho} \\ \rho\dot{\theta} \\ \dot{z} \end{bmatrix} \tag{7.23}$$

The inertial acceleration of C ($\bar{a}$) is defined in F_p as

$$\bar{a}_p = \dot{\bar{V}}_p = \begin{bmatrix} \ddot{x} \\ \ddot{y} \\ \ddot{z} \end{bmatrix} \tag{7.24}$$

and by using the appropriate transformation matrices, $\bar{a}_{pc}$ is

$$\bar{a}_{pc} = \begin{bmatrix} a_r \\ a_\theta \\ a_z \end{bmatrix} = \begin{bmatrix} \ddot{\rho} - \rho\dot{\theta}^2 \\ \ddot{\rho\theta} + 2\dot{\rho}\dot{\theta} \\ \ddot{z} \end{bmatrix} \tag{7.25}$$

Using the velocity displacement relationship (Eq. 7.23), the final expression for $\bar{a}_{pc}$ is

$$\bar{a}_{pc} = \begin{bmatrix} \frac{dV_r}{dt} - \frac{V_\theta^2}{\rho} \\ \frac{dV_\theta}{dt} + \frac{V_r V_\theta}{\rho} \\ \frac{dV_z}{dt} \end{bmatrix} \tag{7.26}$$

For the random missile orientation model, the force is obtained through a coordinate transformation from the wind frame (F_w) into F_{pc} as follows

$$\bar{f}_{pc} = \begin{bmatrix} f_r \\ f_\theta \\ f_z \end{bmatrix} = \tilde{L}_{pc,w} \begin{bmatrix} f_D \\ f_L \\ f_S \end{bmatrix} \tag{7.27}$$

where

$$\tilde{L}_{pc,w} = \begin{bmatrix} \frac{v_r}{v} & L_r & P_r \\ \frac{v_\theta}{v} & L_\theta & P_\theta \\ \frac{v_z}{v} & L_z & P_z \end{bmatrix} \tag{7.28}$$

the elements of which are the F_w components of unit vectors along f_D, f_L, and f_S directions.

LIST OF REFERENCES

1. Tornado and Tornado Risk Modeling

1- 1 Hoecker, W. H., Jr., "Wind Speed and Air Flow Patterns in the Dallas Tornado of April 2, 1957," Monthly Weather Review, 88(5), 1960.

1- 2 Hoecker, W. H., Jr., "Three-Dimensional Pressure Pattern of the Dallas Tornado and Some Resultant Implications," Monthly Weather Review, 89(12), 1961.

1- 3 Fujita, T. T., Bradbury, D. L., and Black, P. G., "Estimation of Tornado Wind Speed from Characteristic Ground Marks," The University of Chicago, Department of Geophysical Sciences, SMRP Research Paper No. 69, October 1967.

1- 4 Fujita, T. T., "Aerial Survey of the Palm Sunday Tornadoes of April 11, 1965," The University of Chicago, Department of Geophysical Sciences, SMRP Research Paper No. 49, January 1966.

1- 5 Flora, S. D., Tornadoes of the United States, 2nd Edition, University of Oklahoma Press, 1954.

1- 6 Thom, H. C. S., Tornado Probabilities, Monthly Weather Review, 91, October - December 1963.

1- 7 McDonald, R. J., Mehta, D. C., and Minor, J. E., "Tornado Resistant Design of Nuclear Power Plant Structures," Nuclear Safety, Volume 15, No. 4, July - August 1974.

1- 8 Miller, D. R., and Williams, W. A., "Tornado Protection for the Spent-Fuel Storage Pool," Report APED-5696, General Electric Company, November 1968.

1- 9 Fujita, T. T., "Proposed Characterization of Tornadoes and Hurricanes by Area and Intensity," The University of Chicago, SMRP Research Paper No. 91, February 1971.

1-10 Fujita, T. T., "Estimate of Maximum Windspeeds of Tornadoes in Southernmost Rockies," The University of Chicago, SMRP Research Paper No. 105, June 1972.

1-11 Fujita, T. T., "Proposed Mechanism of Suction Spots Accompanied by Tornadoes," Proc. of Severe Local Storms Conference, St. Louis, Missouri, October 1971.

1-12 Fujita, T. T., "Estimate of Maximum Windspeeds of Tornadoes in Three Northwestern States," The University of Chicago, SMRP Research Paper No. 92, 1970.

1-13 Fujita, T. T., "The Lubbock Tornadoes: A Study of Suction Spots," Weatherwise, 23, No. 4, 1970.

1-14 Fujita, T. T., "Estimated Windspeeds of the Palm Sunday Tornadoes," The University of Chicago, SMRP Research Paper No. 53, 1967.

1-15 Doan, P. L., "Tornado Consideration for Nuclear Power Plant Structures," Nuclear Safety, Volume 11, No. 4, July - August 1970.

1-16 Garson, R. C., Catalan, J. M., and Cornell, C. A., "Tornado Risk Evaluation Using Wind Speed Profiles," Journal of the Structural Division, Proceedings ASCE, Volume 101, No. ST5, May 1975.

1-17 Wen, Y. K., and Chu, S. L., "Tornado Risks and Design Wind Speed," Journal of the Structural Division, Proceedings ASCE, Volume 99, No. ST12, December 1973.

1-18 Battan, L. J., The Nature of Violent Storms, Doubleday, New York, 1961.

1-19 Garson, R. C., Catalan, J. M., and Cornell, C. A., "Tornado Design Winds Based on Risk," Journal of the Structural Division, Proceedings ASCE, Volume 101, No. ST9, September 1975.

1-20 Nuclear Regulatory Commission, "Design Basis Tornado for Nuclear Power Plants," Regulatory Guide 1.76, April 1974.

1-21 Nuclear Regulatory Commission, "Technical Basis for Interim Regional Tornado Criteria," WASH-1300, May 1974.

1-22 Mehta, K. C., Minor, J. E., and McDonald, J. R., "The Tornadoes of April 3-4, 1974: Windspeed Analysis," Preprint 2490, ASCE National Structural Engineering Meeting, April 1975.

1-23 McDonald, J. R., Mehta, K. C., Minor, J. E., and Beason, L., "Development of a Windspeed Risk Model for the Argonne National Laboratory Site," Institute for Disaster Research and Department of Civil Engineering, Texas Tech University, May 1975.

1-24 Fujita, T. T., "Estimate of Aerial Probability of Tornadoes from Inflationary Reporting of Their Frequencies," The University of Chicago, SMRP Research Paper No. 89, October 1970.

1-25 Fujita, T. T., and Pearson A. D., "Results of FPP Classification of 1971 and 1972 Tornadoes," Eighth Conference on Severe Local Storms, October 1973.

1-26 Fujita, T. T., "F-Scale Classification of 1971 Tornadoes," The University of Chicago, SMRP Research Paper No. 100, April 1972.

1-27 Battan, L. J., "Duration of Tornadoes," Bulletin of the American Meteorological Society, Volume 40, No. 7, July 1959.

1-28 Pautz, M. E., (Ed.), "Severe Local Storm Occurrences, 1955-1967," U. S. Department of Commerce, Environmental Science Services Administration, ESSA Technical Memorandum WBTM FCST 12, September 1969.

1-29 Glaser, A. H., "An Observational Deduction of the Structure of a Tornado Vortex," First Conference on Cumulus Convection, Portsmouth, N. H., May 1959.

1-30 Kuo, H. L., "On the Dynamics of Convective Atmospheric Vortices," Journal of Atmospheric Sciences, 23, January 1966.

1-31 Kuo, H. L., "Axisymmetric Flows in the Boundary Layer of a Maintained Vortex," Journal of Atmospheric Sciences, 23, January 1971.

1-32 Rossman, F. O., "On the Physics of Tornadoes," First Conference on Cumulus Convection, Portsmouth, N. H., May 1959.

1-33 Fujita, T. T., "A Detailed Analysis of the Fargo Tornadoes of June 20, 1957," U. S. Weather Bureau Research Paper No. 42, U. S. Department of Commerce, 1960.

1-34 Wolford, L. V., "Tornado Occurrences in the United States," U. S. Weather Bureau Technical Paper No. 20, 1960.

1-35 Abdullah, A. J., "Some Aspects of the Dynamics of Tornadoes," Monthly Weather Review, 83(4), April 1955.

1-36 General Electric Standard Safety Analysis Report, Section 3.3-3.5, Docket No. STN-50-447.

1-37 Hall, F., and Brewer, R. D., "A Sequence of Tornado Damage Patterns," Monthly Weather Review, 87, 1959.

1-38 Prossner, N. E., "Aerial Photagraphs of a Tornado Path in Nebraska, May 5, 1964," Monthly Weather Review, 92, 1964.

1-39 Wen, Y. K., "Dynamic Tornadic Wind Loads on Tall Buildings," Journal of the Structural Division, Proceedings ASCE, Volume 101, No. 371, January 1975.

1-40 Goldman, J. L., "The Illinois Tornadoes of 17 and 22 April 1963," The University of Chicago, SMRP Research Paper No. 39, 1965.

1-41 Booker, C. A., "On Transmission Towers Destroyed by the Worchester, Massachusetts, Tornado of June 9, 1953," Bulletin of the American Meteorological Society, 35, 1954.

1-42 Segner, E. P., "Estimates of Minimum Wind Forces Causing Structural Damage in the Dallas Tornado," U. S. Weather Bureau Research Paper No. 41, 169-175.

1-43 Court, A., "Tornado Incidence Maps," ESSA Technical Memorandum ERLTM-NSSL 49, National Severe Storms Laboratory, Norman, Oklahoma, August 1970.

1-44 Fulks, J. R., "On the Mechanics of the Tornado," NOAA Technical Memorandum ERLTM-NSSL4, National Severe Storm Laboratory, Norman, Oklahoma, 1962.

1-45 Hess, W. N., (Ed.), Weather and Climate Modification, John Wiley & Sons, 1974.

1-46 Martin, J. R., "Tornadoes in the United States, 1916-1937," U. S. Weather Bureau, Washington, D. C., 1940.

1-47 Nuclear Regulatory Commission, "Safety Related Site Parameters for Nuclear Power Plants," WASH-1361, January 1975.

1-48 Redmann, G. H., et al., "Wind Field and Trajectory Models for Tornado-Propelled Objects," EPRI 308, Technical Report 1, February 1976.

1-49 Abbey, R. F., "Establishment of Maximum Regional Tornado Criteria For Nuclear Power Plants," Ninth Conference on Severe Local Storms, Norman, Oklahoma, October 21-23, 1975.

1-50 Abbey, R. F., and Fujita, T. T., "Use of Tornado Path Lengths and Gradations of Damage to Assess Tornado Intensity Probabilities," Ninth Conference on Severe Local Storms, Norman, Oklahoma, October 21-23, 1975.

1-51 Beebe, R. C., et al., "A Meteorological and Engineering Approach to the Regionalization of Tornado Wind Criteria for Nuclear Power Plant Design," Dames and Moore, AEC Contract No. AT(11-1)-2396, September 1975.

1-52 Singh, M. P., Morcos, A., and Chu, S. L., "Probabilistic Treatment of Problems in Nuclear Power Plant Design," First ASCE Specialty Conference on Structural Design of Nuclear Power Plant Facilities, Chicago, Illinois, December 1973.

1-53 Abbey, R. F., "Research Efforts in Severe Storms Applied to Nuclear Reactors," Second U. S. National Conference on Wind Engineering Research, Fort Collins, Colorado, June 1975.

1-54 Sun, C. N., Burdette, E. G., and Perry, N. H. L., "Tornado Wind Forces on Structures," Second ASCE Specialty Conference on Structural Design of Nuclear Power Plant Facilities, New Orleans, Louisiana, December 1975.

1-55 Agee, E., Church, C., Morns, C., and Snow, Jr., "Some Synoptic Aspects and Dynamic Features of Vortices Associated with the Tornado Outbreak of April 3, 1974," Monthly Weather Review, Volume 103, April 1975.

1-56 Morton, B. R., "Geophysical Vortices," Progress in Aeronautical Sciences, Oxford: Pergamon, Volume 7, 1966.

1-57 ANSI N-178 (ANS 2.3), "Guidelines for Estimating Tornado, Hurricane, and Other Extreme Wind Parameters at Power Reactor Sites," Draft 1, April 1975.

1-58 Brown, C. W., and Roberts, W. O. J., "The Distribution and Frequency of Tornadoes in the United States From 1880 to 1931," Transactions, American Geophysical Union, 16.

1-59 Tecson, J. J., "Characterization of 1965 Tornadoes by Their Area and Intensity," The University of Chicago, SMRP Research Paper No. 94, February 1972.

1-60 Howe, G. M., "Tornado Path Sizes," Journal of Applied Meteorology, 13, April 1974.

1-61 Burgers, J. M., "A Mathematical Model Illustrating the Theory of Turbulence," Advances in Applied Mechanics, (R. von Mises, Editor), Academic Press, Volume I, 1948.

1-62 Kessler, E., "Tornadoes," Bulletin of the American Meteorological Society, Volume 51, No. 10, October 1970.

1-63 A. D. Little, Inc., "A Study of Wind Velocities in Tornadoes, Phase I," NSSL, C-68491, August 1966.

1-64 Kessler, E., "April 25, 1973, Letter to H. Denton of NRC," NSSL.

1-65 Wen, Y. K., and Ang, A. H. S., "Tornado Risk and Wind Loading Effect on Structures," Proceedings of the 4th International Conference on Wind Effects on Buildings and Structures, London, England, September 1975.

1-66 Golden, J. H., "An Assessment of Windspeeds in Tornadoes," Preprint, Symposium on Tornadoes, Lubbock, Texas, June 1976.

1-67 Pearson, A. D., "Statistics on Tornadoes That Caused Fatalities, 1960-1970," Proceedings, Seventh Conference on Severe Local Storms, Kansas City, Missouri, October 1971.

1-68 Fujita, T. T., "Experimental Classification of Tornadoes in FPP Scale," distributed to NWS Offices, May 1973.

1-69 Hart, G. C., "Estimation of Structural Damage Due to Tornadoes," Preprint, Symposium on Tornadoes, Lubbock, Texas, June 1976.

1-70 Vigansky, J., "General Summary of Tornadoes, 1975," Climatological Data, National Summary, 26(13), 1975.

1-71 Wen, Y. K., "Note on Analytical Modeling in Assessment of Tornado Risks," Preprint, Symposium on Tornadoes, Lubbock, Texas, June 1976.

1-72 Abbey, R. F., "Risk Probabilities Associated With Tornado Windspeeds," Preprint, Symposium on Tornadoes, Lubbock, Texas, June 1976.

1-73 Kessler, E., "Survey of Boundary Layer Winds With Special Reference to Extreme Values," AIAA Paper No. 74-586, AIAA Fluid and Plasma Dynamics Conference, Palo Alto, California, June 1974.

1-74 Purdom, J. F. W., "From Above The 3 April 1974 Tornado Outbreak," Weatherwise, June 1974.

1-75 Fujita, T. T., "Graphic Examples of Tornadoes," Bulletin of the American Meteorological Society, Volume 57, No. 4, April 1976.

1-76 Moller, A., et al., "Field Observations of the Union City Tornado in Oklahoma," Weatherwise, 68, April 1974.

2. Missile Characterization and Plant Modeling

2- 1 Nuclear Regulatory Commission, Regulatory Draft Guide RD-3, "Tornado Generated Missiles."

2- 2 Nuclear Regulatory Commission, TVA Preliminary Topical Report Evaluation, February 1974.

2- 3 Nuclear Regulatory Commission, Response to GESSAR Amendment 31, June 2, 1975.

2- 4 Nuclear Regulatory Commission, Response to Bechtel, March 11, 1975, Letter, April 21, 1975.

2- 5 ANSI N177 Draft Standard, "Plant Design Against Missiles," April 1974.

2- 6 Nuclear Regulatory Commission, "Missiles Generated by Natural Phenomena," Section 3.5.1.4, Standard Review Plan, June 1975.

2- 7 "Guidelines for Tornado Damage Survey," Department of Civil Engineering, Texas Tech University.

2- 8 American Institute of Steel Construction, Manual of Steel Construction, Seventh Edition, 1970.

2- 9 Marks, L. S. (Ed.), Standard Handbook for Mechanical Engineers, Seventh Edition, McGraw-Hill, 1967.

2-10 Code of Federal Regulations, 10 CFR Part 50, Appendix A, General Design Criterion 4, "Environmental and Missile Design Bases."

2-11 Nuclear Regulatory Commission, "Structures, Systems, and Components To Be Protected From Externally Generated Missiles," Section 3.5.2, Standard Review Plan, June 1975.

2-12 Nuclear Regulatory Commission, "Ultimate Heat Sink for Nuclear Power Plants," Regulatory Guide 1.27, Revision 1, March 1974.

2-13 Nuclear Regulatory Commission, "Fuel Storage Facility Design Basis," Safety Guide 13, March 1971.

2-14 Scheibel, R. F., "The Advantages of Modular Nuclear Plant Design," General Engineering Conference, Paper GEC-P137, March 13-14, 1975.

2-15 NUS Corporation, "Commercial Nuclear Power Plants," Edition No. 7, October 1974.

2-16 ANS, "World List of Nuclear Power Plants, Nuclear News," 18(10), August 1975.

3. Missile Trajectory Analysis & Windfield Modeling

3- 1 McDonald, J. R., Minor, J. E. Mehta, K. C., "Tornado Generated Missiles," Specialty Conference or Structural Design of Nuclear Power Plant Facilities, ASCE, Chicago, Illinois, December 17-18, 1973.

3- 2 ASCE Paper 3269, "Wind Forces on Structures," Final Report of the Task Committee on Wind Forces, Committee on Loads and Stresses, Structural Division, American Society of Civil Engineers.

3- 3 Bates, F. C., and Swanson, A. E., "Tornado Design Considerations for Nuclear Power Plants," Research Report, Black & Veach, 1967.

3- 4 Paddleford, D. F., "Characteristics of Tornado Generated Missiles," Westinghouse Electric Corporation, WCAP-7897, April 1969.

3- 5 American National Standards Institute, "American National Standard Building Code Requirements for Minimum Design Loads in Buildings and Other Structures," A 58.1-1972.

3- 6 Iotti, R. C., "Velocities of Tornado Generated Missiles, Ebasco Services, ETR-1003, February 1975.

3- 7 Lee, A. J. H., "A General Study of Tornado Generated Missiles," ASCE Specialty Conference on Structural Design of Nuclear Plant Facilities, Chicago, Illinois, December 17-18, 1973.

3- 8 Tennessee Valley Authority, "The Generation of Missiles by Tornadoes," TVA-TR74-1, November 1974.

3- 9 Suarez, M. A., "Selection of Design Basis Tornado," Nuclear Power Plants.

3-10 Sargent & Lundy, "Tornado-Generated Missile Study," Appendix 3A Bryon/Braidwood PSAR, February 1975.

3-11 Gilbert Associates, "Design Parameters for Tornado Generated Missiles," Report No. GAI-TR-102, Revision 1, January 1975.

3-12 Bhattacharyya, A. K., Boritz, R. C., and Niyogi, P. K., "A Consistent Method for Determining Effects of Tornado Missiles on Nuclear Power Plant Design," Second ASCE Specialty Conference on Structural Design of Nuclear Power Plant Facilities, New Orleans, Louisiana, December 8-10, 1975.

3-13 Lee, A. J. H., "Trajectory of Tornado Missiles and the Design Parameters," Second ASCE Specialty Conference on Structural Design of Nuclear Power Plant Facilities, New Orleans, Louisiana, December 8-10, 1975.

3-14 Huang, W., and McLaughlin, J. M., "Tornado Generated Missiles," Second ASCE Specialty Conference on Structural Design of Nuclear Power Plant Facilities, New Orleans, Louisiana, December 8-10, 1975.

3-15 Costello, J. F., and Sadeh, W. Z., "Drag Forces on Tornado Borne Missiles," Second ASCE Specialty Conference on Structural Design of Nuclear Power Plant Facilities, New Orleans, Louisiana, December 8-10, 1975.

3-16 Beeth, D. R., and Hobbs, S. H., "Analysis of Tornado Generated Missiles," Topical Report B&R-001, Brown & Root, Houston, Texas, May 1975.

3-17 Bhattacharyya, A. K., Boritz, R. C., and Niyogi, P. K., "Characteristics of Tornado Generated Missiles," UEC-TR-002-0, United Engineers, October 1975.

3-18 Duke Power Project 81, "A Report on Tornado Generated Missiles," Appendix 3A, 1970.

3-19 Dergarabedian, P., and Fendell, F., "One- and Two-Cell Tornado Structure and Funnel-Cloud Shape," Journal of the Atmospheric Sciences, Volume XXI, No. 1, July - August 1973.

3-20 Carrier, G. F., "The Intensification of Hurricanes," J. Fluid Mech., Volume 49, 1971.

3-21 Carrier, G. F. "A Model of the Mature Hurrican," J. Fluid Mech., Volume 47, 1971.

3-22 Burggraf, O. R., Stewartson, K., and Belcher, R., "Boundary Layer Induced by a Potential Vortex," The Physics of Fluids, Volume 14, No. 9, September 1971.

3-23 Carrier, G. F., "Swirling Flow Boundary Layers," J. Fluid Mech., Volume 49, 1971.

3-24 Dergarabedian, P., and Fendell, F., "Parameters Governing the Generation of Free Vortices," The Physics of Fluids, Volume 10, No. 11, November 1967.

3-25 Davies-Jones, R. P., and Vickers, G. T., "Numerical Simulation of Convective Vortices," NOAA Technical Memorandum, ERL NSSL-57, November 1971.

3-26 Kessler, E., "Tornadoes," Bulletin of the American Meteorological Society, Volume 51, No. 10, October 1970.

3-27 Ward, N. B., "The Exploration of Certain Features of Tornado Dynamics Using a Laboratory Model," Journal of the Atmospheric Sciences, Volume 29, No. 6, September 1972.

3-28 Stephenson, A. E., "Tornado Missile Drop Tests of 12-Inch Pipes," Sandia Laboratories, Janaury 1977.

3-29 Davies-Jones, R. P., and Golden, J. H., "On the Relation of Electrical Activity to Tornadoes," Journal of Geophysical Research, Volume 80, No. 12, April 20, 1975.

3-30 Davies-Jones, R. P., and Golden, J. H., "Reply," Journal of Geophysical Research, Volume 80, No. 33, November 20, 1975.

3-31 Golden, J. H., and Purcell, D., "Photogeometric Velocities for the Great Bend, Kansas, Tornado: Accelerations and Asymmetries," Ninth Conference on Severe Local Storms, Norman, Oklahoma, October 21-23, 1975.

3-32 Golden, J. H., and Davies-Jones, R. P., "Photogrammetric Windspeed Analysis and Damage Interpretation of the Union City, Oklahoma, Tornado, May 24, 1973," Preprints, Second U. S. National Conference on Wind Engineering Research, Fort Collins, Colorado, June 23-25, 1975.

3-33 Ying, S. J., and Chang, C. C., "Exploratory Model Study of Tornado-Like Vortex Dynamics," Journal of the Atmospheric Sciences, Volume 27, No. 1, January 1970.

3-34 Serrin, J., "The Swirling Vortex," Phil. Trans. Roy. Soc. London, 271, 1972.

3-35 Chi, S. W., "Numerical Modeling of the Three-Dimensional Flows in the Ground Boundary Layer of a Maintained Axisymmetrical Vortex," Tellus, XXVI, 4, 1974.

3-36 Melaragno, M. G., "Tornado Forces and Their Effects on Buildings," Kansas State University, 1968.

3-37 Reynolds, G. W., "Venting and Other Building Practices as Practical Means of Reducing Damage From Tornado Low Pressures," Bulletin of the American Meteorological Society, Volume 39, No. 1, January 1958.

3-38 Vickery, B. J., and Clark, A. W., "Lift or Across-Wind Response of Tapered Stacks," Journal of the Structural Division, Proceedings of the American Society of Civil Engineers, Volume 98, No. ST1, January 1972.

3-39 Dessens, J., "Influence of Ground Roughness on Tornadoes: A Laboratory Simulation," Journal of Applied Meteorology, Volume 11, February 1972.

3-40 Lewellen, W. S., and Teske, M., "Turbulence Modeling and Its Application to Atmospheric Diffusion, Part II: Critical Review of the Use of Invariant Modeling," ESRL, Environmental Monitoring Series, EPA-600/4-75-016b, December 1975.

3-41 Davies-Jones, R. P., "The Dependence of Core Radius on Swirl Ratio in a Tornado Simulator," Journal of the Atmospheric Sciences, Volume 30, No. 7, October 1973.

3-42 Brown, R. A., Burgess, D. W., and Crawford, K. C., "Twin Tornado Cyclones Within a Severe Thunderstorm: Single Doppler Radar Observations," Weatherwise, Volume 26, No. 2, April 1973.

3-43 Kessler, E., "On Tornadoes and Their Modification," Technology Review, Volume 74, No. 6, May 1972.

3-44 Hsu, C. T., and Tesfamariam, H., "Turbulent Modeling of a Vortex Boundary Layer Flow," Engineering Research Institute, Iowa State University, ERI-76126, February 1976.

3-45 Hsu, C. T., and Tesfamariam, H., "Computer Simulation of a Tornado-Like Vortex Boundary Layer Flow," Engineering Research Institute, Iowa State University, ERI-76231, February 1976.

3-46 Danielsen, E. F., "A Conceptual Theory of Tornadogenesis Based on Macro-, Meso-, and Microscale Processes," Ninth Conference on Severe Local Storms, Norman, Oklahoma, October 21-23, 1975.

3-47 Blechman, J. B., "The Wisconsin Tornado Event of April 21, 1974: Observations and Theory of Secondary Vortices," Ninth Conference on Severe Local Storms, Norman, Oklahoma, October 21-23, 1975.

3-48 Fujita, T. T., "New Evidence From April 3-4, 1974, Tornadoes," Ninth Conference on Severe Local Storms, Norman Oklahoma, October 21-23, 1975.

3-49 Vickery, B. J., and Kao, K. H., "Drag or Along-Wind Response of Slender Structures," Journal of the Structural Division, Proceedings of the American Society of Civil Engineers, Volume 98, No. ST1, January 1972.

3-50 Minor, J. E., Mehta, K. C., and McDonald, J. R., "Failure of Structures Due to Extreme Winds," Journal of the Structural Division, Proceedings of the American Society of Civil Engineers, Volume 98, No. ST11, November 1972.

3-51 Sherman, Z., "Residential Buildings Engineered to Resist Tornadoes," Journal of the Structural Division, Proceedings of the American Society of Civil Engineers, Volume 99, No. ST4, April 1973.

3-52 Lilly, D. K., "Tornado Dynamics," National Center for Atmospheric Research, NCAR Manuscript No. 69-117.

3-53 Davenport, A. G., "Gust Loading Factors," Journal of the Structural Division, Proceedings ASCE, Volume 93, No. ST3, June 1967.

3-54 Davenport, A. G., "The Application of Statistical Concepts to the Wind Loading of Structures," Proceedings, Institution of Civil Engineering, Volume 19, 1961.

3-55 Golden, J. H., "The Life Cycle of Florida Keys' Waterspouts. I," Journal of Applied Meteorology, Volume 13, September 1974.

3-56 Golden, J. H., "Scale Interaction Implications for the Waterspout Life Cycle. II," Journal of Applied Meteorology," Volume 13, September 1974.

3-57 Lewis, W., and Perkins, P. J., "Recorded Pressure Distribution on the Outer Portion of a Tornado Vortex," Monthly Weather Review, Volume 81, No. 12, December 1953.

3-58 Sarpkaya, T., "Lift, Drag, and Added-Mass Coefficients for a Circular Cylinder Immersed in a Time-Dependent Flow," Journal of Mechanics, Transactions of the ASME, March 1963.

3-59 Sarpkaya, T., and Garrison, C. J., "Vortex Formation and Resistance in Unsteady Flow," Journal of Applied Mechanics, Transactions of the ASME, March 1963.

3-60 Lewellen, W. S., "Theoretical Models of the Tornado Vortex," Preprint, Symposium on Tornadoes, Lubbock, Texas, June 1976.

3-61 Davies-Jones, R. P., "Laboratory Simulation of Tornadoes," Preprint, Symposium on Tornadoes, Lubbock, Texas, June 1976.

3-62 Costello, J. F., "Trajectories of Tornodo-Borne Missiles," Preprint, Symposium on Tornadoes, Lubbock, Texas, June 1976.

3-63 Cermak, J. E., and Atkins, R. E., "Wind Loads on Structures," Preprint, Symposium on Tornadoes, Lubbock, Texas, June 1976.

3-64 Fujita, T. T., et al.,"Photogrammetric Analyses of Tornadoes," Preprint, Symposium on Tornadoes, Lubbock, Texas, June 1976.

3-65 McDonald, J. R., "Tornado Generated Missiles and Their Effects," Preprint, Symposium on Tornadoes, Lubbock, Texas, June 1976.

3-66 Mehta, K. C., et al., "Engineering Aspects of the Tornadoes of April 3-4, 1974," Committee on Natural Disasters, Natural Academy of Sciences, 1975.

3-67 Shanahan, J. A., "Tornado Structure - Interaction," Preprint, Symposium on Tornadoes, Lubbock, Texas, June 1976.

3-68 Simiu, Emil, and Cartes, M., "Tornado Borne Missile Speeds," National Bureau of Standards, NBSIR 76-10-50, April 1976.

3-69 Etkin, B., Dynamics of Atmospheric Flight, John Wiley & Sons, New York, 1972.

3-70 Lilly, D. K., "Tornado Dynamics," National Center for Atmospheric Research, NCAR Manuscript No. 69-117, Boulder, Colorado, 1969.

3-71 Minor, J. E., "Applications of Tornado Technology in Professional Practice," Preprint, Symposium on Tornadoes, Lubbock, Texas, June 1976.

3-72 MacDonald, A. J., Wind Loadings on Buildings, Halsted Press, 1975.

3-73 Mehta, K. C., "Windspeed Estimates: Engineering Analysis," Preprint, Symposium on Tornadoes, Lubbock, Texas, June 1976.

3-74 Eagleman, J. R., Muirhead, V. U., and Willems, N., Thunderstorms, Tornadoes, and Building Damage, D. C. Heath, 1975.

3-75 Marte, J. E., Kuntz, D. W., and Redman, G. H., "Aerodynamic Coefficients of Missile Shapes," Preprint, Symposium on Tornadoes, Lubbock, Texas, June 1976.

3-76 Shampine, L. F., and Gordon, M. K., Computer Solution of Ordinary Differential Equations: The Initial Value Problem, W. H. Freeman, San Francisco, 1975.

3-77 Lew, H. G., "Method of Accelerated Successive Replacement Applied to Boundary Layer Equations," AIAA Journal, Volume 6, 1968.

3-78 Hoerner, S. F., Fluid-Dynamic Drag, Published by the Author, Midland Park, New Jersey, 1965.

3-79 Schlichting, H., Boundary Layer Theory, McGraw-Hill, New York, 1965.

3-80 Chi, S. W., and Costopolous, T., "Wind Loadings on Ground Structures in Intense Atmospheric Vortices - 1," National Science Foundation, GK-41469, March 1975.

3-81 Redman, G. H., et al., "Aerodynamic Data For Planks," Letter Communication through EPRI, Jet Propulsion Laboratory, September 14, 1976.

3-82 Surry, D., "Turbulence In a Wind Tunnel and Its Use In Studying The Turbulence Effects on The Aerodynamics of a Rigid Circular Cylinder," Wind Effects on Buildings and Structures.

3-83 Joubent, P. N., et al., "The Drag of Bluff Bodies Immersed in a Turbulent Boundary Layer," Wind Effects on Buildings and Structures.

3-84 Poreh, M., "On the Motion of Autorotating Elongated Prismatic Bodies," Fluid Dynamics and Diffusion Laboratory, Colorado State University, NBS Contract No. 1101-5064-35873, August 1976.

3-85 Longinow, A., et al., "Debris Motion and Injury Relationships in All Hazard Environments," IITRI, DCPA Contract DCPA 01-74-C-0251, July 1976.

3-86 Sentman, L. H., and Neke, S. E., "Drag Coefficients for Tumbling Satellites," J. Spacecraft, Volume 4, No. 9, September 1967.

3-87 Shampine, L. F., et al., "Solving Nonstiff Ordinary Differential Equations - The State of the Art," SIAM Review, Volume 18, No. 3, July 1976.

4. Missile Interactions

4- 1 McNeill, R. L., "Rapid Penetration of Terrestrial Materials - The State of the Art," Proceedings of a Conference held at Texas A&M University, February 1-3, 1972.

4- 2 Stephenson, A. E., "Tornado Vulnerability at Nuclear Production Facilities," Sandia Laboratories, April 1975.

4- 3 Dunlap, J. A., and Wiedner, K., "Nuclear Power Plant Tornado Design Consideration," Journal of the Power Division, ASCE, March 1971.

4- 4 Bechtel Topical Report, "Design of Structures for Missile Impact," BC-TOP-9A, Revision 2, September 1974.

4- 5 Bechtel Topical Report, "Tornado and Extreme Wind Design Criteria for Nuclear Power Plants," BC-TOP-3A, August 1974.

4- 6 Nuclear Regulatory Commission, "Tornado Loadings," Section 3.3.2, Standard Review Plan.

4- 7 Nuclear Regulatory Commission, "Barrier Design Procedures," Section 3.5.3, Standard Review Plan.

4- 8 Austin, C. F., "Penetration into Concrete: A Review of the State of the Art," NWC TP 5337, Naval Weapons Center, China Lake, California, October 1972.

4- 9 Russell, C. R., Reactor Safeguards, Pergamon Press, New York, New York, 1962.

4-10 Wessman, H. E., and Rose, W. A., Aerial Bombardment Protection, John Wiley & Sons, New York, New York, 1942.

4-11 Amirikian, A., "Design of Protective Structures," Report NP-3726, Bureau of Yards and Docks, Department of the Navy, August 1950.

4-12 Beth, R. A., "Concrete Penetration," NDRC Report No. A-319, OSRD Report No. 4856, ATI-60 153, Division 2, National Defense Research Committee of the Office of Scientific Research and Development, March 20, 1945.

4-13 Chelapati, C. V., Kennedy, R. P., and Wall, I. B., "Probabilistic Assessment of Aircraft Hazard for Nuclear Power Plants," Nuclear Engineering and Design, 19, 1972.

4-14 Gwaltney, R. C., "Missile Generation and Protection in Light-Water-Cooled Power Reactor Plants," USAEC Report ORNL-NSIC-22, Oak Ridge National Laboratory, September 1968.

4-15 "Comparative Test of the Effectiveness of Large Bombs Against Reinforced Concrete Structures (Anglo-American Bomb Tests - Project 'Ruby')," Final Report, Project No. 1-46-7, Air Proving Ground Command, Elgin Field, Florida, October 1946.

4-16 Lee, A. J. H., "On the Missile Protection Design of Reinforced Concrete," Symposium on Structural Design of Nuclear Power Plant Facilities, Pittsburgh, Pennsylvania, April 20, 1972.

4-17 Colp, J. (Ed.), "Rapid Penetration of Terrestrial Materials," Proceedings of a Conference held at Texas A&M University, February 1-3, 1972.

4-18 Tan, C. P., "Concrete Containments for Reactors - State of Art," Journal of the Structural Division, Proceedings of the American Society of Civil Engineers, July 1970.

4-19 Beth, R. A., "Final Report on Concrete Penetration," NDRC Report No. A-388, OSRD Report No. 6459, ATI-18 718, Division 2, National Defense Research Committee of the Office of Scientific Research and Development, Washington, D. C., March 1946.

4-20 "Code Requirements for Nuclear Safety Related Concrete Structures," Proposed Addition to ACI Standard 349-76, Appendix C, American Concrete Institute Journal, February 1977.

4-21 Trexel, C. A., "Tests and Design of Bombproof Structures of Reinforced Concrete," Bureau of Yards and Docks, Navy Department, Washington, D. C., September 1941.

4-22 Robertson, H. P., "Terminal Ballistics," A Preliminary Report, Committee on Passive Protection Against Bombing, National Research Council, Washington, D. C., January 1941.

4-23 Effects of Impact and Explosion, Summary Technical Report of Division 2, National Defense Research Committee, Volume 1, Washington, D. C., 1946.

4-24 McNeilly, V. H., "Richochet of Bombs off Various Surfaces When Released at 300 Miles Per Hour," Report No. 256, Ballistic Research Laboratory, Aberdeen Proving Ground, Maryland, November 1941.

4-25 Stipe, J. G., et al., "Ballistic Tests on Concrete Slabs," Interim Report No. 28, Committee on Fortification and Design, National Research Council, Washington, D. C., June 1944.

4-26 Hansen, R. J., "Resistance of Laminated Concrete Slabs to Perforation," Interim Memorandum No. M-9, Committee on Passive Protection Against Bombing, National Research Council, Princeton, New Jersey, May 1943.

4-27 Austin, C. F., and Pringle, J. K., "Variables of Concrete and Their Effect on Penetration by Projectiles," Naval Weapons Center, China Lake, California, November 1971.

4-28 Samuely, F. J., and Hamann, C. W., Civil Protection, 1939.

4-29 Hagg, A. C., and Sankey, G. O., "The Containment of Disk Burst Fragments by Cylindrical Shells," Westinghouse Research Laboratories, June 1973.

4-30 Science Applications, Inc., "Calculation of Turbine Missile Strike Probabilities of Critical Areas on the Floating Nuclear Plant Using the Midas Code," February 1974.

4-31 Science Applications, Inc., "The Midas Code, Volume I, Description," June 1974.

4-32 Twisdale, L. A., and Garcia, B. H., "Penetration of Reinforced Concrete by Turbine Generated Missiles," Carolina Power & Light Company, December 1973.

4-33 Science Applications, Inc., "Method of Prediction of Damage and Probability of Damage to Floating Nuclear Plant from Turbine Disc Failure," Submitted to Offshore Power Systems, April 25, 1974.

4-34 Riera, J. D., "On the Stress Analysis of Structures Subjected to Aircraft Impact Forces," Nuclear Engineering and Design, 8, 1968.

4-35 Yang, H. T. Y., and Godfrey, D. A., "Structural Analysis of Aircraft Impact on a Nuclear Containment Vessel and Associated Structures," Nuclear Engineering and Design, 11, 1970.

4-36 Yeh, G. C., "Probability and Containment of Turbine Missiles," ASME-IEEE Joint Power Generation Conference, Meeting Preprint JPG-74-11, September 1974.

4-37 Vassallo, F. A., "Missile Impact Testing of Reinforced Concrete Panels," Calspan Report No. HC-5609-D-1, Prepared for Bechtel by Calspan Corporation, January 1975.

4-38 Rotz, J. V., "Results of Impact Tests on Reinforced Concrete Panels," Second ASCE Specialty Conference on Structural Design of Nuclear Power Plant Facilities, New Orleans, Louisiana, December 8-10, 1975.

4-39 Bergman, E., Welch, R. E., and Longinow, A., "Wall Panel Resistance to Tornado Borne Debris," First ASCE Specialty Conference on Structural Design of Nuclear Power Plant Facilities, Chicago, Illinois, December 1973.

4-40 O'Connell, W. J., and Baschiere, R. J., "Design Applications of Turbine Missile Impact Analysis," Second ASCE Specialty Conference on Structural Design of Nuclear Power Plant Facilities, New Orleans, Louisiana, December 8-10, 1975.

4-41 Gupta, Y. M., and Seaman, L., "Dynamic Behavior of Reinforced Concrete Under Missile Impact Loading," Second ASCE Specialty Conference on Structural Design of Nuclear Power Plant Facilities, New Orleans, Louisiana, December 1975.

4-42 Stephenson, A., Sliter, G., and Burdette, E., "Full-Scale Tornado Missile Impact Tests Using a Rocket Launcher," Second ASCE Specialty Conference on Structural Design of Nuclear Power Plant Facilities, New Orleans, Louisiana, December 1975.

4-43 Ting, R. M. L., "Non-Composite and Composite Steel Panels for Tornado Missile Barrier Walls," Second ASCE Specialty Conference on Structural Design of Nuclear Power Plant Facilities, New Orleans, Louisiana, December 1975.

4-44 Rice, J. S., Bahar, L. Y., and Ebner, A., "Reaction-Time Relationship and Structural Design Relationship of Reinforced Concrete Slabs and Shells for Aircraft Impact," Second ASCE Specialty Conference on Structural Design of Nuclear Power Plant Facilities, New Orleans, Louisiana, December 1975.

4-45 Sun, C., Burdette, E. G., and Barnett, R. O., "Missile Penetration," Journal of the Structural Division, Proceedings of the American Society of Civil Engineers, Volume 102, No. ST5, May 1976.

4-46 Kennedy, R. P., "A Review of Procedures for the Analysis and Design of Concrete Structures to Resist Missile Impact Effects," For Presentation at ELCALAP Seminar, September 1975.

4-47 Yitzhaki, D., "Punching Strength of Reinforced Concrete Slabs," Journal of the American Concrete Institute, Proceedings, V, 63, No. 5, May 1966.

4-48 Recht, R. F., and Ipson, T. W., "Ballistic Perforation Dynamics," Journal of Applied Mechanics, Transactions of the ASME, September 1963.

4-49 Rotz, J. V., "Evaluation of Tornado Missile Impact Effects on Structures," Preprint, Symposium on Tornadoes, Lubbock, Texas, June 1976.

4-50 Stephenson, A. E., "Tornado-Generated Missiles - Full-Scale Testing," Preprint, Symposium on Tornadoes, Lubbock, Texas, June 1976.

4-51 Stephenson, A. E., "Full-Scale Tornado - Missile Impact Tests," Interim Report, Electric Power Research Institute, RP399, April 1976.

4-52 Mehta, K. C., McDonald, J. R., Minor, J. E., and Sanger, A. J., "Response of Structural Systems to the Lubbock Storm," Texas Tech University, TTU SRR 03, October 1971.

4-53 McCaffery, R. J., "Solutions of Impact Problems for Structural Dynamic Analyses," ASCE Specialty Conference on Structural Design of Nuclear Plant Facilities, New Orleans, Louisiana, December 1975.

4-54 Thompson, R. G., "The Response of Residential Wall Construction Concepts to Missile Impact," Institute For Environmental Technology, Texas Tech University, July 1973.

4-55 Zankov, Z. O., Shanahan, J. A., and White, M. P., "Missile Tests of Quarter-Scale Reinforced Concrete Barriers," Symposium on Tornadoes, Lubbock, Texas, June 1976.

4-56 Williamson, R. A., and Alvy, R. R., "Impact Effect of Fragments Striking Structural Elements," Holmes & Narver, Inc., November 1973.

4-57 Structural Analysis and Design of Nuclear Plant Facilities, ASCE Committee on Nuclear Structures and Materials, Stevenson, J. D., Chairman, Draft, 1976.

4-58 Neville, A. M., Properties of Concrete, Halsted Press, 1973.

4-59 Norris, C. H., et al., Structural Design For Dynamic Loads, McGraw-Hill, 1959.

4-60 Newmark, N. M., and Haltiwanger, J. D., Air Force Design Manual, AFSWC-TDR-62-138, Kirtland Air Force Base, New Mexico, December 1962.

4-61 Structures to Resist the Effects of Accidental Explosions, TM 5-1300, Department of the Army, Navy, and Air Force, June 1969.

4-62 Baker, W. E., Hokanson, J. C., and Cervantes, R. A., "Model Tests of Industrial Missiles," Southwest Research Institute, San Antonio, Texas, May 1976.

4-63 Clark, J. E., Tornado Missile Impact Barrier Evaluation, Sandia Laboratories, R422202, February 1976.

4-64 Cottrell, W. B., and Savolainen, A. W., (Eds.), U. S. Reactor Containment Technology, USAEC Report ORNL-NSIC-5, Chapter 6, Oak Ridge National Laboratory, August 1965.

4-65 Stephenson, A. E., and Sliter, G. E., "Full-Scale Tornado-Missile Impact Tests," EPRI Program, Washington, D. C., November, 1976.

4-66 Kennedy, R. P., and Chelapati, R. P., "Conditional Probability of a Local Flexural Wall Failure for a Reactor Building as a Result of Aircraft Impact," HN 70-8082-5, Holmes & Narver, 1970.

4-67 Suarez, M. A., "Impactive Dynamic Analysis," Proceedings, Symposium on Structural Design of Nuclear Power Plant Facilities, University of Pittsburgh, Pittsburgh, Pennsylvania, December 1972.

4-68 Thigpon, L., "Projectile Penetration of Elastic-Plastic Earth Media," Journal of the Geotechnical Engineering Division, Proceedings ASCE, Volume 100, No. GT3, March 1974.

4-69 Kennedy, R. P., "Effects of Aircraft Crash Into a Concrete Reactor Containment Building," Holmes & Narver, Anaheim, California, July 1966.

4-70 Old, C. C., and Johnson, B. W., "An Evaluation of Formulas For Penetrations," Interim Progress Report 1, Contract 4G3-02-001030-C, Science Applications, Inc., Sunnyvale, California.

5. Related Probability Models

5- 1 Swan, S. W., and Meleis, M., "A Method of Calculating Turbine Missile Strike and Damage Probabilities," Bechtel Power Corporation.

5- 2 "Hypothetical Turbine Missiles - Probability Occurrence," General Electric Memo Report, March 1973.

5- 3 "Hypothetical Turbine Missiles - Sample Calculations," General Electric Memo Report, March 1973.

5- 4 Semanderes, S. N., "Methods of Determining the Probability of a Turbine Missile Hitting a Particular Plant Region," Westinghouse Electric Corporation, WCAP-7861, February 1972.

5- 5 "Hypothetical Turbine Missiles - Detailed Sample Calculations," General Electric Memo Report, December 1973.

5- 6 Cornell, C. A., "Engineering Seismic Risk Analysis," Bulletin of the Seismological Society of America, Volume 58, No. 5, October 1968.

5- 7 Bush, S. H., "Probability of Damage to Nuclear Components Due to Turbine Failure," Nuclear Safety, Volume 14, No. 3, May - June 1973.

5- 8 Shaffer, D. H., et al., "Analysis of the Probability of the Generation and Strike of Missiles from a Nuclear Turbine," Westinghouse Electric Corporation, March 1974.

5- 9 Gangloff, W. C., and Salvatori, R., "Probability as a Design Parameter Plant Design Against Missiles," ASME Winter Meeting, Detroit, Michigan, November 1973.

5-10 Lohrding, R. K., and McKay, M. D., "Using Risk Analysis as a Tool for Decision Making in the Nuclear Industry," Los Alamos Scientific Lab.

5-11 Rothstein, H., and Lloyd, R., "Turbine Missile Studies - Missile Strike Probabilities," Ebasco Internal Report, July 1974.

5-12 Godbout, P. J., "A Generalized Methodology for the Probabilistic Assessment of Aircraft Crash on Nuclear Power Plants," ANS Annual Meeting, New Orleans, Louisiana, June 1975.

5-13 Johnson, B. W., et al., "General Analysis of Turbine Missile Hazards to Nuclear Power Plants," Science Applications, Inc., SAI-75-507-SV.

5-14 O'Connell, W. J., and Baschiere, R. J., "Design Applications of Turbine Missile Impact Analysis," Paper Presented at the Second ASCE Specialty Conference on Structural Design of Nuclear Plant Facilities," New Orleans, Louisiana, December 1975.

5-15 Johnson, B., et al., "Analysis of the Turbine Missile Hazard to the Nuclear Thermal Power Plant at Pebble Springs, Oregon," Science Applications, Inc., January 1976.

5-16 Meyers, B. L., and Morrow, W. M., "Tornado Missile Risk Model," Topical Report, Bechtel Power Corporation, BC-TOP-10, June 1975.

5-17 Twisdale, L. A., et al., "Tornado Missile Risk Analysis," EPRI NP-154, Project 616-1, Topical Report 1, January 1976.

5-18 Yeh, G. C., "Probability and Containment of Turbine Missiles," ASME-IEEE Joint Power Generation Conference, Meeting Preprint JPG-74-11, Miami Beach, Florida, September 1974.

6- 1 Hahn, G. J., and Shapiro, S. S., Statistical Models in Engineering, John Wiley & Sons, New York, 1967.

6- 2 Hammersley, J. M., and Handscomb, D. C., Monte Carlo Methods, Methven & Co., London, 1964.

6- 3 Tocher, K. D., The Art of Simulation, D. Van Nostrand Co., Princeton, New Jersey, 1963.

6- 4 Harling, J., "Simulation Techniques in Operations Research - A Review," Journal of Operations Research, 6, 307, 1958.

6- 5 Mood, A. M., Introduction to the Theory of Statistics, McGraw-Hill Book Company, New York, 1950.

6- 6 Feller, W., An Introduction to Probability Theory and Its Applications, Volume I, 3rd Edition, John Wiley & Sons, Inc., New York, 1968.

6- 7 Pritsker, A. A. B., and Kiviat, P. J., Simulation With GASP II, Prentice-Hall, Inc., Englewood Cliff, New Jersey, 1969.

6- 8 Schriber, T. J., General Purpose Simulation System/360: Introductory Concepts and Base Studies, The University of Michigan, Ann Arbor, Michigan, 1968.

6- 9 Morris, P. A., "Modeling Experts," ORSA/TIMS Joint National Meeting, November 1975.

6-10 Crane, M. A., "Techniques of Response Surface Estimation With Applications in Computer Simulation," Control Analysis Corporation, Technical Report No. 89-19.

6-11 McGrath, E. J., Basin, S. L., Barton, R. W., Erving, D. C., Jaquette, S. C., and Ketler, W. R., et al., Techniques for Efficient Monte Carlo Simulation, ORNL-RSIC-38, Volumes 1, 2, 3, April 1975.

6-12 Kahn, H., and Marshall, A. W., "Methods of Reducing Sample Size in Monte Carlo Computation," Journal of Operations Research Society of America, 8, 169, 1960.

6-13 Kahn, H., Application of Monte Carlo, The Rand Corporation, Santa Monica, 1956.

6-14 Teichrow, D., and Lubin, J., "Computer Simulation - Discussion in the Technique and Comparison of Languages," Communications of the Association for Computer Machinery, IX, No. 10, October 1966.

6-15 Siff, F. H., "Variance Reduction in Simulation Studies - Conditional Monte Carlo," Presented at the Joint National Meeting - ORSA/TIMS, Las Vegas, Nevada, November 1975.

6-16 Kennedy, W. J., "Recent Advances in Techniques for Generating Pseudo-Random Numbers," Presented at the Joint National Meeting - ORSA/TIMS, Las Vegas, Nevada, November 1975.

6-17 Gentle, J. E., "A Survey of Variance Reduction and Robust Procedures in Monte Carlo Analysis," Presented at the Joint National Meeting - ORSA/TIMS, Las Vegas, Nevada, November 1975.

6-18 Turnquist, M. A., "A Bayesian Approach to the Design of Simulation Experiments," Presented at the Joint National Meeting - ORSA/TIMS, Las Vegas, Nevada, November 1975.

6-19 Coveyou, R. R., Cain, V. R., and Yost, K. J., "Adjoint and Importance in Monte Carlo Applications," Nuclear Science and Engineering, 27, 1967.

6-20 Carter, L. L., Cashwell, E. D., Particle Transport Simulation With The Monte Carlo Method, ERDA Critical Review Series, 1975.

6-21 Schaeffer, N. M., Reactor Shielding for Nuclear Engineers, U. S. Atomic Energy Commission, TID-25951, 1973.

6-22 Raiffa, H., Decision Analysis, Addison-Wesley, 1968.

6-23 Gearing, C. E., "A Fuzzy Set - Theoretic Generalization of Bayes Theorem," Presented at the 1976 Joint National Meeting of ORSA/TIMS, Philadelphia, Pennsylvania, April 1976.

6-24 Benjamin, J. R., and Cornell, C. A., Probability, Statistics, and Decisions for Civil Engineers, McGraw-Hill, 1970.

6-25 Mardia, K. V., "Linear-Circular Correlation Coefficients and Rhythometry," Research Report No. 2, University of Leeds, Leeds, England, September 1975.

6-26 Tang, W. H., and Ang, A. H. S., "Modeling, Analysis, and Updating of Uncertainties," Preprint, ASCE National Structural Engineering Meeting, San Francisco, California, April 1973.

6-27 Tang, W. H., "A Bayesian Evaluation of Information for Foundation Engineering Design," International Conference on Applications of Statistics and Probability to Soil and Structural Engineering, Hong Kong, September 1971.

6-28 Ang, A. H. S., and Tang, W. H., Probability Concepts in Engineering Planning and Design, Wiley, New York, 1975.